FACULTY OF TEXTILE ENGINEERING TUL

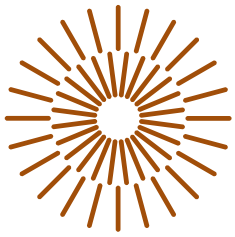

Fiber Structures for Electromagnetic Radiation Shielding

Vlákenné struktury pro stínění elektromagentického záření

Habilitation Thesis

Ing. Veronika Tunáková, Ph.D.

2023

Annotation

This habilitation thesis is a set of published scientific papers or engineering papers supplemented with a commentary according to §72 paragraph 3 point Act No. 111/1998 Coll. on universities. In total, the set of scientific paper contains 18 research works published in impact factor journals, 1 conference paper indexed in Scopus database, and 2 utility models. The chosen scientific papers are mainly focused on the usage of different methods for development of textiles with increased electrical conductivity and increased electromagnetic shielding ability. They are also devoted to the properties of these special textiles in connection with their practical use, and options of designing these special fabrics. Measurement methods of electromagnetic shielding effectiveness together with the possibilities of electromagnetic shielding modeling are also discussed. At the end of this thesis is presented a brief description of applications of textiles that are able to shield electromagnetic field.

Keywords: Composites; Electric conductivity; Electromagnetic shielding; Fiber structures; Measurement methods; Modeling.

Contents

Introduction

Electromagnetic interference (EMI) can be defined as unwanted electromagnetic radiation produced by electrical circuits that can adversely affect the operation of surrounding electronic devices or cause damage to living organisms. In recent decades, the level of so-called electromagnetic smog has increased significantly, especially that, which relates to the development of new high-frequency electronic systems and telecommunication equipment. This phenomenon has led to the active development of new and effective solutions for the provision of shielding from interfering electromagnetic radiation in various applications. Electromagnetic interference shielding refers to the blocking of incoming electromagnetic waves through absorption, reflection, or multiple reflection, whereby the shielding material resists penetration by electromagnetic radiation.

The ability of a material to shield electromagnetic field is usually expressed in terms of the electromagnetic shielding efficiency (SE), which is expressed in dB. SE describes how well the shield reflects or absorbs electromagnetic radiation. It is frequency dependent and affected by several factors such as shield material parameters (conductivity, permeability and permittivity), shield thickness, type of electromagnetic field source, distance from the source to the shield, etc.

Professional literature reveals that the most common method used for shielding from electromagnetic fields involves reflection from metallic materials, generally foils or plates. The disadvantages of these solutions include their limited flexibility due to the high rigidity and high density of these materials, as well as certain corrosion issues and the limited capacity to control the efficiency of the electromagnetic shielding (SE). Therefore, an increasing amount of attention is being paid to the development of polymeric-based shielding materials which have the advantages of having a low weight and being comparatively inexpensive.

Textile materials are a special type of the polymeric-based materials which, in addition, excel in other characteristics such as permeability to air and water vapor, flexibility, handle and more. Their SE is obviously very low, and for their improvements it is necessary to use special techniques based on surface or volume modifications often by active particles or combination with conductive metal fibers.

This habilitation thesis represents a set of published scientific papers accompanied by a commentary in the field of fiber-based EMI shielding materials. In total, the set of scientific paper contains 18 research works published in impact factor journals, 1 conference paper indexed in Scopus database, and 2 utility models. The full texts of the 10 selected papers are given in the appendices to this thesis. The remaining articles can be viewed using the links attached to the citations of individual papers, which are displayed both under individual chapters and in the summary of the literature used in this thesis. Basic knowledge of aspects of EMI shielding and microwave absorption, including their fundamentals and applications, especially with regard to development and evaluation of textile structures, are covered by this thesis. It provides:

- The basic concepts determining electromagnetic shielding.
- A thorough review of different methods for the development of textiles with increased electrical conductivity in terms of the conductive additive used, and a summary of the influence of various parameters which, in addition to the material composition, also affect the functionality of the electromagnetically shielding fabric.
- Research of properties of special electrically conductive textiles in connection with their practical use, and options of designing and enhancing the properties of these special fabrics.
- Discussion about measurement techniques and standards in EMI shielding, including description of a new measuring method, and modeling and prediction options of electromagnetic shielding effectiveness.

- Short description of various applications of textiles with the ability to shield the electromagnetic field.

The first chapter briefly summarizes basic knowledge of EMI shielding and introduces EMI SE, as an important index to quantitatively evaluate the shielding performance.

Because the presence of electrically conductive component is one of the key requirements for the creation of electromagnetically shielding barriers, the second chapter acquaints the reader with various methods of creating textiles with increased electrical conductivity. Increased attention will be paid to the integration of metal fibers and wires into the fabric structure, and application of conductive polymer and metal coatings on textile substrates. The properties are explained together with possible limitations of the new materials. The influence of the moisture content of the material on its final shielding ability will also be discussed. In the same chapter will be in more detail described the parameters that can affect the level of electromagnetic shielding efficiency of the surface partition. More precisely, the amount and the distribution of the conductive component in textile sample will be discussed. Furthermore, structural properties such as the type and pattern of the fabric, its thickness and basis weight, porosity and other influential variables will be examined.

The level of electrical conductivity or electromagnetic shielding effectiveness is a major request in area of development of such functional materials. Depending on the purpose of use, these special textiles are subject to additional requirements, which may include requirements for air and water vapor permeability, and requirements for mechanical properties such as strength, flexibility or other special requirements. Third chapter will discuss other properties of these special textiles in connection with their practical use. In addition, the possibilities of patterning and increasing the aesthetic properties of chosen electrically conductive textiles will be introduced.

In current literature, it is possible to encounter various principles of evaluation of electromagnetic shielding of planar structures. The fourth chapter will therefore be devoted to the methodology of evaluation of this quantity, together with the evaluation and comparison of different measuring methods. A new simple measuring method based on shielded box will also be introduced. In addition, the possibilities of prediction and modeling of this quantity will be discussed on the basis of knowledge of electrical and geometric properties of textiles.

The last, no less important chapter summarizes various uses of electrically conductive and/or electromagnetically shielding textiles, which include e.g. making clothes both for casual everyday wear, and meeting the requirements of personal protective clothing for workers, who are exposed to high levels of electromagnetic fields in their work. In addition to that will be demonstrated technical applications, such as the use of special textiles used to protect sensitive devices, or to protect data on payment cards or other types of cards or data chips.

1 Electromagnetic shielding phenomenon

Electromagnetic shielding is desirable to protect the environment and working area from radiation produced by electromagnetic equipment and computers, and also to protect sensitive circuits. EMI shielding is generally defined as the barrier of the propagation of electric and magnetic waves from one area to another by using electrically conductive or magnetic materials. Shielding is therefore a technique of ensuring the required level of attenuation of electromagnetic waves using a well-designed shield.

"SE of material is defined as the ratio between the transmitted (P_t) and incident power (P_i) of the electromagnetic wave" [1]. SE is usually presented in decibels and expressed by:

$$SE[\text{dB}] = -10\log(P_t/P_i). \tag{1}$$

The total shielding effectiveness (SE_{total}) includes two main mechanisms of attenuation of electromagnetic waves due to: (a) reflection (SE_R), the main mechanism for metal based shields

and (b) absorption (SE_A) of the radiation power connected with consequent dissipation of the wave inside the material. The total SE is the sum of the SE via absorption (SE_A), reflection (SE_R) and multiple reflections (SE_M), which is:

$$SE_{total} = SE_A + SE_R + SE_M. \tag{2}$$

The occurrence of multiple reflections requires the presence of a large specific surface or inter-facial areas in the shielding element. If the shield is made of a well-conducting material and its thickness is significantly greater than the penetration depth and SE_A is $\geq$ 10 dB, then $SE_M \to 0$ and can be neglected [2].

The transmittance T is calculated by the ratio of P_t to P_i:

$$T = P_t/P_i. \tag{3}$$

Thus, SE_{total} can be written as:

$$SE_{total} = -10\log T. \tag{4}$$

Then, A_{eff}, effective absorbance considering level of incident electromagnetic field in the shielding element can be written as:

$$A_{eff} = (1 - R - T)/(1 - R), \tag{5}$$

where, R is the reflectance [2]. Due to effective absorbance and reflectance the SE can be described as:

$$SE_R = -10\log(1 - R). \tag{6}$$

$$SE_A = -10\log(1 - A_{eff}) = -10\log[T/(1 - R)]. \tag{7}$$

Reflection loss occurs by partial reflection of incident energy at a material interface, e.g. between air and a surface of metal coated fabric. "SE_R increases with increasing electrical conductivity σ, while it decreases with increasing permeability μ_r" [3]. It is independent of the thickness of the shield. "The absorption loss SE_A is related to the physical characteristics of shield material and it is independent of the type incident electromagnetic field (unlike reflection loss)" [2]. When the electromagentic wave passes through the material, there is an exponential reduction of its amplitude. In summary, reflection loss is a function of ratio σ/μ_r, while absorption attenuation is a function of product $\sigma \cdot \mu_r$ [1, 2].

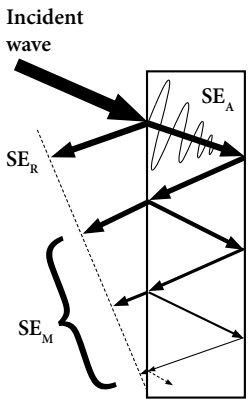

Figure 1: Mechanisms of electromagnetic wave attenuation.

It follows that the most suitable materials for shielding the electromagnetic field have high electrical conductivity and high magnetic permeability and therefore, the highest electromagnetic shielding ability can generally be achieved with barriers made of metals. However, the aim is to replace metals with composite materials, mainly due to their required low weight, favorable mechanical properties and price.

Not only does the shielding efficiency depend on the material, and on the thickness of the material, from which the shielding element was made, but also on the frequency of the electromagnetic radiation source, the distance from the radiation source to the shielding element, and also on the number and shape of various discontinuities. These include mainly gaps, pores, cracks, holes, etc.

2 Development of textiles with increased conductivity

Electrical conductivity is one of the crucial parameters for improving resistance to electromagnetic radiation, reducing the tendency to accumulate electrostatic charge and the construction of intelligent textiles containing conductive paths. Electrically conductive textiles are often used in special clothing and technical applications, where the main purpose is to replace conventional metals or other materials using flexible fiber-based structures.

Most synthetic fibers used in textiles are electrical insulators with a volume resistivity in the order of 10^{11} - 10^{14} Ωcm. This is much more than the required resistivity for electromagnetic shielding needs. For example, the required resistivity for anti-static materials is in the range of $10^4 - 10^{11}$ Ωcm; while for materials designed to shield the electromagnetic field, the resistivity of less than 10^2 Ωcm is required.

Traditional textile materials are mostly dielectric materials, whereas their electric conductivity depends on the moisture content and other impurities. In general, it can be stated, that fabrics made of traditional textile fibers (natural or manufactured) are in standard climatic conditions transparent to electromagnetic radiation, see Fig. 2 where is shown the dependence of SE on frequency for fabrics made of traditional textile materials.

The main goal of the study published by *Tunáková et al.* [4] was to determine whether the presence of increased moisture content (human sweat) in non-conductive knitted fabrics significantly affects its ability to shield electromagnetic field. Based on the results from the study, it can be summarized, that the SE did not increase above 1 dB for higher frequencies

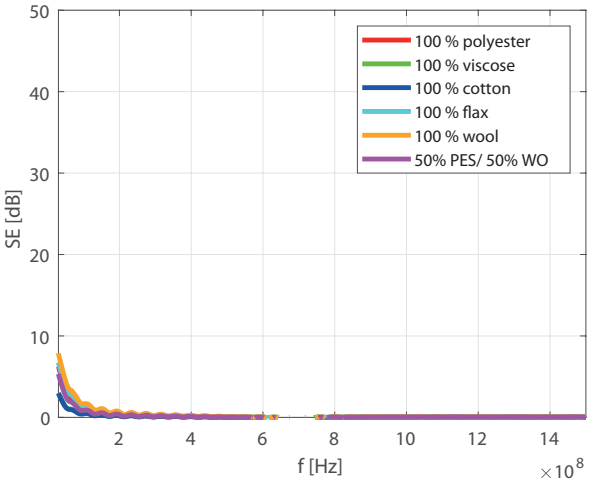

Figure 2: Dependence of SE on frequency for chosen woven fabrics made of traditional textile materials.

($f > 400$ MHz), even when using alkaline synthetic sweat solution (having electric conductivity of the solution 10 mS/cm) in the highest content (~ 200 %) applied on 100 % cotton fabric. It follows from the above that it is not possible to achieve functional shielding barriers by increasing the moisture content, and therefore it is necessary to implement special electrically conductive components to the fiber structure.

Electrically conductive fabrics can be made using an electrically conductive base element - fiber. Electrically conductive fibers can be divided into the following categories: metal fibers, metal and electrically conductive polymer coated fibers, carbon fibers, polymer fibers filled with conductive elements, bi-component fibers, and electrically conductive polymer fibers. In the next sub-chapters will be described individual groups of electrically conductive fibers / electrically conductive fiber structures relating to the author's publication and research outputs.

The 'ideal' electrically conductive fiber would be a material with:

- high electrical conductivity;
- high mechanical tenacity;
- wash resistance;
- is comparatively cheap and available in large quantities.

In general, the electrically conductive fabrics may be formed by yarns containing the fibers mentioned above. Another possibility for the production of electrically conductive textiles is their plating with metals, coating with conductive polymers or impregnation with conductive particles in form of pastes or inks.

2.1 Metal fibers and wires

In recent years, electrically conductive fabrics have received increased attention due to electromagnetic shielding and other applications such as electrostatic charge dissipation. These special fabrics can be made of electrically conductive fibers, for example metal fibers/wires. Metal fibers in general can be produced in filament or staple lengths, and can be incorporated with traditional non-conductive fibers/yarns produce fabrics with different levels of electrical conductivity [5–7].

Winding and twisting represents methods how to incorporate endless electrically conductive component (e.g. thin metal wire) to the staple or multifilament fiber core yarn, see Fig. 3(a). Knitted fabrics with incorporated stainless steel filaments (diameter 0.12 mm) were studied by *Tunáková et al.* and published in [8]. It was found that despite the high content of the metal component, relatively low electromagnetic shielding effectiveness (SE $<$ 10 dB) for knitted fabrics was achieved for frequency $f \sim 1.5$ GHz. This phenomenon is probably caused by asymmetric structure of knitted fabric, which is quite different compared to highly effective metal wire meshes that contain wires parallel to each other with equidistant spacing, together with additional wires oriented orthogonal to the first set [9]. This assumption was confirmed by layering knitted samples oriented at 90° to each other. In this case, the SE of the two-layer sandwich was increased up to 20 dB [8]. It should be noted that the use of continuous metal wires of relatively high diameter and the associated relatively high bending stiffness can cause problems in both processing and use.

Staple length fibers, a non-continuous fibers of relatively short length are, in general, preferred over filament fibers for yarn production due to desirable characteristics of staple fiber yarns - such as comfort, warmth, softness and appearance [12]. Therefore, the researchers focused on textiles made specifically from blended yarns produced by staple fiber spinning technology, containing different portion of a thin metal fiber of staple length [13–15]. In the article [11] *Tunáková et al.* presented the current state of fabrication and characterization of multifunctional light weight flexible electromagnetic shielding fabrics. In this case, stainless steel (SS)

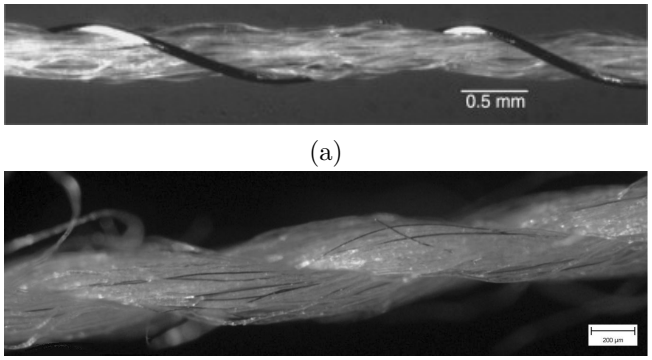

(a)

(b)

Figure 3: (a) Silver wire wounded around non-conductive core yarn [10], (b) blended yarn containing thin metal fiber of staple length.

staple length fibers (diameter 9 μm) and polypropylene fibers were mixed into the yarn Fig. 3(b) to achieve a certain level of electric conductivity. Fiber components were blended together at the draw frame. Up to the draw frame, each raw material was processed separately. Subsequently, the following effects of input variables were studied: metal fiber content, conductive yarn placement, thickness of the shield, type of fabric (woven, knitted), material composition of non-conductive component, moisture content on electromagnetic shielding effectiveness as an output variable. The main findings of this study can be summarized as follows. By controlling the amount of SS (through variation in blend ratio and through hybrid yarn density), the SE of the fabric (woven/knitted) can be easily managed especially with regard to the requirements for the end use of these special fabrics. Woven sample with the highest conductive component content (75 %) reaches the highest SE $\sim$ 50 dB for f= 1.5 GHz, see Figure 4. Generally, it can be said that conductive materials with SE around 40 - 50 dB (corresponding to 99.99 % - 99.999 % of blocked energy) can prevent electromagnetic interference emitted from 90 % of current commercial electronic devices.

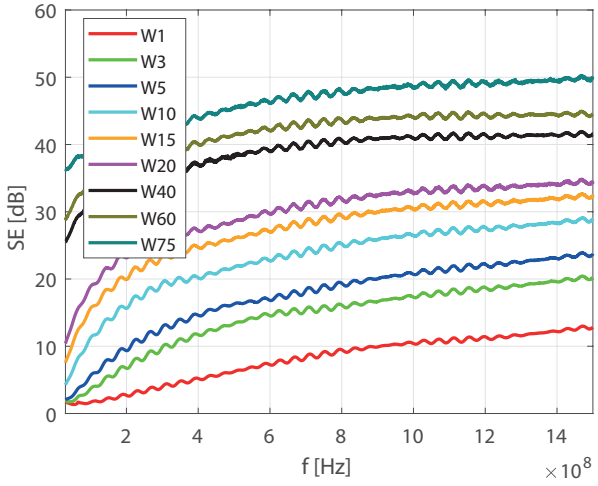

Figure 4: Dependence of SE on frequency for woven fabrics containing different portion of SS fiber. [11]

An increase in the shielding ability of these textiles can be achieved in these ways:

- by increasing the content of the conductive component in hybrid yarn, respectively, decrease electric resistivity of fabric,
- by increasing the hybrid yarn density in fabric (set of warp and weft yarns), which corresponds with metal fiber content,
- by increasing the thickness using e.g. multilayered system which provides blocking of the direct path of electromagnetic wave,
- by increasing the moisture content which increases electrical conductivity and therefore SE,
- by nonconductive component exhibiting hydrophilic property according to preferable higher total moisture content,
- by more compact structure — woven fabrics are usually preferred to single knitted fabrics.

It was proved, that different textile fibers can be used in a mixture with ultra-thin metal fibers in staple length. *Tunáková at al.* in the article [16] described behavior of woven fabrics made of blended yarns containing staple metal fiber and meta-aramid fibers in order to ensure shielding ability as well as mechanical properties, for example for the design of protective clothing. Developed metal composite textile shields possess advantageous properties such as satisfactory flexibility, drapability, durability, comfort properties. They can be manufactured by traditional textile production techniques, joined by sewing, washed without loss of functionality, etc.

2.2 Conductive coatings

Electrically conductive fibers can also be formed by coating the fibers with metals, galvanic materials, metal salts or electrically conductive polymers. Large number of fiber types used as an substrate and achievement of good conductivity without changing the properties of the fiber itself is an advantage of this method. Conductive layer can be applied to the surface of fibers, yarns and even textiles with the aim of creating electrically conductive textile structures. However, coating adhesion can cause problems.

Coating of fibers or yarns or even textile fabrics with a fine metal layer is another common method for achieving increased electrical conductivity. A thin layer of silver, copper or gold can be applied on the fiber surface using electrochemical, electroless, vapor deposition or spray coating techniques to transform nonconductive surface to conducive one. Satisfactorily low electrical resistance is achievable by these processes. However, the metallic layer on such materials is very susceptible to mechanical friction and rubbing. The metallic coating can be damaged during the textile production process or washing. Also, the price of such metal coated yarns is comparatively high and therefore not suitable for the mass market (100–1000 EUR/kg) [10].

Tunáková et al. [17] studied the mechanical, electrical and electro-mechanical properties of commercially available metal coated yarn, more precisely silver coated multifilaments having polyamide core creating yarn with fineness 2×63 tex. It was found that the electrical resistance of metal coated yarn is high ($< 50\ \Omega/\mathrm{m}$) and thus fabrics made from these yarns will have a relatively high ability to shield the electromagnetic field.

Tunáková participated in the preparation and characterization of electrically conductive cotton fabrics by in-situ deposition of copper particles published in [18]. During this study the effect of copper sulfate solution concentration and number of dipping the substrate in a bath

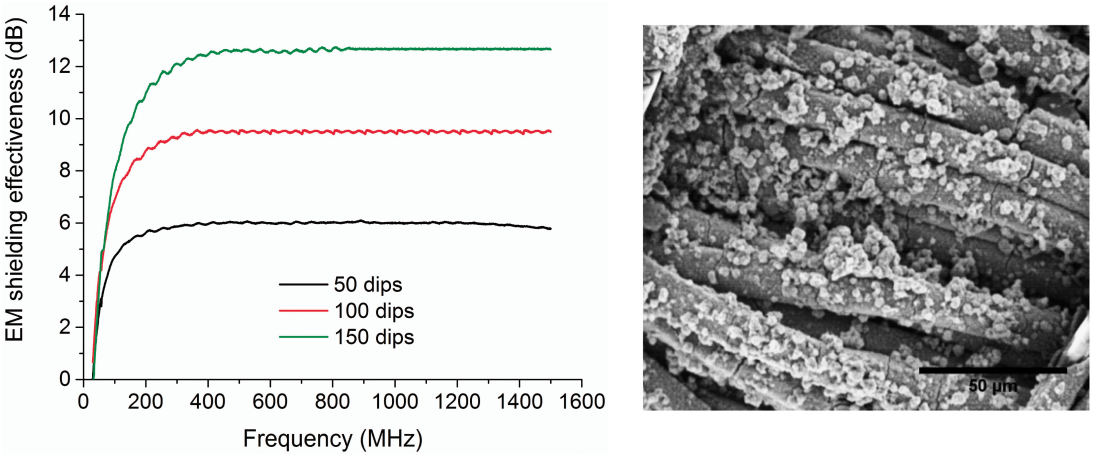

(a) (b)

Figure 5: (a) Dependence of SE on frequency and (b) SEM image of copper coated cotton fabric by 2 g/200 ml [18].

was explored. A cotton fabric with an area density of 150 g/m^2 in a plain weave was used as the substrate for plating. It was found, that cotton fabric samples coated by 2 g/200 ml had SE in range from 5 to 13 dB at frequency range form 300 - 1500 MHz depending on the number of dipping cycles, see Fig. 5. It was further found that SE increases with the increasing number of dips, which was explained by an increase in EM wave reflection due to a sufficiently dense, uniform network of conductive copper particles on the surface. It seems that the SE is independent on frequency for higher frequencies ($f > 400$ MHz) for these copper coated samples, which could be a very important characteristic given the intended purpose of use. It can also be mentioned that the presence of deposited copper particles ensures higher strength and elongation at break as well as increased antibacterial capacity of the coated samples.

Tunáková et al. [19, 20] further examined activation of electrically non-conductive nonwoven sample by electroless copper plating. This 100 % PES filament cross laminated nonwoven fabric excels in its low thickness ($\sim$ 0.07 mm) and high porosity. The diameter of each filament is approx. 10 µm, which ensures also high specific surface area of sample. Prior to the coating, the plasma pre-treatment of sample was used to increase surface tension. Samples were then auto catalytically activated by tin and silver. Finally, metal coating of the sample was performed in copper salt solution; consumption of copper was 3 g/m^2. The coating took place using a copper tartrate complex, by an oxidation-reduction reaction with formaldehyde. It was found that the optimal pH value of the bath, to eliminate copper from the solution, is around 12.8. The highest electrical conductivity results were obtained using 800 W plasma treated substrate, followed by activation with tin and silver. The optimal copper bath temperature was found to be 23 °C. Under these conditions, comparable low electrical resistance of copper coated samples was achieved, namely 23.4 Ω for sample dimensions 40 mm × 20 mm, whereas the electrical resistance of PES substrate was $\sim$ 10E+12 Ω with the same sample dimensions. SE of this highly electrically conductive copper coated samples is shown in Fig. 6. It is visible that copper coated nonwoven sample has comparable high SE ($\sim$ 50 dB) especially with regard to its low thickness and mass per unit area ($<$ 20 g/m^2). The results of this research originated from the diploma thesis [20] with *Tunáková* as a supervisor and partial results were published in [19].

Coating of fibers or yarns or even fabrics with intrinsically conducting polymers precedes problems with process-ability of self-supporting conducting polymer fibers and has wide industrial applications. Electrically conductive polymers have been attracting much attention in the last 20 years due to the fact that they excel in both the physical and chemical properties of

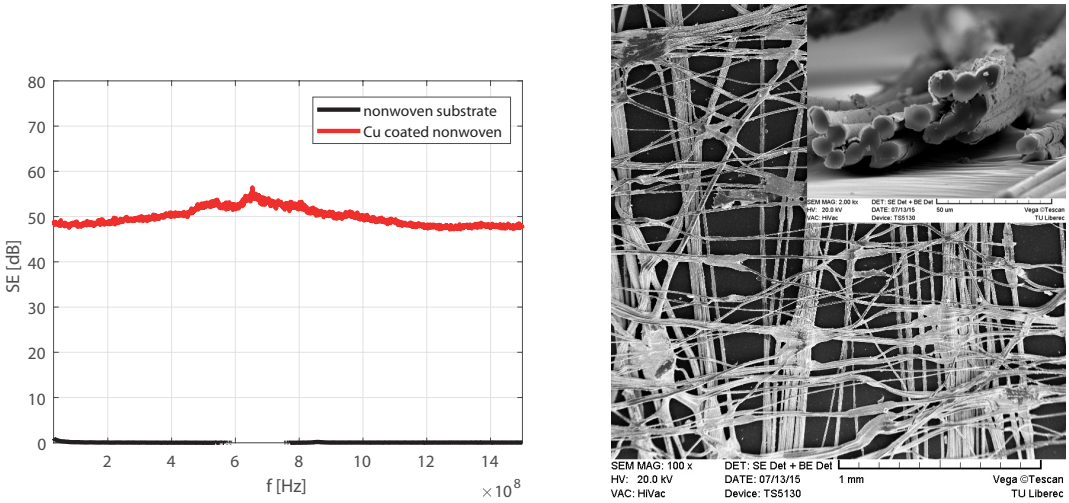

(a) (b)

Figure 6: (a) Dependence of SE on frequency, (b) SEM image for copper coated ultra thin nonwoven fabric [19]

organic polymers, and the electrical properties of metals. "They have a wide range of practical applications due to their low cost, conductive ability, and ease of synthesis [21]." Among the most studied are polyaniline, polyacetylene, polypyrrole and poly(3,4-ethylenedioxythiophene) (PEDOT), nevertheless more than 25 conductive polymers have been reported till now. [21].

"Intrinsically conductive polymers combine high electrical conductivity (as compared with carbons), ease processability, low density (e.g. density of polypyrrole (PPy) is 1.5 g/cm^3 far less than that of metals, such as 8.9 g/cm^3 for copper), and corrosion resistance together with absorption shielding mechanism (differing from the reflection one for metals)" [21]. The problem in processing these polymers is their decomposition below the melting point and therefore the impossibility of processing them from the melt. Low solubility also makes problems with their spinnability. The deposition of a submicron layer on a textile substrate is the most widely used practical solution for the application of conductive polymers, whereas polypyrrole is one of conductive polymers commonly used for commercial applications due to its long-term stability [21].

Tunáková et al. in paper [22], describe the process for the preparation of woven fabrics composed of 100 % polyester yarns coated with electrically conductive polypyrrole (PET/PPy). The key process parameters for the preparation of PET/PPy composites through in-situ oxidative polymerization in aqueous solution were studied with the help of Design of experiment methodology to develop textile composite with electromagnetic shielding efficiency 15±3 dB for frequency 1.5 GHz. It means that electromagnetic shielding effectiveness (SE) cannot be lower than 12 dB, but exceeding the upper limit is not forbidden. This requirement has arisen from the statement that, for personal shielding (general use), electromagnetic SE value should be in the range from 10 dB to 20 dB in the frequency spectrum of 0.8 – 2.5 GHz [23]. Ferric chloride ($FeCl_3$) was used as an oxidizing agent, and p-toluenesulfonic acid (PTSA) was used as a dopant, in fixed amount. Polymerization temperature, time, and monomer concentration were chosen at 3 different levels as input parameters (factors). It was found that all selected factors and their interactions have statistically significant effect on the resulting SE, whereas monomer concentration has the highest positive influence. SE of PET/PPy textile composites ranged from 0 to 17 dB at frequency 1.5 GHz depending on process parameters of polymerization, see Fig. 7. The highest electromagnetic SE (16.7 dB at frequency 1.5 GHz) was exhibited

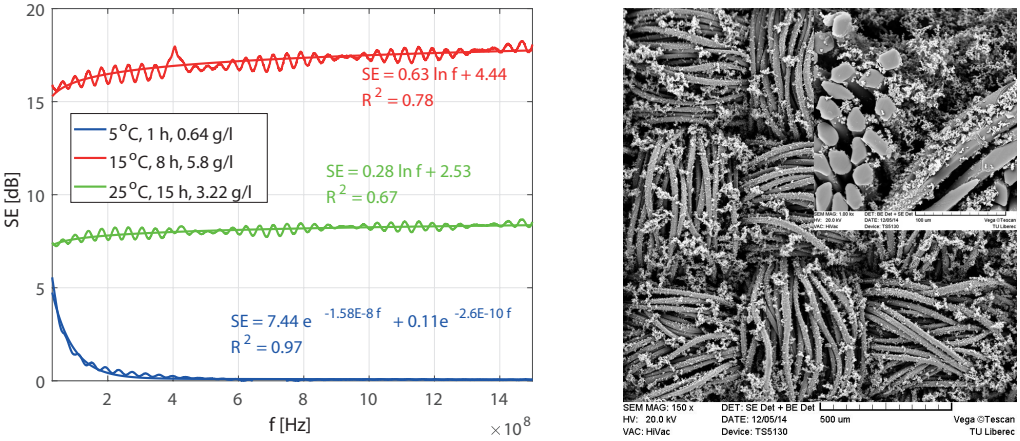

(a) (b)

Figure 7: (a) The dependence of SE on frequency for three representatives of PET/PPy textile composites: sample with low SE, intermediate SE and the highest SE [22]; (b) SEM images of PET/PPy textile composites prepared by following adjustments: 15 °C , 15 h, 5.8 g/l.

by a sample prepared with the following input parameters: 15 °C polymerization temperature, 8 h polymerization time, 5.8 g/l monomer concentration.

Experimental data were used to derive an empirical model linking the output and inputs using Akaike Information Criteria along with traditional null-hypothesis testing during regression analysis:

$$SE[\text{dB}] = -7.99 + 0.68T + 0.76t + 4.09c - 0.01Tt - 0.04Tc - 0.02T^2 - 0.02t^2 - 0.25c^2 + e, \quad (8)$$

where T is polymerization temperature [°C], t is polymerization time [h] and c is monomer concentration [g/l].

Optimizer tool available, e.g., in Minitab (optimization for target value) was used to obtain PET/PPy textile composites with electromagnetic shielding efficiency with at least 12 dB for frequency 1.5 GHz. Globally determined optimized parameters (polymerization temperature 6.7 °C, polymerization time 10 h and monomer concentration 5.8 g/l) for creating polypyrrole/polyester textile composite with electromagnetic shielding ability higher than 12 dB were successfully verified. Moreover, evaluation of weight increase and color of PPy coated samples confirmed that there is a relation between these two parameters and the SE of samples, which can be helpful for quick evaluation of sample functionality without direct SE measurement (demanding on the laboratory equipment).

2.3 Carbon-based materials

Carbon-based materials, such as graphene, carbon nanotubes, carbon fiber, and carbon black have gained great popularity as a component in the preparation of shielding materials mainly due to their high electrical conductivity, good mechanical performance, lightweight, flexibility, and large aspect ratio.

"Carbon fiber has been described as a fiber containing at least 90% carbon obtained by the controlled pyrolysis of appropriate fibers" [24]. The existence of carbon fiber is attributed Edison's patent originated from 1879, in which carbon filaments were manufactured. Unique properties of carbon fibers such as strength, electrical conductivity, stability on exposure to reactive media, low density, low-to-negative coefficient of thermal expansion, and resistance to

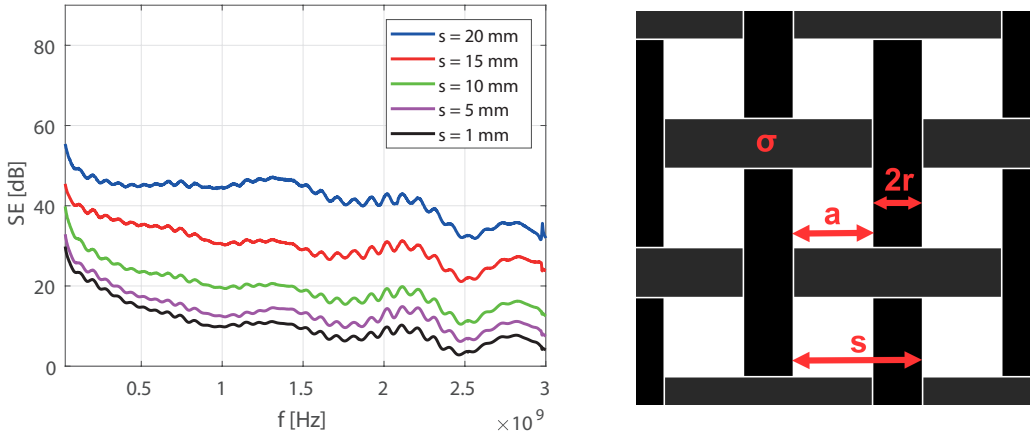

(a) (b)

Figure 8: (a) The dependence of SE on frequency for woven samples with different carbon roving spacing s [26], (b) schematics of samples in plain weave, where σ [S/m] is electric conductivity of carbon roving, a [mm] is a width of square aperture and s [mm] is carbon roving spacing.

shock heating have provided growth of areas of their application. Carbon fibers can be used for production of sorption materials, electrostatic discharge materials, catalysts, and reinforcements for composites [25].

The development of flexible air/water vapor permeable composites designed for shielding the electromagnetic field has received an increasing amount of attention in recent years. A great deal of the attendant research has dealt with the development and investigation of SE composites with textile-based reinforcements. *Tunáková et al.* in paper [26] investigated effect of the warp and weft sett and the thickness of the warp and weft threads of woven fabric in plain weave on SE, whereas Aksaca continuous carbon-fiber roving ($T = 196$ tex) having electrical conductivity $\sigma = 5.8{\cdot}10^4$ S/m was used as a thread element. As expected, the sample with the lowest warp and weft sett (carbon roving spacing $s = 20$ mm) was found to have the lowest SE (SE = 9.5 dB for $f = 1.5$ GHz), while that with the highest warp and weft sett ($s = 1$ mm) had the highest SE (SE = 45 dB for $f = 1.5$ GHz), see Fig. 8. The dependence of SE on the carbon roving spacing can be described using an exponential function. A slight increase in the SE can also be achieved by increasing the thickness of the weft and warp yarns. These electromagnetic shielding woven reinforcements can be used for production of composites that excel at low thickness, low weight and high ability to transport air and water vapor while maintaining SE of reinforcement.

Activated carbon is a processed carbon material with a highly developed porous structure and a large internal specific surface area (500–3000 m^2g^{-1}) [27]. Activated carbons are used extensively in industrial purification, waste water treatment and chemical recovery operations. Activated carbon can be made from a wide range of high-carbon raw materials, such as coconut shells, wood, fruit stones, solid waste, synthetic polymers or for example acrylic fibers, whereas "the main categories of clothing and textile waste are composed of synthetic materials such as acrylic, nylon and polyester fibers and natural materials such as wool, flax and cotton" [28]. As stated in [28], "textile waste is considered as one of the fastest growing sectors in terms of household waste" and therefore its processing into activated carbon can be promising. At the same time, the fibrous nature of textile waste material is very suitable for the production of fibrous activated carbon. Preparation of activated carbon nonwoven fabric with ability to shield electromagnetic field from acrylic waste was described in paper [29] with *Tunáková* as a co-author. "The acrylic fibrous waste obtained as industrial waste was successfully converted

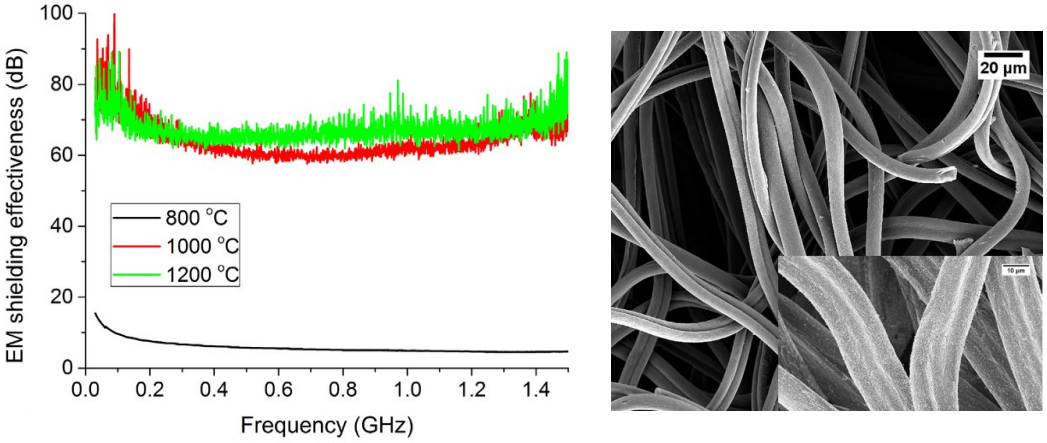

(a) (b)

Figure 9: (a) The dependence of SE on frequency for activated carbon fibers prepared by pyrolysis at 800 °C, 1000 °C, and 1200 °C; (b) SEM image of acrylic fibrous precursor and activated carbon web at 1200 °C (smaller image) [29].

into activated carbon fibrous structure by a single step physical activation via pyrolysis, in the presence of atmospheric air and CO_2 using controlled thermal treatment with temperatures 800 °C, 1000 °C, and 1200 °C using the heating rate of 300 °C h^{-1}" [29]. Whereas, uniform dispersion of graphite layers, low fiber diameter, larger surface area, higher porosity and higher electrical conductivity connected with higher SE ability could be achieved at higher pyrolysis temperature, see Fig. 9, where is shown the dependence of SE on frequency together with SEM images of activated carbon fibers. Acrylic precursor is almost transparent to electromagnetic field especially in higher frequencies. It is visible that the higher activation temperature, the higher SE, whereas further increase in the temperature above 1200 °C is no longer significant.

2.4 Other materials

In the previous chapters were mentioned widely used methods for the preparation of textiles with increased electrical conductivity, especially in connection with the research activities of the author of this work. Other principles of increasing electrical conductivity of fiber/composite will be briefly listed below, including **filling the non-conductive matrix with electrically conductive additives**.

Conventional polymeric materials are excellent electrical insulators, having resistivity in the range of 10^{15}–10^{18} Ωcm. They can be made electrically conductive by the addition of a variety of metal/carbon or metallised fillers and reinforcements, such as grafite, metal particles and flakes, carbon black, metal coated graphite fibers, carbon fibers and nanofibers, stainless steel fibers etc.

Nonwoven non-conductive samples were coated by aqueous dispersion of thermoplastic acrylic polymer enriched by (a) iron powder (50 wt%) and (b) aluminum powder (50 wt%) during the elaboration of diploma thesis [30] with *Tunáková* as a consultant. Dependence of SE on frequency for these two samples is shown in Fig. 10. It is visible, that SE ability of metal powder pastes is rather poor, it does not exceed 5 dB at 1.5 GHz despite the relatively high content of metal particles.

In man-made fibers, polymers can be made electrically conductive by adding electrically conductive particles to the spinning mass, but a problem arises with the inclusion of the particles. To gain proper conductivity of conductive fiber, it is necessary to use a large amount of at least 15

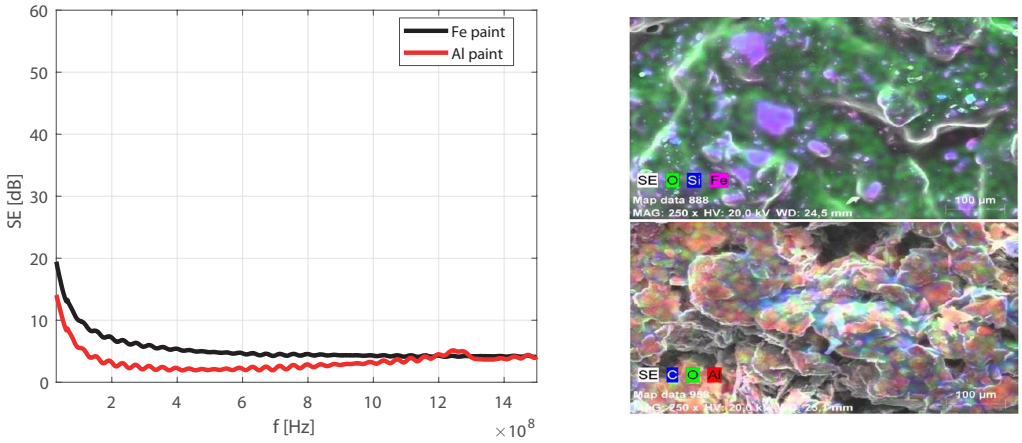

(a) (b)

Figure 10: (a) The dependence of SE on frequency for nonwoven sample coated by paste containing iron and aluminum powders; (b) SEM images of iron and aluminum powder containing paste deposited on nonwoven fabric surface [30].

wt% conductive particles. This large amount of conductive particles causes the fiber-producing process to be difficult, complex and expensive. Furthermore, it is impossible to include the electrically conductive particles inside the natural fibers.

In a similar way, oxides due to their fascinating magnetic properties, oxides of Ti, Fe, Mn, Ni, Cu, Mg, Li, Zn and Si, are often employed as fillers in polymeric coatings or during fiber spinning [31]. MXenes, representing 2D nanomaterials family, become popular among researchers due to their excellent intrinsic electrical conductivity, Joule heating performance, layered structure and polar surface chemistry that is tuneable. This material can be engineered into films, aerogels, fibers etc. [31].

Disadvantages of polymers filled with conductive additives include: high materials cost, problems with processing of filled composites, low performance compromises, poor surface finishes and appearance. The uniform conductivity of the composite is a major problem as well, due to the heterogeneity of the system. In general, beside polymers, cement and ceramics can be also filled with electrically conductive particles to get the required electromagnetic shielding function.

2.5 Influence of fabric structure

As follows from the above, in addition to the type and content of the conductive component in the fabric, its structure also plays a very important role during the development of electrically conductive, or electromagnetic shielding textiles made with the addition of electrically conductive fibers. In the next paragraphs, woven fabrics, knitted fabrics and non-woven fabrics will be discussed, incl. the influence of their structure on SE.

When comparing **woven, knitted and non-woven** fabrics containing similar type and content of the conductive component in form of electrically conductive fibers, differing only in spatial arrangement of fibers in the structure of fabric, it seems that the use of woven fabrics is the most advantageous for shielding the electromagnetic field, thanks to their symmetrical grid-like structure and also thanks to the high number of contact points in the binding points (fiber - fiber, yarn - yarn), which is typical for woven fabrics. Comparison of electromagnetic SE for woven, non-woven and knitted fabric (see Fig. 11, Table 1) made of mixture of non-conductive fibers (polyester, polypropylene) and similar amount of metal fibers ($\sim$ 15 %) in staple length

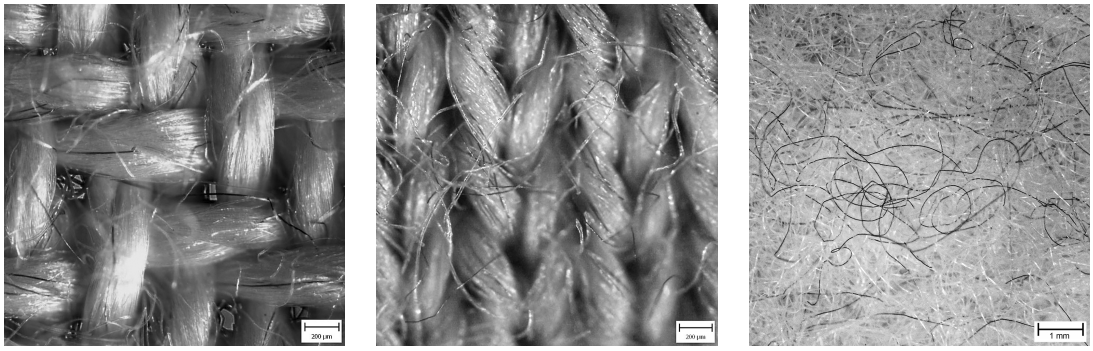

(a) (b) (c)

Figure 11: Mixture of non-conductive and conductive fibers (staple metal fibers) arranged into: (a) woven (twill 2/2), (b) knitted (single jersey) and (c) non-woven fabric (needle-punched).

Table 1: Description of woven, knitted and non-woven sample containing metal fibers in staple length subjected to study of SE.

Fabric type	**Structure**	**Metal fiber content** [%]	**GSM** [kgm^{-2}]	**Thickness** [mm]	**Density** [gm^{-3}]
woven	twill 2/2	15	217	0.73	297.3
knitted	single jersey	15	150	0.65	230.1
non-woven	needle-punched	14	257	5.92	43.43

(Bekinox$^{\mathrm{TM}}$, l = 90 mm , d = 9 µm), is shown in Fig. 12(a). It can be observed from the figure that the dependence of SE on f for all three samples has a different shape, with the woven sample showing the highest shielding efficiency over almost the entire frequency band (SE $\geq$ 30 dB for $f >$ 800 MHz). The non-woven fabric has almost constant SE over the entire frequency range (which could be desirable for special applications) reaching about 10 dB. The knitted fabric shows a global maximum of 10 dB around 800 MHz, however, the SE decreases for lower and higher frequencies. Taking into account the grams per square meter (GSM) or thickness of the sample, the woven sample achieves the highest SE. When considering the sample density, the highest shielding is provided by the non-woven sample. The described conclusions are in accordance with the paper [32], which investigates the effect of the content of stainless steel staple fibers (d = 12 µm) in needle punched nonwoven textiles (t = 5 mm) on SE, while the SE of a sample containing 25 % stainless steel fibers is only about 15 dB for f = 1.5 GHz.

During the investigation of woven textile structures with the addition of electrically conductive fibers, it was further established that the **weave of the woven fabric** can also influence the electromagnetic shielding efficiency, while keeping other parameters constant as stated in other articles [33–38]. It follows from the literature research that the effect of fabric weave has still not been sufficiently researched and clarified, as the published results are not consistent. On account of that, the analysis and the study of woven fabric weaves, and their effect on the SE, was deeply studied by author of this document. A weave consists of several parts that together define interlacing (crossing part, float part, distribution of interlacing points in the weave repeat). It is not possible to take only one part of the weave and assess its influence on SE, based on this one parameter. For that reason, the interlacing structure cells of woven fabric were used to describe the weave in paper [39] with *Tunáková* as a co-author. Twice twisted mixed PES yarn spun with 20% of stainless steel fiber was used, in both the warp and weft systems, for the production of experimental single layer dobby woven fabric samples with varied weaves (basic

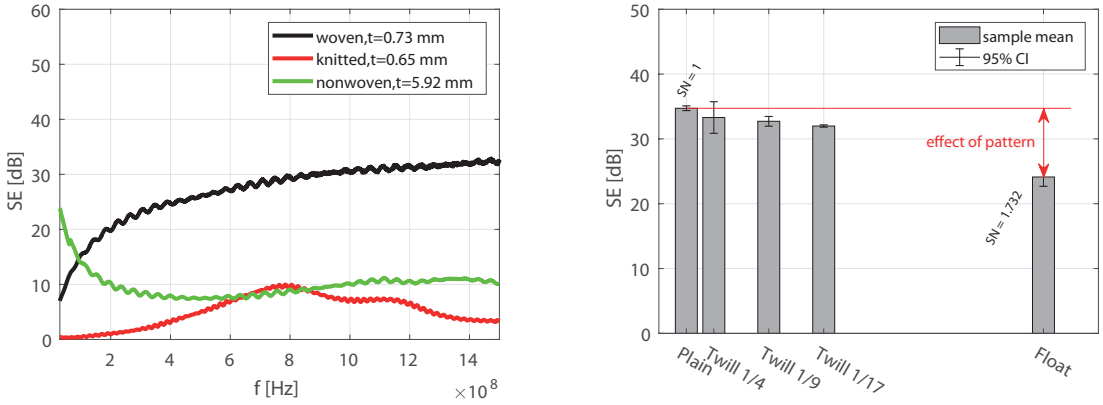

(a) (b)

Figure 12: (a) The dependence of SE on frequency for woven (twill), knitted (single jersey) and nonwoven (needle-punched) sample containing ~ 15 % of extremely thin metal fibers in staple length; (b) comparison of SE ($f = 1.5$ GHz) of woven sample set having different weave.

and derived weaves from the group of symmetrical and asymmetrical weaves). All samples were constructed with the same warp and weft yarn sett. In was found out that plain weave that has the maximum thread crossing given by the interlacing structure cell, *P1* (see paper [39] for more details) shows the highest SE, from the viewpoint of the weave, see Fig. 12(b). Higher thread crossing causes lower porosity (the higher cover factor), which is related to the lower portion of apertures. It is known, from theoretical analysis of propagation of electromagnetic waves through a shield, that the lower portion of discontinuities and apertures inside the shield is beneficial for higher SE. The second extreme case with the lowest SE value is represented by the endless float of the threads given by the interlacing structure cell, *P4*. From the weave viewpoint, the endless float does not create mutual interlacing, nor does it create internal forces, thus woven fabric is not created, but rather a non-interlaced grid. It was further found that a proposed variable called *float coefficient*, *SN*, which is calculated based on the geometrical parameters of different weave types, can be used as an explanatory variable for SE estimation according to:

$$SE[\text{dB}] = -3.59SN + 37.64 + e, \tag{9}$$

because there is a high level of dependence between *SN* and SE (the correlation coefficient $r \sim 0.82$). It is true that the lower the *SN*, the higher the SE. Based on this knowledge, woven samples with a controlled level of SE could be easily designed.

A research into the effect of the **pattern of knitted fabrics** on SE was carried out, as well as a research into the weave of the woven fabrics, showing that the weave of the woven fabrics affects the level of electromagnetic shielding of the samples, while keeping other parameters constant. *Tunáková* has studied the effect of knitted samples pattern on SE with the aim to increase their electromagnetic barrier capability. A set of knitted samples made of the same yarn (a mixture of polypropylene fiber and stainless steel fiber Bekinox$^{\text{TM}}$ having a staple length) was prepared. The samples differed in pattern along with other parameters that were affected by the pattern, see Table 2 for more details. It is observable from Fig. 13(a) that electromagnetic shielding ability of knitted samples having different pattern is unequal. From the point of view of global maxima, the highest SE is achieved by the laid-in knitted sample, which contains the filling yarn placed horizontally, which seems desirable and resembles woven structures. Satisfactory results are also achieved by the single jersey - pique and double face samples, which is probably caused

Table 2: Description of knitted fabric samples.

Pattern	**Metal fiber content** [%]	**GSM** [gm^{-2}]	**Thickness** [mm]	**Density** [kgm^{-3}]
single jersey - plain		149	0.53	281.13
single jersey - pique		186	0.86	216.28
laid-in fabric 3:1	10	168	0.68	247.06
double face		239	1.00	239.00
interlock fabric - plain		199	0.95	209.47

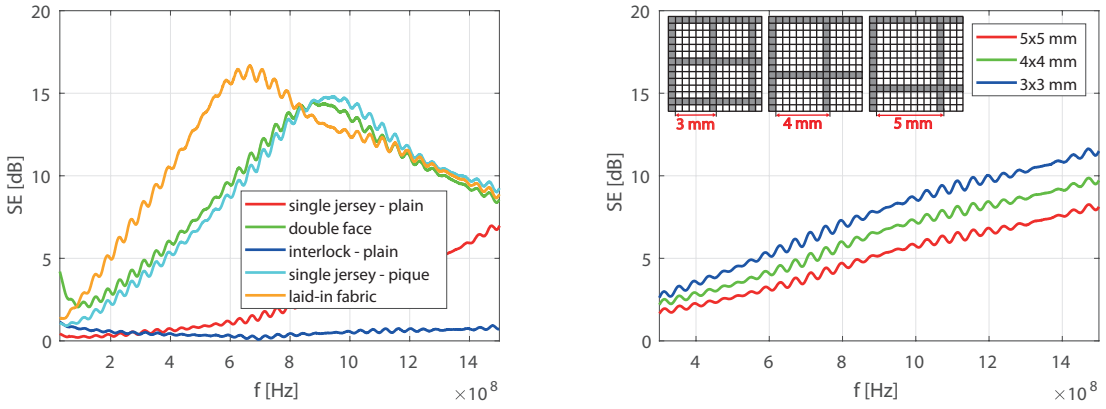

(a) (b)

Figure 13: The dependence of SE on frequency for: (a) knitted sample set having different pattern; (b) woven samples with interwoven electrically conductive grid having different side length.

by both the high grams per square meter and the relatively high thickness. The plain interlock sample achieves low SE values probably due to its open structure and low density.

The conducted experiments show the advantage of using conductive yarn in textiles both in the horizontal and vertical direction. Therefore, the possibility of creating electromagnetically shielding fabrics, which are made of non-conductive yarn and contain only a grid interwoven by electrically conductive yarn, was further investigated and discussed in [11]. As expected, it was found that the larger the spacing of the conductive grid with the same side length is, the lower is the SE of woven fabric, see Fig. 13(b). Furthermore, it was confirmed that a higher content of the conductive component in the yarn forming the grid will cause higher fabric SE. An almost linear increase of SE can also be achieved by increasing the thickness t of the fabric, which is in accordance with the theoretical analysis of SE, especially exploring absorption loss (A), whereas general expression for absorption loss can be written as [1]:

$$A[\text{dB}] = 0.0848t\sqrt{f\mu_r\sigma_r}. \tag{10}$$

where μ_r is relative permeability and σ_r is relative electric conductivity.

It can be examined that it is preferable to use sandwich (layered) system than plane single layer containing the same portion of conductive component in term of conductive component content. This phenomenon is due to the fact that one layer above the other can cover the apertures of the preceding layer and block the direct path of electromagnetic wave.

2.6 Summary

Tunáková et al. published a study [40] to introduce a present state of fiber-based electromagnetic shielding structures. Thirty-two different electro-conductive samples in total having different structure (woven, knitted, nonwoven, foil) and different material composition (carbon, polymer-coated, metal-coated, metal fibers, metal foils) were studied with regard to their SE, electrical conductivity and air permeability. The following paragraphs will summarize the most important findings.

Textile structures made of traditional fibres have been confirmed to be transparent to EM fields. This claim was supported by the very high measured electrical resistivity values of conventional fabrics lying in the insulator range.

The SE of textile structures (knitted, woven, non-woven) with different content and type of conductive components ranges from 1 to 79 dB in the high frequency range. The ability of a material to shield EM fields can be controlled by the correct choice of conductive component type, its content and placement.

Samples made from **metal-coated yarns or fibres** (even when GSM and air permeability are taken into account) appear to give SE in the range of 50-80 dB, giving a "Very good" rating even for professional use according to [23]. The frequency-independent SE of the metal plated textile structures is also very favourable, guaranteeing a constant SE for a given frequency range. The only drawback is their metallic appearance and feel. **The aluminium foils** provide very good shielding with 78 dB but zero air or water vapour permeability and their touch and mechanical properties are very limiting for many applications. The samples made from **hybrid yarns (containing stainless steel staple fibres)**, particularly woven fabrics, represent a promising approach. The SE of these hybrid fabrics ranges between 10 and 50 dB, depending on their structure and metal fibre content, which puts them in the 'Good' class for professional use [23]. The advantage of mixing conductive fibers with non-conductive fibers is the pleasant feel of the resulting woven or knitted fabric and other properties, including an appearance that does not differ from traditional textiles. The use of **carbon rovings** in the form of woven structures is also interesting, especially because of their high shielding ability and satisfactory air permeability, so they can be used as reinforcement for composites.

Other material approaches, such as coatings of non-conductive substrates with conductive polymers, treatment of non-conductive substrates by metal particle filled pastes, the incorporation of carbon particles in nonwoven structures, or the incorporation of conductive fibers in the bulky nonwoven structures, do not seem promising, especially with regard to their lower functionality (SE). Another disadvantage of conductive polymers used as a coating for non-conductive textile substrates is the poor stability in different environmental conditions (high humidity of air, high temperature) together with the expected low resistance to washing.

In addition to the shielding ability of the materials tested, the samples were also evaluated in terms of their electrical conductivity. In [40] it was found that the knowledge of the surface resistivity can be used to estimate its SE, due to the strong inverse relationship ($R^2 = 0.84$) between these two parameters. The prediction ability of this model is limited to samples without an insulating layer on their surface

2.7 Published outputs

Table 3 summarizes author's publications (10 journal papers and 1 conference paper) related to this chapter. The impact factor of the journal, the JIF quartile category and the number of citations of the given paper are displayed.

Table 3: Detailed information about author's publication outputs (journal IF, JIF category quartile and citations given as of 10/3/23) related to this chapter.

Journal Paper	Journal IF	JIF Quartile	Times Cited
[27] S. Naeem, V. Baheti, **V. Tunakova**, et al., "Development of porous and electrically conductive activated carbon web for effective EMI shielding applications," Carbon, vol. 111, pp. 439-447, 2017. DOI: 10.1016/j.carbon.2016.10.026	11.31	Q1	90
[15] **V. Safarova** and J. Militky, "Electromagnetic shielding properties of woven fabrics made from high-performance fibers," Text. Res. J., vol. 84, no. 12, pp. 1255–1267, 2014. DOI: 10.1177/0040517514521118	2.46	Q2	55
[38] S. Palanisamy, **V. Tunakova**, and J. Militky, "Fiber-based structures for electromagnetic shielding - comparison of different materials and textile structures," Text. Res. J., vol. 88, no. 17, pp. 1992–2012, 2018. DOI: 10.1177/0040517517715085	2.46	Q2	29
[17] A. Ali, V. Baheti, J. Militky, Z. Khan, **V. Tunakova**, and S. Naeem, "Copper coated multifunctional cotton fabrics," J. Ind. Text., vol. 48, no. 2, pp. 448–464, 2018. DOI: 10.1177/1528083717732076	2.93	Q1	31
[10] **V. Safarova** and J. Militky, "Multifunctional metal composite textile shields against electromagnetic radiation-Effect of various parameters on electromagnetic shielding effectiveness," Polym. Compos., vol. 38, no. 2, pp. 309–323, 2017. DOI: 10.1002/pc.23588	3.53	Q2	17
[21] **V. Tunakova**, J. Gregr, M. Tunak, and G. Dohnal, "Functional polyester fabric/polypyrrole polymer composites for electromagnetic shielding: Optimization of process parameters," J. Ind. Tex., vol. 47, no. 5, pp. 686–711, 2018. DOI: 10.1177/1528083716667262	2.93	Q1	12
[18] S. Palanisamy, **V. Tunakova**, S. Hu, et al., "Electromagnetic interference shielding of metal coated ultrathin nonwoven fabrics and their factorial design," Polymers, vol. 13, no. 4, p. 484, 2021. DOI: 10.3390/polym13040484	4.97	Q1	6
[3] S. Palanisamy, **V. Tunakova**, J. Militky, and J. Wiener, "Effect of moisture content on the electromagnetic shielding ability of non-conductive textile structures," Sci. Rep., vol. 11, no. 1, p. 11032, 2021. DOI: 10.1038/s41598-021-90516-9	5.00	Q1	5
[7] **V. Tunakova** et al., "Hybrid knitted fabric for electromagnetic radiation shielding," J. Eng. Fiber Fabr., vol. 15, p. 1558925020925397, 2020. DOI: 10.1177/1558925020925397	2.00	Q2	3
[25] **V. Tunakova** and M. Tunak, "Carbon-fiber reinforcements for epoxy composites with electromagnetic radiation protection—prediction of electromagnetic shielding ability," Compos. Sci. Technol., vol. 215, p. 109029, 2021. DOI: 10.1016/j.compscitech.2021.109029	9.88	Q1	6
[37] B. K. Sirková, **V. Tunakova**, M. Tunak, and K. Jezik, "Influence of woven fabric construction parameters on electromagnetic shielding effectiveness: Part I – weave influence," Text. Res. J., vol. 92, no. 21-22, 2022. DOI: 10.1177/00405175221100390	2.46	Q2	0
[16] **V. Safarova**, K. Malachova, and J. Militky, "Electromechanical Analysis of Textile Structures Designed for Wearable Sensors," in Proceedings of Mechatronika 2014, Brno, 2014, pp. 416–422. DOI: 10.1109/MECHATRONIKA.2014.7018294	-	-	3

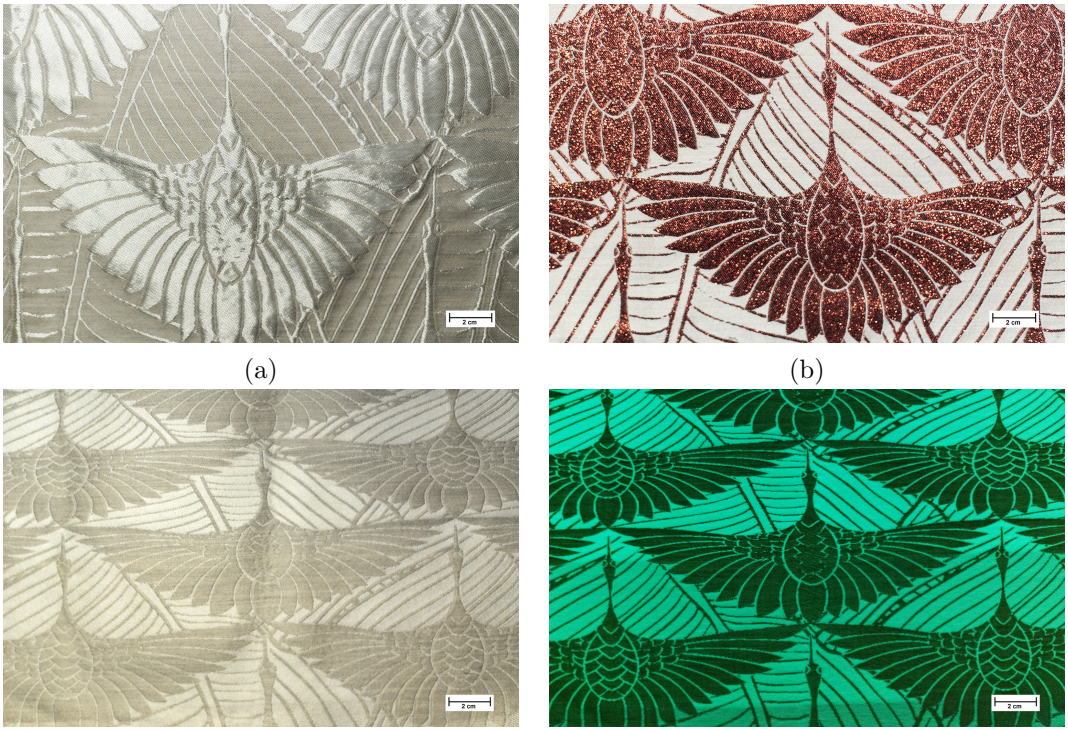

Figure 14: Macroscopic images of woven fabrics containing stainless steel fibers and: (a) glass roving; (b) fancy metallic yarn, (c,d) luminescent yarn as a second weft system with the aim of an effective pattern.

3 Performance in use and patterning of electrically conductive textiles

Electrically conductive textiles are no longer an unknown quantity in the textile industry. These special textiles are mainly used in antistatic applications, in smart textiles, and especially for achieving shielding from electromagnetic radiation.

Besides technical applications, electrically conductive textiles are often developed for the design of protective clothing, which is defined according to Mao [41] as "any device or appliance designed to be worn or held by an individual for protection against one or more health and safety hazards." As stated by Shi et al. [42], **aesthetic properties** (including fashion, color, and style) should also be considered when designing protective clothing for daily use. **Price** is another important factor to consider when introducing clothing with EM radiation protection to the market.

Another significant concern for the commercialization of advanced textiles with special functionality such as electromagnetic shielding ability is their **wash and wear durability** and the ensurement of their projected functional life span. One of the most damaging and destructive processes in the life cycle of special textiles is the washing process, including water, detergents, high temperatures, mechanical forces, etc., which does not receive enough attention compared to other performance properties.

On the grounds of that, this chapter will be dedicated to the description of the author's achievements in the field of increasing the visual appearance of electrically conductive textiles prepared for electromagnetic field shielding. The second part of this chapter will discuss the washing resistance of selected textiles that are resistant to electromagnetic radiation.

It seems that in the case of textiles containing metal staple fibers in their structure, it is

possible to apply two main methods for changing the appearance of the electrically conductive fabrics. It involves the use of colored fibers as non-conductive component, the preparation of yarns with the addition of conductive fibers, and the subsequent construction of the textile using traditional methods such as knitting or weaving. However, this approach is not flexible enough, especially when it is necessary to prepare special conductive yarns with different properties. Moreover, the application of original forms, text, and designs of the product is very limited during patterning by weaving and knitting.

The author of this habilitation thesis conducted an experiment using electrically conductive yarn containing 20 % of stainless steel staple fiber in weft system only, or in weft and warp system, to produce various woven designs. For this purpose was used a rapier weaving machine with an electronic jacquard shedding mechanism to apply more than one weft system. As a second weft system was used colored metallic yarn, glass thread and effective luminescent yarn, see Fig. 14 where images of fabrics are displayed. Figure 16(a) shows dependence of SE on frequency of woven patterned fabrics using luminescent yarn as a second weft. Two samples are compared: first of them contains electrically conductive weft only (warp was made of 100 % cotton yarns), the second sample was made up of both electrically conductive warp and weft. It can be seen from the Fig. 16(a) that it is advantageous to use electrically conductive yarn in both systems. If, for instance, only the electrically conductive warp is used, the resulting electromagnetic shielding ability is less than one quarter, compared to using electrically conductive both weft and warp. In the case of multi-weft fabrics, colored or special yarn can be incorporated, which does not affect the SE, but ensures visual properties of these electrically conductive textiles.

Design-oriented finishing, including bleaching, dyeing, and printing, is a technique that is applied on gray cloth directly after it is woven or knitted, this offers another option for affecting the visual characteristics of the electrically conductive fabrics. The author has no experience with dyeing textiles containing metal fibers, however, it was described in [43] that direct and reactive dyes have a great negative influence on electrical resistance of stainless steel yarns. While the whole fabric is uniformly covered (usually with one color) during dyeing, in the printing process are repeated patterns printed all over the fabric, or on certain part of the fabric, creating sharply defined print patterns for which one or more colors are used. Digital fabric printing is a process in which a pattern or an image from a digital file is transferred onto fabric using inkjet-based printers. There are two main digital printing methods: sublimation digital printing and direct digital printing. In a paper authored by *Tunáková, et al.* [44], have been made attempts to transfer the design in the form of picture on stainless steel fiber containing woven fabrics, by digital printing to enhance the visual properties of these special fabrics. It can be summarized that it is possible to produce patterned electrically conductive fabrics by digital printing, see images of printed electrically conductive fabrics at Fig. 15. No problems were evident in the

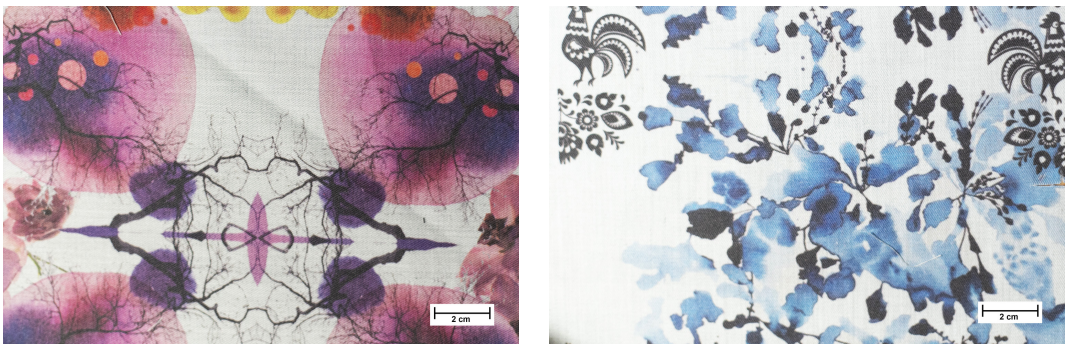

(a) (b)

Figure 15: Macroscopic images of digital printed woven fabrics containing stainless steel fibers.

actual printing process. Due to the presence of metal fibers in the structure of the fabric, the colors of the design differ from the printed colors on the fabric surface (they are darker). A slight increase in the SE of the printed samples is attributed to a decrease in the sample porosity after printing, see Fig. 16(b).

Another option for surface treatments is the use of laser. Laser beam enables to cause controlled deformation on textile surfaces and thus creates new designs by making use of the polymeric and heat-sensitive materials in the structure of the fabric. Designing the surface of electrically conductive (stainless steel fiber containing) fabrics by laser beam was tested and described by *Tunáková, et al.* in a paper [45]. In this study, it was found that some properties of irradiated samples are influenced positively with increasing intensity of laser treatment (such as visual effect, electromagnetic shielding effectiveness), while change in mechanical properties was undesirable. The increase of electromagnetic shielding ability is dedicated to the increase in electrical conductivity of the sample, caused by carbonization of the sample during laser irradiation, accompanied by change of color (from light grey to brown). Visual effect and mechanical properties can be controlled by laser intensity. As optimum laser intensity was determined 20% to 35%, using gray scale. Laser intensity 20% does not cause the desired visual effect, and at the same time, laser intensity above GS 35% is too high, initiating too large degradation of the sample which is accompanied by loss of mechanical properties and functionality restricting its practical usage. Figure 17(a) shows dependence of SE on laser intensity, described by gray scale at $f = 1.5$ GHz. At lower laser intensities, the effect on SE is negligible (statistically insignificant). With further increase of laser irradiation intensity, SE slightly increases. After getting over gray scale "critical value" (GS $> 51\%$), the sample becomes fragile, cracks appear and therefore the SE of the sample decreases because of easier penetration of electromagnetic wave through the sample. Dependence of SE on gray scale can be approximated using power function. From Fig. 17(b) the decrease of strength of sample is observable with increasing laser irradiation intensity. Fig. 18 shows SEM images of untreated sample and laser irradiated sample, where cotton fibers (twisted ribbon appearance), polyester fibers (circular cross-section) and stainless steel fibers (lighter one) are recognizable. After the exposition to the laser, stainless steel fibers remained unaffected having smooth surface, while various sizes of pores on the cotton fibers were created, which resulted in a sponge-like structure

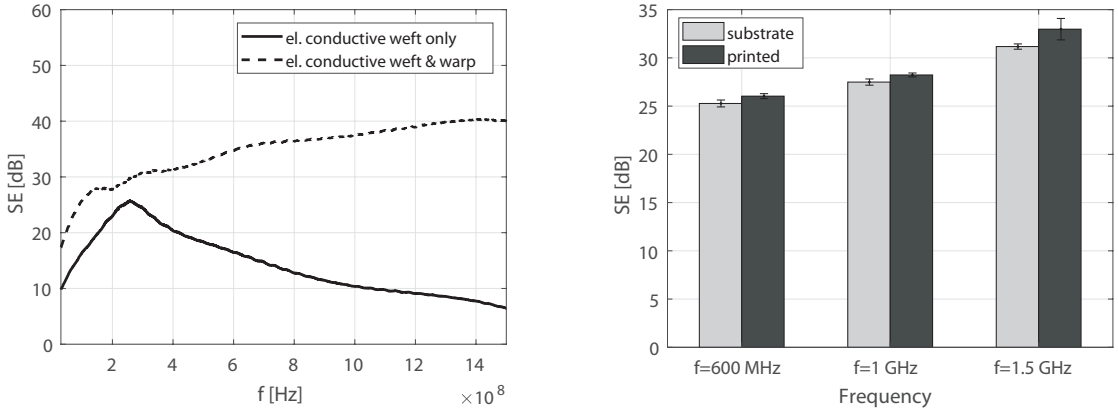

(a) (b)

Figure 16: (a) The dependence of SE on frequency for multi-weft woven fabric that created visual effect, using luminescent yarn, when using yarn containing 20 % of stainless steel fibers as weft system or for both yarn systems; (b) SE of digitally printed fabric containing 10 % of stainless steel fibers in warp and weft system - effect of print.

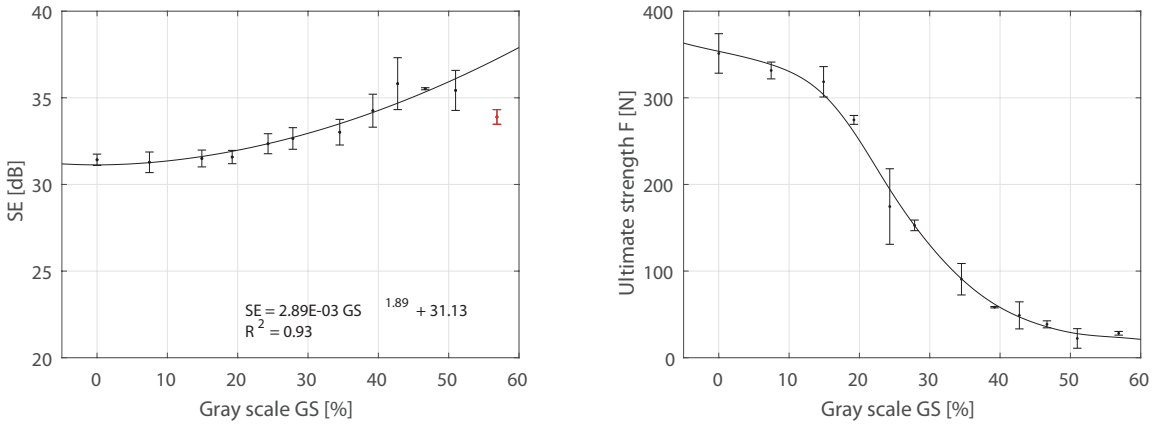

(a) (b)

Figure 17: The dependence of (a) SE, (b) fabric strength on laser intensity expressed by gray scale (GS) for laser irradiated electrically conductive fabrics.

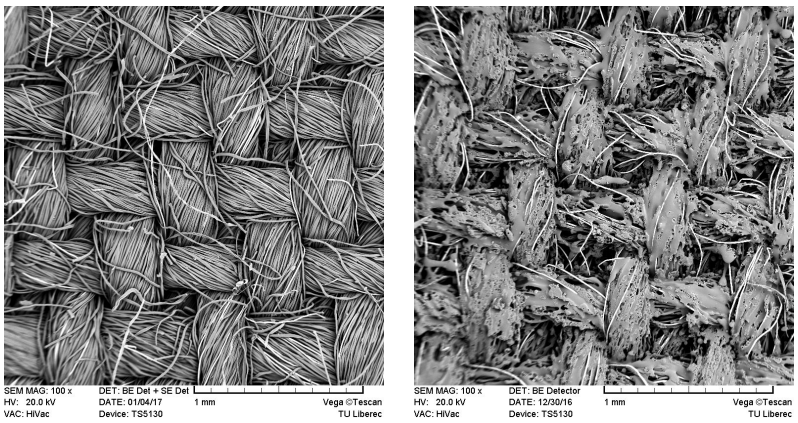

(a) (b)

Figure 18: SEM images of: (a) untreated sample; (b) sample irradiated by laser with intensity 34.5% expressed by gray scale.

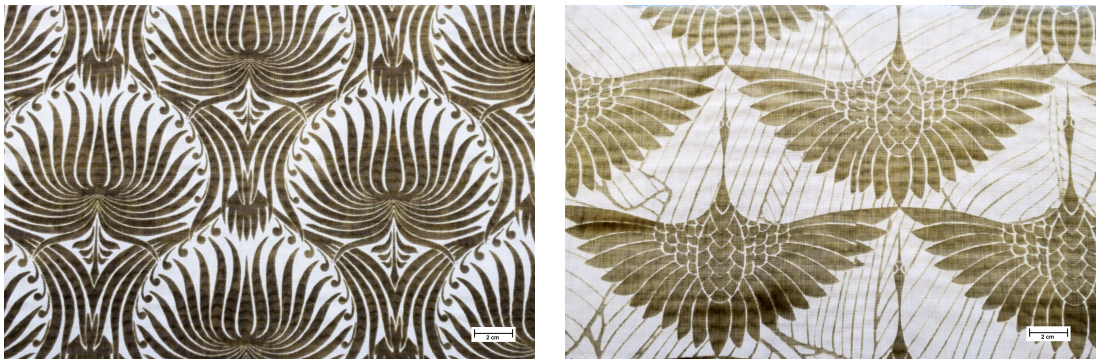

(a) (b)

Figure 19: Laser engraved electrically conducive fabrics using median GS of: (a) 42.7 %, (b) 27.5 %.

and polyester fibers start to melt. In Fig. 19 are presented patterned electrically-conductive fabrics created by laser beam, with optimized intensity.

As mentioned above, washing/dry cleaning is one of the factors in life cycle of special textiles that could negatively affect/limit the use of products made from them. "Washing/dry cleaning process is so destructive that it can cause a complete loss of material protective properties due to the synergism of water, chemical agents, mechanical agitation, as well as heat treatment", as reported in a paper [46], where copper plated filaments were used for production of woven interlining. *Tunáková* and the team [47] investigated and described the effect of washing and drying on the electromagnetic shielding ability of knitted fabrics and woven fabrics containing very fine stainless steel fibers in their structure. The main aim of the mentioned study was to find out if this treatment step can limit the use of these textiles. It was found, that despite the relatively significant increase in electrical resistivity during washing and drying of the samples, the samples did not totally lose their EM shielding ability. After applying 20 cycles of wet processing, SE at frequency 1.5 GHz dropped by 9.5 % to 29.4 dB for the woven sample compared to reference (unwashed) samples, see Fig. 20(a). EM SE remained almost the same for the knitted sample at frequency 1.5 GHz after 20 cycles of washing/ drying, see Fig. 20(b). Wet processing had a lower effect on the EM SE of knitted samples compared to the woven ones (based on regression analysis and t-tests). The following factors were found to be crucial when creating conductive washing resistance fabrics, compared to available conductive fabrics:

- conductive material selection - for example: stainless steel generally does not corrode, rust or stain with water, compared to other metals,
- the type of conductive component selection - all-metal fibers prevent cracking of the conductive layer as in the case of metal-coated fibers or yarns during washing, extremely low fiber diameter declines bending rigidity of metal fibers and prevents fiber breaking in use, as in the case of metal fibers with higher diameter, conductive fiber length similar to non-conductive fiber length helps to prepare compact yarns without fiber migration, while being used,
- yarn production technology - twist generally helps to prevent fiber slippage due to helical configuration of fibers on the yarn surface,

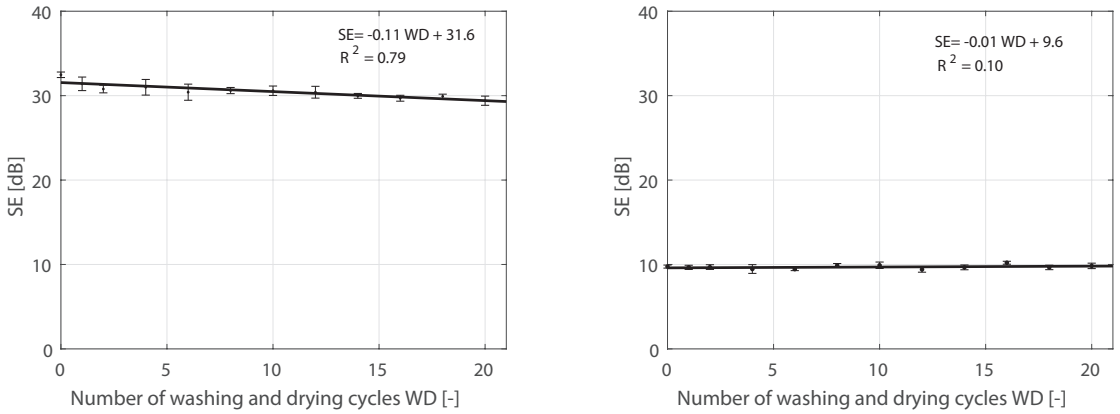

(a) (b)

Figure 20: The dependence of SE on washing and drying cycles (WD) for: (a) woven fabric, (b) knitted fabric containing 15 % of stainless steel fibers.

- fabric construction - for example twill weave is stronger and more durable than the plain weave.

Since the author of this work also focused on the coating of textiles with conductive polymer polypyrrole, the next paragraph will summarize stability findings of polypyrrole-coated fabrics subjected to repeated washing and drying, and abrasion and other utility properties such as air permeability and flammability. The experiments were carried out as part of a master's qualification thesis [48], where *Tunáková* was the supervisor. The aim of the diploma thesis was to verify the service life of the electrically conductive polypyrrole (PPy) coating, which seemed to be critical, based on a survey of the available literature, and to test the possibilities of improving the service life of this coating. The process parameters of the polymerization process were taken from author's previous study [22]. It was possible to achieve an increase in electrical conductivity using chemical deposition of the conductive PPy polymer by in-situ methodology on woven polyester substrate having SE around 14 dB over the entire studied frequency band, see Fig. 21(a). Polypyrrole treated fabrics were subjected to repeated washing and drying, chosen as one of indicators of durability. During the washing and drying cycles, a gentle program for synthetic materials was used for 10 samples, with working temperature of the bath 40 °C and mild detergent. PPy coated samples were washed four times in total. It was found that the life span of conductive polymer coated fabrics is relatively low. Even after the first wash, SE was reduced by more than 50 % of the original value. After applying 4 washing and drying cycles, the SE of the sample was only around 2 dB, see Fig. 21(b). The dependence of SE of the PPy coated fabrics on number of washing and drying cycles can be described using a logarithmically decreasing function. The low durability was also supported by the evaluation of the abrasion of the PPy coated samples in both dry and wet conditions, with the resulting lowest possible degree of durability. It should be mentioned that the air permeability of the samples after the application of conductive polymer decreased significantly (down to 20 % of the original value of the air permeability of the substrate), which was caused by blocking of the pores between the yarns by PPy particles. With the presence of conductive polymer, the burning characteristics of the samples also completely changed. Polyester substrate burned faster, but it was self-extinguishing. When burning, the melt of the polymer was dripping, which was dangerous due to the further spread of the fire. PPy coated fabric burned very slowly and did not tend to self-extinguish, whereas black smoke was emitted at the beginning of burning. In the next step, two selected options for increasing the adhesion between the substrate and

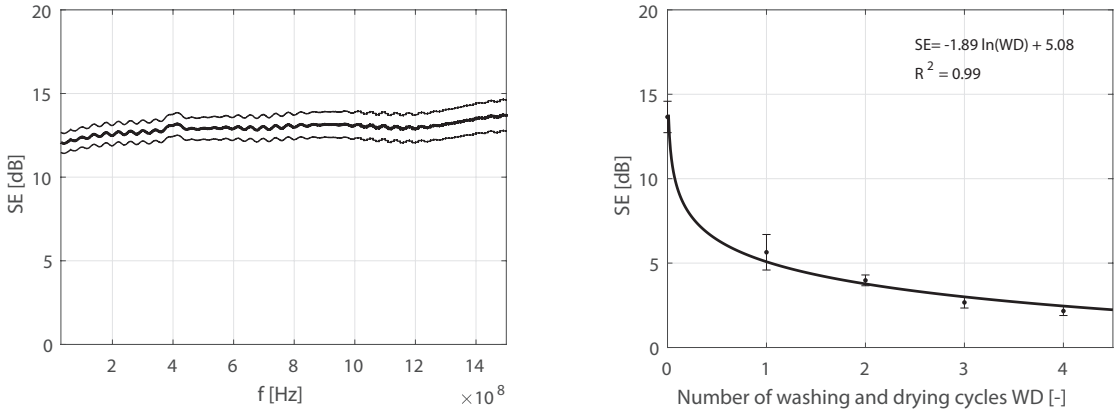

(a) (b)

Figure 21: The dependence of mean values of SE on: (a) frequency - mean values bounded with 95% CI of mean (sample without washing), (b) washing and drying cycles (WD) for PPy coated woven sample.

PPy particles were tested by increase of substrate surface hydrophilicity, using pretreatment by ozone and hydrolysis (in boiling 5 w/v% sodium hydroxide solution). It was found that only sodium hydroxide pretreatment had a statistically significant effect on the hydrophilicity of the polyester substrate. The decrease in SE of PPy coated pretreated samples is slower when repeated washing is applied, however, the initial SE of the pretreated samples is lower (of about 9 dB), in comparison to the samples without any pretreatment. For further experimental work in the field of increasing the electromagnetic shielding efficiency and, at the same time, the life span of the conductive treatment on the surface of the polyester substrate, it is recommended to incorporate surface modification of the substrate using plasma, silanization [49] or modification of the entire polymerization process. The use of combination of reduced graphene oxide (rGO) and PPy seems interesting, having good adhesion between the active material and substrate, where rGO provides a high surface area and stable conductive framework for PPy deposition, whereas PPy is able to boost the charge conduction property of the coated fabric as reported in [50]. Another possibility is the use of lamination or coatings in order to increase the protection of the conductive treatment, taking account of the fact that the protective layer for SE preservation can also be electrically non-conductive.

Table 4 summarizes author's publications (3 journal papers) related to this chapter. The impact factor of the journal, the JIF quartile category and the number of citations of the given paper are displayed.

Table 4: Detailed information about author's publication outputs (journal IF, JIF category quartile and citations given as of 10/3/23) related to this chapter.

Journal Paper	Journal IF	JIF Quartile	Times Cited
[45] **V. Tunakova**, L. Technikova, and J. Militky, "Influence of washing/drying cycles on fundamental properties of metal fiber-containing fabrics designed for electromagnetic shielding purposes," Tex. Res. J., vol. 87, no. 2, pp. 175–192, 2017. DOI: 10.1177/0040517515627168	2.46	Q2	20
[42] **V. Tunakova**, M. Tunak, P. Tesinova, M. Seidlova, and J. Prochazka, "Fashion clothing with electromagnetic radiation protection: aesthetic properties and performance," Text. Res. J., vol. 90, no. 21–22, pp. 2504–2521, 2020. DOI: 10.1177/0040517520923047	2.46	Q2	7
[43] **V. Tunakova**, Z. Hrubosova, M. Tunak, M. Kasparova, and J. Mullerova, "Laser surface modification of electrically conductive fabrics: Material performance improvement and design effects," Opt. Laser Technol., vol. 98, pp. 178–189, 2018. DOI: 10.1016/j.optlastec.2017.07.017	4.94	Q1	6

4 Measurement and modeling of electromagnetic shielding effectiveness

Shielding effectiveness relates to a material's ability to reduce transmission of propagating fields in order to electromagnetically isolate one region from another.

While the SE of metal plates can be estimated based on their physical and geometric characteristics, which can provide a quick and cost-effective way to evaluate the shielding performance of different materials and configurations, this approach is not fully applicable for SE prediction of textile structures having complex shapes or boundary conditions of which the SE must be

often measured. The purpose of any SE test procedure is to quantitatively measure the insertion loss which results from introducing the test sample.

In practice, two test principles are commonly used to measure SE of given flat material made of fibers. It is a measurement that uses shielded space (box, chamber, waveguide, see standard: [51]), and measurement of shielding efficiency using transmission line (coaxial transmission line, transverse electromagnetic cell, see standards: [52, 53]).

Each above-mentioned method has some advantages and limitations. For example, the coaxial transmission line method, according to the ASTM D4935-18 or ASTM ES-7 standard for planar materials using a plane-wave is the preferred method. The measurement set-up consists of two coaxial adapters (sample holders) and a network analyzer, while signals from the source to the receiver are transmitted via coaxial cables. The principle of the design of flanged coaxial line sample holder is based on transmission line theory. "For the coaxial transmission line, the principal mode of propagation is the transverse electromagnetic (TEM) wave" [54]. The material under the test is inserted between the parts of the holder, and it is exposed to electric fields in all directions over the full 360° within the coaxial holder. The flanges are fastened together by means of insulating screws to avoid direct electrical contact between the two parts of the holder. In this way, the sample gets compressed when inserted between two flanges of the holder, which is more significant for nonwoven textiles. The measurements can be made at a specific frequency range (from 30 MHz to 1.5 GHz). "The results obtained in different laboratories are comparable" as described in [53]. Generally, ring shaped sample together with reference sample is needed, that is why the preparation of samples is quite time-consuming. Measurement uncertainty should fall within ± 5 dB [55]. Besides that, the mass of the ASTM D 4935-10 tester holder is about 18 kg, and therefore the manipulation during assembly and disassembly is not entirely easy.

"The shielded box (enclosure) method is frequently used for comparative measurements of test samples made of different shield materials" [56]. Using this methodology, the sample is inserted to the open area of one wall of the box, whereas the receiving antenna is inside. The electromagnetic field is generated outside the box and the intensity of signals is compared. The drawback of this method is that the frequency range is limited by 500 MHz [56]. The shielded room method avoids this disadvantage, but at the cost of significantly larger sample size.

Therefore, there is a need for the development of an experimental method for the fast determination of the electromagnetic shielding effectiveness of textile samples of several centimeters in size, and without the necessity of special preparation of test samples. In a paper [57] *Tunáková et al.* presented new measurement method and equipment which is based on a waveguide principle. It is similar to the arrangement with the shielded box method, but it is easier to handle. The main advantages are: a small required sample, of the size of only a few tens of cm^2, no necessity for sample preparation of special shapes or dimensions, rapid measurements, and simple and cheap equipment. However, it also has certain limitations; equipment (waveguide) with specific parameters is required for a particular narrow frequency range. The proposed method is designated especially for rapid comparative measurements of newly fabricated samples of relatively small size.

Basic part of the device is a rectangular hollow waveguide with conducting walls. A receiving wire (antenna) is placed inside of this waveguide, while a textile sample is placed at the entrance to the waveguide. The end of the waveguide is filled with foam saturated with carbon particles, absorbing the electromagnetic field which passed through the sample. The fabric sample is oriented perpendicularly to the electromagnetic waves. Transmitting antenna is placed in front of the waveguide input. Simulation of electromagnetic wave entering the waveguide and electric field inside the waveguide is shown in Figure 22(a). A progressive wave passing from the entrance to the end is excited outside the waveguide. The electromagnetic field distribution within the wave guide is known, considering the lengths of the inner sides of waveguide, and considering the

frequency. It is possible to measure S-parameters (scattering parameters describing the input-output relationship between ports in an electrical system) with a vector analyzer, by which it is possible to determine transmitted and reflected electromagnetic waves. The main advantage of this approach is great shielding of the surrounding man-made noise. On the other hand, for a particular narrow frequency range, a waveguide with specific dimensions is required. It is assumed that the lengths a,b of the inner sides satisfy $b \leq a$, as shown in Figure 22(b). The waveguide is filled with air (relative magnetic permeability $\mu_r \approx 1$ and relative permittivity $\varepsilon_r \approx 1$). Due to Maxwell's equations, the fields within the waveguide always have a specific form, called modes. The dimensions of a hollow metallic waveguide determine which wavelengths it can support, and in which modes. Typically, the waveguide is operated only with a single mode. Generally, it is selected the possible mode of the lowest order. Frequencies below the waveguide's cutoff frequency will not propagate. For example, the dimensions of the waveguide, in which TE_{10} mode will be excited, for example for source frequency 1.8 GHz (frequency of GSM mobile used in most parts of the world: Europe, Middle East, Africa, Australia, Oceania and most of Asia is 1.8 GHz), the dimensions were determined as: $a = 120$ mm, $b = 60$ mm with corresponding cutoff frequency $f_c = 1.25$ GHz. Dimensions of a waveguide for source frequency 2.45 GHz (frequency of microwave oven, wi-fi broadcast), were determined as: $a = 90$ mm, $b = 45$ mm having cutoff frequency $f_c = 1.67$ GHz, whereas the f_c has to be lower than source frequency. More information can be found in [57]. The usability of the proposed method was confirmed by a two-sample t-test performed on nine samples differing in their electrical conductivity. Concerning the intermediately conducting samples, the measured SE using both the ASTM D4935 method and the new waveguide method, were in good agreement, with only a small shift of results considered, and therefore a correction model was proposed. It was found that the waveguide method is not appropriate for samples with high conductivity (conductivity higher than 6E-03 S.m^1), where reflection predominates. The new waveguide method embodies higher variability of measured SE values, compared to the ASTM D4935 method, although the total variability of the waveguide method is satisfactory (lower than 30 %). The proposed method is suitable for SE testing of different types of textile, polymeric materials, or special composites, where only small samples are accessible and quick testing is required. Aside from the operational reasons and purchase costs, the ASTM D4935 method remains one of the most useful methods for evaluating electromagnetic shielding effectiveness of textile samples with satisfactory repeatability and reproducibility.

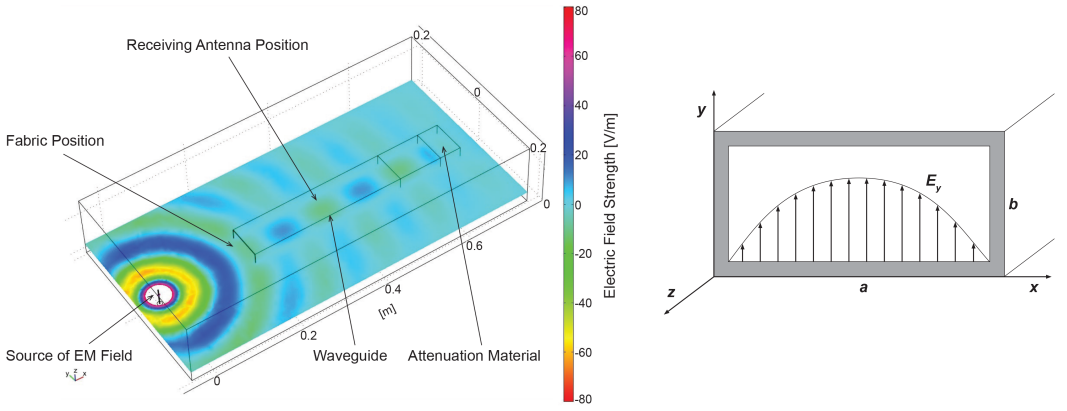

(a) (b)

Figure 22: (a) Simulation of electromagnetic wave entering the waveguide, (b) electric field inside the waveguide.

It should be concluded that the results measured by different methods for electromagnetic shielding effectiveness may not always be directly comparable, as different methods may have different measurement conditions, assumptions, and limitations. Therefore, it is important to carefully consider the advantages and limitations of each method, and to select the most appropriate method for the specific application. More information about comparison of measurement of textile sample by different methods can be found in *Tunáková* Ph.D. thesis [58].

Recently, an increasing amount of attention has been paid to the effective evaluation of the SE using non-experimental methods, which can be divided into two main categories. The disadvantages of the first category involves full-wave solvers based on numerical methods, such as the finite-difference time domain, the method of moments, the transmission line matrix, and various hybrid methods [59–61]. The disadvantage of these methods lies in the complexity of the associated computing resources and computer memory. The second non-experimental category involves analytical methods used for the rapid computation of the SE for certain structures in widespread use, such as rectangular enclosures.

With respect to textile-structure-based shielding materials, a limited number of scientific papers have dealt with the attendant SE simulation or prediction. For example, in a paper [62], the authors formed a three-ply continuous CF woven (satin weave) reinforced composite, and simulated the SE using the plane-wave shielding theory. However, the simulated SE results were not in good agreement with the experimentally-measured SE. In a paper [63], the electromagnetic characteristics of a frequency-selective fabric composite (plain weave of continuous CF with square elements with an 8 mm aperture) were simulated, using CST Microwave Studio 5.1 software, and the data related to the electrical conductivity, fiber undulation, and aperture-to-cell ratio of carbon rovings. The results were in excellent agreement with the experimentally-measured data. In a paper [64], the CST Microwave Studio software was also used for SE simulation, with the results again demonstrating good agreement with the experimental results, especially with the thin compact carbon woven/epoxy samples. The SE of hybrid fabrics containing different contents of staple stainless-steel fibers was predicted in a paper authored by *Tunáková et al.* [65], based on the assumption that the total SE of fabric is a linear combination of the SE, due to apertures (SE_{aper}) at high frequencies and the SE of compact materials at low frequencies (SE_{fabric}). Here, all equations were taken out of the published literature, with good agreement obtained only for samples with lower electric conductivity, and apertures of smaller dimensions. Reference [66] includes a detailed derivation of SE for SE_{fabric} and SE_{aper}, with a general equation of SE tested on woven fabrics made of blended yarns with high conductivity ($\sigma > 244$ S/m). Calculated SE was compared with the experimental data with absolute agreement. However, the derived calculations were somewhat complicated.

In a paper [26], *Tunáková et al.* presented a simple analytical model to predict the SE of carbon-fiber reinforcements in plain weave intended for the preparation of electromagnetic shielding epoxy composites. Given that the geometry of a bonded-junction wire-mesh screen is highly similar to that of low-density woven fabrics made of electrically conductive threads, a simple analytical computation method [9] was adopted and used to predict the SE based on the knowledge of only a few parameters, i.e., the geometrical properties of the woven fabric (length of aperture and diameter of multifil) and the electrical conductivity of the carbon multifil.

Assuming that the aperture dimensions are small, relative to the wavelength, the SE of a planar mesh screen with bonded junctions can be described, using the equivalent sheet impedance of the mesh [67]. The total shielding effectiveness (in dB) can be calculated based on the electrical conductivity and radius of the wire, the length of the aperture, and the angle of the incidence as follows [9]:

$$SE_{tot}(\omega, \theta) = 10\log\{|T_1(\omega, \theta)|^2 + |T_2(\omega, \theta)|^2\}, \tag{11}$$

where ω is the angular frequency ($\omega = 2\pi f$), f [Hz] is the frequency, and $T_1(\omega, \theta)$ and $T_2(\omega, \theta)$

are the transmission coefficients for the polarization of the transverse electric and transverse magnetic modes, respectively, which can be calculated using the following equations [9]:

$$T_1(\omega,\theta) = \frac{\frac{2Z_{S1}(\omega)}{Z_0}\,cos\theta}{1+\frac{2Z_{S1}(\omega)}{Z_0}\,cos\theta}, \tag{12}$$

$$T_2(\omega,\theta) = \frac{\frac{2Z_{S2}(\omega)}{Z_0}}{cos\theta+\frac{2Z_{S2}(\omega)}{Z_0}}, \tag{13}$$

where Z_0 is the free-space impedance ($Z_0 = 376.73\ \Omega$), and Z_{S1} and Z_{S2} are the eigenvalues of the mesh impedance operator, which are given as follows [9]:

$$Z_{S1}(\omega) = Z_\omega a + j\omega L, \tag{14}$$

$$Z_{S2}(\omega) = Z_{S1} - \frac{j\omega L}{2} sin^2\theta, \tag{15}$$

where a [m] is the length of a square aperture, Z_ω is the wire impedance per unit length (approximated by its DC electrical resistance per unit length), and L is the sheet inductance. These variables can be calculated as follows [9]:

$$L = \frac{\mu_0 a}{2\pi} ln\{(1-e^{-2\pi r/a})^{-1}\}, \tag{16}$$

$$Z_\omega = (\pi r^2 \sigma)^{-1}, \tag{17}$$

where μ_0 is the vacuum permeability ($\mu_0 = 1.256\ 10^6$ H/m), r [m] is the wire radius, and σ [S/m] is the electrical conductivity.

The polarization-independent SE for sample 1 from [26] (using Equation 11) is shown in Figure 23(a). The results indicated that this simple analytical model for determining the SE

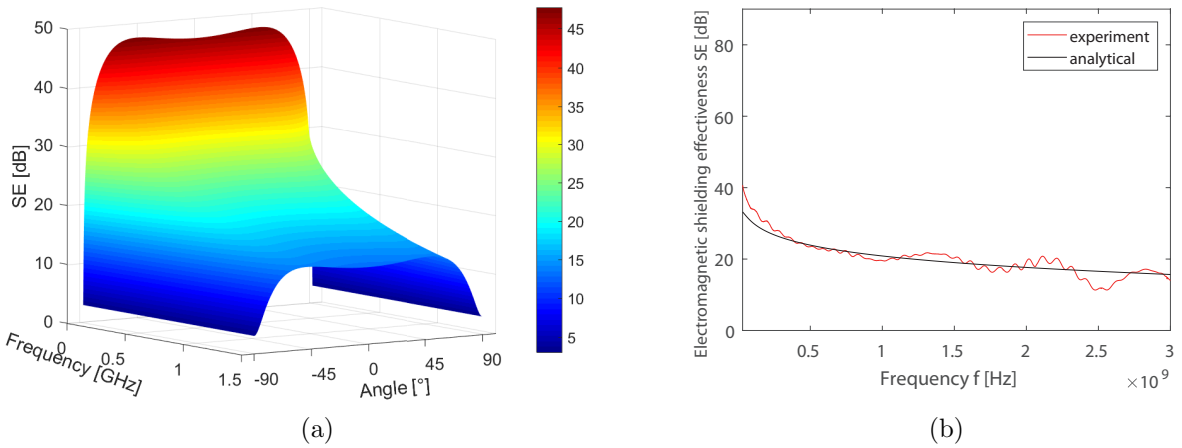

(a) (b)

Figure 23: (a) SE as a function of frequency and incidence angle for sample no. 1 [26], (b) dependence of SE on frequency for the experimental (measured by ASTM D4935) and analytical data for sample no. 4 [26].

works well for highly porous woven reinforcements made of carbon roving, for given frequency bands, and it is in good agreement with the experimental measurement of SE using the ASTM D4935 standard method, see comparison of measured and analytical data for sample no. 4 [26] in Figure 23(b). The mean absolute error between the measured and modeled data was less than the random error of the method used to measure the SE. In addition, it was found that averaging all the angles of incidence presents a good solution for randomization in the coaxial transmission line measurement method for SE. It can also be stated that the tested simulation could be suitable for predicting the SE with other textile structures, especially woven fabrics made from electrically conductive yarns, forming both the warp and weft system, while the high porosity may be a limiting factor.

Table 5 summarizes author's publications (2 journal papers (one of which was already mentioned in Chapter 2)) related to this chapter. The impact factor of the journal, the JIF quartile category and the number of citations of the given paper are displayed.

Table 5: Detailed information about author's publication outputs (journal IF, JIF category quartile and citations given as of 10/3/23) related to this chapter.

Journal Paper	Journal IF	JIF Quartile	Times Cited
[63] **V. Safarova**, M. Tunak, and J. Militky, "Prediction of hybrid woven fabric electromagnetic shielding effectiveness," Textile Research Journal, vol. 85, no. 7, pp. 673–686, 2015. DOI: 10.1177/0040517514555802	2.46	Q2	24
[25] **V. Tunakova** and M. Tunak, "Carbon-fiber reinforcements for epoxy composites with electromagnetic radiation protection—prediction of electromagnetic shielding ability," Composites Science and Technology, vol. 215, p. 109029, 2021. DOI: 10.1016/j.compscitech.2021.109029	9.88	Q1	6

5 Applications

Electromagnetic shielding fabric is a type of material that is designed to block or reduce the electromagnetic radiation that can be emitted by electronic devices. These fabrics are made from a variety of materials, including copper, nickel, silver, and other conductive metals or other electrically conductive materials, as summarized in Chapter 2.

Therefore they have many possible applications such as in radiofrequency protective suits, tents, curtains or tapestry, protection of people, equipment and sensitive electronic devices from the harmful effects of electromagnetic radiation. These textiles, due to their increased electrical conductivity, can also be used for production of smart clothing with incorporated conductive paths (when sufficient electrical conductivity achieved), electrostatic dissipative materials for clothing or equipment, clean room working clothes, etc.

One of the most common applications of electromagnetic shielding fabric is in the construction of protective clothing for workers who are exposed to high levels of electromagnetic radiation. This includes workers in the electronics industry, as well as those who work with medical equipment such as magnetic resonance machines. Protective clothing is in general defined according to [41] as "any device or appliance designed to be worn or held by an individual for protection against one or more health and safety hazards." The fabric can be used to make protective suits, gloves, and other clothing items that shield the wearer from the harmful effects of radiation. For example, authors of paper [68] introduced a protective clothing against

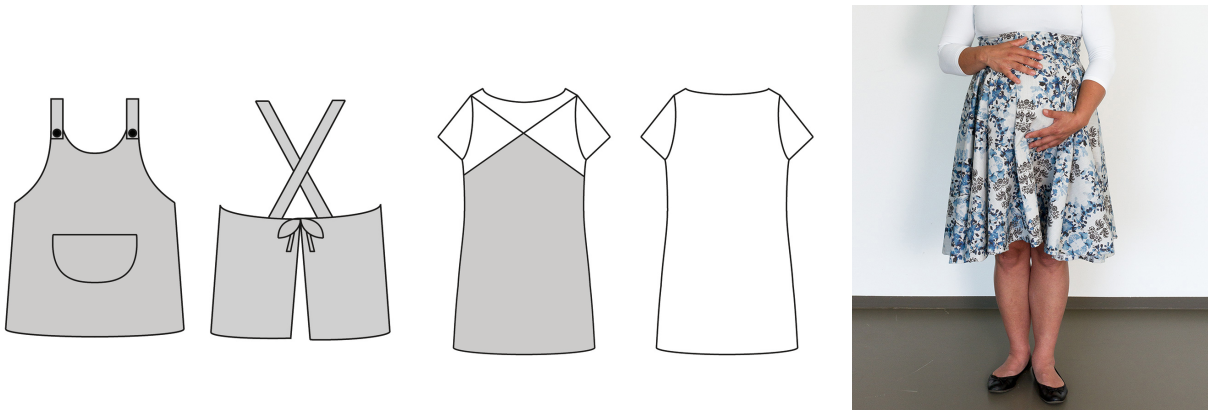

(a) (b) (c)

Figure 24: (a,b) Schematic illustration (the gray color indicates the use of electromagnetic shielding fabric), (c) photo of the design of radio-frequency protective clothing [44].

high-frequency EM fields based on synthetic yarns with the addition of silver nanoparticles. The main advantage of this solution is the reduction in the weight of the garment, using nanoparticles instead of metal wires. The suit, described in a paper [69], originally developed to provide personnel protection in large electric-field gradients near overhead high-voltage 50/60 Hz power transmission lines, was claimed to provide whole-body protection for radio-frequency workers. In particular, these special fabrics can also be applicable for casual wear intended for specific groups of people, which include people having a pacemaker, people who are increasingly susceptible to EM radiation, pregnant women or young children. When designing any clothing system, the specific requirements for aesthetics, functionality, thermophysiological comfort (including mobility), and durability should be considered; functionality (protection) together with thermophysiological comfort properties is the fundamental requirement for any protective clothing [41]. For that reason *Tunáková* at al. [44] presented a study, in which electrically conductive woven fabric was modified by digital printing, and in which the essential requirements for designing the EM radiation protective clothing for daily use were studied, whereas it was summarized that the presented fabric (raw or printed) does not have significantly different comfort properties, compared to common textile fabrics, which makes it possible for its application as fabric in clothing design, see the schematic illustration of the design of radio-frequency protective clothing and the photo of functional clothing, for example for pregnant woman, in Figure 24. The described technical solution was protected by a utility model [70].

Another application of electromagnetic shielding fabric is in the construction of shielding enclosures for electronic devices. These enclosures are designed to block electromagnetic interference and protect sensitive electronic components from damage. They are commonly used in the telecommunication industry to protect cell towers, satellite equipment, and other sensitive electronic devices from interference. Electrically shielding textiles or fiber-based composite structures are used especially where there is a requirement for low weight, flexibility and/or also for air and water vapor permeability. *Tunáková* consulted a master's thesis [71], which dealt with the development and testing of textile-based shielding cover intended for a protection of sensitive devices, see Figure 25. The cover was tested in the EMC laboratory by the aspects of disruptive signals with respect to the shielded device, and to the surroundings of the shielded device as well.

Electromagnetically shielding textiles could also offer a practical solution to protecting personal data, because Radio frequency identification (RFID) technology is used widely in many industries for identification, tracking, and inventory management purposes. The data transmit-

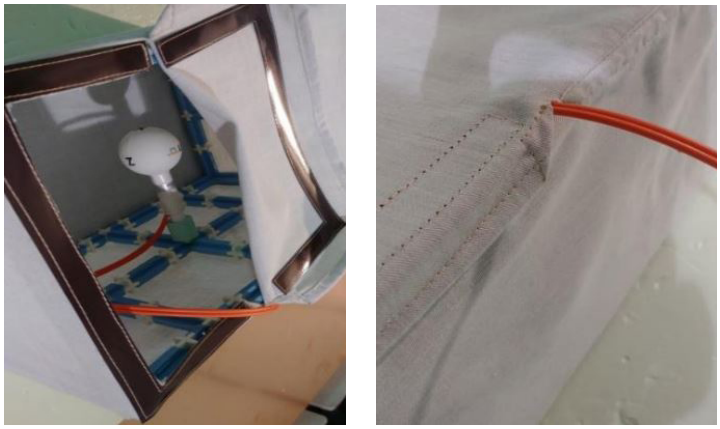

(a) (b)

Figure 25: Photo documentation of the shielding cover developed and tested in the diploma thesis [71]: (a) service opening solution, (b) wiring outlet.

ted by RFID tags can be intercepted and read by unauthorized parties, leading to potential security breaches. Electromagnetically shielding textiles are an effective solution to protect data by creating a Faraday cage around the object or person wearing them. A Faraday cage is an enclosure made of conductive material that blocks electromagnetic waves, including radio frequency signals. *Tunáková et al.* [72]designed a lightweight data protective cover for a credit card, where flat and smooth composite non-woven fabric, made of synthetic fibers surface coated by metal, represents the main functional part. The textile created in this way can be attached to other textile layers or between textile layers, using common textile techniques, typically using gluing or polymer interlayers, or lamination using a flexible matrix, etc. The composite nonwoven has very high air and water vapor permeability and very low bending rigidity and thickness. The described technical solution is protected by a utility model [72]. Another example of usage of highly electrically conductive fabrics represents the car theft protection by shielding RFID signals from keyless go systems. In the bachelor's thesis [73] (for which *Tunáková* was a consultant) the main goal was to propose a suitable technical solution against the threat of misuse of electronic car keys that are equipped with KESSY technology.

Electromagnetic shielding fabric is also used in the automotive or avionic industry to protect electronic components from electromagnetic interference. Modern cars contain a large number of electronic devices, and these devices can be sensitive to electromagnetic radiation. Shielding fabric can be used to protect these devices from interference and prevent malfunctions. Also in the aerospace and defense industries, electromagnetic interference can disrupt the communication systems of airplanes and spacecraft. The use of electromagnetically shielding textiles in the construction of these vehicles can prevent such interference and ensure their safe operation. For this particular use can be advantageously used porous, low thickness carbon-fiber reinforced composites with excellent flexibility and superior electromagnetic radiation protection developed by *Tunáková et al.* [74]. A quality index evaluation approach using weighted and normalized data was implemented to choose a composite with properties that best fit their intended use. The highest quality index was achieved by the composite containing plain-woven reinforcement with warp and weft sett 18 dm^1, using carbon tape 2 mm wide. This composite provides electromagnetic shielding 36 dB at 1.5 GHz, having high air permeability 1000 mm/s, relatively low bending rigidity of around 2.5 Nmm, and thickness of only 0.37 mm.

In addition, electromagnetic shielding fabrics or composites can be used in the construction of buildings to protect them against electromagnetic radiation. This is particularly important in areas where there are high levels of electromagnetic radiation, such as areas near power lines or

cell phone towers. Shielding fabric can be used to line walls and ceilings, creating a shield that blocks radiation from entering the building. As an example can be mentioned [75] the research in which *Tunáková*, as a co-author, investigated the effect of carbon fiber content of plaster-based composites on SE and mechanical properties. It can be concluded that that sample (t = 10 mm) containing 2 % of carbon fiber (d = 1.8 µm, l = 8 mm) in cement matrix reaches SE about 50 dB at f = 1.5 GHz. At the same time, this type of composite showed interesting mechanical properties.

Last but not least, it should be mentioned that the ability of the fabric shield of the electromagnetic field could be used for wireless strain sensing, because it was found out, that highly electrically conductive and at the same time highly deformable knitted fabrics, show change in electrical conductivity and the related ability to shield the electromagnetic field under the tensile stress. This behavior of knitted fabrics was studied while working on dissertation thesis [76] under the supervision of *Tunáková*. Some of the results based on this thesis have been already published [77].

Table 6 summarizes author's publications (4 journal papers (one of which was already mentioned in Chapter 2) and 2 utility models) related to this chapter. The impact factor of the journal, the JIF quartile category and the number of citations of the given paper are displayed.

Table 6: Detailed information about author's publication outputs (journal IF, JIF category quartile and citations given as of 10/3/23) related to this chapter.

Journal Paper	Journal IF	JIF Quartile	Times Cited
[42] **V. Tunakova**, M. Tunak, P. Tesinova, M. Seidlova, and J. Prochazka, "Fashion clothing with electromagnetic radiation protection: aesthetic properties and performance," vol. 90, no. 21, pp. 2504–2521, 2020. DOI: 10.1177/0040517520923047	2.46	Q2	7
[68] **V. Tunakova**, "Protective clothing against radiofrequency electromagnetic radiation or a part of clothing against radiofrequency electromagnetic radiation," CZ Utility Model, 30754, 2017. UPV	-	-	-
[70] J. Militky, **V. Tunakova**, Z. Hrubosova, and J. Vecernik, "A textile for the protection of electronic information carriers," CZ Utility Model, 31290, 2017. UPV	-	-	-
[72] **V. Tunakova**, M. Tunak, and J. Novotna, "Porous, low thickness carbon-fiber reinforced epoxy composites with excellent flexibility and superior electromagnetic radiation protection," Journal of Industrial Textiles, vol. 53, p. 15280837231159867, 2023. DOI: 10.1177/15280837231159867	2.93	Q1	0
[73] A. Samkova, P. Kulhavy, **V. Tunakova**, and M. Petru, "Improving electromagnetic shielding ability of plaster-based composites by addition of carbon fibers," Advances in Materials Science and Engineering, vol. 2018, p. 3758364. DOI: 10.1155/2018/3758364	2.10	Q3	4
[75] S. Palanisamy, **V. Tunakova**, M. Tunak, and J. Militky, "Textile-based weft knit strain sensor: Experimental investigation of the effect of stretching on electrical conductivity and electromagnetic shielding," Journal of Industrial Textiles, vol. 52, 2022. DOI: 10.1177/15280837221142825	2.93	Q1	0

6 Conclusion

This habilitation thesis is conceived as a summary of published scientific and professional works, in which the author of this thesis is the main author or co-author, to demonstrate the contribution of the author to the field of textile technology and materials science. In order to emphasize the topicality of the studied topic, the novelty, and the motivation of the author for research activities, the work is supplemented with citations from other research works that have been published in the given area. For this purpose, 18 articles published in journals with an impact factor, 1 conference paper indexed in the Scopus database, and 2 technical solutions protected by a utility model, were selected. Ten selected papers with the highest citation response are listed in the appendices of this habilitation thesis.

The contents of the habilitation thesis include a summary of different methods for development of textiles with increased electrical conductivity and increased electromagnetic shielding ability. The influence of various parameters which, in addition to the material composition, that also affect the functionality of electromagnetic shielding fabrics, is also mentioned. One of the chapters is further devoted to the properties of special textiles in connection with their practical use, and options of designing these special fabrics. Measurement methods of SE together with the possibilities of SE modeling are also discussed. At the end of the work is presented a brief description of applications of textiles that are able to shield electromagnetic field.

Electromagnetic shielding textiles and composites with textile reinforcement are still important in various applications, from aerospace and defense to consumer electronics and medical devices. These materials are designed to protect sensitive electronic equipment from electromagnetic interference, which can cause malfunctions, data loss, or even system failure. They can also shield people from exposure to electromagnetic radiation.

Research in this field is essential, in order to develop new and improved materials that provide effective electromagnetic shielding and also meet other requirements such as durability, flexibility, or air and water vapor permeability. The properties of these materials depend on various factors, including the type of fiber, weave or knit structure, thickness, and coating or laminating treatments. Therefore, exploration of different combinations of these variables and optimization of the design for specific applications is needed. Furthermore, development of new approaches to incorporate multiple functionalities into a single material, or to combine different materials in a layered or hybrid structure, can be also required.

In addition to the material development, research in the field of electromagnetic shielding textiles and composites also involves the development of measurement methods and modeling techniques, to assess the shielding effectiveness of different structures under various conditions. These methods may involve experimental tests in controlled environments, numerical simulations using electromagnetic field solvers, or statistical analysis of large datasets. These methods can help researchers to understand the underlying mechanisms of electromagnetic shielding, and to optimize the design of shielding materials for various applications.

Further examination of hybrid layered composites, considering different SE mechanisms (reflection, absorption); usage of nanostructures with an emphasis on the percolation threshold of conductive component on SE; or a deeper study of the effect of fabric construction parameters on SE, could develop an insight into fiber structures for electromagnetic radiation shielding.

Declaration

I would like to take this opportunity to thank all the co-authors of the papers I have presented as part of the habilitation thesis. I honestly declare that in all cases my share in preparation, implementation, and interpretation of the results was greater than or equal to that of all other co-authors.

References

[1] H. Ott, *Electromagnetic Compatibility Engineering*. Wiley, 2009.

[2] S. A. Mirmohammadi, S. Sadjadi, and N. Bahri-Laleh, "10 - Electrical and electromagnetic properties of cnt/polymer composites," in *Carbon Nanotube-Reinforced Polymers* (R. Rafiee, ed.), Micro and Nano Technologies, pp. 233–258, Elsevier, 2018.

[3] A. L. Caro, "Modelling of textile reinforced composite barriers against electromagnetic radiation," Ph.D. thesis, Universitat Politecnica de Calalunya, 2011.

[4] S. Palanisamy, V. Tunakova, J. Militky, and J. Wiener, "Effect of moisture content on the electromagnetic shielding ability of non-conductive textile structures," *Scientific Reports*, vol. 11, no. 1, p. 11032, 2021. DOI: 10.1177/0040517514521118.

[5] A. Asghar, M. Ahmad, M. Yahya, M. Ali, A. A. Aziz, N. A. Rahman, S. Z. U. Hassan, and M. Kashif, "An alternative approach to design conductive hybrid cover yarns for efficient electromagnetic shielding fabrics," *Journal of Industrial Textiles*, vol. 48, no. 1, pp. 38–57, 2018.

[6] A. O. Kizilçay, E. Delihasanlar, F. G. K. Abdulla, and A. H. Yuzer, "Electromagnetic shielding characterization of conductive knitted fabrics," *Progress in Electromagnetics Research*, vol. 56, pp. 33–41, 2017.

[7] K. Marciniak, K. E. Grabowska, Z. Stempien, I. L. Ciesielska-Wróbel, A. Rutkowska, and D. Taranek, "Woven fabrics containing hybrid yarns for shielding electromagnetic radiation," *Fibres & Textiles in Eastern Europe*, vol. 24, no. 6, pp. 109–115, 2016.

[8] V. Tunakova, M. Tunak, V. Bajzik, L. Ocheretna, S. Arabuli, O. Kyzymchuk, and V. Vlasenko, "Hybrid knitted fabric for electromagnetic radiation shielding," *Journal of Engineered Fibers and Fabrics*, vol. 15, 2020. DOI: 10.1177/1558925020925397.

[9] D. Mansson and A. Ellgardt, "Comparing analytical and numerical calculations of shielding effectiveness of planar metallic meshes with measurements in cascaded reverberation chambers," *Progress In Electromagnetics Research C*, vol. 31, pp. 123–135, 2012.

[10] J. Eichhoff, A. Hehl, S. Jockenhoevel, and T. Gries, "7 - Textile fabrication technologies for embedding electronic functions into fibres, yarns and fabrics," in *Multidisciplinary Know-How for Smart-Textiles Developers*, pp. 191–226, Woodhead Publishing, 2013.

[11] V. Safarova and J. Militky, "Multifunctional metal composite textile shields against electromagnetic radiation - effect of various parameters on electromagnetic shielding effectiveness," *Polymer Composites*, vol. 38, no. 2, pp. 309–323, 2017. DOI: 10.1002/pc.23588.

[12] I. Elhawary, "Chapter 9 - fibre to yarn: Staple-yarn spinning," in *Textiles and Fashion*, pp. 191–212, Woodhead Publishing, 2015.

[13] S. Varnaite and J. Katunskis, "Influence of washing on the electric charge decay of fabrics with conductive yarns," *Fibres & Textiles in Eastern Europe*, vol. 17, no. 5, pp. 69–75, 2009.

[14] O. Kayacan, "The effect of washing processes on the electromagnetic shielding of knitted fabrics," *Textile and Apparel*, vol. 24, pp. 356 – 362, 2014.

[15] C.-I. Su and J.-T. Chern, "Effect of stainless steel-containing fabrics on electromagnetic shielding effectiveness," *Textile Research Journal*, vol. 74, no. 1, pp. 51–54, 2004.

[16] V. Safarova and J. Militky, "Electromagnetic shielding properties of woven fabrics made from high-performance fibers," *Textile Research Journal*, vol. 84, no. 12, pp. 1255–1267, 2014. DOI: 10.1177/0040517514521118.

[17] V. Safarova, K. Malachova, and J. Militky, "Electromechanical analysis of textile structures designed for wearable sensors," in *Proceedings of the 2014 16th International Conference on Mechatronics (mechatronika 2014)*, pp. 416–422, IEEE, 2014. DOI: 10.1109/MECHATRONIKA.2014.7018294.

[18] A. Ali, V. Baheti, J. Militky, Z. Khan, V. Tunakova, and S. Naeem, "Copper coated multifunctional cotton fabrics," *Journal of Industrial Textiles*, vol. 48, no. 2, pp. 448–464, 2018. DOI: 10.1177/1528083717732076.

[19] S. Palanisamy, V. Tunakova, S. Hu, T. Yang, D. Kremenakova, M. Venkataraman, M. Petru, and J. Militky, "Electromagnetic interference shielding of metal coated ultrathin nonwoven fabrics and their factorial design," *Polymers*, vol. 13, no. 4, p. 484, 2021. DOI: 10.3390/polym13040484.

[20] K. Malachova, "Modification of textile surfaces by electroless plating," Master's thesis, Technical University of Liberec, Czech Republic, 2017.

[21] R. Cherrington and J. Liang, "2 - Materials and deposition processes for multifunctionality," in *Design and Manufacture of Plastic Components for Multifunctionality*, pp. 19–51, Oxford: William Andrew Publishing, 2016.

[22] V. Tunakova, J. Gregr, M. Tunak, and G. Dohnal, "Functional polyester fabric/polypyrrole polymer composites for electromagnetic shielding: Optimization of process parameters," *Journal of Industrial Textiles*, vol. 47, no. 5, pp. 686–711, 2018. DOI: 10.1177/1528083716667262.

[23] Committee for Conformity Assessment on Accreditation and Certification of Functional and Technical Textiles, "Specified requirements of electromagnetic shielding textiles." https://www.ftts.org.tw/images/fa003E.pdf.

[24] P. Morgan, *Carbon Fibers and Their Composites*. Materials Engineering, Taylor & Francis, 2005.

[25] J. Donnet and R. Bansal, *Carbon Fibers*. CRC Press, 1998.

[26] V. Tunakova and M. Tunak, "Carbon-fiber reinforcements for epoxy composites with electromagnetic radiation protection—prediction of electromagnetic shielding ability," *Composites Science and Technology*, vol. 215, p. 109029, 2021. DOI: 10.1016/j.compscitech.2021.109029.

[27] M. A. Nahil and P. T. Williams, "Activated carbons from acrylic textile waste," *Journal of Analytical and Applied Pyrolysis*, vol. 89, no. 1, pp. 51–59, 2010.

[28] D. Czajczyńska, L. Anguilano, H. Ghazal, R. Krzyżyńska, A. Reynolds, N. Spencer, and H. Jouhara, "Potential of pyrolysis processes in the waste management sector," *Thermal Science and Engineering Progress*, vol. 3, pp. 171–197, 2017.

[29] S. Naeem, V. Baheti, V. Tunakova, J. Militky, D. Karthik, and B. Tomkova, "Development of porous and electrically conductive activated carbon web for effective EMI shielding applications," *Carbon*, vol. 111, pp. 439–447, 2017. DOI: 10.1016/j.carbon.2016.10.026.

[30] A. Petrikova, "Solving the issue of electromagnetic radiation shielding," Master's thesis, Technical University of Liberec, Czech Republic, 2012.

[31] F. Safdar, M. Ashraf, A. Javid, and K. Iqbal, "Polymeric textile-based electromagnetic interference shielding materials, their synthesis, mechanism and applications – A review," *Journal of Industrial Textiles*, 2021. Article in Press.

[32] M. S. Ozen, E. Sancak, A. Beyit, I. Usta, and M. Akalin, "Investigation of electromagnetic shielding properties of needle-punched nonwoven fabrics with stainless steel and polyester fiber," *Textile Research Journal*, vol. 83, no. 8, pp. 849–858, 2013.

[33] R. Perumalraj and B. Dasaradan, "Electromagnetic shielding effectiveness of doubled copper-cotton yarn woven materials," *Fibres & Textiles in Eastern Europe*, vol. 18, no. 3, p. 80, 2010.

[34] A. Bedeloglu, "Investigation of electrical, electromagnetic shielding, and usage properties of woven fabrics made from different hybrid yarns containing stainless steel wires," *The Journal of The Textile Institute*, vol. 104, no. 12, pp. 1359–1373, 2013.

[35] Z. Liu and X. Wang, "Influence of fabric weave type on the effectiveness of electromagnetic shielding woven fabric," *Journal of Electromagnetic Waves and Applications*, vol. 26, no. 14-15, pp. 1848–1856, 2012.

[36] J. Krishnasamy, A. Ramasamy, A. Das, and A. Basu, "Effect of fabric cover and pore area distribution of carbon/stainless steel/polypropylene hybrid yarn-woven fabric on electromagnetic shielding effectiveness," *Journal of Electronic Materials*, vol. 45, no. 6, pp. 3087–3100, 2016.

[37] A. Das, J. Krishnasamy, R. Alagirusamy, and A. Basu, "Electromagnetic interference shielding effectiveness of ss/pet hybrid yarn incorporated woven fabrics," *Fibers and Polymers*, vol. 15, no. 1, pp. 169–174, 2014.

[38] N. Erdumlu and C. Saricam, "Electromagnetic shielding effectiveness of woven fabrics containing cotton/metal-wrapped hybrid yarns," *Journal of Industrial Textiles*, vol. 46, no. 4, pp. 1084–1103, 2016.

[39] B. K. Sirkova, V. Tunakova, M. Tunak, and K. Jezik, "Influence of woven fabric construction parameters on electromagnetic shielding effectiveness: Part I – weave influence," *Textile Research Journal*, vol. 92, no. 21-22, pp. 4020–4040, 2022. DOI: 10.1177/00405175221100390.

[40] S. Palanisamy, V. Tunakova, and J. Militky, "Fiber-based structures for electromagnetic shielding - comparison of different materials and textile structures," *Textile Research Journal*, vol. 88, no. 17, pp. 1992–2012, 2021. DOI: 10.1177/0040517517715085.

[41] N. Mao, "3 - High performance textiles for protective clothing," in *High Performance Textiles and their Applications*, pp. 91–143, Woodhead Publishing, 2014.

[42] S. Hui, W. Jianping, C. Xiaona, and W. Yanzhen, "Research on electromagnetic shielding clothing," in *Proceedings of 2011 Cross Strait Quad-Regional Radio Science and Wireless Technology Conference*, IEEE, 2011.

[43] S. K. Bahadir, S. Jevsnik, D. Fakin, and U. K. Sahin, "Color and electrical resistance evaluation of cotton fabrics composed of stainless steel yarns treated with direct and reactive dyes," *Textile Research Journal*, vol. 86, no. 13, pp. 1356–1371, 2016.

[44] V. Tunakova, M. Tunak, P. Tesinova, M. Seidlova, and J. Prochazka, "Fashion clothing with electromagnetic radiation protection: aesthetic properties and performance," vol. 90, no. 21, pp. 2504–2521, 2020. DOI: 10.1177/0040517520923047.

[45] V. Tunakova, Z. Hrubosova, M. Tunak, M. Kasparova, and J. Mullerova, "Laser surface modification of electrically conductive fabrics: Material performance improvement and design effects," vol. 98, pp. 178–189, 2018. DOI: 10.1016/j.optlastec.2017.07.017.

[46] B. Saravanja, M. Kresimir, P. Tanja, and D. Ujevic, "Impact of dry cleaning on the electromagnetic shield characteristics of interlining fabric," *Fibres & Textiles in Eastern Europe*, vol. 23, no. 1, pp. 104–108, 2015.

[47] V. Tunakova, L. Technikova, and J. Militky, "Influence of washing/drying cycles on fundamental properties of metal fiber-containing fabrics designed for electromagnetic shielding purposes," vol. 87, no. 2, pp. 175–192, 2017. DOI: 10.1177/0040517515627168.

[48] E. Pokorna, "Adhesive properties of polypyrrole modified textiles," Master's thesis, Technical University of Liberec, Czech Republic, 2016.

[49] K. Mosnackova, M. Chehimi, P. Fedorko, and M. Omastova, "Polyamide grafted with polypyrrole: formation, properties, and stability," *Chemical Papers*, vol. 67, no. 8, pp. 979–994, 2013.

[50] M. Barakzehi, M. Montazer, and F. Sharif, "Electrically and electrochemically active composite based on polyester/reduced graphene oxide/polypyrrole with remarkable washing durability," *Journal of Textiles and Polymers*, vol. 8, no. 2, pp. 15–22, 2020.

[51] "IEE-STD-299. Standard Method for Measuring the Effectiveness of Electromagnetic Shielding Enclosures," standard, Institute of Electrical and Electronics Engineerss, New Jersey, USA, 2006.

[52] "ASTM ES-7. Test Method for Electromagnetic Shielding Effectiveness of Planar Materials," standard, American Society for Testing and Materials, Conshohocken, USA, Mar. 2013.

[53] "ASTM D4935-18. Standard Test Method for Measuring the Electromagnetic Shielding Effectiveness of Planar Materials," standard, American Society for Testing and Materials, Conshohocken, USA, 2013.

[54] S. Tezel, Y. Kavuşturan, G. A. Vandenbosch, and V. Volski, "Comparison of electromagnetic shielding effectiveness of conductive single jersey fabrics with coaxial transmission line and free space measurement techniques," *Textile Research Journal*, vol. 84, no. 5, pp. 461–476, 2014.

[55] T. W. Wieckowski and J. M. Janukiewicz, "Methods for evaluating the shielding effectiveness of textiles," *Fibres & Textiles in Eastern Europe*, vol. 14, no. 5, pp. 18–22, 2006.

[56] S. Geetha, K. K. Satheesh Kumar, C. R. K. Rao, M. Vijayan, and D. C. Trivedi, "Emi shielding: Methods and materials—A review," *Journal of Applied Polymer Science*, vol. 112, no. 4, pp. 2073–2086, 2009.

[57] V. Safarova, M. Tunak, M. Truhlar, and J. Militky, "A new method and apparatus for evaluating the electromagnetic shielding effectiveness of textiles," *Textile Research Journal*, vol. 86, no. 1, pp. 44–56, 2016. DOI: 10.1177/0040517515581587.

[58] V. Safarova, "Textile structures with enhanced electromagnetic shielding ability," Ph.D. thesis, Technical University of Liberec, Czech Republic, 2014.

[59] D. Su, H. Liu, S. Yang, Z. Zhao, and D. Sui, "An analytical method for calculating the shielding effectiveness of an enclosure with an oblique rectangular aperture," *Chinese Journal of Electronics*, vol. 28, no. 4, pp. 850–855, 2019.

[60] W. Shen, S. Wang, W. Li, H. Jin, and H. Zhang, "An extended hybrid analytical model for shielding effectiveness prediction of multi-cavity structure with numerous apertures," *Progress In Electromagentic Research*, vol. 96, pp. 181–190, 2020.

[61] M. Robinson, T. Benson, C. Christopoulos, J. Dawson, M. Ganley, A. Marvin, S. Porter, and D. Thomas, "Analytical formulation for the shielding effectiveness of enclosures with apertures," *IEEE Transactions on Electromagnetic Compatibility*, vol. 40, no. 3, pp. 240–248, 1998.

[62] S. Rea, D. Linton, E. Orr, and J. McConnell, "Electromagnetic shielding properties of carbon fibre composites in avionic systems," *Microwave Review*, vol. 11, no. 1, p. 29 – 32, 2005.

[63] S.-E. Lee, K.-Y. Park, K.-S. Oh, and C.-G. Kim, "The use of carbon/dielectric fiber woven fabrics as filters for electromagnetic radiation," *Carbon*, vol. 47, no. 8, pp. 1896–1904, 2009.

[64] D. Munalli, G. Dimitrakis, D. Chronopoulos, S. Greedy, and A. Long, "Electromagnetic shielding effectiveness of carbon fibre reinforced composites," *Composites Part B: Engineering*, vol. 173, p. 106906, 2019.

[65] V. Safarova, M. Tunak, and J. Militky, "Prediction of hybrid woven fabric electromagnetic shielding effectiveness," *Textile Research Journal*, vol. 85, no. 7, pp. 673–686, 2015. DOI: 10.1177/0040517514555802.

[66] M. Neruda and L. Vojtech, "Electromagnetic shielding effectiveness of woven fabrics with high electrical conductivity: Complete derivation and verification of analytical model," *Materials*, vol. 11, no. 9, 2018.

[67] K. Casey, "Electromagnetic shielding behavior of wire-mesh screens," *IEEE Transactions on Electromagnetic Compatibility*, vol. 30, no. 3, pp. 298–306, 1988.

[68] L. Vojtech and M. Neruda, "Design of radiofrequency protective clothing containing silver nanoparticles," *Fibres & Textiles in Eastern Europe*, vol. 5, no. 101, pp. 141–147, 2013.

[69] K. Joyner, P. Copeland, and I. MacFarlane, "An evaluation of a radiofrequency protective suit and electrically conductive fabrics," *IEEE Transactions on Electromagnetic Compatibility*, vol. 31, no. 2, pp. 129–137, 1989.

[70] V. Tunakova, "Protective clothing against radiofrequency electromagnetic radiation or a part of clothing against radiofrequency electromagnetic radiation," CZ Utility Model, 30754, 2017. UPV.

[71] V. Vitek, "The study of features of conductive fabric in term of EMC," Master's thesis, Technical University of Liberec, Czech Republic, 2019.

[72] J. Militky, V. Tunakova, Z. Hrubosova, and J. Vecernik, "A textile for the protection of electronic information carriers," CZ Utility Model, 31290, 2017. UPV.

[73] P. Knizak, "Product to protect the electronic key from misusage," Master's thesis, Technical University of Liberec, Czech Republic, 2020.

[74] V. Tunakova, M. Tunak, and J. Novotna, "Porous, low thickness carbon-fiber reinforced epoxy composites with excellent flexibility and superior electromagnetic radiation protection," *Journal of Industrial Textiles*, vol. 53, 2023. DOI: 10.1177/15280837231159867.

[75] A. Samkova, P. Kulhavy, V. Tunakova, and M. Petru, "Improving electromagnetic shielding ability of plaster-based composites by addition of carbon fibers," *Advances in Materials Science and Engineering*, vol. 2018, p. 3758364. DOI: 10.1155/2018/3758364.

[76] S. Palanisamy, "Knitted conductive fabrics with enhanced electromagnetic interference shielding," Ph.D. thesis, Technical University of Liberec, Czech Republic, 2023.

[77] S. Palanisamy, V. Tunakova, M. Tunak, and J. Militky, "Textile-based weft knit strain sensor: Experimental investigation of the effect of stretching on electrical conductivity and electromagnetic shielding," *Journal of Industrial Textiles*, vol. 52, 2022. DOI: 10.1177/15280837221142825.

Appendix 1

V. Tunakova and M. Tunak, "Carbon-fiber reinforcements for epoxy composites with electromagnetic radiation protection—prediction of electromagnetic shielding ability," Composites Science and Technology, vol. 215, p. 109029, 2021.

Composites Science and Technology 215 (2021) 109029

Contents lists available at ScienceDirect

Composites Science and Technology

journal homepage: www.elsevier.com/locate/compscitech

Carbon-fiber reinforcements for epoxy composites with electromagnetic radiation protection—prediction of electromagnetic shielding ability

Veronika Tunakova *, Maros Tunak

Technical University of Liberec, Faculty of Textile Engineering, Studentska 2, 46117, Liberec, Czech Republic

ARTICLE INFO

Keywords:
Carbon fibres
Fabrics/Textiles
Polymer-matrix composites (PMCs)
Electromagnetic interference shielding (EMI)
Electrical properties

ABSTRACT

The development of flexible air/water vapor permeable composites designed for shielding the electromagnetic field has received an increasing amount of attention in recent years. A great deal of the attendant research has dealt with the development and investigation of electromagnetic shielding (SE) composites with textile-based reinforcements. However, little attention has been paid to the simple prediction of their SE ability, especially in terms of industrial applications. In this study, we investigated the design and properties of carbon-fiber reinforcements for use in epoxy composites that provide SE protection. Here, we selected the Aksaca electrically conductive continuous carbon-fiber roving and prepared different reinforcements with woven structures before investigating the effects of the weft and warp sett and the thickness of the warp and weft threads on the SE ability. To measure the shielding effectiveness, we used the coaxial transmission line method, while an analytical approach was adopted to predict the shielding effectiveness of the carbon reinforcements and to compare the calculated values with the experimental data. The SE effectiveness of the reinforcements varied from 10 to 45 dB at a frequency of 1.5 GHz, with good agreement between the calculated and experimental results.

1. Introduction

Electromagnetic interference can be defined as the electromagnetic radiation produced by electrical circuits that can adversely affect the operation of surrounding electronic devices or cause damage to living organisms. In recent decades, the level of so-called electromagnetic smog has increased significantly, especially that related to the development of new high-frequency electronic systems and telecommunication equipment. This phenomenon has led to the active development of new and effective solutions for the provision of shielding from interfering electromagnetic radiation in various applications.

Electromagnetic interference shielding refers to the blocking of incoming electromagnetic waves through absorption, reflection, or multiple reflection, whereby the shielding material resists penetration by the electromagnetic radiation.

The attendant literature reveals that the most common method used for the shielding from electromagnetic fields involves reflection via metallic materials, generally foils or plates. The disadvantages of these solutions include their limited flexibility due to the high rigidity and high density of these materials, as well as certain corrosion issues and the limited capacity to control the efficiency of the electromagnetic shielding (SE). In addition, electromagnetic smog cannot be eliminated via reflection from a shield alone. Therefore, an increasing amount of attention is being paid to the development of absorbent polymeric-based shielding materials, which have the advantages of having a low weight (density of >2 g/cm^3 compared with metals with densities of >3 g/cm^3) and being comparatively inexpensive and formable. However, most polymeric materials are electrical insulators that are entirely transparent to electromagnetic radiation. By incorporating an electrically conductive component of any one of various types and shapes, shielding from the electromagnetic field can also be achieved. As such, composite materials are gaining popularity [1–3]. Carbon-fiber (CF)-reinforced polymers are a special type of composite material in which the CF provides strength, stiffness, and electrical conductivity, while the polymer provides a cohesive matrix that protects and holds the fibers together. This type of composite material is most commonly used in the aircraft industry.

In fact, CF is electrically conductive due to the planar layered structure of the carbon atoms, which provides a certain degree of SE for materials containing CFs in their structure. As such, CFs are preferred to other forms of carbon filler, such as graphite or carbon black [4]. However, since the cost of CFs is almost four times higher than that of

* Corresponding author.
E-mail address: veronika.tunakova@tul.cz (V. Tunakova).

https://doi.org/10.1016/j.compscitech.2021.109029
Received 9 March 2021; Received in revised form 29 August 2021; Accepted 1 September 2021
Available online 8 September 2021

traditional polymer materials, the CF content becomes critical in this type of composite. Various researchers (e.g. Refs. [5–9]) have demonstrated that the SE can be improved and that the amount of CF used can be reduced by controlling the discontinuous CF orientation. In Ref. [7], it was demonstrated that the higher the CF content, the higher the SE, with the orientation of the CF perpendicular to the casting of the composite film providing even higher SE (up to 150 dB/mm at $f = 10$ GHz). It has also been confirmed that a high aspect ratio (ratio of the length of a fiber to its diameter) is preferable [10]. Meanwhile, the experiments performed in Ref. [11] indicated that both the electric conductivity and the SE of a given composite will increase with a higher short CF content (a composite with a filler loading of 30 phr has an SE of approximately 60 dB at a frequency of 10 GHz), while the dependence of the SE on the electric conductivity can be approximated using a logarithmic function. The SE value also tends to increase with an increase in composite thickness, while the magnetic permeability of any given composite will increase with a higher short CF content and with an increase in frequency.

Compared with the traditional discontinuous CFs, a composite with higher SE can be realized through the use of continuous CFs as a woven reinforcement under the same conditions (e.g., the CF content) [12]. The mechanism behind this improvement is the formation of a highly electrically conductive symmetrical network of carbon multifils (containing thousands of closely arranged fibers), which are required for SE. Another reason for the higher SE of this type of composite relates to how reflection is a dominant factor in the total shielding effectiveness [13]. The preparation and properties of continuous CF-reinforced composites have been reported in a number of studies [14–17]. For example, nickel-coated CF-reinforced composites were studied in terms of their mechanical properties and their ability to shield the electromagnetic field in Ref. [17]. Here, in addition to achieving unique mechanical properties, it was found that the SE increased from 20 to 30 dB due to metallization. In Ref. [16], the authors demonstrated how the SE of their carbon fabric/epoxy samples increased with a higher fiber volume fraction (the resin reduced the contact between the fibers). Despite the fact that a larger thickness and a greater number of fabric layers of the composite does not provide higher electric conductivity, specimens with more layers tend to demonstrate greater protection against electromagnetic radiation. It can thus be stated that the SE is not only related to the conductivity of the material but is also dependent on the power that is dissipated along the thickness and reflected at different interfaces.

The SE is the key parameter in the evaluation of the electromagnetic compatibility of electronic systems. One of the most important factors in reducing the SE relates to the presence of apertures on the surface of the shielding enclosure [18]. However, in practical applications, apertures are both desirable and necessary for ensuring sufficient air permeability, ventilation, and cooling, as well as ease of maintenance. In this context, less attention is generally paid to the structure of the carbon fabric reinforcements, especially in terms of weave and related porosity. A woven reinforcement in a plain weave of continuous carbon, boron, and carbon–boron fibers was studied in Ref. [19]. Here, the authors found that the highest SE (around 45 dB for a frequency of 1.5 GHz) was provided by the CF due to its higher electrical conductivity compared with boron fibers. However, more details regarding the structure of the woven reinforcements (e.g., the sett of the warp or weft, the fineness of the multifils or fibers) were not reported. Meanwhile, the SEs of plain weave, balanced twill weave, and uniform-direction conductive continuous CFs were studied in Ref. [12], with the experimental results indicating that the SEs of the composites containing woven reinforcement were higher than those obtained with the uniform-direction CF at the same weight percentage content. In fact, the highest SE of 96 dB was obtained with two balanced twill-weave reinforced composites. Elsewhere, a number of hybrid and 100% carbon woven fabrics were investigated in Ref. [20], with the authors comparing various different patterns, including plain, twill, and satin weaves. Here, as was expected, the plain and twill weaves, which were made of 100% continuous CF roving, achieved a higher SE than the satin, which was attributed to the number of intersection points. Meanwhile, in Ref. [21], various designs of frequency-selective composites containing reinforcements woven from continuous CFs and dielectric fibers in periodic patterns were outlined.

Overall, the literature review revealed that to obtain a fabric with a high capacity to shield against the electromagnetic field, it is advantageous to use continuous, highly electrically conductive CFs, with the plain-weave-type being the preference.

Recently, an increasing amount of attention has been paid to the effective evaluation of the SE using non-experimental methods, which can be divided into two main categories. The first involves full-wave solvers based on numerical methods, such as the finite-difference time domain, the method of moments, the transmission line matrix, and various hybrid methods [18,22,23]. The disadvantage of these methods lies in the complexity of the associated computing resources and computer memory. The second non-experimental category involves analytical methods used for the rapid computation of the SE for certain structures in widespread use, such as rectangular enclosures.

With respect to textile-structure-based shielding materials, a limited number of scientific papers have dealt with the attendant SE simulation or prediction. For example, in Ref. [24], the authors formed a three-ply continuous CF woven (satin weave) reinforced composite and simulated the SE using the plane-wave shielding theory. However, the simulated SE results were not in good agreement with the experimentally measured SE. In Ref. [21], the electromagnetic characteristics of a frequency-selective fabric composite (plain weave of continuous CF with square elements with an 8-mm aperture) were simulated using CST Microwave Studio 5.1 software and the data related to the electrical conductivity, fiber undulation, and aperture-to-cell ratio of carbon rovings, with the results being in excellent agreement with the experimentally measured data. In Ref. [16], the CST Microwave Studio software was also used for SE simulation, with the results again demonstrating good agreement with the experimental results, especially with the thin compact carbon woven/epoxy samples. The SE of hybrid fabrics containing different contents of staple stainless-steel fibers was predicted in Ref. [25] based on the assumption that the total SE of a fabric is a linear combination of the SE due to apertures (SE_{aper}) at high frequencies and the SE of compact materials at low frequencies (SE_{sheet}). Here, all equations were taken from the published literature, with good agreement obtained only for samples with lower electric conductivity and apertures of smaller dimensions. Reference [26] includes a detailed derivation of SE for SE_{fabric} and SE_{aper}, with a general equation of SE derived for woven fabrics made of blended yarns with high conductivity ($\sigma > 244$ S/m), which was then compared with the experimental data with absolute agreement. However, the derived calculations were somewhat complicated.

All the above research indicates the need for both deeper research into the SE efficiency of carbon-based woven fabrics in terms of their structure, especially the porosity, and the verification of the possibility of SE prediction based on the knowledge of the geometric parameters and electrical conductivity of rovings. With this in mind, the current research was aimed at experimentally identifying the factors that affect the SE ability of CF woven reinforcements, while a further crucial objective was to verify an uncomplicated approach suitable for calculating the SE of woven, electrically conductive reinforcements based on various input parameters. As such, we used the coaxial transmission line method, the ASTM 4935-18 standard method, to experimentally investigate the SE of composite reinforcements with woven structures made of carbon continuous multifils. This standard is one of the most commonly used standards for the SE evaluation of planar materials. We also selected this standard in view of the intended use of the composite, that is, within the aircraft industry. Avionic systems contain numerous onboard, frequency-generating systems, including frequency synthesizers, digital circuits, telemetry systems, and switching power supplies. Therefore, SE in the frequency range starts at VHF radio frequencies,

while ending at L-band microwave frequencies is desirable. Specifically, we explored the effects of the warp and weft sett and multifil fineness on the SE. Given that the geometry of a bonded-junction wire-mesh screen is highly similar to that of low-density woven fabrics made of electrically conductive threads, we were able to use an extremely simple analytical computation method [27] to predict the SE based on the knowledge of only a small number of parameters, i.e., the geometrical properties of the woven fabric (length of aperture and diameter of multifil) and the electrical conductivity of the carbon multifil. Following this, we compared the SE values obtained experimentally with those computed analytically, with the findings subsequently discussed.

1.1. Electromagnetic shielding effectiveness of woven fabrics

The SE ability of any shield varies depending on the frequency, geometry, and material of the shield, as well as the type of attenuated field, the angle of incidence, and the polarization [26]. The total SE of a solid material with no apertures (SE_{sheet}) is equal to the sum of the absorption loss (A), the reflection loss (R), and a correction factor to account for multiple reflections (B) in the shield. In contrast, the term B can be neglected for electric fields and plane weaves [26]:

$$SE_{sheet} = 10\log_{10}\left(\frac{1}{|S_{21}|^2}\right) = A_{sheet} + R_{sheet} + B_{sheet} = 10\log_{10}\left(\frac{1}{1-|S_{11}|^2}\right) + 10\log_{10}\left(\frac{1-|S_{11}|^2}{|S_{21}|^2}\right) = 20\log_{10}\frac{E_i}{E_t} = 20\log_{10}\frac{H_i}{H_t} = 10\log_{10}\frac{P_i}{P_t}, \quad (1)$$

where E_i, H_i, and P_i are the electric field intensity, magnetic field intensity, and power, respectively, measured without the presence of the tested material, while E_t, H_t, and P_t are the same physical quantities measured in the presence of the tested material, and S_{ij} represents the scattering parameters [28].

The absorption loss and reflection loss of the shield with no apertures can be written after simplification as follows [29]:

$$A_{sheet} = 0.0848t\sqrt{\frac{K}{K_C}}f, \quad (2)$$

$$R_{sheet} = C + 10\log\left(\frac{K}{K_C f}\right), \quad (3)$$

where C is the constant, K [S·cm^{-1}] is the volume conductivity, K_C is the copper conductivity, f [MHz] is the frequency, and t [m] is the thickness of the shield.

In the previous formulations, a solid shield with no apertures was assumed. In practice, however, most shields are not solid. In the case of fabrics, the inter-yarn pores represent the apertures. All types of discontinuities (e.g., seams, ventilation holes, etc.) considerably reduce the effectiveness of the shield, while with a higher frequency, the intrinsic SE of the shield material is of less concern than the leakage through the apertures [30,31]. The total SE of a porous material can be expressed as a linear combination of the SE due to apertures at high frequencies and the SE of compact materials at low frequencies [31]:

$$SE = e^{-0.017L\sqrt{f}}SE_{sheet} + \left(1 - e^{-0.017L\sqrt{f}}\right)SE_{aper}, \quad (4)$$

where L is the maximum aperture length and SE_{aper} is the SE of an aperture depending mainly on the geometrical dimensions of the aperture. More details regarding different approaches for the calculation of SE_{aper} can be found in Refs. [31,32].

Woven structures, especially in the plane wave, have a similar geometry to wire mesh, meaning a simple analytical solution for the SE can be applied. Assuming that the aperture dimensions are small relative to the wavelength, the SE of a planar mesh screen with bonded junctions can be described using the equivalent sheet impedance of the mesh [33]. The power transmission coefficient or the total shielding effectiveness (in dB) can be calculated based on the electrical conductivity and radius of the wire, the length of the aperture (see Fig. 1), and the angle of the incidence as follows:

$$SE_{tot}(\omega,\theta) = 10\log_{10}\left\{|T_1(\omega,\theta)|^2 + |T_2(\omega,\theta)|^2\right\}, \quad (5)$$

where ω is the angular frequency ($\omega = 2\pi f$), f [Hz] is the frequency, and $T_1(\omega,\theta)$ and $T_2(\omega,\theta)$ are the transmission coefficients for the polarization of the transverse electric and transverse magnetic modes, respectively, which can be calculated using the following equations:

$$T_1(\omega,\theta) = \frac{\left(\frac{2Z_{S1}(\omega)}{Z_0}\right)cos\theta}{1 + \left(\frac{2Z_{S1}(\omega)}{Z_0}\right)cos\theta}, \quad (6)$$

$$T_2(\omega,\theta) = \frac{\left(\frac{2Z_{S2}(\omega)}{Z_0}\right)}{cos\theta + \left(\frac{2Z_{S2}(\omega)}{Z_0}\right)}, \quad (7)$$

where Z_0 is the free-space impedance ($Z_0 = 376.730\ \Omega$), and Z_{S1} and Z_{S2} are the eigenvalues of the mesh impedance operator, which are given as follows:

$$Z_{S1}(\omega) = Z_\omega a + j\omega L, \quad (8)$$

$$Z_{S2}(\omega) = Z_{S1} - \frac{j\omega L}{2}sin^2\theta, \quad (9)$$

where a [m] is the length of a square aperture, Z_ω is the wire impedance per unit length (approximated by its DC electrical resistance per unit length), and L is the sheet inductance. These variables can be calculated as follows:

$$L = \frac{\mu_0 a}{2\pi}ln\left\{\left(1 - e^{-2\pi r/a}\right)^{-1}\right\}, \quad (10)$$

$$Z_\omega = \left(\pi r^2\sigma\right)^{-1}, \quad (11)$$

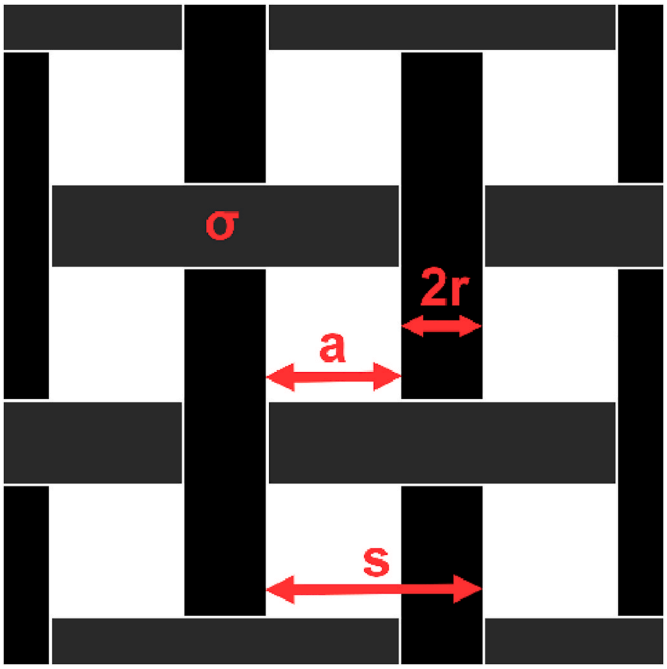

Fig. 1. Planar mesh screen with bonded junctions.

where μ_0 is the vacuum permeability ($\mu_0 = 1.256{\cdot}10^{-6}$ H/m), r [m] is the wire radius, and σ [S/m] is the electrical conductivity.

The relationships described above are primarily intended for meshes with square apertures; however, it was reported in Ref. [27] that non-square (hexagonal) aperture meshes can also be handled with an aperture of an equivalent square-area shape.

2. Electrical characteristics of fibers and threads

The resistance, R, of a wire of fiber (annular cross section) with length L can be calculated using the following formula:

$$R = \frac{L\rho}{A} = \frac{4L\rho}{\pi d^2}, \tag{12}$$

where R [Ω] is the resistance of the conductor, L [m] is the length of the conductor, ρ [Ω·m] is the electrical resistivity of the conductor, A [m^2] is the cross-sectional area, and d [m] is the nominal diameter of the fiber [34].

Meanwhile, the electric resistivity, ρ, also known as specific electrical resistance [Ω·m], is a measure of how strongly a wire opposes an electric current. A low resistivity indicates that the wire readily allows movement of an electrical charge. Copper has a resistivity of 0.0171 Ω·mm^2/m and is therefore one of the best conductors of electric current (slightly behind pure silver) [34]:

$$\rho = \frac{RA}{L} = \frac{\pi d^2 R}{4L}. \tag{13}$$

Electrical conductivity, σ, also known as specific conductance [S/m], is the reciprocal of the electrical resistivity and represents a material's ability to conduct an electric current:

$$\sigma = \frac{1}{\rho}. \tag{14}$$

Finally, the linear electrical resistance, R_L, [Ω·m] is the electrical resistance of a conductor per unit length. The R_L does not take into account the cross-sectional area of the conductor and is often used for the basic electric resistance evaluation of longitudinal textile structures such as yarns.

$$R_L = \frac{R}{L}. \tag{15}$$

In the area of textile technology, the materials are studied in terms of their weight rather than their bulk. Furthermore, the cross-sectional area of textile yarns is not well defined, as this area is complicated by the space between its fibers. As such, this area can be more easily obtained indirectly from the mass and density of the specimen than by direct measurement. As the main definition of fineness is the linear density (mass per unit length), it is more suitable to use mass-based quantities related to the linear density [34]. Therefore, the mass specific resistance, R_S, is used and is defined as the resistance in ohms between the ends of a 1-m-long specimen with a mass of 1 kg, with the unit being Ω·kg/m^2. These two quantities can be expressed as follows:

$$R_S = \rho D, \tag{16}$$

where D is the density of the material [kg/m^3].

However, in practice, it is more convenient to express R_S in Ω·g/cm^2. With these units, the resistance, R, of an arbitrary specimen is given by the following relationship:

$$R = R_S \frac{l}{NT} 10^5, \tag{17}$$

where l is the distance between the end of the specimen [cm], N is the number of the ends in the yarn or fiber, and T is the linear density of the yarn or fiber [tex] [34]. Using Equations (15)–(17), it is possible to compare the electrical conductivity of linear textile structures (e.g., yarns, rovings, strands, etc.) with different fineness and density values.

3. Materials and methods

3.1. Continuous carbon-fiber roving

To prepare the woven reinforcements, we used Aksaca carbon roving, type A-35, which is comprised of continuous fibers of a polyacrylonitrile precursor, the main physical and chemical properties of which are shown in Table 1. Meanwhile, Fig. 2 presents microscopic images of the CFs in carbon roving A-35.

3.2. Carbon-fiber woven reinforcements

Using the carbon roving, we created eleven types of reinforcement in the form of a plain weave fabric with a different total warp and weft sett. The same method was used to prepare all the samples. Here, the warp and weft threads were manually interwoven onto the prepared Teflon foil, which served as a non-stick backing for the subsequent construction of the composite, forming a fabric with a plain weave. The term "thread" is often used for carbon roving. The edges of the fabric were secured using adhesive tape to prevent collapse of the reinforcement during handling. The size of the reinforcements was approximately 30 × 30 cm.

As the main goal of this study was to explore the influence of the weft and warp sett and the diameter of the carbon rovings on the resulting SE ability of woven reinforcements, a two-factor factorial design [35] was chosen to comprehensively and systematically study the interaction between various factors in addition to identifying any significant factors. The variable of interest was the SE effectiveness as measured at a frequency of 1.5 GHz. We decided to test three types of weft and warp setts and three diameters of carbon roving, thus, a 3^2 factorial design was used. Coarser warp and weft threads with higher diameter were obtained by combining single carbon rovings of 2× and 3× . Three samples were tested for each combination of warp and weft sett (spacing) and roving diameter, with all 27 tests run in random order. The factor levels are shown in Table 2. Since the warp and weft sett was expected to have the highest effect on the final SE ability of the sample, the sample set was expanded by incorporating a further two samples with higher and lower setts for improved investigation of the effect of the sett on the SE. Table 3 lists the properties of all the samples in the series, while Figs. 3 and 4 show schematics of the reinforcement formations in the samples.

These specific spacings of warp and weft threads were chosen in terms of the carbon material consumption and the air and water vapor permeability of woven structures often required for final application. The sample with the lowest warp and weft sett had five threads per 100 mm, which corresponded to a 20-mm carbon roving spacing (s, see Fig. 1) in both the warp and weft. Meanwhile, the densest sample reinforcement was 100 threads per 100 mm.

3.3. Measurement of the electrical resistance of the carbon roving

To test the electrical resistance of the continuous CF roving, we used the two-probe (four-wire) method according to the SIST EN 16812

Table 1
Physical and chemical properties of Aksaca carbon roving A-35.

Odor	NO
Water solubility	NO
Fineness [tex]	196
No of filaments [−]	3000
Fiber diameter [μm]	7
Density [g/cm^3]	1.75
Strength [MPa]	3500
Young's modulus [GPa]	230
Elongation [%]	1.5

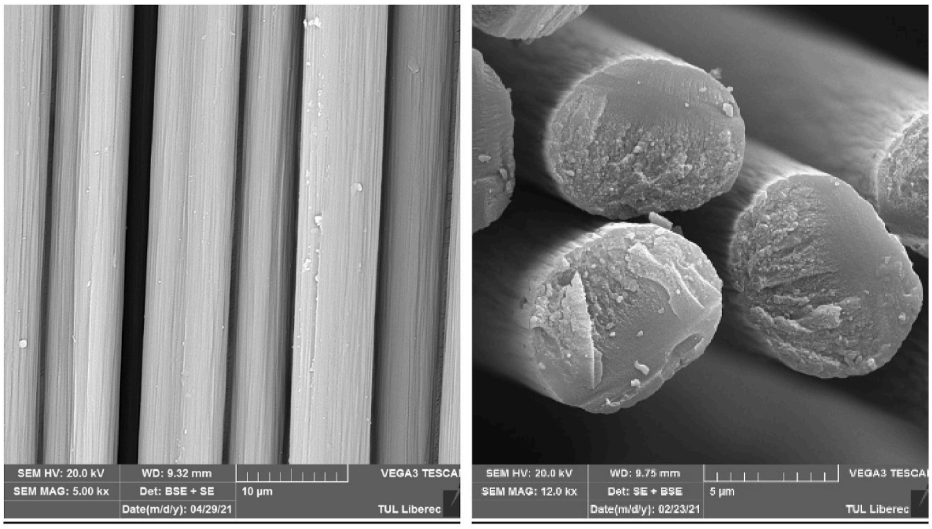

Fig. 2. Microscopic images of the carbon fibers in carbon roving.

Table 2
Input variables, units and levels.

Variable name	Variable unit	Levels		
Spacing (A)	mm	5	10	15
Diameter (B)	mm	2	3	4

Table 3
Main properties of carbon-fiber woven sample set.

Sample code	Warp and weft sett [dm^{-1}]	Carbon roving spacing s [mm]	No. of rovings n [−] weft/warp
1	5	20	1
2	7	15	1
3	7	15	2
4	7	15	3
5	9	10	1
6	9	10	2
7	9	10	3
8	18	5	1
9	18	5	2
10	18	5	3
11	100	1	1

standard [36]. Fig. 5 shows a schematic of the configuration of the two-probe method. Here, we ensured that the same pressure was exerted using 15-mm-wide bulldog clamps, with the rectangular electrodes gripping the measured material made of copper. An Agilent 34401A digital multimeter was used for the measurement, with the samples air-conditioned and the measurements performed at a 40% relative humidity (RH) and a temperature of 22 °C. Meanwhile, the resistance of the samples was measured at different distances from the ends of the specimen (0.05, 0.1, 0.15, 0.2, 0.25, and 0.3 m), with 10 measurements performed at each clamping length (sample size $n = 10$). To determine the mass-specific resistance R_S and to eliminate the contact resistances at the interface between the material and the electrode, we used the linear regression method [37], while the electric resistivity of the samples was calculated using Equations (15)–(17).

3.4. Image analysis of the geometrical dimensions of the reinforcements

Gaining some knowledge of the geometrical properties of the samples was crucial. As noted above, the presence of apertures in the shield is a key factor in reducing the SE. Furthermore, information regarding the dimensions of the woven fabric (length of aperture, diameter of thread) was required for analytically predicting the SE based on the equivalent sheet impedance. Therefore, we obtained images of the carbon roving and woven samples using an HP ScanJet Pro 2500 f1. Seven sample representatives from the entire sample set were subjected to dimensional analysis, namely samples 1, 2, 3, 4, 5, 8, and 11.

To determine the thickness of the carbon roving, we obtained images of the rovings (total length of the rovings = 5.3 m) at a resolution of 600 dpi (1 pix = 0.0423 mm), while to determine the geometrical properties of the woven fabric, we obtained images at a resolution of 300 dpi (1 px = 0.0085 cm), as shown in Fig. 6.

The images were captured as RGB (red, green, blue) image matrices, which were then pre-processed using global thresholding (the Otsu method) and binary morphological operations (morphological opening to remove small objects, morphological closing to fill any holes and remove any incomplete objects) [38]. The thickness of the roving was determined according to its height along its length ($n = 20$), as measured by the number of white pixels from the first to the last white pixel along the y-axis of the image. Characteristics such as the object area and the size of the bounding boxes (smallest rectangle-containing objects) were then extracted from the pre-processed images of the woven samples ($n = 1$).

3.5. Measurement of the electromagnetic shielding effectiveness

The SE of the samples was experimentally measured via a far-field electromagnetic plane wave using the ASTM D 4935-18 standard method [39] for planar materials. This measurement method is valid over a frequency range of 30 MHz to 1.5 GHz; however, as these limits are not exact, the measurements were performed over a frequency range of 30 MHz to 3 GHz, which corresponded to a wavelength of 10–0.1 m. More attention was paid to the SE at 1.5 GHz since this is within the frequency range defined in the standard and also since it is close to the frequency of frequently used sources of electromagnetic liability, such as mobile phones, wireless LAN systems, radars, and GPSs.

The setup consisted of a sample holder with its input and output connected to a network analyzer. An SE test fixture (model EM-2107A; Electro-Metrics, Inc.) was used to hold the sample, with the design and dimensions of the sample holder following the standard method noted above. The measured sample was in the shape of a circle with a diameter of 13.31 cm. To generate and receive the electromagnetic signals, we

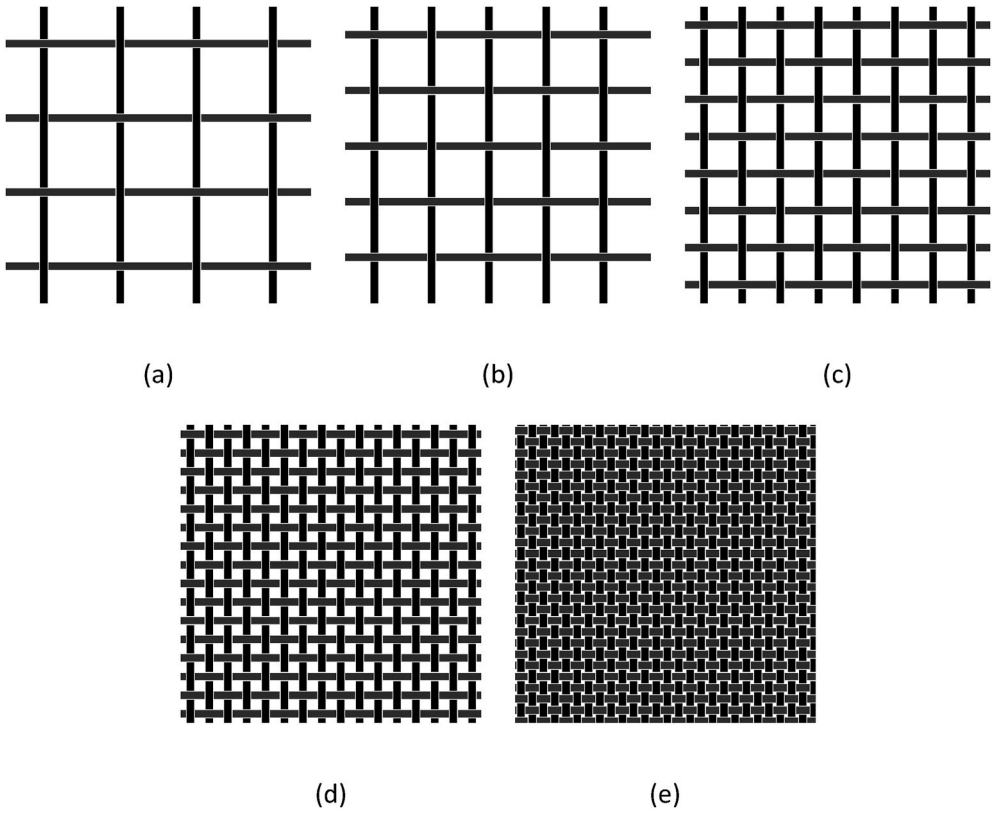

Fig. 3. Schematics of samples with the same roving diameter $d = 2r$, but different roving spacing s: (a) $s = 20$ mm, (b) $s = 15$ mm, (c), $s = 10$ mm, (d) $s = 5$ mm, and (e) $s = 1$ mm.

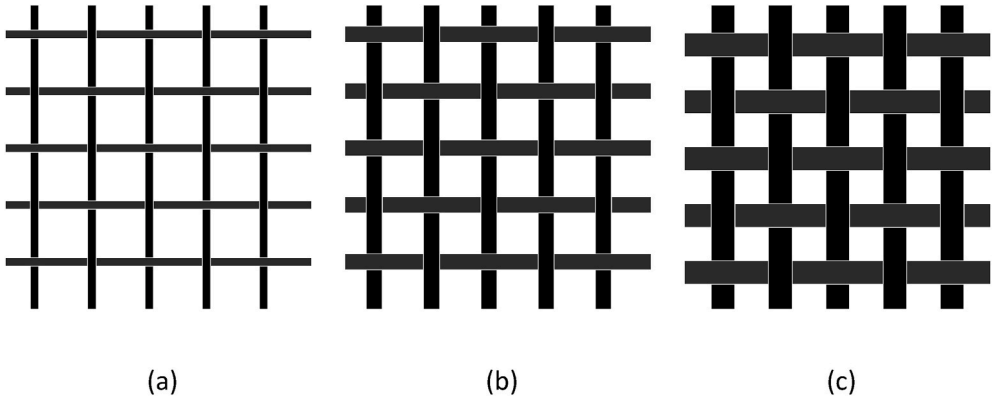

Fig. 4. Schematics of samples with the same roving spacing, $s = 15$ mm, but different roving diameters: (a) $2r$, (b) $2 \times 2r$, and (c) $3 \times 2r$.

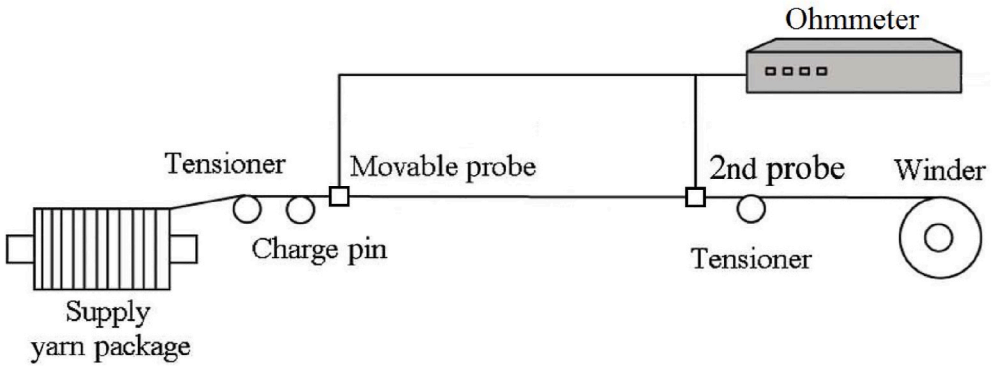

Fig. 5. Configuration of electrical resistance measurement of samples.

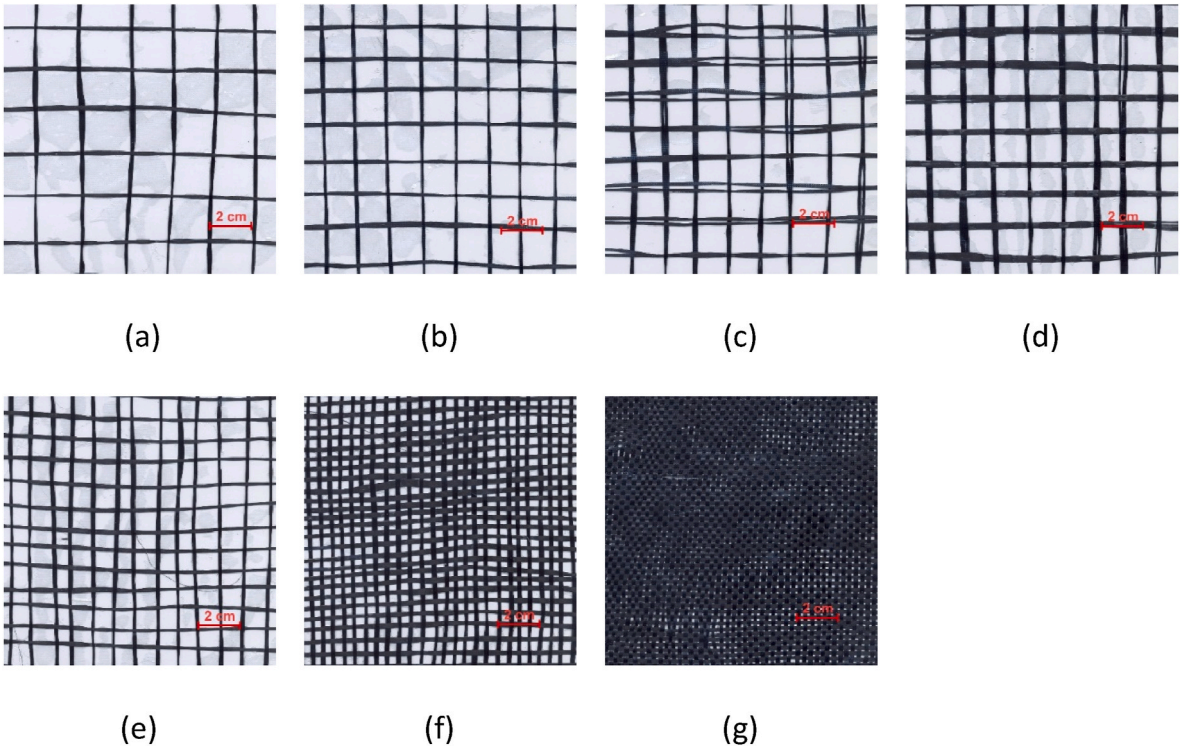

Fig. 6. Images of all the samples in the set: (a)–(e): sample 1–5, (f) sample 8, (g) sample 11.

used a Rohde & Schwarz ZN3 network analyzer, while the insertion–loss method was used to determine the SE of the fabric. The samples were air-conditioned prior to testing ($T = 22\ °C \pm 3\ °C$, $RH = 50\ \% \pm 10\ \%$), with the measurements performed ($n = 3$) at three different randomly chosen sample locations to facilitate the subsequent statistical analysis.

4. Results and discussion

4.1. Electrical properties of the carbon roving

Fig. 7 shows the dependence on the clamping length L of the electrical resistance R and of the electrical resistance when considering the fineness of the carbon roving $R{\cdot}T{\cdot}10^{-5}$. Here, the linear least squares method was used to fit the model to the data. The slope of the linear regression model indicates the R_L and R_S values in accordance with Equations (15) and (17), while the intercept of the regression line represents the sum of the contact resistances at the interface between the material and both electrodes. Meanwhile, Table 3 shows the mean R_L and R_S values and the 95% confidence intervals of the means. Using the R_S values, we also calculated the electrical resistivity ρ and the conductivity σ values (based on the knowledge of material density D according to Equations (14) and (16), which are summarized in Table 4. The electrical conductivity of a single carbon roving was used in the

Table 4
Electrical properties of carbon roving (mean value $\bar{x}$, standard deviation *std* and margins of error of means $MOE_{0.95}$ used for construction of 95% confidence interval of mean).

Variable	$\bar{x}$	*std*	$MOE_{0.95}$
R_L [Ω/m]	154	29.36	6.6
R_s [mΩ·g·cm^{-2}]	3.02	0.54	0.13
ρ [Ω·m]	$1.73{\cdot}10^{-5}$	$2.93{\cdot}10^{-6}$	$7{\cdot}10^{-7}$
σ [S/m]	$5.80{\cdot}10^{4}$	$1.09{\cdot}10^{4}$	$2.6{\cdot}10^{3}$

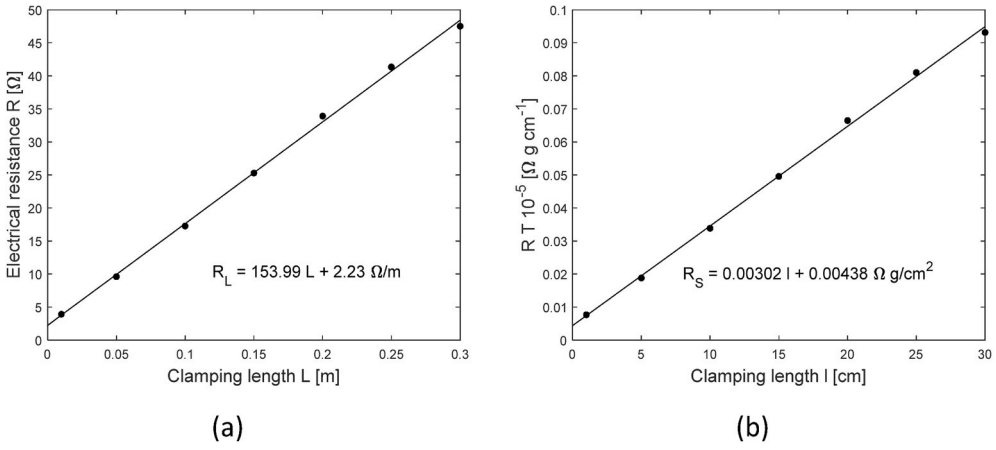

Fig. 7. Dependence of (a) electrical resistance and (b) electrical resistance when taking into account the carbon-roving fineness on clamping length.

analytical computation of the SE.

4.2. Physical dimensions of the reinforcements

Table 5 shows the $\bar{x}$, the *std*, and the $MOE_{0.95}$ used for the construction of the 95% confidence intervals (95% CI = $<\bar{x}- MOE_{0.95}; \bar{x}+ MOE_{0.95}>$) of the carbon-roving diameters (*2r*), which confirmed that the diameter of the coupled threads was not a simple multiple of the single thread since the individual rovings overlapped.

Table 6 shows the mean values, the standard deviations, and the margins of error of the means of the following variables: the area of a single aperture A_a [cm^2], the width of the aperture *w* [cm], the height of the aperture *h* [cm], and the porosity *P* [%] of the woven samples. As the table shows, the area of a single pore and the width and height of the apertures decreased with an increase in warp and weft setts (samples 1, 2, 5, 8, and 11), while the area of a single pore and the pore dimensions decreased with an increase in thread fineness in samples 2, 3, and 4. The porosity behaved in similar fashion, i.e., it decreased with an increase in warp and weft setts and decreased with an increase in thread fineness, as shown in Fig. 8. An examination of the width and height of the apertures indicated that the apertures were square in samples 1, 2, 3, and 5 since there was no statistically significant difference between their widths and heights. As shown in Table 6, the widths of the apertures in samples 4, 8, and 11 were only slightly higher than their heights. For this reason, we converted the aperture area A_a of all the samples to a square with side length *a*, which was used for the analytical SE computation.

4.3. Analysis of the electromagnetic shielding effectiveness of the reinforcements

Table 7 summarizes the experimentally measured mean values, standard deviations, and margins of error of the SE means for all the samples and the frequencies of 600 MHz, 1, 1.5, and 3 GHz. Here, it was clear that carbon roving reinforcements with a SE ranging from 9 to 45 dB at a frequency of 1.5 GHz were prepared.

4.4. Factorial design analysis

The results of the analysis of variance (ANOVA) for the factorial design are presented in Table 8. Here, *SS* is the sum of squares, *df* is the degrees of freedom, *MS* is the mean squared error, which is *SS/df* for each source of variation, the *F*-statistic is the ratio of the mean squared errors, and the *p*-value is the probability that the test statistic can take a value greater than the value of the computed test statistic. The SE was measured at a frequency of 1.5 GHz.

Here, it was clear that both factors, *A* (spacing) and B (diameter), were statistically significant since all of the *p*-values were below the significance level ($\alpha = 0.05$). Meanwhile, a two-factor interaction was also significant. The main effect of *A* dominated this process, accounting for over 75 % of the total variability, while the main effect of *B* accounted for around 20 % and the percentage contribution of the interaction was <1 %. A normal probability plot of the residuals and the other usual diagnostics indicated that both the normality and the constant variance assumptions were met. The spacing–diameter plot is shown in Fig. 9, with the main effect plots indicating that variable *A* had a negative main effect, i.e., an increase in the variable moved the electromagnetic SE upward, while variable *B* had a positive main effect. Overall, the main effect of the spacing was higher than that of the diameter.

The regression model that describes this experiment (first-order model with interactions) can be written in the following form:

$$SE = \beta_0 + \beta_1 A + \beta_2 B + \beta_{12} AB + \varepsilon, \quad (18)$$

where *SE* [dB] is the function fitted to a response, β_i is the regression coefficient to be estimated, *A* and *B* are the factors, and ε is the residual. The regression coefficients can be estimated using the least square method in this model, with the final equation having the following form:

$$SE = 20.58 - 1.01A + 8.25B \pm 0.31AB + \varepsilon. \quad (19)$$

Fig. 10 shows the three-dimensional response surface together with the contour plot for that case.

The obtained model (Equation (19)) could be also used to create a graphical representation of the experimental region. The resultant response-surface contour plot (Fig. 10) indicates how the response related to two continuous design variables. Here, it was clear that the higher the carbon roving diameter and the lower the carbon roving spacing (i.e., higher warp and weft sett), the higher the SE.

4.5. Effect of carbon roving spacing and carbon roving diameter on the electromagnetic shielding

Fig. 11a shows the dependence of the mean SE values on the frequency for samples 1, 2, 5, 8, and 11, with the shading around the mean values indicating their 95% intervals. Here, it was clear that the SE decreased slightly with an increase in frequency (decreasing wavelength) for all the samples, which was in accordance with the theoretical assumptions. It should be noted that the lowest examined frequency (30 MHz) corresponded to a wavelength of 10 m, while the highest measured frequency corresponded to a wavelength of 0.1 m, meaning the aperture length of all samples was small ($a < 1.8$ mm) in relation to the wavelength of the electromagnetic wave for the entire studied frequency range. It was also observed that the wider the carbon thread spacing *s* (the lower the aperture size *a*), the lower the SE ability of the sample. The sample with the lowest warp and weft sett was found to have the lowest SE ($SE = 9.5$ dB for $f = 1.5$ GHz), while that with the highest warp and weft sett had the highest SE ($SE = 45$ dB for $f = 1.5$ GHz). Meanwhile, the higher the spacing and porosity, the lower the carbon material consumption and the higher the air and water vapor permeability. Fig. 11b shows the dependence of the SE on the carbon roving at a certain frequency, i.e., 1.5 GHz, where, with an increase in *s*, the SE behavior was more visible. The solid line in this figure represents the data approximation using an exponential function with a high coefficient of determination ($R^2 = 0.99$). It should be noted that the specific spacing of the carbon threads, or the sett of the warp and the weft of the fabric, must be chosen in view of the requirements of the final application.

Fig. 12a shows the dependence of the SE on the frequency for samples 2, 3, and 4, i.e., those with different degrees of fineness in their warp and weft threads in the carbon rovings ($s = 15$ mm). Again, it was clear that the SE decreased slightly with an increase in frequency and that this was distinct over the entire frequency range, i.e., the greater the number of rovings forming the warp and weft threads, the greater the SE. Meanwhile, Fig. 12b shows the relationship between the SE and the number of rovings that made up the warp and weft threads for the frequency of 1.5 GHz, which could be approximated using a logarithmic function with a very good fit ($R^2 = 0.98$). The same behavior was also observed with the other sets of samples ($s = 10$ mm, $s = 5$ mm) with different degrees of warp and weft thread fineness.

Furthermore, the mechanism behind the shielding ability of the prepared carbon reinforcements intended for the formation of composites was investigated in terms of the chosen sample set. The SE

Table 5
Diameters of carbon threads (mean value, standard deviation and 95% confidence interval).

Sample	Thread diameter *2r* [mm]		
	$\bar{x}$	*std*	$MOE_{0.95}$
Single roving	1.95	0.29	0.13
Dual-coupled roving	3.12	0.81	0.38
Triple-coupled roving	4.18	1.76	0.82

Table 6
Characteristics of pores and porosity of samples.

Sample code	A_a [cm^2]			w [cm]			h [cm]			P [%]	a [cm]
	$\bar{x}$	*std*	$MOE_{0.95}$	$\bar{x}$	*std*	$MOE_{0.95}$	$\bar{x}$	*std*	$MOE_{0.95}$		
1	3.22	0.40	0.08	1.86	0.18	0.03	1.84	0.14	0.03	76.25	1.80
2	1.74	0.34	0.05	1.35	0.18	0.03	1.34	0.17	0.02	70.03	1.32
3	1.40	0.30	0.04	1.25	0.21	0.03	1.21	0.17	0.02	60.56	1.19
4	1.35	0.26	0.04	1.24	0.16	0.02	1.15	0.14	0.02	56.93	1.16
5	0.62	0.25	0.02	0.82	0.25	0.02	0.80	0.24	0.02	64.09	0.79
8	0.09	0.03	0.00	0.33	0.06	0.00	0.29	0.09	0.00	34.78	0.30
11	0.01	0.00	0.00	0.08	0.05	0.00	0.07	0.03	0.00	5.74	0.07

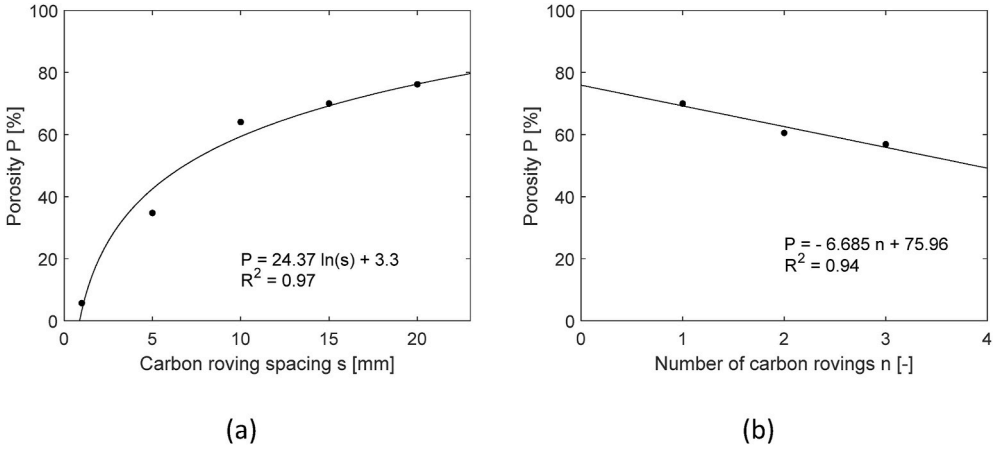

Fig. 8. Dependence of porosity on: (a) carbon roving spacing and (b) number of carbon rovings forming the weft and warp threads.

Table 7
Measured SE of all samples.

Sample code	Measured electromagnetic shielding effectiveness SE [dB]											
	f = 600 MHz			f = 1 GHz			f = 1.5 GHz			f = 3 GHz		
	$\bar{x}$	*std*	$MOE_{0.95}$	$\bar{x}$	*std*	$MOE_{0.95}$	$\bar{x}$	*std*	$MOE_{0.95}$	$\bar{x}$	*std*	$MOE_{0.95}$
1	13.90	0.39	3.45	9.85	0.88	2.18	9.49	0.31	0.78	4.06	0.30	0.75
2	16.60	0.34	0.84	19.58	0.90	2.25	20.34	1.20	2.98	14.00	0.86	2.13
3	21.13	1.53	3.81	18.07	0.48	1.20	16.95	0.49	1.23	10.90	0.58	1.46
4	22.74	1.25	3.11	12.44	1.98	4.91	13.21	1.78	4.42	7.49	1.63	4.07
5	23.01	0.54	1.35	29.07	0.59	1.48	28.61	0.42	1.06	22.59	0.13	0.33
6	28.25	0.43	1.08	24.58	0.45	1.14	24.04	0.35	0.87	17.63	0.06	0.17
7	31.09	0.56	1.40	19.54	1.19	2.95	18.78	1.24	3.08	12.49	1.20	2.99
8	34.77	0.57	1.43	43.44	0.80	2.01	42.60	1.03	2.56	37.59	0.75	1.86
9	42.09	0.06	0.17	38.61	0.30	0.74	37.71	0.66	1.64	32.37	0.50	1.25
10	46.81	0.40	1.00	30.41	0.46	1.16	29.11	0.45	1.12	23.78	0.44	1.10
11	45.00	0.92	2.30	44.41	1.23	3.06	45.01	0.63	1.57	31.94	3.31	8.24

Table 8
Analysis of variance for the factorial design.

Source	*SS*	Percent Contribution	*df*	*MS*	*F*	*p-value*
A	1784.3	78.65	2	892.148	952.26	0
B	467.28	20.60	2	249.38	249.38	0
A*B	33.94	0.75	4	9.06	9.06	0.0003
Error	16.86		18			
Total	2302.38		26			

effectiveness through absorption (A) and reflection (R) was calculated (in dB) based on the measured scattering parameters S_{21} and S_{11} according to Equation (1) for samples 1, 2, 5, 8, and 11, with the results presented in Fig. 13. It should be noted that the lower the spacing of the carbon rovings s in the woven reinforcement, the higher the SE through R. It was also observed that the R underwent an almost linear decrease with an increase in frequency. Meanwhile, the SE through A variation with an increase in frequency was extremely small. Much like with R, the A increased with a reduction in spacing s. On comparing the mean values of A and R over the entire frequency range, it was clear that R was the dominant mechanism for samples 1, 2, and 8, while for samples 5 and 11, A was the main contributor to the SE.

4.6. Analytical computation of electromagnetic shielding

As carbon roving reinforcement is considered to be a metal mesh, we analytically computed the SE using Equations (5)–(11). In terms of input variables, we used the mean aperture width a [m] (see Table 6), the mean conductivity of the carbon roving $\sigma = 5.80 \cdot 10^4$ S/m (see Table 4), and the mean diameter of the carbon roving $2r$ [m] (see Table 5). Thus, in addition to the physical dimensions of the mesh (wire/roving diameter, aperture width) and its conductivity, the analytical approach

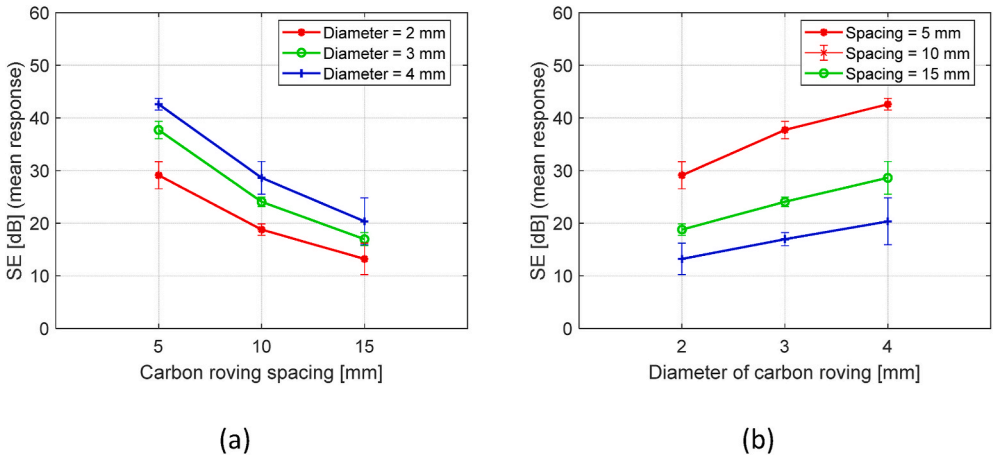

Fig. 9. Dependence of SE on: (a) carbon roving spacing and (b) diameter of carbon rovings forming the weft and warp threads.

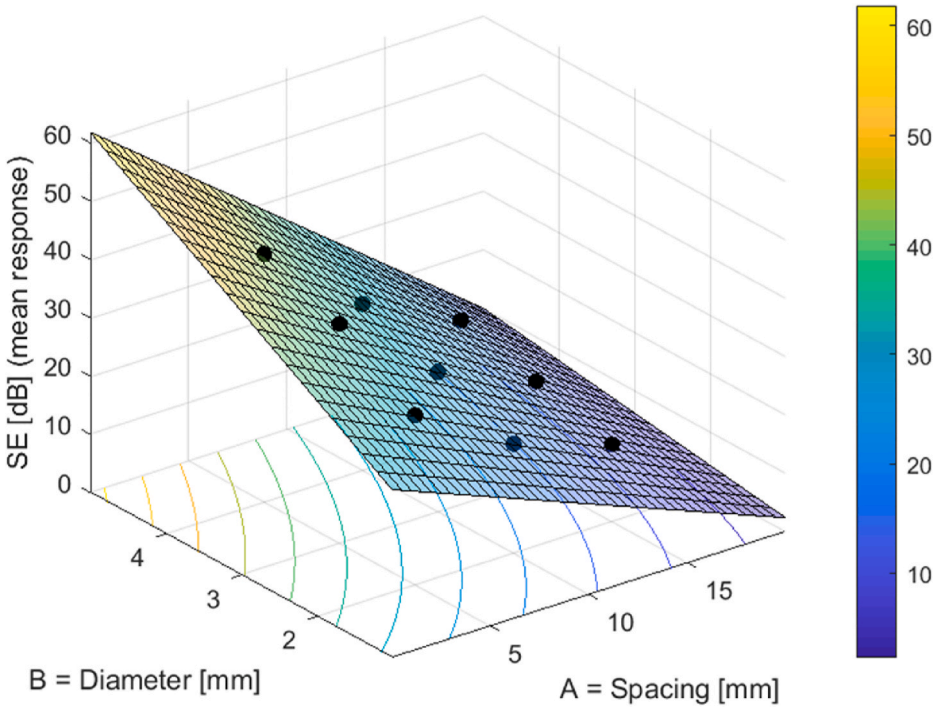

Fig. 10. The response surface graph for dependent variable SE ($f = 1.5$ GHz).

incorporated the dependence of the SE values on both the angle of incidence and the frequency.

To explore the dependence of the SE behavior on the frequency and the angle of incidence, we calculated and plotted the polarization-independent SE for sample 1 (using Equation (5)). As Fig. 14 shows, the sample SE was significantly lower for fields with higher incidence angles than for fields with incidences normal to the surface ($\theta = 0°$), while it was also clear that a higher frequency resulted in a lower SE.

As reported in Ref. [27], the output data must be modified to enable comparisons with the experimental data, especially when using the experimental method we selected to evaluate the SE. To use the coaxial transmission line method to measure the SE, it was assumed that the angle of incidence of the fields relative to the inserted sample was randomized, which was why we calculated the arithmetic mean of the inner sum in Equation (5) (over the angles of incidence in the interval $<-\pi/2 : \pi/2>$) prior to taking the logarithm, as described by the following equation:

$$SE_{tot} = 10 \log_{10}\left\{\frac{1}{n}\sum_{i=1}^{n}\left(\frac{1}{2}|T_1(\omega,\theta)|^2 + \frac{1}{2}|T_2(\omega,\theta)|^2\right)\right\}. \quad (20)$$

Using the assumption described above, we used the average of the angle of incidence for each frequency and the computed SEs, as shown in Table 9, for four chosen frequencies representing the entire frequency range.

4.7. Comparison of calculated and experimentally verified electromagnetic shielding effectiveness values

Fig. 15 shows a comparison of the experimental values and the analytically computed SE values for the basic set of samples. The shaded areas around the mean values show the 95% confidence intervals of the means for the measured and modelled curves. Here, there was excellent agreement between the predicted and experimentally measured values, especially for samples with a higher porosity (samples 1–5 and sample 8,

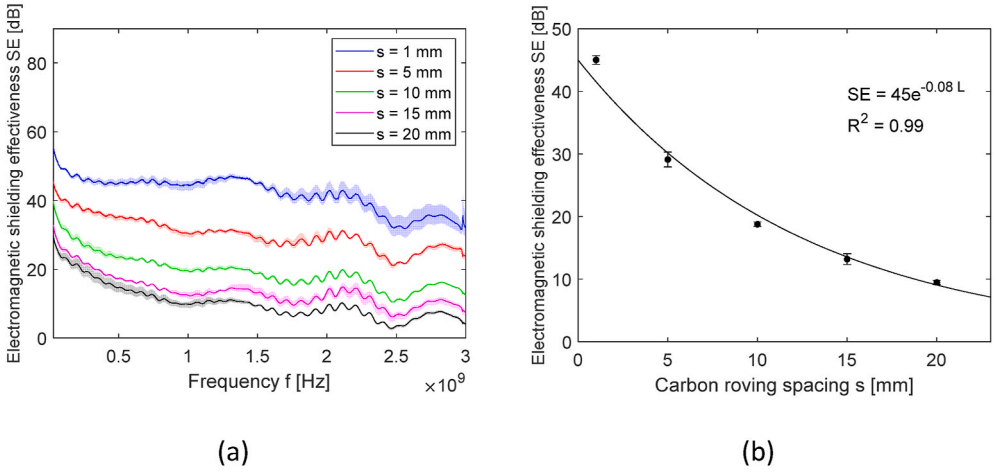

Fig. 11. Dependence of SE on (a) frequency and (b) carbon-roving spacing (f = 1.5 GHz) for samples 1,2,5,8 and 11.

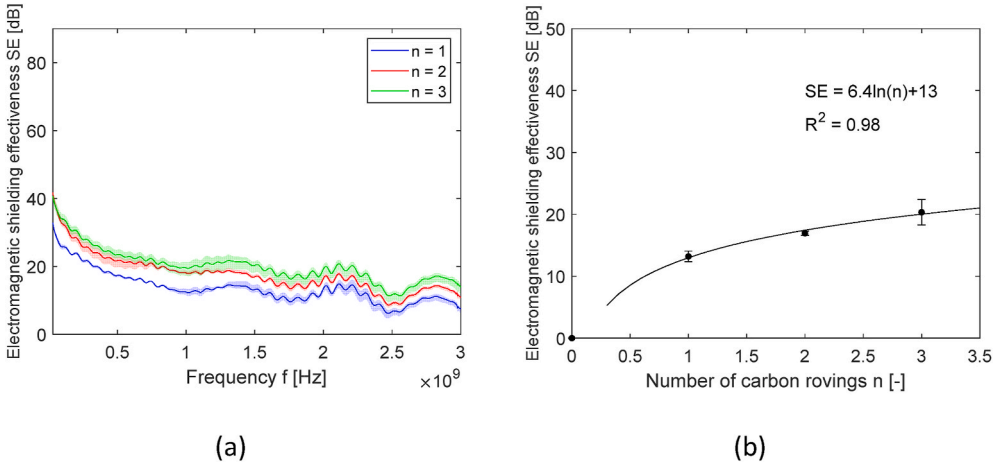

Fig. 12. Dependence of SE on (a) frequency and (b) a number of carbon rovings (f = 1.5 GHz) for samples 2, 3, and 4.

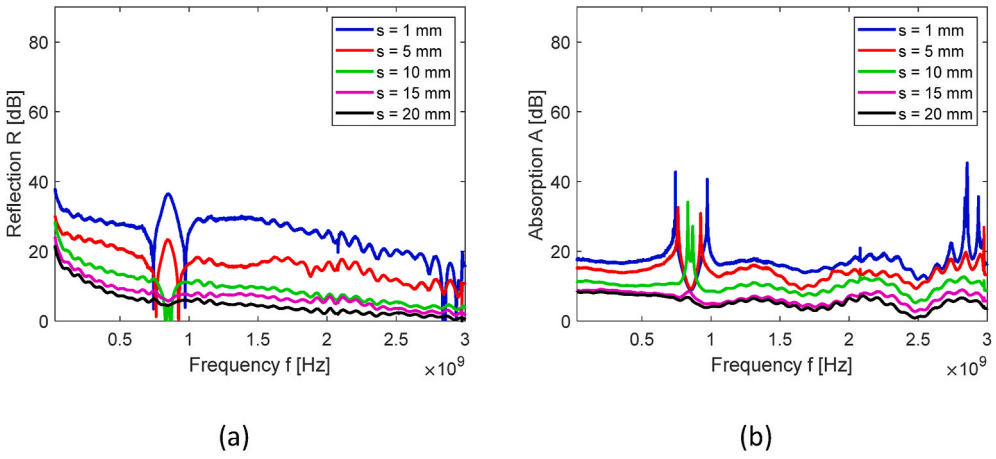

Fig. 13. Dependence of electromagnetic shielding by (a) reflection R, (b) absorption A on frequency for samples 1, 2, 5, 8, and 11.

when $P > 30$ %). In addition, the modelled data effectively followed the trend of the SE decreasing with an increase in frequency. A large difference between the experimental values and the analytically calculated data was observed for sample 11, which had a compact structure, a porosity of approximately 5%, and an aperture width of only 0.7 mm. For this compact sample, the model was suitable only for SE prediction for higher frequencies (f > 2.5 GHz), which confirms that the model is appropriate for extremely porous wire meshes. However, we also found that this simple model based on only a few parameters can be used for woven structures made of electrically conductive warp and weft threads that have sufficiently high porosity.

To numerically express the difference between the experimental

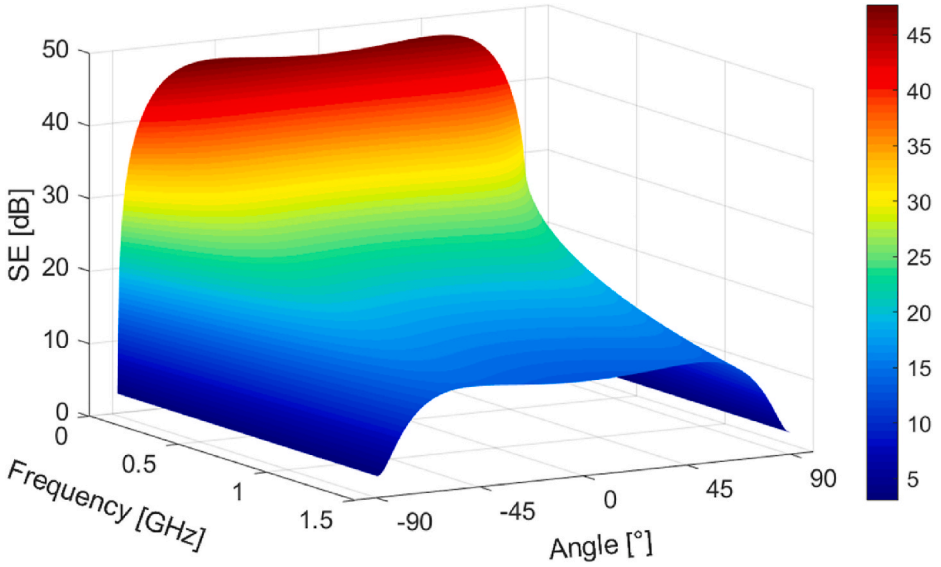

Fig. 14. Electromagnetic shielding effectiveness *SE* as a function of frequency *f* and angle of incidence θ for sample 1.

Table 9
Predicted SEs for all samples.

Sample code	Predicted electromagnetic shielding effectiveness SE [dB]							
	$f = 600$ MHz		$f = 1$ GHz		$f = 1.5$ GHz		$f = 3$ GHz	
	$\bar{x}$	$MOE_{0.95}$	$\bar{x}$	$MOE_{0.95}$	$\bar{x}$	$MOE_{0.95}$	$\bar{x}$	$MOE_{0.95}$
1	16.14	0.18	13.19	0.19	11.03	0.20	7.26	0.20
2	18.72	0.18	15.93	0.19	13.88	0.20	10.18	0.21
3	21.43	0.32	18.78	0.33	16.86	0.35	13.37	0.37
4	23.41	1.13	20.86	1.18	19.01	1.23	15.68	1.32
5	23.18	0.26	20.61	0.27	18.75	0.28	15.41	0.30
8	32.42	0.45	30.81	0.62	29.42	0.68	26.78	0.75
11	33.98	0.00	33.98	0.00	33.98	0.00	33.98	0.00

values and the model, we computed the mean absolute error (MAE) [40] for all frequencies (200 points in the frequency range 30 MHz–3 GHz), as shown in Table 10. Statistically, the MAE is a measure of errors between paired observations of the same phenomenon, and can be defined as follows:

$$MAE = \frac{\sum_{i=1}^{n} \left| SE_{analytical} - SE_{experiment} \right|}{n}. \quad (21)$$

As Table 10 shows, for all the samples apart from sample 11, the MAE was <3 dB, which confirmed the suitability of the model for porous woven samples made of conductive warp and weft threads. In addition, the random error of the coaxial transmission line method, as reported in the standard (see Ref. [23]), was ±5 dB. Therefore, the MAEs of all the samples used in this study (except sample 11) were within the range of the random error of the measurement method.

5. Conclusion

In this paper, we investigated the CF reinforcements used in the preparation of SE epoxy composites. A total of seven plain-weave samples were created using carbon roving (fineness of single carbon roving $T = 196$ tex) for the weft and warp threads. The samples differed in the two following respects: warp and weft sett (spacing between threads) and warp and weft thread thickness (by combining two and three carbon rovings).

First, we experimentally determined the SE efficiency according to the ASTM 4935-18 standard in terms of a frequency range of 30 MHz–3 GHz before we studied the effect of the warp and weft sett and the warp and weft thread thickness on the SE. As expected, the sample with the lowest warp and weft sett was found to have the lowest SE (SE = 9.5 dB for $f = 1.5$ GHz), while that with the highest warp and weft sett had the highest SE (SE = 45 dB for $f = 1.5$ GHz). The dependence of SE on the carbon roving spacing can be described using an exponential function. A slight increase in the SE can also be achieved by increasing the thickness of the weft and warp yarns.

Next, we tested the suitability of applying an extremely simple analytical model to predict the effect of reinforcements on the SE. For this purpose, we used image analysis to determine the geometric dimensions of the reinforcements (aperture width a) and carbon rovings (diameters of weft and warp threads $2r$). Meanwhile, we measured the electric conductivity (σ) of the carbon roving using the two-probe method, excluding the contact resistances at the interfaces of the material and both electrodes. These input variables were substituted into specific equations obtained from the literature, which were originally intended for the analytical determination of the SE of a planar wire-mesh screen with bonded junctions. We selected this simple analytical solution due to the geometric similarity of the structure of the porous plain weave and that of the wire mesh.

Our results indicated that this simple analytical model for determining the SE works well on highly porous woven reinforcements made of carbon roving for given frequency bands and with the experimental measurement of SE using the ASTM 4935-18 standard method. The MAE between the measured and modelled data was less than the random error of the method used to measure the SE. In addition, it was found that averaging all the angles of incidence presents a good solution for randomization in the coaxial transmission line measurement method for

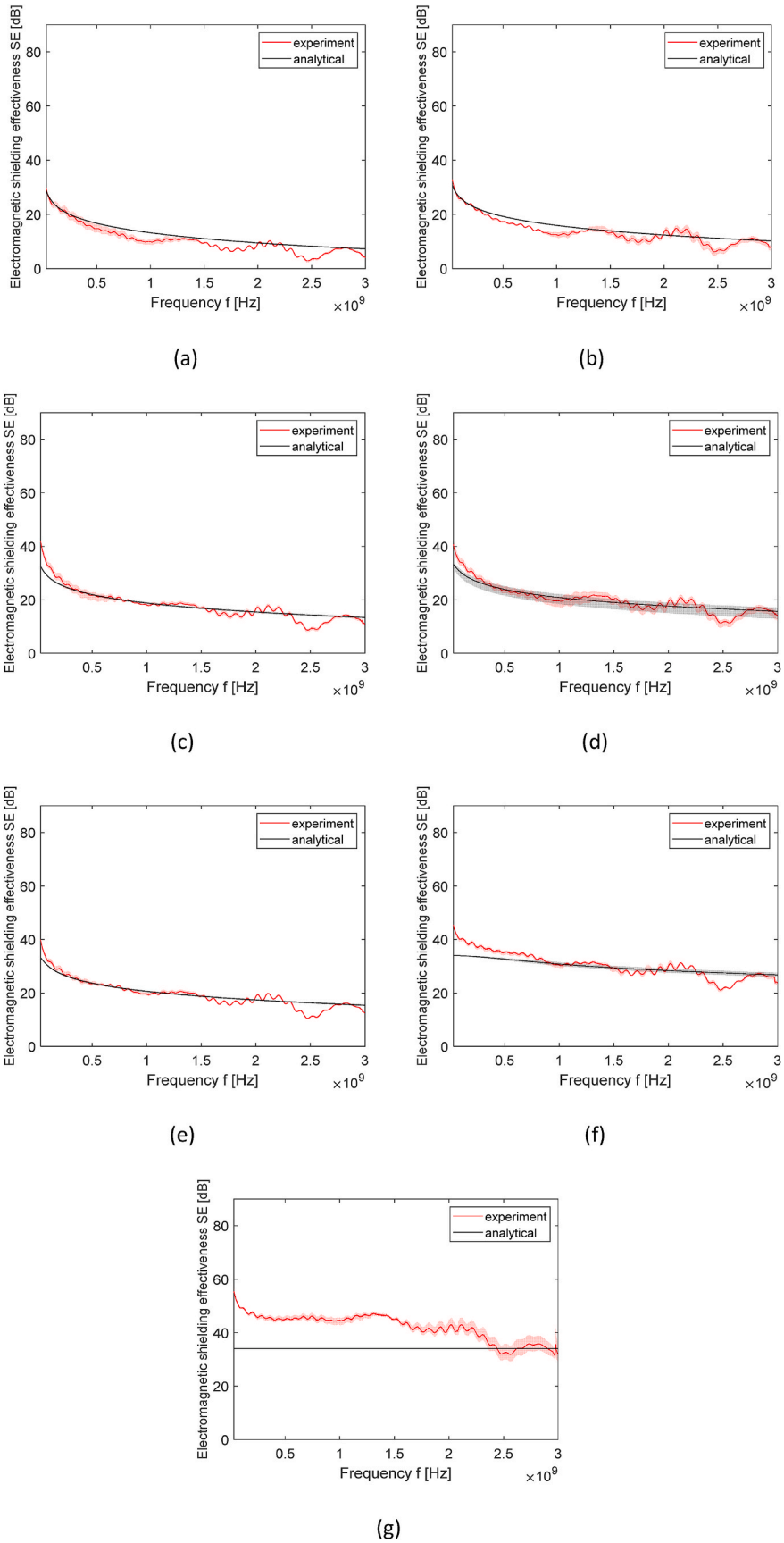

Fig. 15. Dependence of SE on frequency for the experimental and analytical data for the whole sample set: a–g: samples 1–5, 8, 11.

Table 10
Mean absolute error between experimental and modelled data.

Sample code	MAE [dB]
1	1.95
2	1.69
3	1.31
4	1.44
5	1.23
8	2.04
11	8.34

SE. It can also be stated that the tested simulation could be suitable for predicting the SE with other textile structures, especially woven fabrics made from electrically conductive yarns forming both the warp and weft system, while the high porosity may be a limiting factor.

Using the analytical SE solution, low cost, porous carbon woven reinforcements that are permeable to air and water vapor can be designed and obtained to produce epoxy composites with the desired SE. Various applications in the aircraft industry, including large, shielded enclosures and shielding for cable trenches could be interesting applications for these composites.

Author statement

Veronika Tunakova - conceptualization, methodology, experimental, original draft preparation.

Maros Tunak - data curation, visualization, software.

Declaration of competing interest

The authors declare that they have no known competing financial interests or personal relationships that could have appeared to influence the work reported in this paper.

Acknowledgements

This work was a supported research project CZ.01.1.02/0.0/0.0/15_019/0004465 entitled Extreme shielding textile materials for special applications granted by the Ministry of Industry and Trade of the Czech Republic and the Ministry of Education, Youth and Sports of the Czech Republic and the European Union – European Structural and Investment Funds in the frames of Operational Programme Research, Development and Education – project Hybrid Materials for Hierarchical Structures (HyHi, Reg. No. CZ.02.1.01/0.0/0.0/16_019/0000843).

References

[1] Q. Xiao, Z. Chen, J. Liao, Y. Li, L. Xue, T. Guan, Electromagnetic interference shielding performance and mechanism of Fe/Al modified SiC/SiC composites, J. Alloys Compd. 887 (2021) 161359, https://doi.org/10.1016/j.jallcom.2021.161359.

[2] X. Zhang, X. Wang, P. Sha, B. Wang, Y. Ding, S. Du, High-efficiency electromagnetic wave absorption of epoxy composites filled with ultralow content of reduced graphene/carbon nanotube oxides, Compos. Sci. Technol. 189 (2020) 108020, https://doi.org/10.1016/j.compscitech.2020.108020.

[3] B.D.S. Deeraj, G. George, N.R. Dhineshbabu, S. Bose, K. Joseph, Electrospun ZrO2@carbon nanofiber mats and their epoxy composites as effective EMI shields in Ku band, Mater. Res. Bull. 144 (2021) 111477, https://doi.org/10.1016/j.materresbull.2021.111477.

[4] D.D.L. Chung, Electromagnetic interference shielding effectiveness of carbon materials, Carbon 2 (2001) 279–285, https://doi.org/10.1016/S0008-6223(00)00184-6.

[5] W.S. Jou, The hight electromagentic shielding of woven carbon fiber composites appiled to optoelectronics devices, in: CLEO/Pacific Rim 2003. The 5th Pacific Rim Conference on Lasers and Electro-Optics, IEEE Cat. No.03TH8671), Taipei, Taiwan, 2003, p. 755, https://doi.org/10.1109/CLEOPR.2003.1277291.

[6] W.S. Jou, T.L. Wu, S.K. Chiu, W.H. Cheng, The influence of fiber orientation on electromagnetic shielding in liquid-crystal polymers, J. Electron. Mater. 3 (2002) 178–184, https://doi.org/10.1007/s11664-002-0203-7.

[7] B. Wen, X. Wang, Y. Zhang, Ultrathin and anisotropic polyvinyl butyral/Ni-graphite/short-cut carbon fibre film with high electromagnetic shielding performance, Compos. Sci. Technol. 169 (2019) 127–134, https://doi.org/10.1016/j.compscitech.2018.11.013.

[8] C. Unterweger, T. Mayrhofer, F. Piana, J. Duchoslav, D. Stifter, C. Poitzsch, C. Fürst, Impact of fiber length and fiber content on the mechanical properties and electrical conductivity of short carbon fiber reinforced polypropylene composites, Compos. Sci. Technol. 188 (2020) 107998, https://doi.org/10.1016/j.compscitech.2020.107998.

[9] S. Hwang, Tensile, electrical conductivity and EMI shielding properties of solid and foamed PBT/carbon fiber composites, Compos. B Eng. 98 (2016) 1–8, https://doi.org/10.1016/j.compositesb.2016.05.028.

[10] P.B. Jana, A.K. Mallick, S.K. De, Effects of sample thickness and fiber aspect ratio on EMI shielding effectiveness of carbon fiber filled polychloroprene composites in the X-band frequency range, I.E.E.E. Trans. Electromagn. Compat. 34 (1992) 478–481, https://doi.org/10.1109/15.179281.

[11] M. Rahaman, T.K. Chaki, D. Khastgir, Shielding with conductive polymer and carbon fiber composites, Plast. Res. 3 (2012), https://doi.org/10.1002/spepro.003964.

[12] W.S. Jou, A novel structure of woven continuous-carbon fiber composites with high electromagnetic shielding, J. Electron. Mater. 33 (2004) 162–170, https://doi.org/10.1007/s11664-004-0175-x.

[13] X. Luo, D.D. Chung, Electromagnetic interference shielding using continuous carbon-fiber carbon-matrix and polymer-matrix composites, Compos. B Eng. 30 (3) (1999) 227–231, https://doi.org/10.1016/S1359-8368(98)00065-1.

[14] S. Das, T. Yokozeki, A brief review of modified conductive carbon/glass fibre reinforced composites for structural applications: lightning strike protection, electromagnetic shielding, and strain sensing, Composites Part C: Open Access 5 (2021) 100162, https://doi.org/10.1016/j.jcomc.2021.100162.

[15] M.C. Lin, J.H. Lin, L. Bao, Applying TPU blends and composite carbon fibers to flexible electromagnetic-shielding fabrics: long-fiber-reinforced thermoplastics technique, Compos. A 138 (2020), https://doi.org/10.1016/j.compositesa.2020.106022.

[16] D. Munalli, G. Dimitrakis, D. Chronopoulos, S. Greedy, A. Long, Electromagnetic shielding effectiveness of carbon fibre reinforced composites, Compos. B Eng. 173 (2019) 106906, https://doi.org/10.1016/j.compositesb.2019.106906.

[17] S. Zhu, R. Shi, M. Qu, J. Zhou, C. Ye, L. Zhang, H. Cao, D. Ge, Q. Chen, Simultaneously improved mechanical and electromagnetic interference shielding properties of carbon fiber fabrics/epoxy composites via interface engineering, Compos. Sci. Technol. 207 (2021), https://doi.org/10.1016/j.compscitech.2021.108696.

[18] D. Su, H. Liu, S. Yang, Z. Zhao, D. Sui, An analytical method for calculating the shielding effectiveness of an enclosure with an oblique rectangular aperture, Chin. J. Electron. 28 (2019) 850–854, https://doi.org/10.1049/cje.2019.02.006.

[19] S.I. Mıstık, E. Sancak, S. Ovalı, M. Akalın, Investigation of electromagnetic shielding properties of boron, carbon and boron–carbon fibre hybrid woven fabrics and their polymer composites, J. Electromagn. Waves Appl. 31 (2017) 1289–1303, https://doi.org/10.1080/09205071.2017.1348257.

[20] G. Pamuk, Ö. Kayacan, O. Kayacan, Ş. Seçkin Uğurlu, Electromagnetic shielding effectiveness of carbon yarn-based woven fabrics, J. Ind. Textil. (2019) 1–18, https://doi.org/10.1177/1528083719896769. Article in Press.

[21] S.E. Lee, K.Y. Park, K.S. Oh, C.G. Kim, The use of carbon/dielectric fiber woven fabrics as filters for electromagnetic radiation, Carbon 47 (2009) 1896–1904, https://doi.org/10.1016/j.carbon.2009.02.013.

[22] W. Shen, S. Wang, W. Li, H. Jin, H. Zhang, An Extended hybrid analytical model for the shielding effectiveness prediction of a multi-cavity structure with numerous apertures', Prog. Electromagn. Res. M 96 (2020) 181–190, https://doi.org/10.2528/PIERM20081201.

[23] M.P. Robinson, T.M. Benson, C. Christopoulos, J.F. Dawson, M.D. Ganley, A. C. Marvin, S.J. Porter, D.W.P. Thomas, Analytical formulation for the shielding effectiveness of enclosures with apertures, I.E.E.E. Trans. Electromagn. Compat. 40 (1998) 240–248, https://doi.org/10.1109/15.709422.

[24] S. Rea, D. Linton, E. Orr, J. McConnell, Electromagnetic shielding properties of carbon fibre composites in avionic systems, Microw. Rev. (2005) 29–32.

[25] V. Šafářová, M. Tunák, J. Militký, Prediction of hybrid woven fabric electromagnetic shielding effectiveness, Textil. Res. J. 85 (2015) 673–686, https://doi.org/10.1177/0040517514555802.

[26] M. Neruda, L. Vojtech, Electromagnetic shielding effectiveness of woven fabrics with high electrical conductivity: complete derivation and verification of analytical model, Materials 11 (2018) 1657, https://doi.org/10.3390/ma11091657.

[27] D. Mansson, A. Ellgardt, Comparing analytical and numerical calculations of shielding effectiveness of planar metallic meshes with measurement in cascaded reverberation chambers, Prog. Electromagn. Res. C 31 (2012) 123–135, https://doi.org/10.2528/PIERC12061506.

[28] P. Karimi, M. Ostoja-Starzewski, I. Jasiuk, Experimental and computational study of shielding effectiveness of polycarbonate carbon nanocomposites, J. Appl. Phys. 120 (2016) 145103, https://doi.org/10.1063/1.4964691.

[29] V. Šafářová, M. Tunák, J. Militký, Prediction of hybrid woven fabric electromagnetic shielding effectiveness, Textil. Res. J. 85 (2015) 673–686, https://doi.org/10.1177/0040517514555802.

[30] H.W. Ott, H.W. Ott, Electromagnetic Compatibility Engineering, John Wiley & Sons, Hoboken, N.J, 2009.

[31] A.R. Henn, R.M. Cribb, Modeling the shielding effectiveness of metallized fabrics, in: International Symposium on Electromagnetic Compatibility, 1992, pp. 283–286, https://doi.org/10.1109/ISEMC.1992.626095. Anaheim, CA.

[32] M. Neruda, L. Vojtech, Electromagnetic shielding effectiveness of woven fabrics with high electrical conductivity: complete Derivation and verification of analytical model, Materials 11 (2018) 1657, https://doi.org/10.3390/ma11091657.
[33] K.F. Casey, Electromagnetic shielding behavior of wire-mesh screens, I.E.E.E. Trans. Electromagn. Compat. 30 (1988) 298–306, https://doi.org/10.1109/15.3309.
[34] W.E. Morton, J.W.S. Hearle, Physical Properties of Textile Fibres, CRC Press [u.a.], Boca Raton, Fla, 2008, 4.
[35] D.C. Montgomery, Design and Analysis of Experiments, tenth ed., Wiley, Hoboken, NJ, 2020.
[36] Sist En 16812, Textiles and textile products - electrically conductive textiles - determination of the linear electrical resistance of conductive tracks, ITEK (2016). https://standards.iteh.ai/catalog/standards/sist/7898845e-5fb2-4699-8671-10b7fadae459/sist-en-16812-2016, 2016. Accessed: Feb. 27, 2021.
[37] V. Safarova, L. Hes, J. Militky, An approach to electrical resistance measurement eliminating contact resistance problem, in: 2014 International Conference on Applied Electronics, Pilsen, Czech Republic, 2014, pp. 259–262, https://doi.org/10.1109/AE.2014.7011715.
[38] R.C. Gonzalez, R.E. Woods, Digital Image Processing, fourth ed., Global edition, Pearson, New York, NY, 2018.
[39] ASTM 4935-18, Test method for measuring the electromagnetic shielding effectiveness of planar materials, J. ASTM Int. (JAI) (2018), https://doi.org/10.1520/D4935-18.
[40] A. Stetco, F. Dinmohammadi, X. Zhao, V. Robu, D. Flynn, M. Barnes, J. Keane, G. Nenadic, Machine learning methods for wind turbine condition monitoring: a review, Renew. Energy 133 (2019) 620–635, https://doi.org/10.1016/j.renene.2018.10.047.

Appendix 2

V. Tunakova, M. Tunak, P. Tesinova, M. Seidlova, and J. Prochazka, "Fashion clothing with electromagnetic radiation protection: aesthetic properties and performance," vol. 90, no. 21, pp. 2504–2521, 2020.

Textile Research Journal

Original article

Textile Research Journal
2020, Vol. 90(21–22) 2504–2521

DOI: 10.1177/0040517520923047
journals.sagepub.com/home/trj
SAGE

Fashion clothing with electromagnetic radiation protection: aesthetic properties and performance

Veronika Tunakova[1], Maros Tunak[1], Pavla Tesinova[1], Marie Seidlova[1] and Jiri Prochazka[2]

Abstract

At present, much attention is focused on developing clothing fabrics with advanced functionality without compromising their visual, mechanical, or comfort properties. A fabric's ability to prevent the penetration of electromagnetic radiation is an interesting added feature. In the published literature, there are many references describing the development and investigation of electromagnetic shielding textile structures using different electrically conductive additives. However, little attention has been given to the aesthetic and comfort properties of these special fabrics. Moreover, the availability of everyday fashion containing electromagnetic radiation protection is very limited. For this study, woven fabric made from a mixture of traditional fibers and extremely thin discrete stainless steel fibers developed in the authors' previous research was used as a substrate. The fabric was digitally printed to provide an interesting design effect suitable for use in clothing and for making clothes for everyday wear. The main objective of this work is to determine whether digital printing is a suitable tool for changing the color and pattern of this metal fiber-containing fabric. The individual goals are (a) to examine the fabric's color fastness to washing and (b) to investigate whether the surface modification of the fabric adversely affects its functionality. Results show that it is possible to change the color and pattern of metal fiber-containing fabric by digital printing easily, whereas the associated decrease of porosity causes an increase of this special fabric functionality. The electromagnetic shielding effectiveness of the fabric after printing is around 33 dB for frequency 1.5 GHz. However, washing has a negative effect, causing both the electromagnetic shielding ability decrease (to 27 dB for frequency 1.5 GHz after 20 washing and drying cycles) and color fading (the color fastness grade is around 1–2 after 20 washing and drying cycles). Furthermore, the basic transport properties of printed electrically conductive fabric are compared with those of fabric made from traditional material and positive results are found. The incidence of pilling after washing is also evaluated, whereas the first pills are observed after the eighth washing and drying cycle. Finally, clothing prototypes that could be prepared from printed fabric are presented.

Keywords

digital printing, durability, color fastness, comfort, electromagnetic radiation, protective clothing

Electrically conductive textiles are no longer an unknown quantity in the textile industry. These special textiles are mainly used in antistatic applications, in smart textiles, and especially for achieving shielding from electromagnetic (EM) radiation. Besides technical applications, electrically conductive textiles are often developed for the design of protective clothing, which is defined according to Mao[1] as "any device or appliance designed to be worn or held by an individual for protection against one or more health and safety hazards."

[1]Faculty of Textile Engineering, Technical University of Liberec, Czech Republic
[2]Sintex, a.s., Czech Republic

Corresponding author:
Veronika Tunakova, Faculty of Textile Engineering, Technical University of Liberec, Studentska 2, Liberec 463 17, Czech Republic.
Email: veronika.tunakova@tul.cz

EM radiation cannot be avoided as it comes from both natural and artificial sources. There is no doubt that EM fields have biological effects;[2] however, there is still not enough knowledge about the extent to which these effects are reversible and when they are irreversible and harmful to health. The use of EM radiation-emitting devices (radio and TV transmitters, mobile phones, radars, medical, diagnostic devices, etc.) makes life not only easier but also more pleasant. In short, human existence is not possible without them. However, in 2011, the World Health Organization in cooperation with the International Agency for Research on Cancer classified radio-frequency EM radiation into Group 2B, with potentially carcinogenic effects to humans.[2] This decision was made despite the lack of convincing evidence of the radiation's carcinogenicity, but currently, this possibility cannot be ignored.

For the above reasons, the demand for protective clothing of this type is relatively high, especially from a preventive point of view. In particular, this is applicable for casual wear intended for specific groups of people, which include people living with a pacemaker, workers who are exposed to EM radiation, people who are increasingly susceptible to EM radiation, pregnant women, and young children. When designing any clothing system, the specific requirements for aesthetics, functionality, thermophysiological comfort (including mobility), and durability should be considered; functionality (protection) together with thermophysiological comfort properties is the fundamental requirement for any protective clothing.[1]

As stated by Shi et al.,[3] aesthetic properties (including fashion, color, and style) should also be considered when designing protective clothing for daily use. Price is another important consideration in introducing clothing with EM radiation protection to the market.

To shield from EM fields, the very basic requirement for textile materials is to have a sufficient conductive component content in its structure. Currently, most of the traditionally used textile fibers in the clothing industry electrically insulate in a dry state, which means fabrics made from traditional textile fibers are transparent to EM fields and offer no protection to the wearer.

At present, the use of very fine electrically conductive fibers (metal fibers or metal-coated fibers) in staple or filament lengths[4–6] is a popular way of incorporating the conductive component into the textile structure. These fibers can be mixed with traditional textile fibers (both natural and synthetic) to prepare electrically conductive yarns with the desired level of electrical conductivity while preserving positive mechanical and manufacturing properties. From these electrically conductive yarns, woven or knitted fabrics with EM shielding abilities can be easily prepared. Staple length fibers are preferred over filament fibers, especially when preparing fabrics for clothing purposes; staple length fiber-based textile structures have better thermophysiological comfort properties. Due to the substance of a traditional fiber, its appearance is promising. Its color can be changed using different colored nonconductive fibers (colors for metal or metal-coated fibers are very limited), and the finished fabric can be dyed, printed, etc.

It is essential to note that the following fiber and fabric properties should be acknowledged when designing electrically conductive protective clothing for daily use: (a) all used fibers should be fine ($t < 1$ tex); (b) fabrics should be lightweight ($GSM < 250\,\mathrm{g/m^2}$); (c) fabrics should have low resistance to bending and shearing to guarantee deformability and a pleasant drape; (d) fabrics should satisfy the overall requirements for clothing comfort, including air and water vapor permeability; and (e) fabrics should be washable without loss of functionality (e.g., EM shielding ability).

It is possible to characterize the performance EM shielding effectiveness (SE) of the EM shield

$$SE = 10\log\frac{P_t}{P_i} = 20\log\frac{E_t}{E_i} = 20\log\frac{H_t}{H_i}\ [\mathrm{dB}] \quad (1)$$

where H_t, E_t, and P_t are the electric field strength, magnetic field strength, and EM field density values measured in the presence of the textile material, respectively. H_i, E_i, and P_i are the same values measured without the textile material. Requirements for EM SE of protective textiles are given in FTTS-FA-003:2005,[7] where class I contains textiles for professional use and class II represents textiles for general use (including casual wear, office uniforms, maternity dresses, and aprons). The grading of textiles with EM shielding ability for general use (class II) according to FTTS-FA-003:2005[7] is presented in Table 1.

There is no question that the color, design, visual texture, and feel of the fabric are most likely to attract a consumer to an item of clothing or fabric. That is why changing the visual characteristics of fabrics according to consumer expectations and thus increasing the added value of newly developed fabrics with special functions are important.[8] In the case of electrically conductive textiles where metal or metal-coated fibers are incorporated into the yarn structure, two major methods for affecting the appearance of the fabric are available. The preparation of yarns with different properties, such as color and fineness, and their use during the production of fabric by weaving and knitting is one of the methods. However, this approach is not flexible enough, especially when it is necessary to prepare special conductive

Table 1. Grading of electromagnetic shielding fabrics for general use

Grade	5 Excellent	4 Very good	3 Good	2 Moderate	1 Fair
SE [dB]	$SE > 30$	$30 \geq SE > 20$	$20 \geq SE > 10$	$10 \geq SE > 7$	$7 \geq SE > 5$

yarns with different properties. Moreover, the application of original forms, text, and designs to the product is very limited during patterning by weaving and knitting.

Design-oriented finishing, including bleaching, dyeing, and printing, is a technique that is applied on a gray cloth directly after it is woven or knitted; this offers another option for affecting the visual characteristics of the electrically conductive fabrics. While the whole fabric is uniformly covered (usually with one color during dyeing) in the printing process, repeated patterns are printed all over or on a certain part of the fabric, creating sharply defined print patterns using one or more colors. Digital fabric printing is a new and innovative process, where a pattern or an image from a digital file is transferred onto fabric using inkjet-based printers. There are two main digital printing methods: sublimation digital printing and direct digital printing.

In addition to the development of new lightweight high-efficiency fiber-based EM shielding materials, there is increased focus on the preparation of protective clothing made of composite fabrics containing thin metal or metal-coated fibers and traditional fibers. Several types of metal composite fabrics have been described and applied in personal protective clothing, especially for the protection of workers in environments with increased levels of EM radiation.[9–15] However, little attention has been given to the design and enhancement of the properties of these special fabrics intended for casual wear where functionality is not the only thing to be considered.

Bahadir et al.[16] investigated the dyeing of cotton (CO) fabrics with incorporated stainless steel yarns. Two different dyeing profiles with different concentrations were applied to the bleached substrate, and the color change and linear electrical resistance were evaluated. It was discovered that dyeing has a significant negative effect on conductive yarns and, at the same time, the presence of electrically conductive yarns retards the dyeing process.[16] Tunakova et al.[17] studied laser patterning of metal composite fabric. It can be concluded that laser patterning is a valuable tool in transferring certain designs onto electrically conductive fabric, while its functionality is even increased due to the partial carbonization of textile fibers. However, the mechanical properties of laser-patterned fabric decrease, which significantly limits its use. Vojtech and Neruda[18] introduced protective clothing against high-frequency EM fields based on synthetic yarns with the addition of silver nanoparticles. The main advantage of this solution is the reduction in the weight of the garment using nanoparticles instead of metal wires. However, the visual characteristics of the garment were not discussed in the paper, as the proposed protective clothing was not intended for daily use, and the main requirement was to provide effective EM shielding.

In this paper, the aesthetic properties of electrically conductive fabric containing staple stainless steel (SST) fibers were enhanced using digital printing. The development and EM shielding ability of these special fabrics is dependent on different variables, as previously described in studies by other authors. As these fabrics could be considered for use against radio-frequency radiation in everyday protective clothing, the material's composition and structure were optimized to satisfy firstly the thermophysiological comfort property requirements. This work considers patterning possibilities and production opportunities of the special electrically conductive textile structure by digital printing. The effect of areal printing on SE is evaluated as well as the durability of the printed fabric, which is represented by washing and drying, because a color change during laundering impacts greatly on consumer satisfaction. Furthermore, the basic transport properties (thermal insulation and thermal contact properties together with air permeability (AP)) of the printed conductive fabric are compared with those of fabric made from traditional material; this is to ensure that the evaluation includes the wearing comfort and pilling of printed fabrics after washing. Traditional nonconductive fabrics are totally transparent to EM fields, and consequently, they have zero SE properties. On that basis, traditional fabric was incorporated in this study only for the comparison of transport properties. Fashion garment prototypes made of printed conductive fabric were introduced at the end of the investigation.

Experimental details

Materials

Electrically conductive yarns. Yarns were made of conventional polyester (PET) fibers (59 wt%) and CO fibers (31 wt%) with admixtures of SST fibers (10 wt%) with the trade name BEKINOX. These three components were mixed at the drawing frame, and a ring spinning

Table 2. Characteristics of hybrid yarns (mean values and 95% confidence intervals)

Composition	Linear density [tex]	Tensile strength [cN/tex]	Elongation [%]
10% SS/59% PET/31% CO	31.14 ± 0.96	20.85 ± 0.89	10.22 ± 0.56

SS: stainless steel; PET: polyester; CO: cotton.

Table 3. Characteristics of hybrid fabric used as substrate for surface modification

Composition	Warp/weft count [tex]	Hybrid yarn placement	Fabric structure	Fabric thickness [mm]	Mass per unit area [g/m^2]
10% SS/59% PET/31% CO	31/31	100%	2/1 twill	$0.36 \pm 5.1E\text{-}3$	190.21 ± 1.53

SS: stainless steel; PET: polyester; CO: cotton.

system was used to produce blended single yarns with a linear density of ~31 tex. The basic parameters of the yarns were determined according to the appropriate standards, and are presented in Table 2.

BEKINOX metal fiber is very thin (diameter $d = 8\,\mu m$) and has a staple length ($l = 45\,mm$), which ensures favorable mechanical properties in mixed yarns—especially low bending stiffness. The addition of electrically conductive components of sufficiently high concentration provides increased electrical conductivity (the electrical resistance of the yarn is $\sim 5.76E+02 \pm 1.15E+02\ \Omega$, measured according to Safarova et al.[19] at 1 cm distance from the electrodes), which is a basic requirement for the creation of EM shielding fabrics. It was discovered in previous studies that the addition of 10 wt% of SST fiber is sufficient to exceed the percolation threshold of the conductive component while maintaining typical textile yarn properties. Furthermore, there were no problems with yarn production.

Hybrid fabric. Metal fiber-containing fabric for patterning was created using hybrid yarns as described above. The hybrid fabric has a twill 2/1 weave made from 100% conductive yarn (warp sett 39 1/cm, weft sett 22 1/cm). The characteristics of the hybrid fabric are presented in Table 3. Figure 1 presents scanning electron microscope (SEM) images of the fabric (the lightest and smoothest fibers are metal fibers). The raw fabric has a light gray color due to the presence of metal fibers.

Methods

Digital printing

Digital textile printing was selected because of its low price (approximately €7/m) and flexibility (it is easy to print various colors and detailed designs with small runs of each design). Fabric was printed using the following methods: (a) design preparation in a red, green, blue (RGB) color model (see Figures 2(a) and (b) for examples of designs applied on the conductive fabric); (b) substrate pretreatment to increase washing durability and color richness; (c) feeding of the conductive fabric through the printer using rollers and the application of ink to the fabric's surface. The industrial printer used an $8 \times$ Ricoh Gen5 typehead (with the following colors: $2 \times$ black, light black, cyan, magenta, violet, red, and yellow) together with ElvaJet PR 540 pigment ink (Sensient, Switzerland). 4) The fabric was finished in an infrared oven ($T = 160^{\circ}C$, $t = 3\,min$) to cure the ink.

A color template (see Figure 2(c)) containing a selected spectrum of 11 colors (see Table 4, showing the RGB color coordinates of computer design) was prepared to study the durability of printing on conductive textiles for easier evaluation. This color spectrum was transferred onto the hybrid fabric through digital printing to study the shade change of the individual colors after repeated washing and drying.

Conversion of RGB to CIE 1976 $L^*a^*b^*$ was performed by Color Space Conversion software[20] under the CIE standard illuminant, D65, which simulates daylight with a color temperature of 6504 K. The RGB coordinates of computer design converted to the CIE $L^*a^*b^*$ system are presented in Table 5. Figure 3(a) represents the CIE $L^*a^*b^*$ color coordinates selected for the experiment. Figure 3(b) presents the CIE $L^*a^*b^*$ coordinates of colors on the fabric after printing. The CIE $L^*a^*b^*$ coordinates measured on the printed fabric are presented in Table 6 together with CIE $L^*a^*b^*$ ΔE to compare the CIE $L^*a^*b^*$ values of the design and the CIE $L^*a^*b^*$ values measured on the printed fabric. This comparison was made to study the change in color of the design after printing due to the presence of the metal fiber in the fabric, which causes its light gray color.

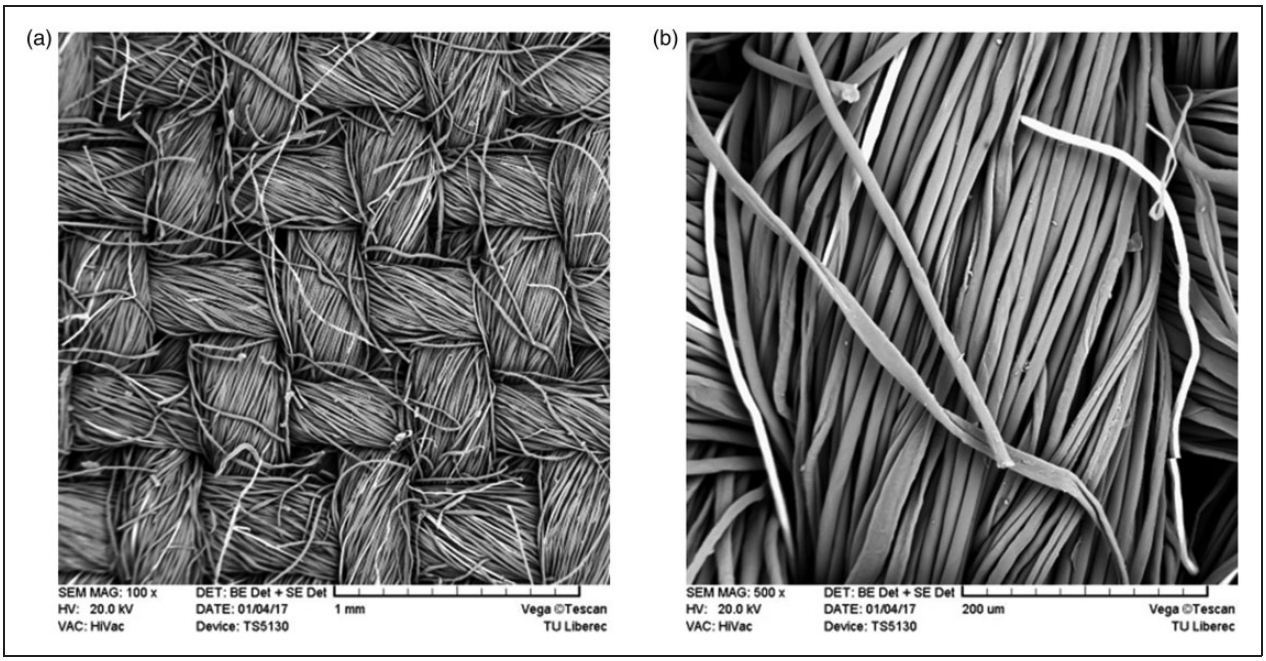

Figure 1. Scanning electron microscope images of conductive fabric with magnification at (a) 100× and (b) 500×.

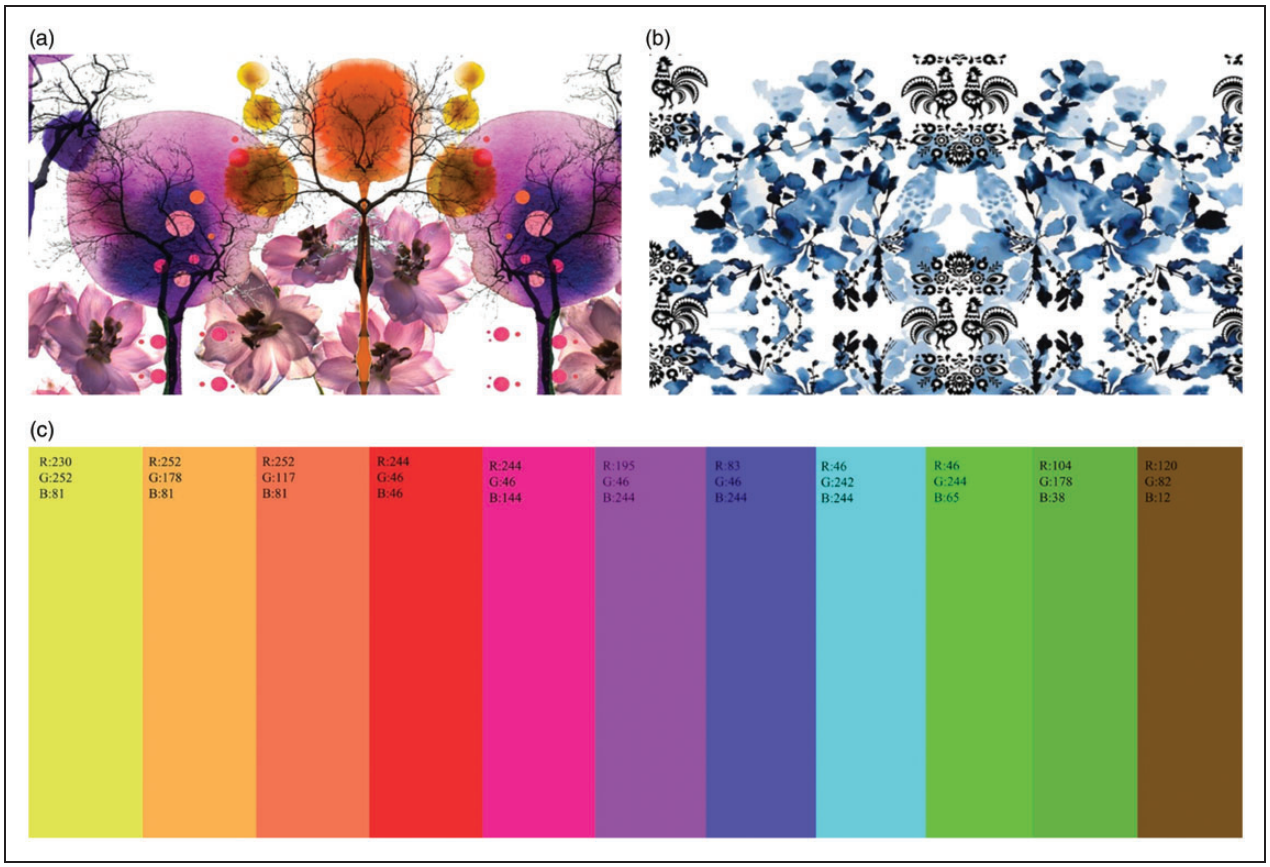

Figure 2. (a), (b) Designs for digital printing. (c) Selected colors for digital printing used in the experiment. (Color online only.)

Table 4. Specifications of red, green, blue color coordinates selected for the experiment—computer design before print

Sample	1	2	3	4	5	6	7	8	9	10	11
Red	230	252	252	244	244	195	83	46	46	104	120
Green	252	178	117	46	46	46	46	242	244	178	82
Blue	81	81	81	46	144	244	244	244	65	38	12

Table 5. The CIE $L^*a^*b^*$ coordinates of selected colors—computer design before print

Sample	1	2	3	4	5	6	7	8	9	10	11
L^*	94.75	77.95	64.82	53.38	55.28	51.79	38.66	87.31	84.51	65.69	37.67
a^*	–28.17	18.03	48.71	71.85	77.53	81.10	66.95	–43.70	–77.87	–45.15	10.50
b^*	75.49	58.68	44.50	49.09	–5.15	–68.95	–91.54	–14.07	68.29	58.86	42.62

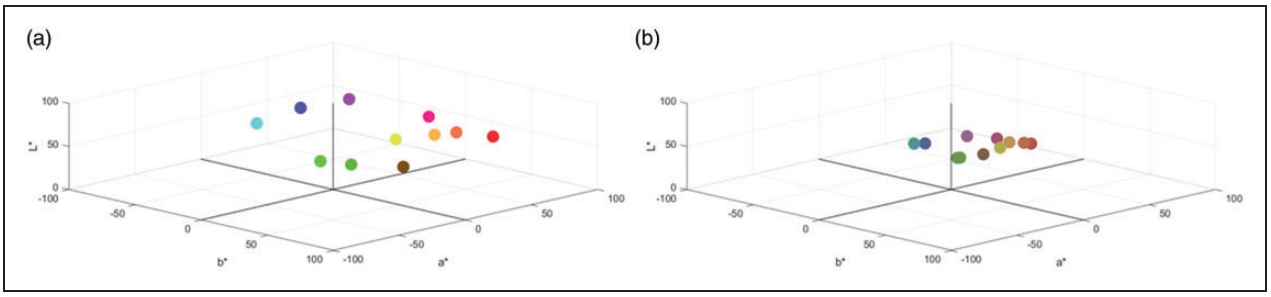

Figure 3. The CIE $L^*a^*b^*$ coordinates of (a) the colors of the computer design and (b) the colors on the fabric after printing.

Table 6. The CIE $L^*a^*b^*$ values of the printed fabric together with CIE $L^*a^*b^*$ E for comparison of shades of colors of the computer design and the printed fabric

	1	2	3	4	5	6	7	8	9	10	11
L^*	69.34	63.86	53.31	47.83	45.43	49.37	43.15	56.73	57.77	57.71	43.43
a^*	−11.08	9.23	28.76	37.94	36.80	23.70	4.78	−18.93	−26.02	−27.37	8.64
b^*	48.12	34.81	26.36	22.54	−2.10	−11.66	−24.48	−9.03	32.79	32.12	15.75
E	41.08	29.08	29.32	43.43	42.02	81.14	91.56	39.67	68.29	33.09	27.53

The washing and drying process

The washing was conducted in accordance with EN ISO 6330 standard[21] in a Miele Professional W6071 washing machine. According to the standard, the 3M procedure was chosen, which is specific to front-loading washing machines. Following the recommendations from the printing company, the washing temperature was set at 30°C with an 800 RPM spin speed to simulate delicate domestic washing. As a detergent, a universal blend (trade name Havon U9 PLUS, pH 7.8) with the composition of a conventional gel laundry detergent was used to replicate normal household operation. After washing, the samples were dried in a hanger in an air-conditioned laboratory. To fill the remaining space in the drum, 100% white CO fabric was added. The washing scheme with the number of washing cycles is presented in Table 7. First, the printed fabric was evaluated after a single wash. The interval was increased then and the printed fabric was washed 20 times, in total.

Color fastness evaluation

The color fastness of the printed fabric was evaluated during repeated maintenance. The procedure was conducted in accordance with the ISO 105-A04 standard,[22] which deals with the method for the instrumental

Table 7. Scheme of washing and drying cycles

Number of washing cycles	1	2	3	4	6	8	10	15	20

evaluation of the degree of embedding of accompanying fabrics. A 2500d Minolta spectrophotometer with 8 mm measuring aperture (illuminant D65 and 10° Standard Observer) was used to measure the color. The color evaluation method was performed as follows: first, the spectrophotometer was calibrated to black and white prior to measurement. Next, certain sections (color samples) of the fabric were evaluated, and the data were displayed in the color space $L^*a^*b^*$. The data were measured 10 times at different locations in each color section. The color of the samples was evaluated after the following washing cycles: 1×, 2×, 4×, 6×, 8×, 10×, 15×, and 20×.

For color difference evaluation, CIE $L^*a^*b^*$ ΔE was used. For two colors in the CIE $L^*a^*b^*$ color space, (L_1^*, a_1^*, b_1^*) and (L_2^*, a_2^*, b_2^*), the color difference is defined as

$$\Delta E = \sqrt{\left(L_2^* - L_1^*\right)^2 + \left(a_2^* - a_1^*\right)^2 + \left(b_2^* - b_1^*\right)^2} \quad (2)$$

where $\Delta E \sim 2.3$ corresponds to a just-noticeable color change according to Hurren.[23]

CIE $L^*a^*b^*$ ΔE values can be compared with the gray scale rating system, which is often used for the visual assessment of the change in the shade of a colored textile. The CIE $L^*a^*b^*$ assigned ΔE values for each gray scale are reproduced in Table 8. Gray scales have a rating of 1–5, with 1 being the worst color performance and 5 being the best.[23]

Three color representatives were chosen from Table 6 for the purposes of data processing and color evaluation demonstration: sample 4 (red), sample 7 (blue), and sample 10 (green). Tables 9–11 present the results of the CIE $L^*a^*b^*$ measurements for selected colors after repeated washing cycles, the sample average, and a 95% confidence interval for the mean (measurements were conducted at 10 different places), together with the CIE $L^*a^*b^*$ ΔE showing the difference between the washed and reference samples.

Table 8. The CIE $L^*a^*b^*$ E assigned values for gray scales

CIE $L^*a^*b^*$ color difference for fading		Color fastness grade
Value	Tolerance	
0.0	<0.40	5
0.8	0.40–1.25	4–5
1.7	1.25–2.10	4
2.5	2.10–2.95	3–4
3.4	2.95–4.10	3
4.8	4.10–5.80	2–3
6.8	5.80–8.20	2
9.6	8.20–11.60	1–2
13.6	>11.60	1

Table 9. Results of CIE $L^*a^*b^*$ coordinate measurements for sample 4 from Table 6 (input red, green, blue [244, 46, and 46])

Washing cycles	L^*	a^*	b^*	E
0	47.83 ± 0.37	37.94 ± 0.48	22.54 ± 0.32	0.00
1	50.06 ± 0.74	35.26 ± 1.09	19.78 ± 1.05	4.45
2	51.00 ± 0.44	33.65 ± 0.72	18.35 ± 0.49	6.78
3	51.86 ± 0.50	32.75 ± 1.05	17.37 ± 0.79	8.36
4	52.36 ± 0.50	32.47 ± 0.66	17.08 ± 0.53	8.96
6	53.09 ± 0.68	30.95 ± 0.91	15.82 ± 0.66	11.04
8	53.15 ± 0.69	31.02 ± 0.70	15.72 ± 0.45	11.08
10	53.82 ± 0.63	30.45 ± 0.81	15.33 ± 0.51	12.00
15	54.54 ± 0.85	29.23 ± 1.00	14.32 ± 0.71	13.72
20	54.46 ± 0.31	29.55 ± 1.08	14.46 ± 0.73	13.40

SE evaluation

The SE of samples was measured according to ASTM D 4935-18[24] for planar materials using a plane-wave, far-field EM wave. The measurements were performed over a frequency range from 30 MHz to 1.5 GHz. The setup consisted of a sample holder with its input and output connected to a network analyzer. A SE test fixture (model EM-2107A, Electro-Metrics, Inc.) was used to hold the sample. The design and dimension of the sample holder followed the standard mentioned above. A Rohde & Schwarz ZN3 network analyzer was used to generate and receive the EM signals. This measurement method determines the SE of the fabric using the insertion–loss method. The samples were air-conditioned before testing ($T = 22°C \pm 3°C$, $RH = 50\% \pm 10\%$), and measurements were conducted at 10 different places on the textile samples to facilitate subsequent statistical analysis. The mean values together with 95% confidence intervals of the SE means for both samples (substrate and printed) for frequencies of 600

Table 10. Results of $L^*a^*b^*$ coordinate measurements for sample 7 from Table 1 (input red, green, blue [83, 46, and 244])

Washing cycles	L^*	a^*	b^*	E
0	43.15 ± 0.46	4.78 ± 0.34	−24.48 ± 0.51	0.00
1	46.25 ± 1.35	4.18 ± 0.37	−22.72 ± 0.84	3.61
2	47.69 ± 1.10	3.95 ± 0.17	−21.97 ± 0.74	5.25
3	49.20 ± 1.25	3.57 ± 0.32	−20.85 ± 0.71	7.15
4	50.37 ± 1.02	3.36 ± 0.23	−20.37 ± 0.74	8.43
6	50.92 ± 1.31	3.35 ± 0.14	−20.09 ± 0.65	9.03
8	51.85 ± 1.16	3.23 ± 0.28	−19.42 ± 0.80	10.19
10	52.92 ± 0.80	2.89 ± 0.24	−18.88 ± 0.67	11.42
15	53.99 ± 1.21	2.69 ± 0.37	−18.20 ± 1.08	12.69
20	54.80 ± 0.68	2.55 ± 0.19	−17.59 ± 0.45	13.71

Table 11. Results of $L^*a^*b^*$ coordinate measurements for sample 10 from Table 1 (input red, green, blue [104, 178, and 38])

Washing cycles	L^*	a^*	b^*	E
0	57.71 ± 0.40	−27.37 ± 0.30	32.12 ± 0.65	0.00
1	59.46 ± 0.57	−25.38 ± 0.47	29.73 ± 0.62	3.57
2	60.15 ± 0.73	−24.10 ± 0.99	28.44 ± 0.90	5.50
3	60.89 ± 0.64	−23.85 ± 0.84	27.95 ± 0.90	6.32
4	61.37 ± 0.37	−23.14 ± 0.83	27.15 ± 0.73	7.49
6	62.07 ± 0.44	−22.44 ± 0.58	26.22 ± 0.52	8.84
8	62.18 ± 0.56	−21.82 ± 0.85	25.37 ± 0.88	9.82
10	62.43 ± 0.50	−21.90 ± 0.59	25.39 ± 0.53	9.87
15	63.20 ± 0.54	−20.67 ± 0.49	24.10 ± 0.55	11.80
20	63.60 ± 0.63	−20.24 ± 0.77	23.33 ± 0.61	12.76

Table 12. Mean values and 95% confidence intervals of means for the *SE* of the substrate

No. of washing and drying cycles [-]	Electromagnetic shielding effectiveness *SE* [dB]		
	$f = 600$ MHz	$f = 1$ GHz	$f = 1.5$ GHz
0	25.27 ± 0.36	27.49 ± 0.32	31.17 ± 0.28
1	25.02 ± 0.21	28.09 ± 0.22	29.99 ± 0.16
2	24.80 ± 0.11	27.20 ± 0.17	30.89 ± 0.12
3	24.54 ± 0.17	26.93 ± 0.22	30.49 ± 0.17
4	23.42 ± 0.33	26.20 ± 0.26	30.21 ± 0.17
6	24.53 ± 0.26	26.46 ± 0.22	31.54 ± 0.83
8	23.52 ± 0.35	25.86 ± 0.21	29.67 ± 0.16
10	23.32 ± 0.27	25.64 ± 0.24	29.55 ± 0.16
15	22.65 ± 0.13	25.39 ± 0.16	29.35 ± 0.21
20	21.68 ± 0.27	24.50 ± 0.21	28.67 ± 0.23

Table 13. Mean values and 95% confidence intervals of means for the *SE* of the printed sample

No. of washing and drying cycles [-]	Electromagnetic shielding effectiveness *SE* [dB]		
	$f = 600$ MHz	$f = 1$ GHz	$f = 1.5$ GHz
0	26.03 ± 0.26	28.23 ± 0.21	32.97 ± 1.11
1	25.36 ± 0.24	28.45 ± 0.26	31.37 ± 1.16
2	24.99 ± 0.25	27.36 ± 0.22	30.93 ± 0.19
3	24.41 ± 0.43	26.83 ± 0.32	30.45 ± 0.31
4	24.19 ± 0.28	26.57 ± 0.22	30.31 ± 0.22
6	23.96 ± 0.37	25.68 ± 0.36	29.92 ± 0.72
8	23.09 ± 0.55	25.08 ± 0.47	28.91 ± 0.45
10	22.48 ± 0.72	24.51 ± 0.60	28.40 ± 0.57
15	21.22 ± 0.85	23.48 ± 0.69	27.51 ± 0.65
20	20.38 ± 0.89	22.70 ± 0.84	26.83 ± 0.77

MHz, 1 GHz, and 1.5 GHz are summarized in Tables 12 and 13.

Pilling evaluation

Pilling of fabrics is a negative and complex issue that is caused by friction or rubbing on the fabric surface during common wearing and maintenance. It was observed that pills appeared on the top of tested fabrics during various washing and drying cycles (WDs). Therefore, pilling evaluation was included in this study. Generally, the pilling evaluation is based on a subjective classification of the sample according to a rating scale containing five grades of pilling: grade 5, no pilling; grade 4, slight pilling; grade 3, moderate pilling; grade 2, severe pilling; and grade 1, very severe pilling. The degree of fabric pilling was evaluated by comparing tested specimens with visual standards (EMPA photographic woven standards for pilling test) after each washing cycle.

Air permeability evaluation

An important factor in the comfort of a fabric is AP, as it plays a role in the transportation of moisture vapor from the skin to the outside atmosphere. An AP tester (FX 3300, TEXTEST Instruments) was used to conduct the AP test. The test pressure was 100 Pa on an area of 20 cm^2. Five measurements were performed according to the ISO 9237 standard.[25] The AP was measured under standard laboratory conditions ($T = 22°C \pm 3°C$, $RH = 50\% \pm 10\%$). To compare the AP values of conductive printed fabric with common (nonconductive) textile fabric, samples of similar material composition and structure (marked as reference) were selected (see Table 14 for more details).

Table 14. Basic characteristics of the reference fabric

Composition	Fabric structure	Fabric thickness [mm]	Mass per unit area [g/m^2]
50% PET/50% CO	2/1 twill	0.45	210

PET: polyester; CO: cotton.

Table 15. Mean values and 95% confidence intervals of means for the air permeability (AP), thermal absorptivity (*b*), and thermal resistance (*R*) values for conductive fabric (substrate, printed) and comparative nonconductive fabric (reference)

Sample type	*AP* [mm/s]	*b* [W $m^{-2}s^{½}$ K^{-1}]	*R* 10^{-3} [K·m^2·W^{-1}]
Substrate	310.0 ± 8.4	150.4 ± 6.2	10.06 ± 0.15
Printed	189.8 ± 10.3	156.6 ± 3.2	9.94 ± 0.13
Reference	63.0 ± 1.4	177.4 ± 5.6	10.2 ± 0.19

The mean values of the estimator (pivot half sums) together with 95% confidence intervals of means for the AP are summarized in Table 15.

Thermophysical properties

The heat transfer characteristics of textile structures are very important in textile comfort evaluation, since it was found that thermophysiological properties greatly influence the fabric's total wear comfort.[26] The heat transfer mechanism through textile fabric is a complex phenomenon comprising all three mechanisms (conduction, convection, and radiation). However, heat transfer by conduction is generally accepted to be more significant than by convection and radiation. Thermal properties were evaluated using an Alambeta instrument,[27] and tests were conducted according to the ISO EN 31092:1994 standard. The samples were air-conditioned before testing ($T = 22°C \pm 3°C$, $RH = 50\% \pm 10\%$). The measurements were conducted at five different places on the textile samples because of subsequent statistical analysis, and samples were air-conditioned under standard laboratory conditions ($T = 22°C \pm 3°C$, $RH = 50\% \pm 10\%$). In all cases, the measuring head temperature was approximately 32°C, and the measuring head pressure was 200 Pa. The thermal comfort of conductive fabric is characterized by thermal absorptivity *b* [$Wm^{-2}s^{½}K^{-1}$] and thermal resistivity *R* [Km^2W^{-1}], which are directly connected both with the protection of the wearer from cold and heat and in providing a warm feeling. In addition, in this case, a reference fabric (see Table 14) was used to compare the thermal properties of the conductive fabric with those of common (nonconductive) textile fabric. The mean values of the estimator (pivot half sums) together with 95% confidence intervals of means for *b* and *R* are summarized in Table 15.

Results and discussion

Effect of digital printing on SE

The main aim was to investigate whether digital printing influences the functionality of hybrid fabric, especially its ability to shield EM fields. Figure 4 presents the variation in SE for woven fabrics after printing with incident frequency in the range between 30 and 1500 MHz. It is evident that both samples have a relatively high ability to shield EM fields. The SE exceeds 30 dB for frequencies higher than 1.2 GHz, and thus the fabric meets the requirements for the excellent grade, according to FTTS-FA-003:2005.[7] It seems that the untreated sample (gray line) reaches the lower SE values throughout the whole frequency band ($SE \sim 31$ dB for $f = 1.5$ GHz) compared with the printed sample. It is assumed that this behavior is related to a decrease in porosity of the printed sample accompanied by the lower penetration of EM waves through the sample. That is why an increase in SE is evident—especially for higher frequencies. It can be observed that the relationship between SE and frequency in both samples (untreated and printed) can be approached by a generalized logarithmic function adapted from Safarova and Militky:[28]

$$SE = a + b\log(f) + c\sqrt{f} \tag{3}$$

where *a*, *b*, and *c* are constants depending on the characteristic impedance of the shield material and the characteristic impedance of the medium surrounding the shield, and *f* is frequency.

To confirm the significance of the effect of digital printing on SE, the variability of the measured parameters represented by 95% confidence intervals was considered (see Figure 4). It is evident that the confidence intervals do not overlap for all studied frequencies; therefore, the statistically significant effect of digital printing on the SE is confirmed at $\alpha = 0.05$.

Effect of washing and drying on SE

Figure 5 presents the dependences of SE on the number of WDs for untreated and printed samples for the 1.5 GHz frequency. When investigating the unprinted sample, the SE drops by about 2.5 dB after 20 WDs, which represents 8% of the original (unwashed) value. In the case of the printed sample, the decrease is about 6 dB and can be observed after the same number of

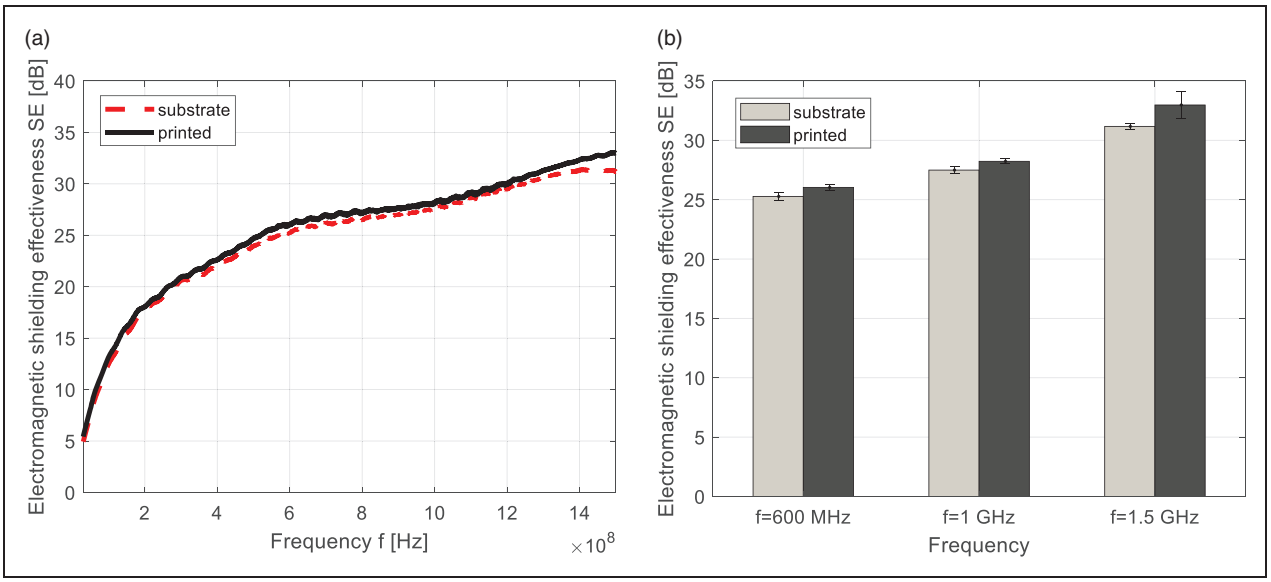

Figure 4. Electromagnetic shielding of the substrate and printed sample: (a) frequency dependence; (b) comparison including variability for chosen frequencies.

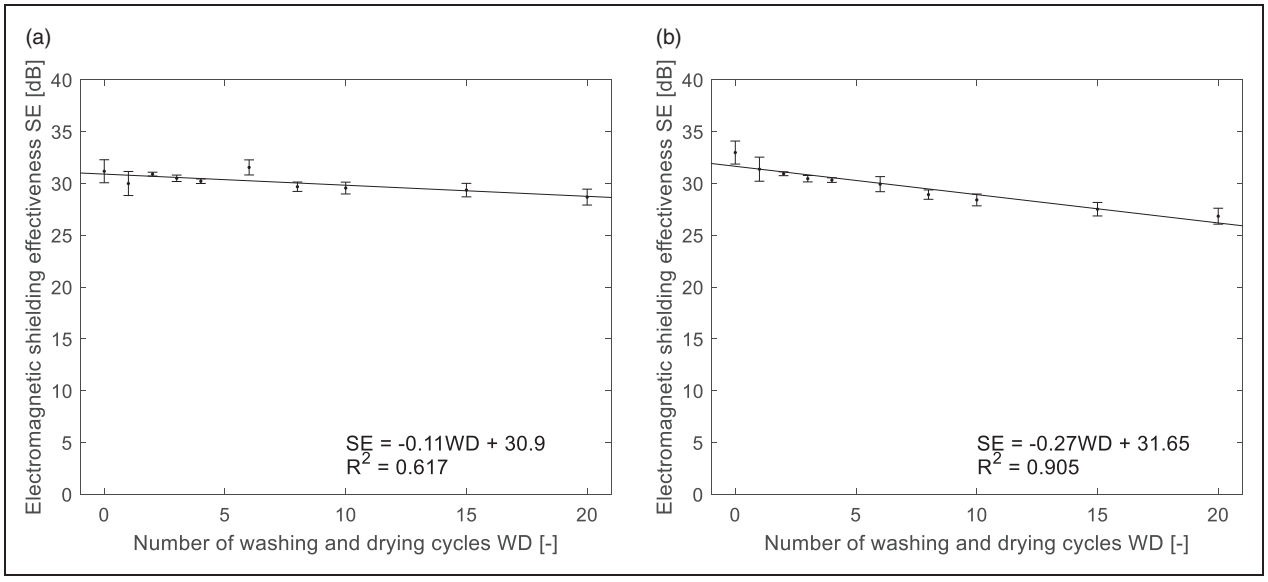

Figure 5. Dependence of shielding effectiveness on washing and drying cycles for (a) substrate and (b) printed samples.

WDs at a frequency of 1.5 GHz (i.e., 18% of the original value). This phenomenon is probably caused by the removal of printing ink and unblocking of pores during the washing procedure. It must be noted that even after 20 WDs, the SE of the samples remains satisfactory at 28.7 and 26.8 dB at the 1.5 GHz frequency for the unprinted and printed samples, respectively.

SE dependence on the number of WDs can be described using a linear function. The solid lines in these graphs correspond to indicate the regression models (straight line) with parameters obtained by the minimizing the sum of squared errors. The corresponding coefficients of determination $R^2 \sim 0.6$ and $R^2 \sim 0.9$ for the unprinted and printed samples, respectively, indicate a good quality fit. It should be noted that this approximation is valid only for the studied range of WDs.

The straight lines indicating the dependence of SE on WDs are not steep, and the slope is relatively low (-0.1 and -0.8). To confirm the influence of WDs on the SE of samples, an analysis of regression model in the form $y = b_1 x + b_2$ was performed in a MATLAB

environment. As an output of linear regression diagnostics, the p-values and coefficients were calculated. The p-value for each term tests the null hypothesis that the coefficient is equal to zero (no effect). A low p-value (below the significance level $\alpha = 0.05$) indicates that the null hypothesis can be rejected. Conversely, a significant p-value (>0.05) indicates that the changes in the predictor are not associated with the changes in the response. The results of the linear regression analysis for both samples (at a frequency of 1.5 GHz) are presented in Table 16. It is evident that the predictor variable WDs is significant because its p-values are <0.05; therefore, the null hypothesis is rejected for all studied frequencies. At the same time, a statistically significant effect of WDs on the SE value is not confirmed at $\alpha = 0.05$.

Table 16. Results of linear regression analysis for samples

Predictor	Coef.	SE Coef.	T	p
Untreated sample				
Constant	30.90	0.28	111.74	0.000
WD	−0.11	0.03	−3.59	0.007
Printed sample				
Constant	31.65	0.29	109.23	0.000
WD	−0.27	0.03	−8.72	0.000

WD: washing and drying cycle.

Color fastness of printed electromagnetic shielding fabric

Figures 6–8 present the CIE $L^*a^*b^*$ coordinates of the measurements after repeated WDs from a three-dimensional (3D) view and the projection of L^* versus a^* for three chosen samples of different colors (red, blue, and green).[29]

Figures 9(a)–(d) present the CIE $L^*a^*b^*$ coordinates for all samples after washing in the form of a 3D view with projections of L^* versus a^*, L^* versus b^*, and b^* versus a^*. All samples exhibit no tendency to shift hue, but there is a decrease in chroma (dullness) after repeated washing. The CIE $L^*a^*b^*$ ΔE values for all samples are presented in Figure 10 (a line chart was chosen due to better visualization), where the color difference between the current sample and the sample before washing is captured. It can be observed that after the first WD, the CIE $L^*a^*b^*$ ΔE value exceeds 2 for all samples, which corresponds to color fastness grade 3 (samples 7 and 10) and grades 2–3 (sample 4) on the gray scale evaluation system. The CIE $L^*a^*b^*$ ΔE value is between 4 and 7 after two WDs (corresponding to grades 3, 2–3, and 2) and 7–12 after 10 WDs (corresponding to grades 2, 1–2, and 1). It seems that the

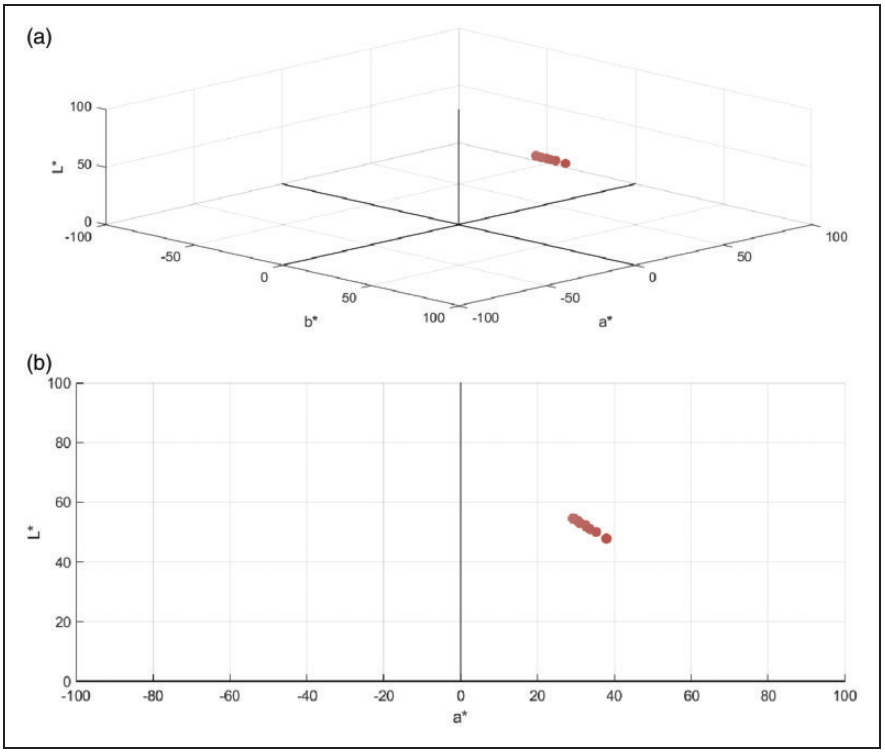

Figure 6. The CIE $L^*a^*b^*$ coordinates for sample 4 after repeated washing cycles.

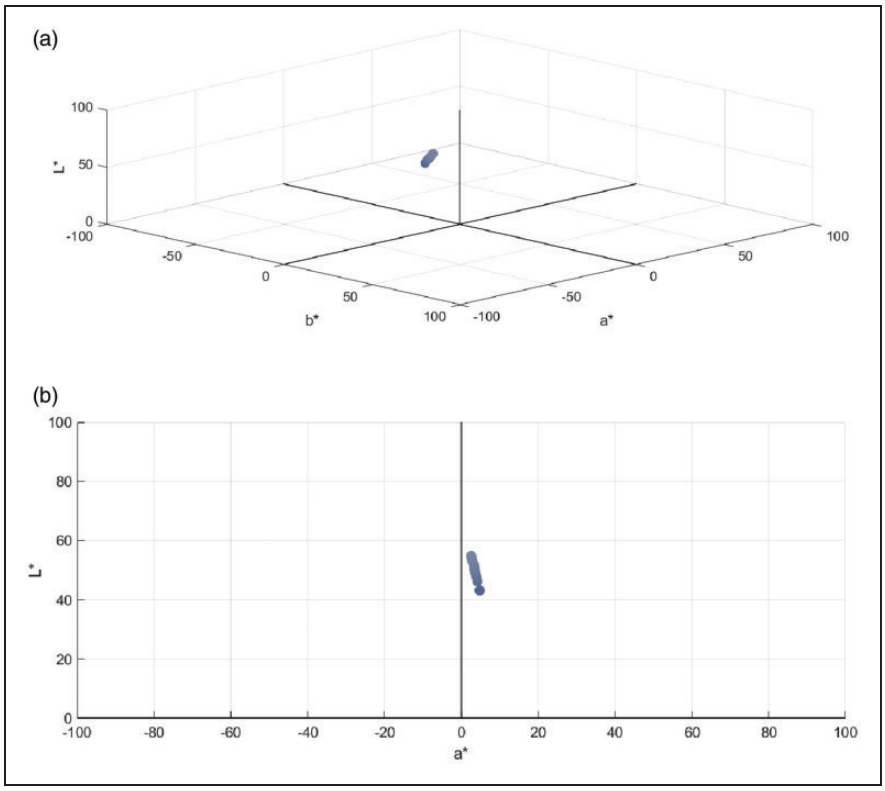

Figure 7. The CIE $L^*a^*b^*$ coordinates for sample 7 after repeated washing cycles.

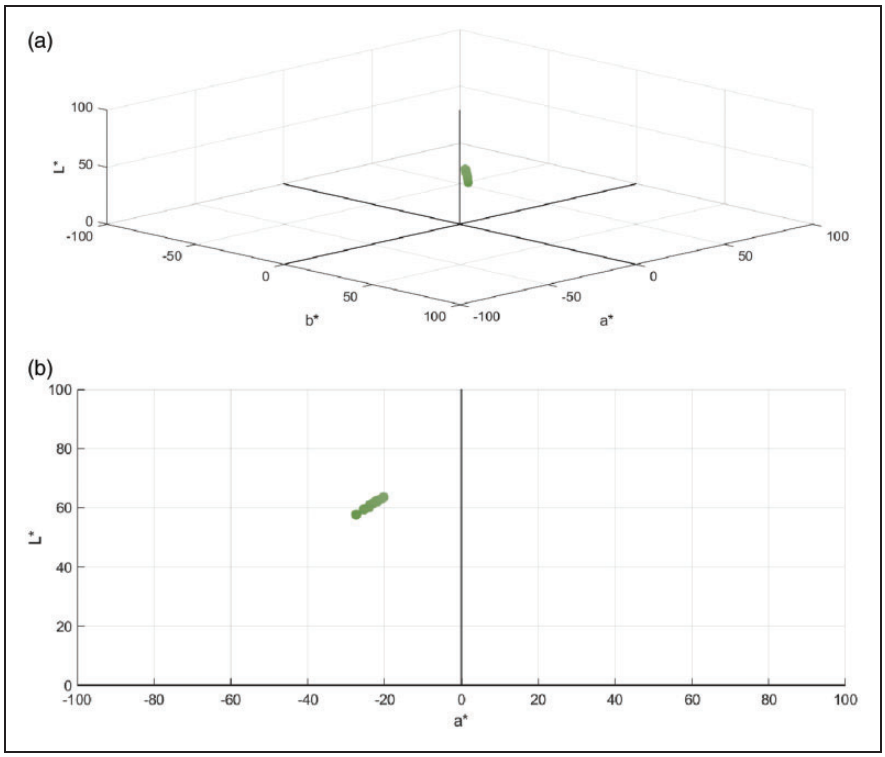

Figure 8. The CIE $L^*a^*b^*$ coordinates for sample 10 after repeated washing cycles.

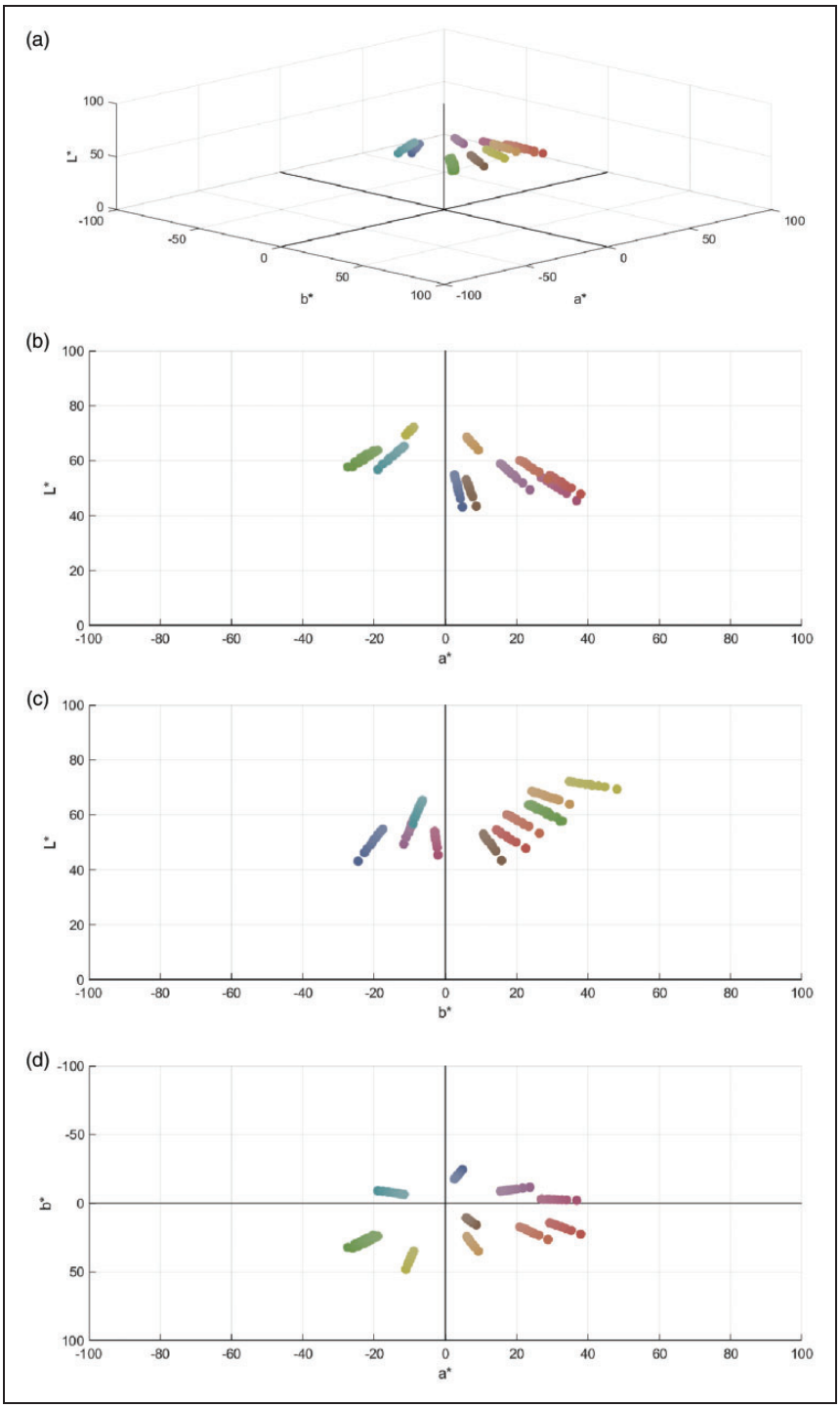

Figure 9. The CIE $L^*a^*b^*$ coordinates after repeated washing for all samples: (a) three-dimensional view; (b) L^* versus a^*; (c) L^* versus b^*; (d) b^* versus a^*.

dependence of CIE $L^*a^*b^*$ ΔE on the number of WDs can be approximated by a logarithmic function; furthermore, it can be assumed that CIE $L^*a^*b^*$ ΔE will be stabilized after further WDs. Images of real samples before and after 20 WDs and the effect of color fading are illustrated in Figure 11.

Pilling evaluation of electromagnetic shielding fabric

It was discovered that pills are created on the surface of printed EM shielding fabric during repeated washing. The first pills were observed after the eighth WD, and after the 20th WD,

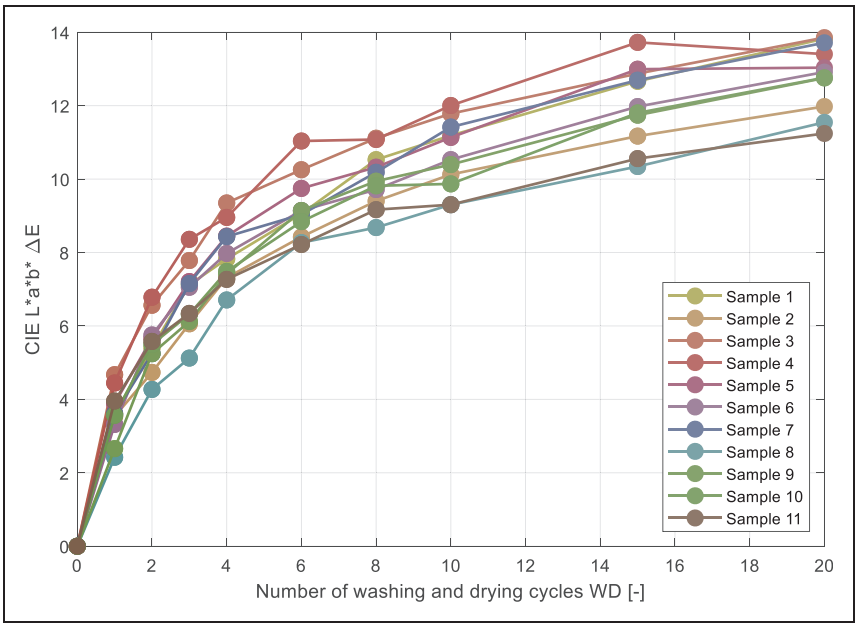

Figure 10. Dependence of CIE $L^*a^*b^*$ ΔE on the number of washing and drying cycles for all samples.

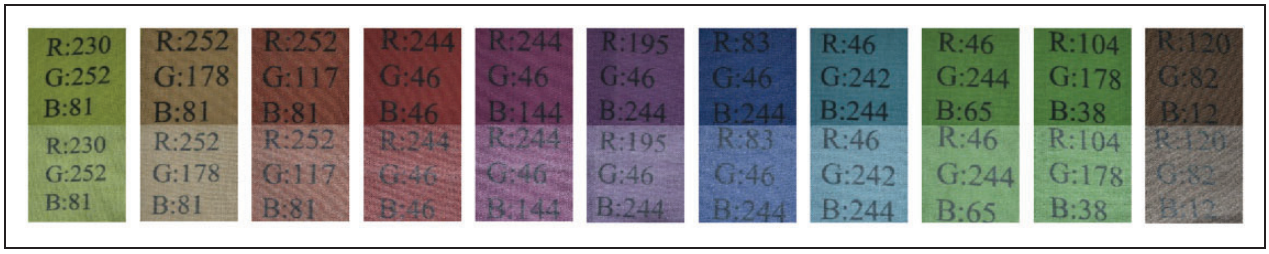

Figure 11. Samples before (above) and after (below) the 20 washing cycles.

Table 17. Pilling evaluation

Number of washing cycles	1	2	3	4	6	8	10	15	20
Pilling category	–	–	–	–	–	W4–5	W3–4	W3–4	W2–3

the fabric was categorized as W2–3, as presented in Table 17.

Transport properties of electromagnetic shielding fabric

The key objective was to determine whether conductive fabric (raw and printed) has similar comfort properties (based on chosen transport properties) to traditional textile fabric. For this investigation, common fabric with a similar material composition and structure was selected. Figure 12 presents the AP comparison for all samples. It is shown that raw EM shielding fabric has the highest ability to transport air. As expected, the AP significantly decreases (to 60% of the value of the substrate) when the fabric is printed (all over its surface). The reference fabric possesses the lowest AP, which is caused by its increased thickness and greater mass per unit area compared with hybrid fabric.

Figure 13(a) compares the thermal absorptivity of all samples. In this case, there is no observable statistically significant effect of printing on the warm/cool feeling of the material. The reference fabric provides a cooler feeling compared with the EM shielding fabric due to the more compact structure of the reference fabric. Figure 13(b) compares the thermal resistance of all samples. When studying variability with 95% confidence intervals of means, it can be concluded that all

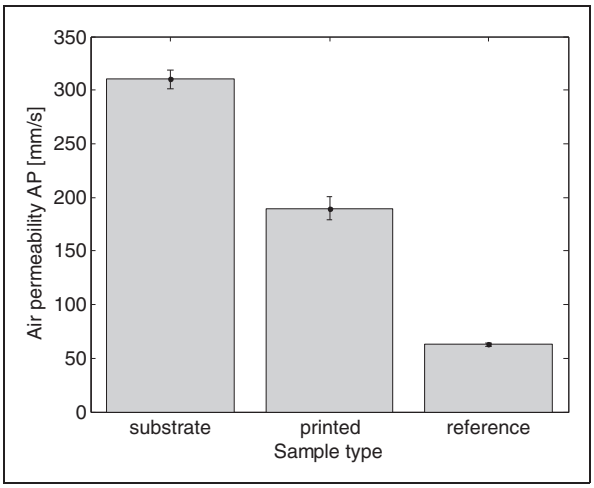

Figure 12. Comparison of air permeability in all samples.

compared fabrics have the same ability to protect the wearer from both cold and heat.

In summary, EM shielding fabric (raw or printed) does not have significantly different comfort properties from common textile fabric, which makes it possible for application as a fabric in clothing design.

Fashion clothing with electromagnetic radiation protection

While the performance of traditional protective clothing depends on the structural design of the garment and the fabric properties, the latter is essential. Conversely, clothing for daily use with a protective function should also satisfy current fashion requirements, including color, shape, design, and style.

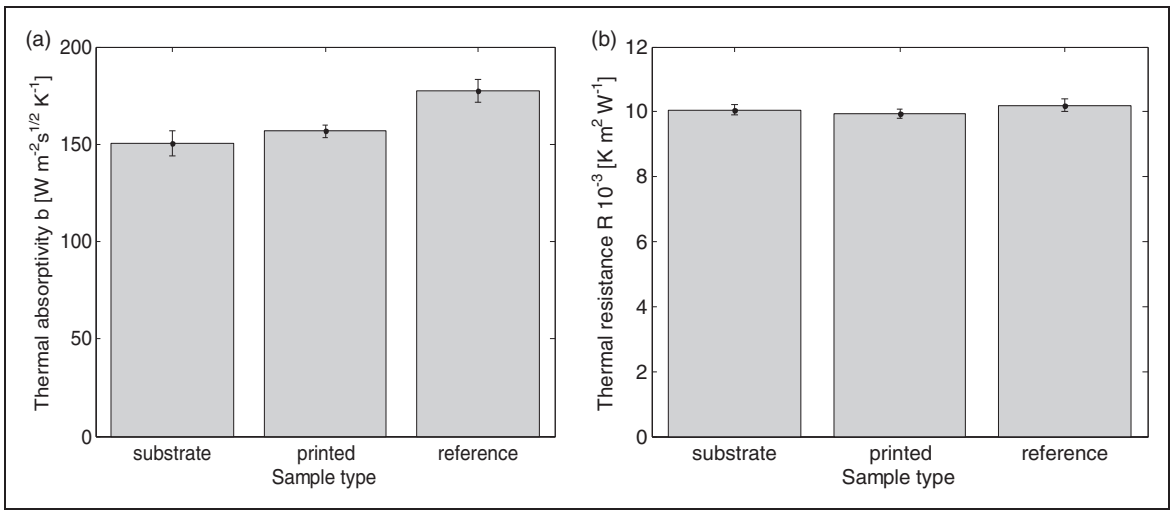

Figure 13. Comparison of basic thermal properties of all samples: (a) thermal absorptivity; (b) thermal resistance.

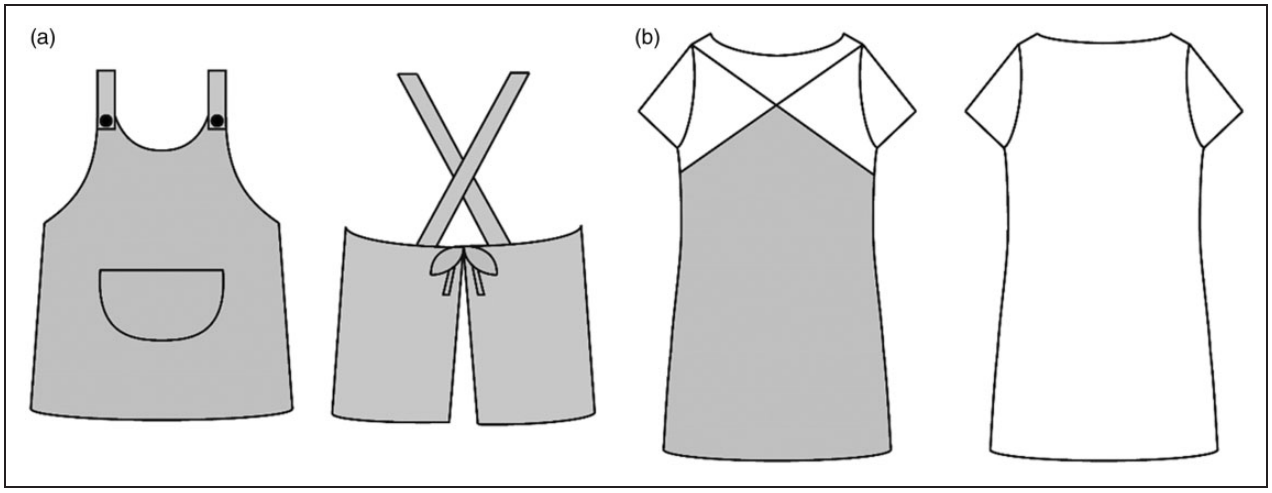

Figure 14. Schematic illustration of the design of radio-frequency protective clothing. The gray color indicates the use of electromagnetic shielding fabric.

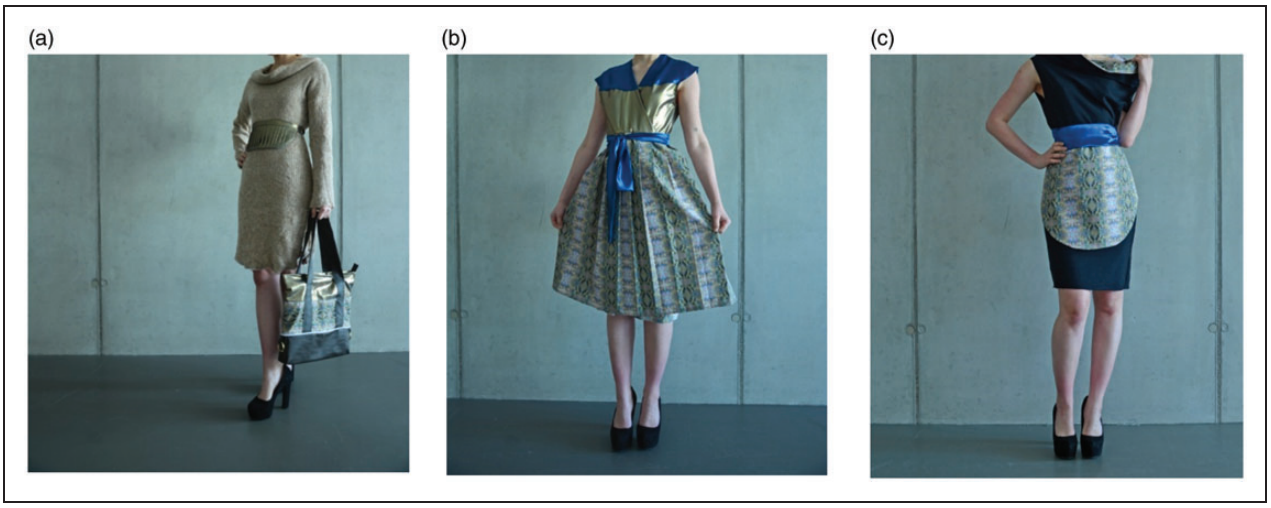

Figure 15. Fashion clothing with electromagnetic radiation protection.

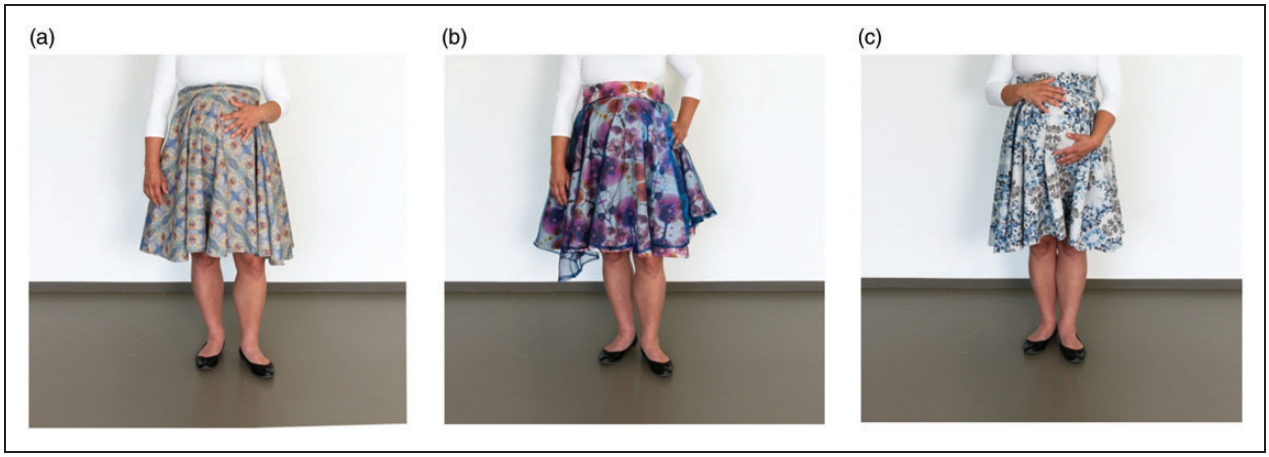

Figure 16. Fashion clothing with electromagnetic radiation protection intended for pregnant women.

It is impossible to design EM radiation clothing to completely protect the human body from EM radiation, because each aperture (placket, button holes, etc.), openings (collar, lack bottom, hem, etc.), and free spaces (uncovered head) in the clothing will allow the EM waves to penetrate into the human body. Nevertheless, recent findings on EM radiation and human health aim to protect at least the torso where sensitive organs (reproductive system, the fetus in pregnant women, etc.) are located. Figure 14 presents a schematic design of women's protective clothing; the gray color denotes the use of EM shielding fabric.

Figure 15 presents photographs of real EM shielding clothes for daily use. Figure 15(a) presents a woman's dress. In this case, EM shielding fabric was used to line the torso section. The upper fabric is a knitted nonconductive fabric, and the handbag in the image is also made of this special fabric, which protects information stored in the radio-frequency identification (RFID) tags in passports, credit cards, and other personal documents from unauthorized reading. The skirt part of the dress in Figure 15(b) is sewn directly from EM shielding fabric, whereas the top of the dress is made from nonconductive fabric. The apron presented in Figure 15(c) is made from EM shielding fabric. Moreover, conductive fabric is used both as a lining and a decorative element of the dress presented in this figure. The black fabric is a knitted nonconductive fabric. Figure 16 presents fashion clothing (the skirt is made directly from conductive fabric) with EM radiation protection intended for pregnant women. It should be noted that this special fabric can be subjected to traditional techniques of the garment manufacturing process, including cutting, sewing, and pressing/finishing.

Conclusion

In this paper, electrically conductive and EM shielding woven fabric was modified by digital printing, and the essential requirements for designing EM radiation protection clothing for daily use were studied.

It was found that an electrically conductive fabric satisfies the requirements for functionality. Its EM shielding at higher frequencies (i.e., the working frequencies of cell phones, radars, wireless networks, etc.) is higher than 30 dB, which classifies the fabric as excellent according to the grading published in FTTS-FA-003:2005.[7] A slight increase in the SE of the printed samples is attributed to a decrease in sample porosity after printing. It has been shown that WDs have a statistically significant effect on SE. The shielding ability of the fabric slightly decreases with an increasing number of WDs, but even after 20 cycles, the fabric's SE remains higher than 25 dB at a frequency of 1.5 GHz.

It was confirmed that it is possible to produce a patterned electrically conductive fabric by digital printing. No problems were evident in the actual printing process. Due to the presence of metal fibers in the fabric's structure, the colors of the design differ from the printed colors on the fabric surface; more precisely, they are darker compared with the design, and the CIE $L^*a^*b^*$ ΔE value is about 48. It was revealed that repeated washing has a statistically significant effect on color fastness for all studied color samples, whereas a decrease in chroma with an increasing number of WDs was observed. The CIE $L^*a^*b^*$ ΔE value (which describes the color difference between the washed sample and the reference sample) was higher than 2 after the initial washing and between 7 and 12 and 11 and 14 after the 10th and 20th WDs, respectively. This corresponds to grade 3, 2–3 after the first washing; grade 2, 1–2, 1 after the 10th washing; and grade 1 after the 20th washing. Based on this finding, it is recommended to investigate alternative methods for patterning electrically conductive fabric to obtain higher levels of color fastness. The creation of pills was observed after the eighth WD.

Basic air, heat, and mass transport parameters were measured and compared with the properties of nonconductive fabric of similar material composition and structure. Thermal resistance, thermal absorptivity, and AP were chosen as representative indicators of wearing comfort. It can be summarized that EM shielding fabric (raw or printed) does not have significantly different comfort properties from common textile fabrics, which makes it possible for application as a fabric in clothing design.

Finally, the design and preparation of radio-frequency protective clothing for daily use were discussed, and some prototypes of protective clothes made from printed electrically conductive fabric were produced and documented.

Declaration of conflicting interests

The authors declared no potential conflicts of interest with respect to the research, authorship, and/or publication of this article.

Funding

The authors disclosed receipt of the following financial support for the research, authorship, and/or publication of this article: This work was supported in part by the Technology Agency of the Czech Republic (research project of TG01010117 PROSYKO, the Ministry of Industry and Trade of the Czech Republic and the Ministry of Education, Youth and Sports of the Czech Republic (research project CZ.01.1.02/0.0/0.0/15_019/0004465 entitled Extreme shielding textile materials for special applications), and the European Union - European Structural and Investment Funds in the frames of Operational Programme Research, Development and Education (project Hybrid Materials for Hierarchical Structures (HyHi, Reg. No. CZ.02.1.01/0.0/0.0/16_019/0000843)).

References

1. Mao N. High performance textiles for protective clothing. In: Lawrence CA (ed) *High performance textiles and their applications*. Sawston: Woodhead Publishing, 2014, pp.91–143.
2. World Health Organization. *Establishing a dialogue on risks from electromagnetic fields*. Geneva: WHO, 2002.
3. Shi H, Wand J and Chen X. Research on electromagnetic shielding clothing. In: *proceedings of cross strait quad-regional radio science and wireless technology conference*, paper number: 12291690, pp. 211–213, IEEE, Harbin, China, 27–30 July 2011.
4. Yu ZC, Zhang JF, Lou ChW, et al. Investigation and fabrication of multifunctional metal composite knitted fabrics. *Text Res J* 2015; 85: 188–199.
5. Cheng K, Lee LM, Ramakrishna S, et al. Electromagnetic shielding effectiveness of stainless steel/polyester woven fabric. *Text Res J* 2001; 71: 42–49.
6. Su Ch and Chern J. Effect of stainless steel-containing fabrics on electromagnetic shielding effectiveness. *Text Res J* 2004; 74: 51–54.
7. FTTS-FA-003:2005 Specified requirements of electromagnetic shielding textiles.
8. Ondogan Z, Pamuk O, Ondogan EN, et al. Improving the appearance of all textile products from clothing to home textile using laser technology. *Optic Laser Technol* 2005; 37: 631–637.
9. Ortlek HG, Alpyildiz T and Kilic G. Determination of electromagnetic shielding performance of hybrid yarns knitted fabrics with anechoic chamber. *Text Res J* 2013; 83: 90–99.
10. Duran D and Kadoglu H. Electromagnetic shielding characterization of conductive woven fabrics produced

with silver-containing yarns. *Text Res J* 2015; 85: 1009–1021.
11. Safarova V and Militky J. Electromagnetic shielding properties of woven fabrics made from high-performance fibers. *Text Res J* 2014; 84: 1255–1267.
12. Shinagawa S, Kumagai Y and Urabe K. Conductive papers containing metallized polyester fibers for electromagnetic interference shielding. *J Porous Mater* 1999; 6: 185–190.
13. Lu Y and Xue L. Electromagnetic interference shielding, mechanical properties and water absorption of copper/bamboo fabric (Cu/BF) composites. *Compos Sci Technol* 2012; 72: 828–834.
14. Avloni J, Lau R, Ouyang M, et al. Polypyrrole-coated nonwovens for electromagnetic shielding. *J Ind Text* 2008; 38: 55–68.
15. Yildiz Z, Usta I and Gungor A. Electrical properties and electromagnetic shielding effectiveness of polyester yarns with polypyrrole deposition. *Text Res J* 2012; 82: 2137–2148.
16. Bahadir SK, Jevsnik S, Fakin D, et al. Color and electrical resistance evaluation of cotton fabric composed of stainless-steel yarns treated with direct and reactive dyes. *Text Res J* 2016; 86: 1356–1371.
17. Tunakova V, Hrubosova Z, Tunak M, et al. Laser surface modification of electrically conductive fabrics: material performance improvement and design effects. *Optic Laser Technol* 2018; 98: 178–189.
18. Vojtech L and Neruda M. Design of radiofrequency protective clothing containing silver nanoparticles. *Fibre Text East Eur* 2013; 101: 141–147.
19. Safarova V, Hes L and Militky J. An approach to electrical resistance measurement eliminating contact resistance problem. In: Pinker J (ed) *proceedings of international conference of applied electronics*, paper number: 14855859, pp. 259–262. IEEE: Pilsen, Czech Republic, 8–10 September 2015.
20. Color Space Conversion. Matlab Documentation, https://www.mathworks.com/help/vision/ref/colorspaceconversion.html#bqdn5yt-1 (accessed 27 November 2019).
21. EN ISO 6330:2012. Textiles – domestic washing and drying procedures for textile testing.
22. ISO 105-A04:1989. Textiles – test for colour fastness.
23. Hurren Ch. Dyeing and colouring tests for fabrics. In: Hu J (ed) *Fabric testing*. Boca Raton, FL: Taylor & Francis, 2008, pp.255–274.
24. STM 4935-18:2018. Standard test method for measuring the electromagnetic shielding effectiveness of planar materials.
25. ISO 9237:1995. Textiles – determination of the permeability of fabrics to air.
26. Bajzik V, Hes L and Dolezal I. Changes in thermal comfort properties of sportswear and underwear due to their wetting. *Ind J Fibre Text Res* 2016; 41: 161–166.
27. Boguslawska-Baczek M and Hes L. Determination of heat transfer by radiation in textile fabrics by means of method with known emissivity of plates. *J Ind Text* 2014; 44: 115–129.
28. Safarova V and Militky J. Multifunctional metal composite textile shields against electromagnetic radiation – effect of various parameters on electromagnetic shielding effectiveness. *Polym Compos* 2017; 38: 309–323.
29. Plot Lab Color Coordinates. MATLAB File Exchange, https://www.mathworks.com/matlabcentral/fileexchange/44965-plot-lab-color-coordinates (accessed 27 November 2019).

Appendix 3

S. Palanisamy, **V. Tunakova**, and J. Militky, "Fiber-based structures for electromagnetic shielding - comparison of different materials and textile structures," Text. Res. J., vol. 88, no. 17, pp. 1992–2012, 2018.

Textile Research Journal

Original article

Textile Research Journal
2018, Vol. 88(17) 1992–2012

DOI: 10.1177/0040517517715085
journals.sagepub.com/home/trj
SAGE

Fiber-based structures for electromagnetic shielding – comparison of different materials and textile structures

Sundaramoorthy Palanisamy, Veronika Tunakova and Jiri Militky

Abstract

In this study, 32 different electro-conductive fabrics and seven different non-conductive fabrics were taken for an analysis of their electromagnetic shielding ability, electrical resistivity and air permeability. According to the present state of development of electromagnetic shielding textile structures, a diverse set of samples was selected, including stainless steel, copper, silver, aluminum, carbon and polypyrrole as a conductive component. The ASTM D4935 coaxial transmission line method was used to study the electromagnetic shielding and the ASTM D257 ring electrode method was used to evaluate the surface and volume electrical resistivity of all the samples. Air permeability was considered as an additional important parameter for the production of electromagnetic radiation protective fabrics designed for technical or clothing applications. It was confirmed that textile structures made of conventional textile fibers are transparent to an electromagnetic field. The electromagnetic shielding effectiveness of non-conductive samples is less than 0.2 dB regardless of material composition. On the other hand, the electromagnetic shielding effectiveness of electro-conductive samples containing different content and types of conductive component ranges from 1 to 79 dB at the high-frequency range, whereas the woven sample containing 75 wt% of staple metal fiber provides excellent shielding ability together with high air permeability. It was confirmed that, in particular, the surface resistivity can be used to predict the electromagnetic shielding ability of fabric samples due to a strong inverse relationship between these two parameters.

Keywords

electromagnetic shielding effectiveness, textile, electro-conductive, non-conductive, electrical resistivity, air permeability

Recently, the usage of electrical and electronic devices has grown rapidly. Many devices, such as alternating current (AC) motors, digital computers, calculators, printers, modems, electronic typewriters, digital circuits, transmission lines and electronic home appliances, including Wi-Fi routers and cellular phones, emit electromagnetic (EM) waves that can result in some electromagnetic interference (EMI) problems.[1] The EM spectrum contains an array of EM waves increasing in frequency from extremely low frequency and very low frequency through radio frequency (RF) and microwaves to infrared (IR) light, visible light, ultraviolet (UV) light, X-rays and gamma rays.[2] Many devices, such as cell phones with frequencies of 900, 1800, 2100 and 2600 MHz, microwave ovens of 2450 MHz, radar signal communication systems extending from 1 to 10,000 MHz and FM/AM radio broadcasts of 30–300 MHz and 300–3000 kHz, contribute to such exposure.[3] The use of electronic equipment causes EM radiation, which can be harmful for the performance of electronic and electrical equipment and also for human health.[4] Therefore, it has become essential to shield against all interference sources of the EM energy.[5] When an EM wave enters an organism, it causes heat to come out by vibrating the molecules.

Faculty of Textile Engineering, Technical University of Liberec, Czech Republic

Corresponding author:
Sundaramoorthy Palanisamy, Faculty of Textile Engineering, Technical University of Liberec, Studentská 2, Liberec 461 17, Czech Republic.
Email: sundaramoorthy.palanisamy@tul.cz

The heat developed in the tissues is mainly a result of the Foucault currents flowing in the liquids of the cells. Shielding is necessary to prevent the negative effects of the EM waves. EM shielding can be described as the prevention of EM radiation transmission by a material.[6]

Currently, many EM shielding studies exist that use electro-conductive textile materials. The incorporation of conductive fillers and fabric surface coatings are the two major methods to develop EMI shielding fabrics.[7] Several methods for developing EM radiation shields are available, such as ionic plating, electroless plating, cathode sputtering, conductive paints, vacuum metallization, zinc paints, zinc flame spraying, zinc arc spraying and conductive fillers, such as copper, stainless steel (SS) and aluminum in different forms (fibers, particles, wires). The above-mentioned methods can be categorized under two headings, being the surface treatments and the fillers. The surface treatments are often time consuming, laborious and costly. The conductive fillers in the form of particulates, fibers and filaments are increasingly being used for shielding of EM radiation.[8] The application of EM shielding with textile materials is used more widely and normally instead of metal screens and other traditional shielding materials, because metal screening materials have many disadvantages, particularly weight, corrosion, difficulty in adjusting the shielding effectiveness (SE) and limited mechanical flexibility, while textile materials are generally lighter (having lower density), more flexible and cheaper.[9]

EM shielding, based on polymers with conductive fillers, has been gaining more significant roles in a variety of technological domains and is becoming the research focus of numerous studies as a part of a growing research trend. Conductive filler particles, such as silver, copper, gold, etc., and carbon particles, such as carbon nanotubes, were used for EM shielding applications in many studies, giving excellent results.[10,11] Conductive polymers, on the other hand, allow an excellent control of the electrical stimulus, possess very good electrical and optical properties, have a high conductivity/weight ratio and can be made biocompatible, biodegradable and porous. The conductive polymers, such as polypyrrole (PPy), polyaniline, polyacetylene, etc., have been described for their EM shielding applications in many scientific studies.[12–15]

Electrically conductive fibers are very often used for EM shielding applications because natural or synthetic fibers, for example, cotton, polyester (PES), polyamide, polyacrylic and cellulose acetate fibers, exhibit very poor electric conductivity. Currently, there are many metal-coated textile fibers, metal fibers, carbon based fibers, etc., available on the market. Carbon-matrix composites with different forms of carbon (fiber, nanotube) were found to be an excellent EMI shielding material with SE of 124 dB, low surface impedance and high reflectivity in the frequency range from 0.3 MHz to 1.5 GHz in this study.[16–18]

Conductive fabrics can also be made of 100% metal fiber yarns, such as SS, copper etc.; however, they are difficult to process. These types of yarns tend to have low flexibility due to the high stiffness of metal fibers, which produces heavier and uncomfortable fabrics. To reduce this effect, totally metallic yarns are replaced by blending with traditional fibers to diminish the overall stiffness of the fabric and to improve the touch properties of the fabrics.[19] Usage of various types of textile structures, such as woven,[4,6] nonwoven,[20,21] weft knit,[22] warp knit,[23] braid,[18] composite,[22,24] etc., containing metal fiber or wire has been reported for EMI shielding. The EM SE results show that by incorporating staple SS fibers (diameter 8 or 12 μm), a textile structure with shielding of 20–45 dB (which means that more than 99.9% of EM was attenuated) and other positive properties (mechanical flexibility, drape, etc.) can be obtained.[25–27] Further, the incorporation of metal wires (SS, copper) used as the core or shell of yarns offers an interesting solution for the limited amount of applications due to their poor mechanical properties.[28,29]

A literature review shows that a number of new fiber-based materials suitable for shielding EM waves have been developed and introduced. Increasing the conductivity of material has certain advantages and disadvantages. The following factors should be considered when selecting between various production methods and materials: cost, thickness, stability, durability, aesthetic appearance, shape, physical strength, expected environment, recyclability and environmental issues. Authors very often use different methods for experimental determination of the EM shielding ability of samples with regard to several active standards[30] and available instrumentation in their work place. Unfortunately, since there are many factors (EM wave propagation principle, material properties, sample size, test setup geometry) that affect the measurement results, the values for SE obtained by different methods cannot be compared. Therefore, the same measurement method and test setup geometry should be used in order to compare different materials.

The main objective of this study is therefore investigation of the EM shielding ability of various electro-conductive textile samples based on the usage of several types and quantities of conductive components (carbon fiber, conductive polymer-coated fabrics, metal-coated fibers, metal-coated fabrics, metal fiber containing yarns, metal foil) and different structural approaches (woven, knitted, nonwoven, foil) by the identical measurement method. Higher attention is dedicated to

shielding of frequencies around 1–1.5 GHz, because these frequencies are close to the working frequencies of common devices (cell phones, radars, wireless routers, etc.). Another partial aim of this study is to confirm that textile samples made of traditional textile fibers are totally unsuitable for the usage mentioned above. To show that EM shielding ability is not the only requirement for the production of protective textiles for technical or clothing purposes was one of the other partial goals and, therefore, the physical characteristics and air permeability of the samples were studied. Consequently, another main goal is to review and generalize the advantages and limitations of different electro-conductive fabrics designed for protective textiles against the EM field for certain applications.

Samples were tested for the EMI SE, electrical resistivity and air permeability according to the standards. The effect of fabric structure (woven, knitted, nonwoven and foils), various electro-conductive sample preparation techniques (metal coating, hybrid metal yarn, carbon materials, conductive polymers, metal paints and metal-coated fibers) and the content of the conductive component on EM shielding properties was studied. An identical methodology, more precisely the coaxial transmission line method according to the ASTM D4935-10, was applied on the whole sample set to avoid difficulties when comparing data gained by different measurement methods. The air permeability, which is connected with the porosity of the material, plays a very important role in both transport properties as well as EM shielding. Electrical conductivity is another important factor, together with the sample's ability to shield the EM field and, for that reason, this parameter was also taken into account.

Materials

Different types of samples having woven (W), knitted (K), nonwoven (NW) and foil (F) structures were used for this study. Seven categories were distinguished among the 39 samples, based on similar types of material, namely: non-conductive (N), carbon (Ca), polypyrrole (PPy) coating, metallic fiber (Mf), metallic coating (Mc), hybrid yarn (H) and aluminum foil (F). These are shown in Table 1.

The seven non-conductive samples consist of natural and synthetic fiber-based woven fabrics. The second category represents three carbon (Ca) samples, two of which are woven fabrics with 100% carbon fiber and the third is nonwoven PES fabric filled with carbon particles. The third category is represented by the only woven fabric sample prepared by in situ chemical oxidative polymerization of the pyrrole on a PES fabric (polymerization temperature 15°C, polymerization time 8 h, monomer concentration 5.8 g/l). In the fourth category are four metal-coated fiber samples that consist of two nonwoven fabrics produced with copper sulfide (CuS)/ silver (Ag) coated on acrylic (polyacrylonitrile; PAN) fiber (brand name Eurostatic) blended with PES fiber in the ratios of 20:80 and 14:86, respectively; a nonwoven fabric with composition of 10% SS fiber ($d = 8\,\mu m$, trade name Bekinox) and 90% PES staple fiber and a plain weave woven fabric fully made-up of 100% Ag-coated PES fiber spun yarn (trade name X-Static). Five different types of metal-coated fabrics are included in the fifth category, which consists of two PES nonwoven fabrics ($220\,g/m^2$) coated with 65% Cu powder paste and 50% Al paste, respectively; two woven rip stop fabrics, one fabric having Ag-plated nylon yarn (trade name Breman) and another fabric having Cu/Ag-plated nylon yarn (trade name Kassel); one flat knitted fabric made-up of Ag-plated nylon yarn (trade name Ballinger). Seventeen fabric samples made of hybrid yarns consisting of SS fiber ($d = 8\,\mu m$, Bekinox) and polypropylene (PP) fiber blended in different ratios represent the sixth category. Four woven twill weave fabrics were produced by hybrid yarn with different compositions of SS fiber (10%, 20%, 40% and 75%) blended with PP fiber (90%, 80%, 60% and 25%), respectively; five woven twill sandwich (Ws) fabric samples were prepared by one, two, three, four and five layers with composition of 1% SS fiber blend with 99% PP fiber. Five knitted samples containing three knitted single jersey (Ks/j) fabrics were produced by a hybrid yarn with different ratios of SS fiber: PP fiber (10:90, 15:85 and 20:80, respectively); another two knitted fabric samples having pique design (Kpq) and double jersey (Kd/j) pattern were produced with the hybrid yarn of 10% SS fiber and 90% PP fiber, respectively. The samples also include three twill weave woven grid (WG) (5 mm × 5 mm) samples consisting of 100% PP yarn in body and hybrid yarn in grid portion (ratio of SS:PP – 1:99, 10:90 and 20:80). All the hybrid yarn fabric samples were made-up of 50 tex yarn for woven fabrics and 25 tex yarn for knitted fabrics. Two Al metal foil samples with thicknesses of 0.04 mm (laminated on both sides) and 0.01 mm (pure food grade) are in the seventh category. Sample details together with sample codings are shown in Table 1. Figure 1 shows microscopic images of some electro-conductive and non-conductive samples at 50× magnification.

Characterization

The sample set was characterized mainly according to its EM shielding ability in the microwave range. Further electrical properties of the sample set were

Table 1. Sample coding, its description and structure

Sample code	Sample details	Structure	Type of design	Yarn count [tex] (warp/weft)
Non-conductive samples				
N Vis W	100% viscose fabric	Woven	3/1 twill	16/28
N PESW	100% PES fabric	Woven	Plain	10/16
N Wo W	100% wool fabric (Figure 1(a))	Woven	2/2 twill	50/50
N Li W	100% linen fabric	Woven	Plain	75/75
N Co W	100% cotton fabric	Woven	Plain	15/15
N Co WL	100% cotton fabric(laminated on one side)	Woven	3/1 twill	30/60
N Gls W	100% glass fabric	Woven	Plain	20/20
Carbon material samples				
Ca W 1	Carbon fabric (Figure 1(b))	Woven	Plain	75/90
Ca W 2	Carbon fabric(Figure 1(c))	Woven	Satin	120/150
Ca NW	Carbon particle coated fabric	Nonwoven	Needle p.	–
Polymer-coated sample				
PPy/PESW	PPy coated PES fabric (Figure 1(d))	Woven	Plain	35/35
Metal-coated fiber samples				
Mf Ag W	100% Ag-coated PES fiber yarn fabric (X-Static) (Figure 1(e))	Woven	Plain	15/15
Mf20EuNW	20%CuS-Ag coated PAN fiber (Eurostatic)/80% PES fabric (Figure 1(f))	Nonwoven	Needle p.	–
Mf14EuNW	14% CuS-Ag-coated PAN fiber (Eurostatic)/86% PES fabric	Nonwoven	Needle p.	–
Mf10SSNW	10% SS/90% PES fiber fabric	Nonwoven	Needle p.	–
Metal-coated samples				
Mc Cu NW	65% Cu powder painted PES fabric	Nonwoven	Needle p.	–
Mc Al NW	50% Al painted PES fabric (Figure 1(g))	Nonwoven	Needle p.	–
Mc Ag K	Ag-plated nylon yarn mesh (Balingen) (Figure 1(h))	Knitted	Flat	5
Mc Ag W	Ag-plated nylon yarn fabric (Breman)	Woven	Rip stop	5/5
Mc Cu/Ag W	Cu-Ag-plated nylon yarn fabric (Kassel) (Figure 1(i))	Woven	Rip stop	10/10
Hybrid yarn (SS/PP) samples				
H 10SS W	Hybrid 10% SS/PP fabric	Woven	2/2 Twill	50/50
H 20SS W	Hybrid 20% SS/PP fabric (Figure 1(j))	Woven	2/2 Twill	50/50
H 40SS W	Hybrid 40% SS/PP fabric	Woven	2/2 Twill	50/50
H 75SS W	Hybrid 75% SS/PP fabric	Woven	2/2 Twill	50/50
H 1SS Ws1	Sandwich 1% SS/PP fabric – 1 layer(Figure 1(k))	Woven	2/2 Twill	50/50
H 1SS Ws2	Sandwich 1% SS/PP fabric – 2 layer	Woven	2/2 Twill	50/50
H 1SS Ws3	Sandwich 1% SS/PP fabric – 3 layer	Woven	2/2 Twill	50/50
H 1SS Ws4	Sandwich 1% SS/PP fabric – 4 layer	Woven	2/2 Twill	50/50
H 1SS Ws5	Sandwich 1% SS/PP fabric – 5 layer	Woven	2/2 Twill	50/50
H 10SS Ks/j	Knitted hybrid 10% SS/PP fabric	Knitted	Single j.	25
H 15SS Ks/j	Knitted hybrid 15% SS/PP fabric (Figure 1(l))	Knitted	Single j.	25
H 20SS Ks/j	Knitted hybrid 20% SS/PP fabric	Knitted	Single j.	25
H 10SS Kpq	PC Pique 10% SS/PP fabric	Knitted	Pique	25
H 10SS Kd/j	Double jersey 10% SS/PP fabric (Figure 1(m))	Knitted	Double j.	25
H 1SS WG	Hybrid 1% SS/PP fabric – 5 mm grid	Woven	2/2 Twill	50/50
H 10SS WG	Hybrid 10% SS/PP fabric – 5 mm grid (Figure 1(n))	Woven	2/2 Twill	50/50
H 20SS WG	Hybrid 20% SS/PP fabric – 5 mm grid	Woven	2/2 Twill	50/50
Metal foil				
F Al	Aluminum foil (Figure 1(o))	Foil	Sheet	–
F Al FG	Aluminum foil food grade	Foil	Sheet	–

PPy: polypyrrole; CuS: copper sulfide; Ag: silver; PAN: polyacrylonitrile; Al: aluminum; PP: polypropylene; PES: polyester; SS: stainless steel.

Figure 1. Microscopic images at 50× magnification of samples: (a)"N Wo W"; (b) "Ca W 1"; (c) "Ca W 2"; (d) "PPy/PESW"; (e) "Mf Ag W"; (f) "Mf 20Eu NW"; (g) "Mc Al NW"; (h) "Mc Ag K"; (i) "Mc Cu/Ag W"; (j) "H 20SS W"; (k) "H 1SS Ws1"; (l) "H 15SS Ks/j"; (m) "H 10SS Kd/j"; (n) "H 10SS WG"; (o) "F Al".

explored because of an assumed correlation with EM shielding ability and a possibility of prediction the EM SE of the sample based on the knowledge of the electrical properties. Moreover, the air permeability together with basic geometrical characteristics of the samples were chosen as very important parameters, especially for the production of protective textiles designed for technical or clothing purposes.

Electrical properties evaluation

The volume and surface resistance of the sample set were measured according to the standard ASTM D257-07,[31] under a 100 V direct current (DC) power supply, using concentric electrodes (pressure of 2.3 kPa was applied), at the temperature $T = 21^{\circ}C$ and the relative humidity $RH = 54\%$ using an air-conditioned room. Samples were placed in the air-conditioned room 24 h prior to testing. The above-mentioned standard is intended for insulating samples and it was chosen due to the wide sample set containing insulating, semi-conductive and conductive samples allowing a comparison of the results. Volume resistance is measured by applying a voltage potential across the opposite sides of the sample and measuring the resultant current through the sample. Volume resistivity, ρ_V [Ω.mm], was calculated from the following equation

$$\rho_v = R_v\left(\frac{S}{t}\right) \quad (1)$$

where R_V [Ω] is the volume resistance reading, t is the thickness of the fabric [mm], S is the surface area of the electrode [mm^2] ($\pi D_2^2/4$), and D_2 is the inner diameter of the outer ring electrode [mm].

Surface resistance is measured by applying a voltage potential between two electrodes of specified configuration that are in contact with the same side of the tested material. Surface resistivity ρ_S [Ω] was calculated from the following equation

$$\rho_s = R_s\left(\frac{\pi D_0}{g}\right) \quad (2)$$

where R_S [Ω] is the surface resistance reading, D_0 is $(D_2 - D_1)/2$, D_1 is the outer diameter of the center electrode [mm], D_2 is the inner diameter of the outer ring electrode [mm] and g is the distance between D_1 and D_2 [mm]. The measurements were carried out at 10 different places on the textile samples because of the subsequent statistical analysis. The mean values and 95% confidence intervals for means of ρ_V and ρ_S are summarized in Table 2.

Electromagnetic shielding effectiveness evaluation

The SE of the sample set was measured according to the ASTM D4935-10 standard[32] for the planar materials using a plane-wave, the far-field EM wave at the temperature $T = 21^{\circ}C$ and the relative humidity $RH = 54\%$ using an air-conditioned room, and samples were placed in the air-conditioned room 24 h prior to testing. The SE of the samples was measured over the frequency range from 30 MHz to 1.5 GHz. The setup consisted of a sample holder with its input and output connected to the network analyzer. A SE test fixture (Electro-Metrics, Inc., model EM-2107A) was used to hold the sample. The design and dimension of the sample holder follows the ASTM method mentioned above. The sample was subjected to pressure of 5.2 kPa during this measurement configuration. A vector analyzer, Rohde & Schwarz ZN3, was used to generate and receive the EM signals. The standard mentioned above determines the SE of the fabric using the insertion-loss method. A reference measurement for the empty cell was required for the SE assessment. A ''through'' calibration with the help of the reference sample was made first. A load measurement was performed on a solid disk shape sample subsequently. The reference and load specimens must be of the same material and thickness. Both the reference and load sample geometries are in accordance with ASTM D 4935-10. The measurements were performed at five different places of the textile samples because of the subsequent statistical analysis. The mean values and 95% confidence intervals for means of the SE for 1.5 GHz frequency are summarized in Table 2.

Fabric properties

The fabric mass per unit area (GSM; w) [g/m^2] was measured using the standard ASTM D 3776[33] and the sample size was 100 cm^2. Fabric thickness (t) was measured using a thickness gauge [mm], as per standards ASTM D1777 (woven, knitted and foil samples) and ASTM D 5729 (nonwoven samples), and pressure of 1 kPa was used. The mean values of these two parameters are shown in Table 2. Air permeability (A) [l/m^2/s] of the samples was measured using the Textest FX 3300 at 100 Pa as per the ISO 9237 standard.[34] The mean values and 95% confidence intervals for the means of A are summarized in Table 2.

Results and discussion

Electromagnetic shielding ability of the samples

Frequency-dependent electromagnetic shielding effectiveness. Figure 2 shows the dependence of the EM SE in dB on the whole measured frequency range

Table 2. Mean values of the sample thickness, mass per unit area, air permeability, surface resistivity, volume resistivity and electromagnetic shielding effectiveness (EM SE) at 1.5 GHz frequency

Sample code	Thickness t [mm]	Mass per unit area w [g/m^2]	Air permeability A [l/m^2/s]	Surface resistivity ρ_s [Ω]	Volume resistivity ρ_v [Ω.mm]	EM SE (f = 1.5 GHz) [dB]
N Vis W	0.30	149	559 ± 19	7.8E + 11 ± 9.1E + 10	4.0E + 12 ± 3.9E + 11	<0.1
N PES W	0.22	87	152 ± 4	4.3E + 11 ± 1.5E + 11	2.0E + 12 ± 7.1E + 11	<0.1
N Wo W	0.54	267	86 ± 3	7.8E + 12 ± 1.2E + 12	6.4E + 13 ± 4.8E + 12	<0.1
N Li W	0.61	221	658 ± 27	8.3E + 10 ± 8.2E + 09	1.0E + 11 ± 6.3E + 09	<0.1
N Co W	0.31	119	171 ± 4	9.8E + 11 ± 9.8E + 10	2.1E + 12 ± 3.6E + 11	<0.1
N Co WL	0.51	276	0	5.2E + 11 ± 6.3E + 10	1.4E + 12 ± 1.1E + 11	<0.1
N Gls W	0.09	85	496 ± 32	4.1E + 13 ± 6.2E + 12	5.4E + 14 ± 1.3E + 14	<0.1
Ca W 1	0.59	190	416 ± 36	3.1E + 02 ± 7.0E + 01	8.3E + 02 ± 1.6E + 02	57 ± 1
Ca W 2	0.85	360	246 ± 7	9.3E + 01 ± 4.5E + 01	2.6E + 02 ± 5.7E + 01	49 ± 0
Ca NW	5.09	700	1110 ± 30	1.3E + 07 ± 9.5E + 06	1.1E + 07 ± 5.3E + 06	4 ± 0
PPy/PES W	0.49	195	73 ± 33	5.0E + 05 ± 1.7E + 05	9.2E + 06 ± 1.1E + 07	12 ± 0
Mf Ag W	0.22	109	24 ± 0	3.5E + 01 ± 1.8E + 01	1.7E + 03 ± 1.7E + 03	67 ± 1
Mf 20Eu NW	7.01	318	985 ± 50	9.4E + 02 ± 8.0E + 01	5.8E + 02 ± 7.8E + 01	12 ± 0
Mf 14Eu NW	6.51	317	1240 ± 112	2.2E + 03 ± 5.1E + 02	1.2E + 03 ± 1.1E + 02	8 ± 1
Mf 10SS NW	6.33	280	1142 ± 33	3.0E + 06 ± 3.5E + 06	7.5E + 05 ± 4.3E + 05	14 ± 1
Mc Cu NW	1.74	580	76 ± 15	4.2E + 12 ± 2.8E + 12	4.7E + 12 ± 1.7E + 12	1 ± 0
Mc Al NW	2.14	550	7 ± 1	1.4E + 10 ± 8.7E + 09	1.1E + 11 ± 1.4E + 11	5 ± 0
Mc Ag K	0.26	48	4820 ± 136	1.5E + 02 ± 1.6E + 02	1.7E + 03 ± 1.2E + 03	50 ± 0
Mc Ag W	0.07	43	178 ± 3	1.1E + 02 ± 7.6E + 01	1.7E + 03 ± 5.4E + 02	54 ± 1
Mc Cu/Ag W	0.09	88	27 ± 1	2.6E + 01 ± 1.1E + 01	7.8E + 02 ± 5.1E + 02	79 ± 3
H 10SS W	0.80	221	193 ± 3	1.7E + 06 ± 2.3E + 05	2.0E + 06 ± 8.8E + 05	29 ± 0
H 20SS W	0.76	208	304 ± 8	1.3E + 05 ± 4.6E + 04	2.2E + 05 ± 9.2E + 04	35 ± 0
H 40SS W	0.71	206	419 ± 11	2.8E + 03 ± 7.6E + 02	4.5E + 03 ± 1.7E + 03	42 ± 0
H 75SS W	0.58	160	1262 ± 39	1.4E + 02 ± 4.0E + 01	5.5E + 02 ± 1.1E + 02	51 ± 0
H 1SS Ws1	0.82	233	134 ± 11	5.8E + 06 ± 6.6E + 06	1.3E + 07 ± 1.3E + 07	12 ± 0
H 1SS Ws2	1.63	467	74 ± 2	5.8E + 06 ± 6.6E + 06	2.1E + 07 ± 2.1E + 07	18 ± 0
H 1SS Ws3	2.45	700	51 ± 3	5.8E + 06 ± 6.6E + 06	7.8E + 12 ± 1.5E + 12	21 ± 2
H 1SS Ws4	3.26	934	37 ± 1	5.8E + 06 ± 6.6E + 06	5.9E + 12 ± 1.4E + 12	25 ± 2
H 1SS Ws5	4.08	1167	30 ± 1	5.8E + 06 ± 6.6E + 06	5.3E + 12 ± 7.7E + 11	29 ± 2
H 10SS Ks/j	0.75	158	1260 ± 47	1.4E + 08 ± 8.3E + 07	7.5E + 05 ± 5.7E + 05	8 ± 3
H 15SS Ks/j	0.71	150	1048 ± 24	2.4E + 07 ± 8.4E + 06	7.7E + 05 ± 6.6E + 05	10 ± 0
H 20SS Ks/j	0.77	156	1420 ± 18	6.1E + 05 ± 3.5E + 05	4.9E + 03 ± 2.5E + 03	9 ± 0
H 10SS Kpq	1.13	186	1320 ± 36	6.9E + 06 ± 4.1E + 06	1.3E + 06 ± 7.5E + 05	10 ± 1
H 10SS Kd/j	1.39	199	1176 ± 28	2.5E + 06 ± 4.8E + 05	6.3E + 05 ± 3.8E + 05	9 ± 0
H 1SS WG	0.82	222	112 ± 3	4.5E + 12 ± 1.5E + 12	5.4E + 14 ± 6.7E + 14	1 ± 0
H 10SS WG	0.82	221	107 ± 5	1.2E + 07 ± 5.9E + 06	1.0E + 07 ± 1.1E + 07	10 ± 1
H 20SS WG	0.83	223	117 ± 7	8.9E + 05 ± 3.0E + 05	1.0E + 06 ± 3.6E + 05	15 ± 0
F Al	0.04	55	0	1.2E + 13 ± 4.0E + 12	4.1E + 14 ± 2.3E + 14	78 ± 5
F A lFG	0.01	24	0	6.1E + 01 ± 1.8E + 01	1.6E + 04 ± 3.6E + 03	78 ± 4

PPy: polypyrrole; Ag: silver; Al: aluminum; PES: polyester; SS: stainless steel.

(from 30 MHz to 1.5 GHz) for all the samples. The frequency-dependent SE curves were divided into six different graphs with respect to different groups of the samples to provide easier inspection.

In this section, frequency-dependent behavior of the sample SE will be analyzed. Further comparison of the samples at certain frequencies will be presented in the following sections. It is seen from Figure 2(a) that

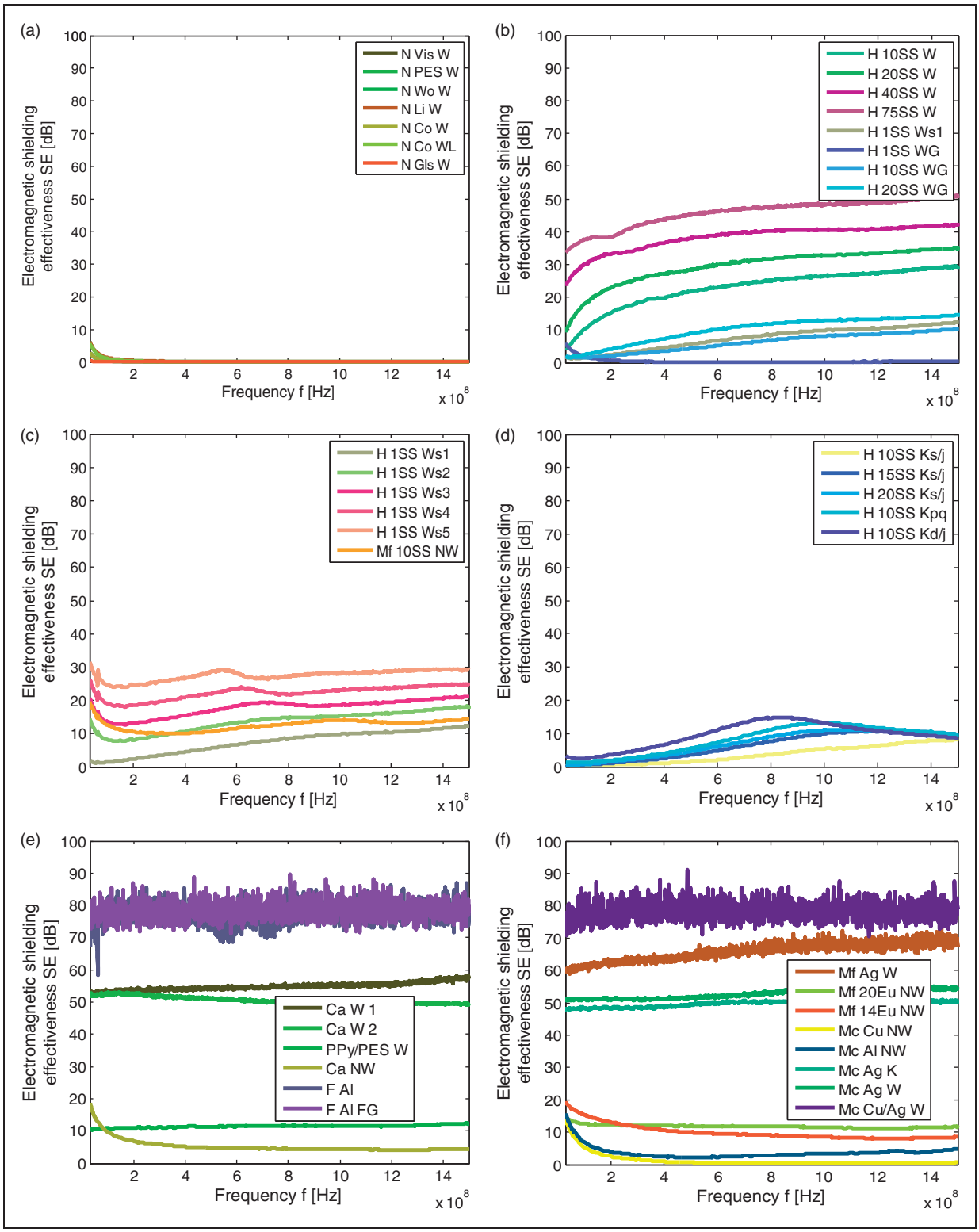

Figure 2. Graphs of the electromagnetic shielding effectiveness *SE* [dB] versus frequency, *f* [Hz] ($f = 30$ MHz–1.5 GHz) for: (a) non-conductive samples; (b) woven hybrid yarn samples containing various percentages of stainless steel (SS); (c) woven hybrid yarn sandwich samples containing 1% SS and 20% SS nonwoven samples; (d) different structures of the knitted hybrid yarn samples containing various percentages of SS; (e) carbon woven and nonwoven samples, polypyrrole-coated sample and Al foil samples; (f) metal-coated fiber samples and metal-coated fabric samples with different structures.

samples made of traditional textile materials, including cotton, wool, linen, PES, viscose or glass fibers, have almost no SE, especially at high frequencies (frequencies higher than 150 MHz).This result was expected, because the major part of the textile fibers belongs to electric insulators, which is associated with the fact that each of the electrons are fixed to the atomic nucleus or shared in atomic bonds. However, the electric conductance of the traditional fibers is not fully neutral and it depends on the content of various additives or the moisture content.[35]

Figure 2(b) shows the EM SE of the hybrid yarn woven samples with different SS fiber content (''H SS W''), which increases logarithmically with the increasing frequency. It is seen that the EM SE values in this group of the samples are increasing (up to 50 dB at 1.5 GHz frequency) with increasing metal fiber content (10%, 20%, 40% and 75% of the SS) in the sample on the whole frequency range. By the incorporation of a higher amount of SS fiber, the electrical conductivity of the sample is increasing and therefore the components of total SE, that is, the reflection and absorption coefficient, are increasing. In this figure (Figure 2(b)), the frequency-dependent EM SE sample group, where hybrid yarns with different metal fiber content form only a conductive grid (conductive yarn spacing is 5 mm in the warp and weft directions) in non-conductive woven fabric (''H SS WG'') are also presented. These groups of samples contain only about 10% of conductive yarns (90% of non-conductive yarns) in its volume, which means that the samples with a conductive grid created by hybrid yarns containing 1%, 10% and 20% of metal fiber contain actually 0.1%, 1% and 2% of staple metal fiber, respectively. It is evident that these grid samples have generally lower shielding ability (up to 15 dB at 1.5 GHz frequency) because they contain lower metal content compared to the samples completely made of hybrid yarns and also have more space (places made of non-conductive yarn) for penetration of the EM waves. The SE is logarithmically increasing with increasing frequency in this case as well (except the sample with a grid created of 1% SS yarn). This logarithmical behavior is in good agreement with the well-known theory.[36] The 1% SS yarn grid sample (''H 1SS WG''), which has 99.6% non-conductive material, shows a similar trend to non-conductive samples (the electric conductivity of the sample is too low to be able to act as a barrier against the EM field).

Figure 2(c) shows the increase of the EM SE value by increasing the number of electro-conductive layers of the woven sample (''Ws''), whereas the EM SE of the single woven sample containing 1% of SS is 12 dB and the EM SE of five layers of the same fabric is 29 dB at 1.5 GHz frequency. This phenomenon can be explained by a higher thickness of the sandwich compared with a single layer fabric, which directly affects the absorption component of the SE and by the presence of multiple reflections of waves in the case of increasing number of the layers. The EM SE of a single woven sample follows the logarithmical dependence on frequency. Sandwiched samples also follow the above-mentioned logarithmical trend, but local maximums in medium frequencies and an increase in very low frequency appears. The local maximum is shifting from higher frequencies (10E + 8 Hz) to lower frequencies (5.5E + 8 Hz) with the increasing number of layers. It is seen that the sandwiched sample containing five layers of woven sample with 1% of SS embodies similar SE ($SE = 30$ dB at 1.5 GHz) as the single layer sample with 10% of SS, which means that layering can create a more effective EM shielding structure. Nevertheless, sample thickness and the GSM increased five-fold (having five layers) and it is expected that the air permeability of the sample is significantly lowered at these sandwiched systems. The nonwoven (NW) sample containing 10% of SS fiber has a lower SE (14 dB at 1.5 GHz) than the woven sample containing the same portion of conductive component (30 dB at 1.5 GHz) despite the higher thickness of the sample, because of the discontinuous link between the conductive fibers in the bulky NW sample. It can also be observed that the frequency-dependent behavior of SE of the nonwoven sample is totally different from the woven samples. The SE of the nonwoven sample is almost constant in the full frequency range.

Knitted (K) samples with SS staple fiber (Figure 2(d)) behave differently compared with the woven samples. The EM SE of the knitted samples increases according to the power function up to a certain frequency and then decreases for single jersey (s/j) (15 and 20 wt%), double jersey (d/j) and pique (pq) knitted fabric samples. It is possible to observe the global maximum (inflection point) of the SE in the frequency range from 700 MHz to 1100 MHz. The higher the metal fiber content in the knitted sample results in the lower position (frequency) of the global maximum and at the same times the higher SE at this point (around 15 dB at 8E + 08 Hz for knitted sample containing 20% of SS). The single jersey knitted sample (10 wt%) differs from this group. It shows a logarithmic increase of the SE with respect to increasing frequency. It is visible that the EM SE is almost the same ($SE = 7$–10 dB) at higher frequencies (around 1.5 GHz) for all the knitted samples with different proportions of metal fiber. When exploring the shielding behavior of knitted samples in the area of frequencies from 200 to 800 MHz, double jersey provides the highest shielding (about 12 dB at 600 MHz) and the second-highest is pique with 8 dB at 600 MHz, both having 10 wt% of the conductive component.

The group of singe jersey knits with a conductive component content ranging from 10 to 20 wt% is behind the other groups, having SE from 2 to 6 dB at 600 MHz. The double jersey and pique structure shows greater shielding than the single jersey in these studied frequencies, because of the higher GSM, that is, higher thickness and higher packing density of the sample, which reduce the EM waves passing through.

Figure 2(e) shows the frequency-dependent EM SE results of the carbon, PPy-coated PES woven and the aluminum foil (F) samples. The Al foils and the PPy polymer-coated woven samples seem to be independent on frequency. This phenomenon can be expected for electrically thin materials or isotropic materials with frequency-independent electrical properties of conductivity, permittivity and permeability.[32] The Al foil samples show high EM SE around 78 dB and the PPy-coated PES woven shows EM SE of around 12 dB. The thinner carbon woven sample (marked 1) shows the EM SE increasing linearly with increasing frequency and embodies the EM SE around 57 dB at 1.5 GHz frequency. On the other hand, the thicker carbon woven sample (marked 2) has the EM SE almost independent at the frequency of around 49 dB. The carbon particle filled nonwoven sample has low EM SE of around 5 dB, which is caused by the fact that there are not enough conductive particles to create a conductive path. It was confirmed that the EM SE is strongly dependent on the continuous link of the conductive portion inside the material and the carbon woven ($\geq$48 dB) has a higher value than the carbon particle (5 dB) due to the continuous conductive link.

Figure 2(f) shows the EM SE results of the metal-coated fiber (Mf) and the metal-coated fabric (Mc) samples against various frequencies. Only this fabric, which is totally made of silver-coated PES fibers, embodies logarithmic growth of the EM SE ($SE = 70$ dB at 1.5 GHz) with increasing frequency. The rest of the samples are almost frequency independent, which means that their SE is almost constant, especially at higher frequencies. The nonwoven samples coated by paste containing a certain content of conductive particles (Al, Cu) embody low SE (<5 dB). The nonwoven samples made of different proportions of Eurostatic fibers have EM SE of around 10 dB, whereas the higher metal-coated fiber content gives slightly higher EM SE. EM shielding of about 50 dB can be reached by the woven and knitted samples coated by Ag, whereas generally woven substrates have an advantage in their periodical grid structure, resulting in higher SE when they are metal coated compared to the metal-coated knitted sample. The highest EM SE is achieved by the woven sample coated by a combination of Cu and Ag ($SE = 82$ dB).

Electromagnetic shielding effectiveness of the samples at 1.5 GHz frequency

The EM shielding ability of the samples was measured in a broad frequency range, but the EM SE at 1.5 GHz frequency was taken for further analysis. This frequency was found to be interesting, because this is close to the frequency used by many devices as a working one (e.g. cell phones, GPS, Wi-Fi routers).

Figure 3 shows the EM SE values measured at 1.5 GHz frequency for all the electro-conductive samples in ascending order for easier comparison. According to the requirements of EM shielding textiles,[37] depending on professional or general use, textiles can be classified in five grades from a fair grade to an excellent grade (see Tables 3 and 4). Professional use comprises professional protective uniforms for electronic manufacturers, shielding of medical equipment, etc., whereas general use is represented by casual wear, maternity clothes, aprons, shielding of consumptive electronic products and communication-related products, etc.

It can be observed that a very low shielding (<5 dB) is provided by the woven sample where electro-conductive mesh is created by the hybrid yarn containing only 1% of the SS, nonwoven samples coated by paste containing Cu and Al particles and the nonwoven sample incorporated with carbon particles. In the case of the hybrid fabric containing only the conductive mesh, the portion of the SS fiber is too low to get over the percolation threshold of the conductive component. In addition, the metal particle containing paste does not contain a sufficient amount of conductive component to obtain the conductive path, because the conductive particles significantly affect the mechanical properties and the process ability of the paste, especially at higher filler levels. The EM SE ranging from 10 to 20 dB is provided by the knitted samples with different content of SS fibers, the sample coated by PPy, the woven samples with electro-conductive mesh containing different SS fiber content, the nonwoven fabrics containing up to 20% of Eurostatic fibers, the nonwoven fabric containing 10% of SS or by the single layer woven fabric totally made of hybrid yarn with the content of SS fiber lower than 10%. In the case of hybrid fabrics containing the staple metal fiber, woven structures are preferred to the knit structures or the loft nonwoven structures because of the periodic mesh structure of woven fabrics contributing to prevent EM field penetration. The mentioned values of SE match the Good grade in the case of general use, but this is unsatisfactory for professional use. The EM SE within the range of 20–30 dB (accordant with the Very good grade for general use, Fair grade for professional use) can be reached by the layered woven samples

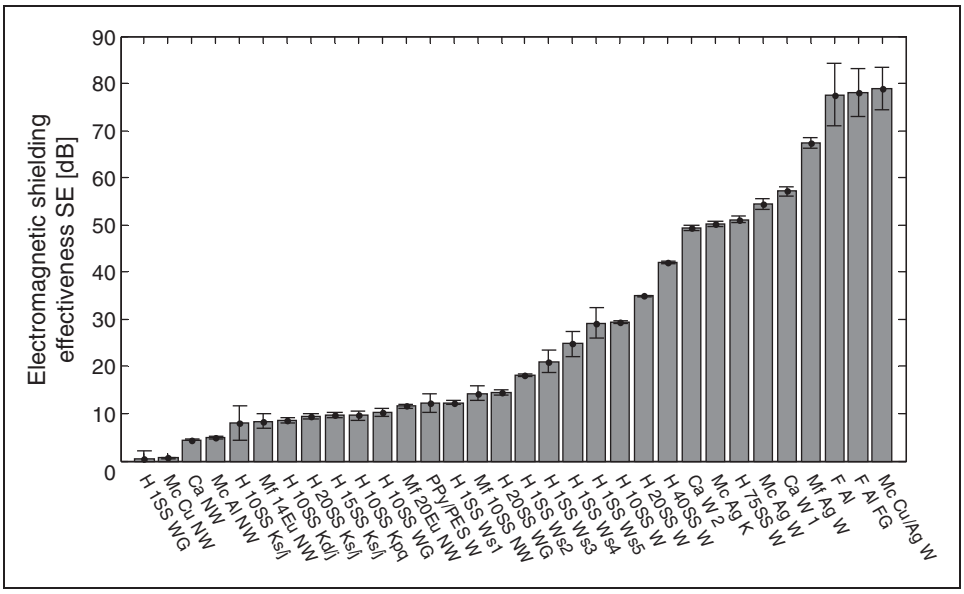

Figure 3. Comparison of mean values of the electromagnetic shielding effectiveness at 1.5 GHz frequency for electro-conductive samples in ascending order.

Table 3. Classification of electromagnetic shielding effectiveness (SE) values based on professional use

Grade	Excellent	Very good	Good	Moderate	Fair
Range	SE > 60 dB	60 dB ≥ SE > 50 dB	50 dB ≥ SE > 40 dB	40 dB ≥ SE > 30 dB	30 dB ≥ SE > 20 dB

Table 4. Classification of electromagnetic shielding effectiveness (SE) values based on general use

Grade	Excellent	Very good	Good	Moderate	Fair
SE range	SE > 30 dB	30 dB ≥ SE > 20 dB	20 dB ≥ SE > 10 dB	10 dB ≥ SE > 7 dB	7 dB ≥ SE > 5 dB

(up to five layers) made of 1% SS hybrid yarn. The EM SE within the range starting from 30–60 dB (corresponding with the Excellent grade for general use, from Moderate to Very good grade for professional use) can be achieved by the woven fabric samples totally made of hybrid yarn with the SS fiber content higher than 10%, carbon filament woven fabrics and silver-coated knitted and woven fabrics. EM shielding higher than 60 dB (satisfying Excellent grade for both general and professional requirements) is guaranteed by usage of the Al foils, coating of traditional fabric by combination of Ag/Cu and the woven sample totally made of silver-coated fiber yarn. These findings are in good agreement with the presumption that for high EM shielding materials, a preferable electro-conductive path in continuous or grid layout has to be provided (coatings on non-conductive substrates, metal foils, provide a sufficient amount of conductive fiber inside the textile structure in the area above the percolation threshold of the conductive component) and the higher electrical conductivity and magnetic permeability of the conductive component have a higher shielding ability. The electrical conductivity of PPy is from 2 to 100×10^2 S/m. The carbon fibers achieve conductivity of about 1×10^6 S/m. Silver, copper and aluminum are the materials with the highest electrical conductivity among metals ($\sigma = 3.5 - 6.3 \times 10^7$ S/m), while SS has a lower electric conductivity ($\sigma = 1.4 \times 10^6$ S/m), but excels in relatively high magnetic permeability ($\mu = 1.5 \times 10^{-3}$ H/m).

In this study, totally different samples with a view to structure, material composition, thickness and GSM were compared. In some applications where the weight of the shield is very important, EM shielding GSM (SE/GSM) products are more important than the absolute high EM SE – it is often possible to

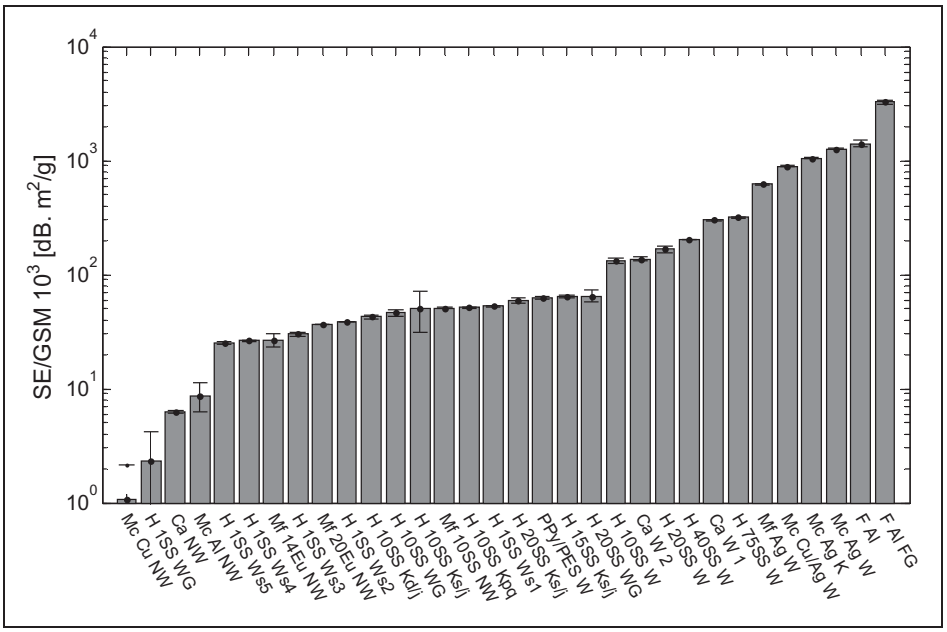

Figure 4. Bar chart of electromagnetic shielding mass per unit area (SE/GSM) (dB m^2/g) of electro-conductive samples in ascending order.

make the shield thicker to make up for a higher shielding ability – and then a material with a high SE/GSM product is desirable. To take into account different GSMs of the samples, relative EM SE (divided by sample GSM) in [dBm^2g^{-1}] was calculated for each sample (see Figure 4; due to visualization, the SE/GSM ratio was multiplied by 10^3 and the logarithmic scale was used). When taking the weight of the sample into consideration, the aluminum foil samples show very good results of the relative EM SE among all the other electro-conductive samples, due to its high SE together with a lower mass. Very good results of relative EM SE were also obtained for the metal-coated fabrics and the fabric totally made of metal-coated fiber yarns. As the mass of the sample increases, a decrease in the SE/GSM value is clearly visible, for example, woven sandwich samples with a huge GSM variation from 233 to 1167 g/m^2 embody the SE/GSM from 0.05 to 0.02 $dB.m^2/g$.

The effect of metal fiber content on electromagnetic shielding effectiveness

As expected, metal fiber content has a strong influence on the EM shielding ability of fabrics. It was confirmed that the EM SE increases with increasing SS fiber content for the woven samples totally made of hybrid yarns containing 1%, 10%, 20%, 40% and 75% SS (see Figure 5(a)) and also for woven samples in which the electro-conductive mesh is created by hybrid yarns containing 1%, 10% and 20% (see Figure 5(b)). The sample with the highest content of metal fiber reaches the highest EM SE of 51 dB for 1.5 GHz frequency, while the sample containing the lowest proportion of conductive component displays the lowest EM SE of 12 dB for 1.5 GHz frequency (Figure 5(a)). The overall SE is increasing according to the power function with metal fiber content (P). At a very low percentage of conductive fiber loading, the SE is more or less equal to zero, like the pure matrix (PP yarn). At 3–7% of metal fiber content, the SE value increases drastically over a very narrow range of conductive fiber concentration, which is called the percolation threshold (P_0). The solid line in this graph corresponds to the linear regression model with a parameter obtained by minimizing the sum of squared differences. A high R^2 value (0.99) confirms the prediction ability of the developed regression models. This linear regression model can be used for prediction of the "P" value for sufficient shielding. Similar behavior, that is, a power increase of shielding ability with increasing content of the SS fiber, was observed in the group of samples containing a grid structure; see Figure 5(b)).

The layer number effect on electromagnetic shielding effectiveness

As mentioned above, it seems that the increase in the number of layers can positively influence the shielding ability of the sandwich. Figure 6 shows the dependence

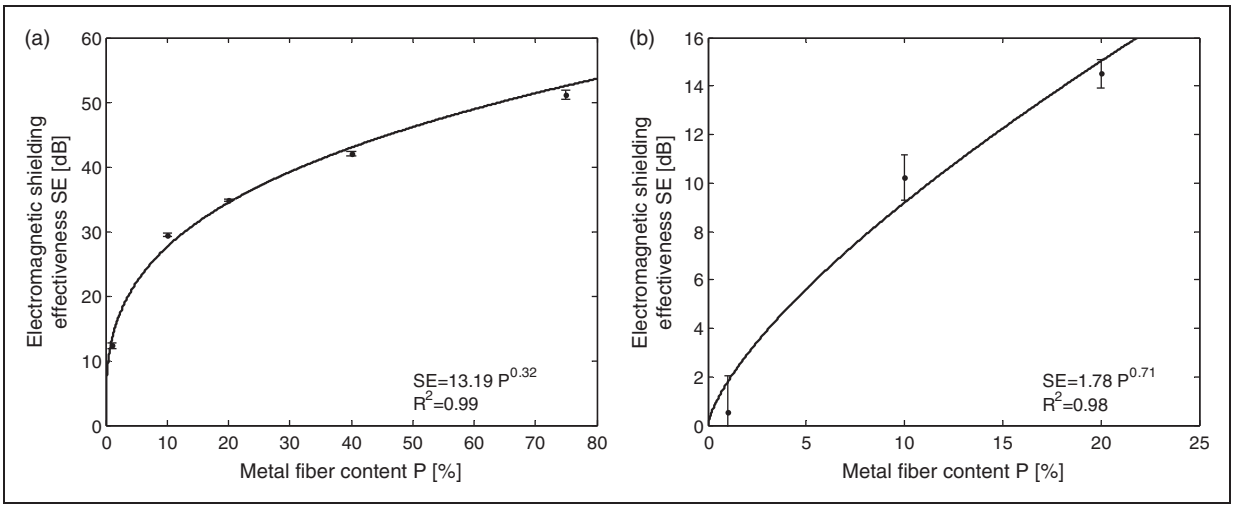

Figure 5. The dependence of the electromagnetic shielding effectiveness on the metal fiber content for: (a) woven samples: H 1SS Ws1, H 10SS W, H 20SS W, H 40SS W and H 75SS W; (b) woven grid samples: H 1SS WG, H 10SS WG and H 20SS WG.

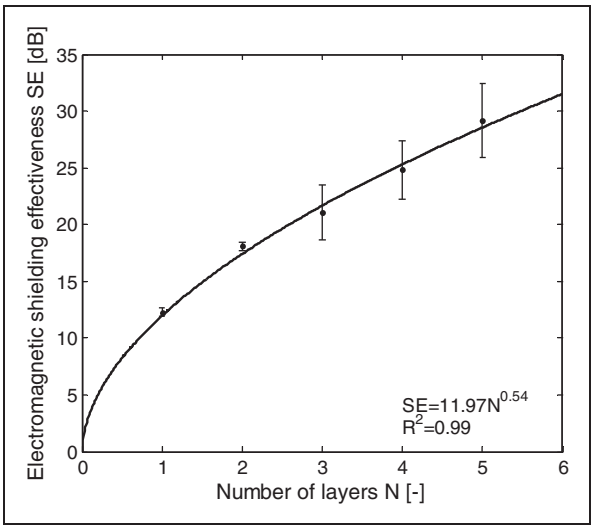

Figure 6. Dependence of the electromagnetic shielding effectiveness on the number of layers of 1% stainless steel woven samples (H 1SS Ws1, H 1SS Ws2, H 1SS Ws3, H 1SS Ws4 and H 1SS Ws5).

of the EM SE on the number of layers for woven samples containing 1% of SS fiber at 1.5 GHz frequency. The EM SE increase with the increasing number of fabric layers (up to 29 dB at 1.5 GHz for five layers) according to the power function (solid line) is shown in Figure 6. This phenomenon is supported by the theory which says that as the thickness (t) of the shield increases, the absorption loss (A) also increases.[38] It can be seen that it is preferable to use sandwich systems compared to a plane single layer containing the same proportion of the conductive component.

Electrical conductivity of the samples

The electrical conductivity of the material is one of the important factors influencing its EM shielding. Therefore, the results of the surface and volume electrical resistivity are discussed below for the non-conductive as well as electro-conductive samples.

The electrical conductivity of the materials is classified into three groups containing insulators, semiconductors and conductors. Insulators are materials having an electrical conductivity $\sigma < 10^{-8}$ S/cm (expressed as volume resistivity $\rho_v > 10^8\,\Omega$.cm), semiconductors have a conductivity $10^{-8}\,\text{S/cm} < \sigma < 10^3\,\text{S/cm}$ ($10^{-3}\,\Omega.\text{cm} < \rho_v < 10^8\,\Omega.\text{cm}$) and, finally, conductors are materials with high conductivities: $10^3\,\text{S/cm} < \sigma$ ($\rho_v < 10^{-3}\ \Omega.\text{cm}$).

The non-conductive samples show very high resistivity ($>10^{10}\,\Omega$) on both surface and volume, but the volume resistivity is higher than the surface for all the samples (see Table 2). Among the non-conductive sample group the linen (Li) fabric shows the lowest resistivity value ($<10^{11}\,\Omega$) and the glass (Gls) fabric shows the highest resistivity value ($>10^{13}\,\Omega$). The difference in resistivity is because of the moisture content of fiber material during the measurement ($T = 21^\circ$C and the relative humidity $RH = 54\%$) with respect to the thickness of the fabric. The commercial moisture regain values (%) of linen, cotton, viscose, wool, PES and glass are 12, 7–8.5, 11, 15–18, 0.4 and 0, respectively, according to ASTM D 1909.[39] The moisture content of wool is higher than the other samples, but the

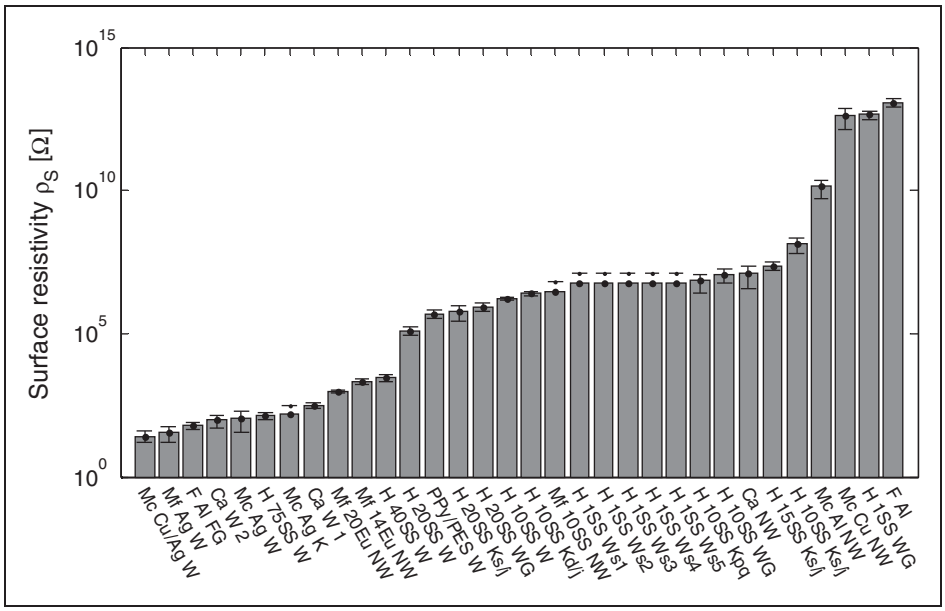

Figure 7. Mean values and 95% confidence intervals of the mean for surface resistivity, ρ_s [Ω] of the electro-conductive sample set.

resistivity is also higher because of the air pockets present in-between the fiber structure of the wool. These findings are consistent with the shielding ability results of the non-conductive samples, confirming that if the sample is an insulator it is transparent to the EM field and simultaneously it has no ability to block the incidental EM field.

Figure 7 shows a bar chart of the surface electrical resistivity (ρ_s) of the electro-conductive samples in ascending order together with 95% confidence interval error bars. All the electro-conductive sample values of the surface resistivity are below 10^8 Ω; only four samples (''Mc Al NW'', ''Mc Cu NW'', ''H 1SS WG'' and ''F Al'') have ρ_s higher than 10^{10} Ω. The highest surface resistivity was in the sample marked ''F Al'', because the conductive aluminum foil is laminated by a non-conductive layer on both sides of the sample. The lowest surface resistivity embodies the samples ''Mc Cu/Ag W'' and ''F Al FG''. Figure 8 shows the mean values and 95% confidence intervals for volume resistivity of the electro-conductive sample group. The volume resistivity value ranges from 10^2 to 10^{14} Ω.mm for all the samples. The carbon woven sample (''Ca W 2'') shows the lowest ρ_v of about 10^2 Ω.mm. The hybrid yarn woven grid sample (''H 1SS WG'') has the highest ρ_v of above 10^{14} Ω.mm, due to the very low SS fiber content by volume. The metal-coated samples do not excel in low-volume resistivity values, because the conductive layer is applied only on their surface, which allows easy transportation of the current on the sample surface (low surface resistivity) but not across the opposite sides of the sample. It is visible that the increase of the metal content percentage (from 10% to 75%) in the hybrid yarn woven samples causes a decrease of the volume resistivity values (from 10^6 to 10^2 Ω.mm).

The effect of metal fiber content on electric resistivity

Figure 9 shows the volume and surface resistivity curves for the samples totally made of SS hybrid yarn (Figures 9(a) and (b)) and for the samples containing a conductive grid (Figures 9(c) and (d)). A strong dependence was found; the volume and surface resistivity decrease by more than four orders of magnitude between 1% and 75% SS fibers in the fabrics totally made of hybrid yarn (Figures 9(a) and (b)). As the SS content in woven hybrid yarn grid samples increases (from 1% to 20%), the surface and volume electrical resistivity decrease (from 10^{12} to 10^5 Ω and from 10^{14} to 10^6 Ω.mm, respectively), as shown in Figures 9(c) and (d). This behavior is in positive correlation with measurement of EM SE, which says ''that the higher metal fiber content having lower electric resistivity and the higher EM shielding effectiveness''. From Figure 9, the percolation threshold (P_0) of the conductive component can be identified (predicted). In this case, the percolation threshold is estimated at a metal fiber loading of 2–5% and 1–3% for the woven samples and woven grid samples, respectively. A drastic change in the conductivity (more precisely a decrease of resistivity) of the material occurs in the vicinity of the percolation threshold under the proviso that the volume fraction of the metal fiber portion becomes sufficient to provide continuous electrical paths through the non-conductive component. It is well known that this

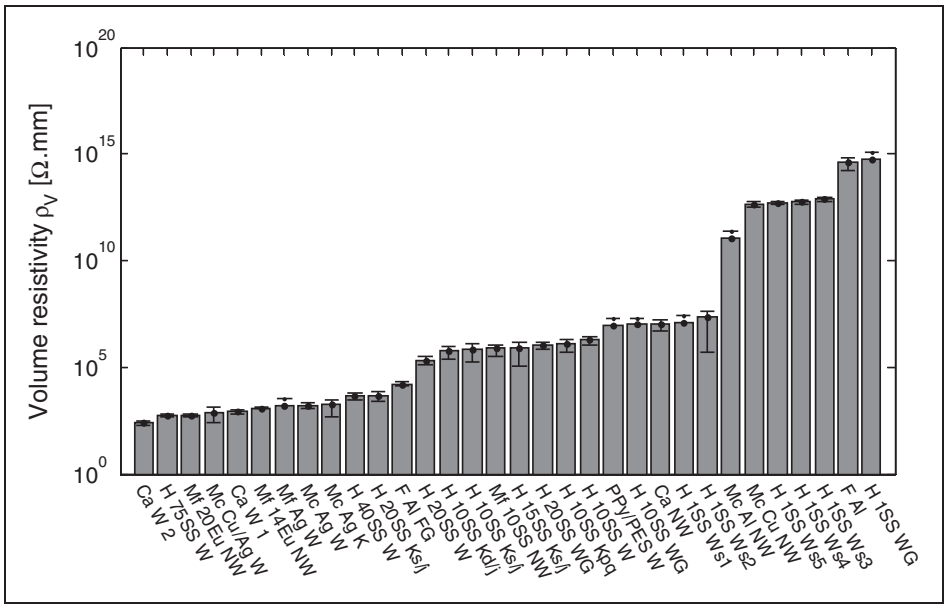

Figure 8. Mean values and 95% confidence intervals of the mean for volume resistivity, ρ_v [Ω.mm] of the electro-conductive sample set.

dependence (resistivity versus metal fiber loading) is different for the range below and above, the so-called percolation threshold P_0. ρ_V and ρ_S are strongly decreasing functions of P below P_0. ρ_V and ρ_S are more slowly decreasing functions of P in the range above P_0. It seems that the resistivity will not increase dramatically with an additional increase of the conductive component (above 75%). The dependence of resistivity (ρ_V and ρ_S) on P can be expressed by a simple power function using Equation (3) (see Figure 9; adopted from Clingerman et al.[40])

$$\rho = \rho_c P^E \tag{3}$$

where ρ is the resistivity, ρ_C is the resistivity for $P = 1\%$ of the conductive component in hybrid yarn and parameter E is dependent on the structure of the conductive component.

The effect of electrical resistivity on shielding effectiveness

It is well known that the SE increases as the electric conductivity and the permittivity of shielding material increases based on the EM shielding theory,[41] but there is a lack of experimental verification and exploration of this dependence for heterogeneous fiber-based structures with different material compositions and structures. In addition, direct measurement of fabric EM SE needs special devices compared to the measurement of electrical properties; therefore, utilization of the presumption that the electrical part of the EM field dominates in sufficiently high frequencies seems to be helpful. Knowledge of the electrical characteristics, which are easily measurable, could be therefore used for the prediction of sample shielding ability. That is why the correlation between the surface and volume resistivity on EM shielding efficiency is studied. The dependence of EM SE on the surface and volume resistivity for the whole sample set is shown in Figures 10(a) and (b). It is possible to observe a trend which says that the decrease of electric resistivity of a sample (i.e. increasing electric conductivity) is connected with the increase of its EM shielding ability. However, few outliers behaving differently from this trend are traceable. One of them is the aluminum foil sample (marked "F Al"), having very high surface and volume resistivity (due to the lamination on both sides of the sample by the non-conductive layer), but showing EM SE of 78 dB at 1.5 GHz frequency (due to the high conductive aluminum foil core). Out of the trend are also sandwiched woven samples ("H 1SS Ws2", "H 1SS Ws3", "H 1SS Ws4" and "H 1SS Ws5") created by multiplying the same woven fabric. They show no change in surface resistivity and uneven changes in volume resistivity values accompanied by an increase of SE caused by the increase of thickness of the sandwich.

Figures 11(a) and (b) shows the dependence of EM SE on electric resistivity for the sample set (the outlying samples described above were removed) approximated by the power function (solid line in the graph). The coefficient of determination $R^2 = 0.84$ and $R^2 = 0.48$ for dependence of EM SE on surface and volume resistivity, respectively, shows that the surface resistivity has

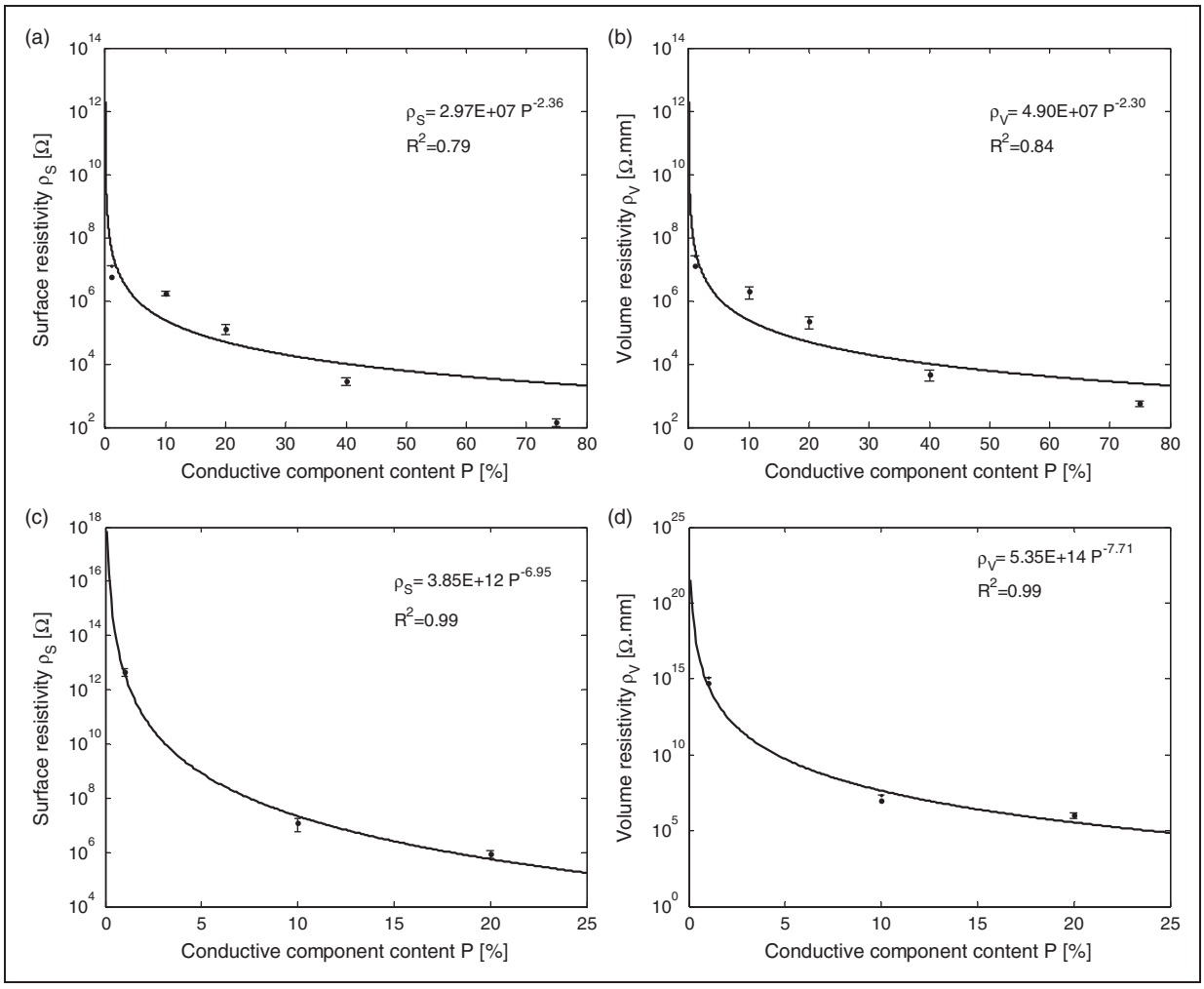

Figure 9. The dependence of electrical resistivity on conductive component content for: (a) and (b) woven samples: "H 1SS Ws1", "H 10SS W", "H 20SS W", "H 40SS W" and "H 75SS W", (c) and (d) woven grid samples: "H 1SS WG", "H 10SS WG" and "H 20SS WG".

better prediction ability compared to the volume resistivity and, therefore, for sufficiently high frequencies it is adequate to measure only the electrical characteristics, especially based on the surface conductivity. The prediction ability of this model is restricted to the samples without an insulating layer.

Air permeability of the electro-conductive samples

Beside functionality (EM shielding ability), the air permeability of the sample is a very important character for various applications as a development of protective clothing, garments, curtain cloths, seats or interior covers, electronic devices covers that should be able to transport heat out, etc. Figure 12 shows a bar chart of the air permeability values [l/m^2/s] for the electro-conductive samples plotted in ascending order together with information about their functionality – the EM shielding ability. The air permeability parameter is mainly dependent on the structure and porosity of the sample. In general, the nonwoven and knitted structures are more open (more porous, having lower packing density) than the woven structures. It is notable that even if the Al foil samples have a very high shielding ability, they show no air permeability ($A = 0$ l/m^2/s) because of the presence of no gaps in the foil. This fact is very limiting for many applications. For the hybrid yarn woven samples ("H 10SS W", "H 20SS W", "H 40SS W" and "H 75SS W"), with an increase in the percentage of metal fiber content (10%, 20%, 40% and 75%), the air permeability increases (from 130 to 1200 l/m^2/s) due to the higher density of metal fiber, which affects the yarn diameter. Yarn containing a certain amount of metal fibers has a lower diameter compared to the diameter of yarn totally made of PP fibers. The copper and aluminum painted nonwoven ("Mc Cu NW" and "Mc Al NW") samples are less permeable for air ($A < 80$ l/m^2/s) than

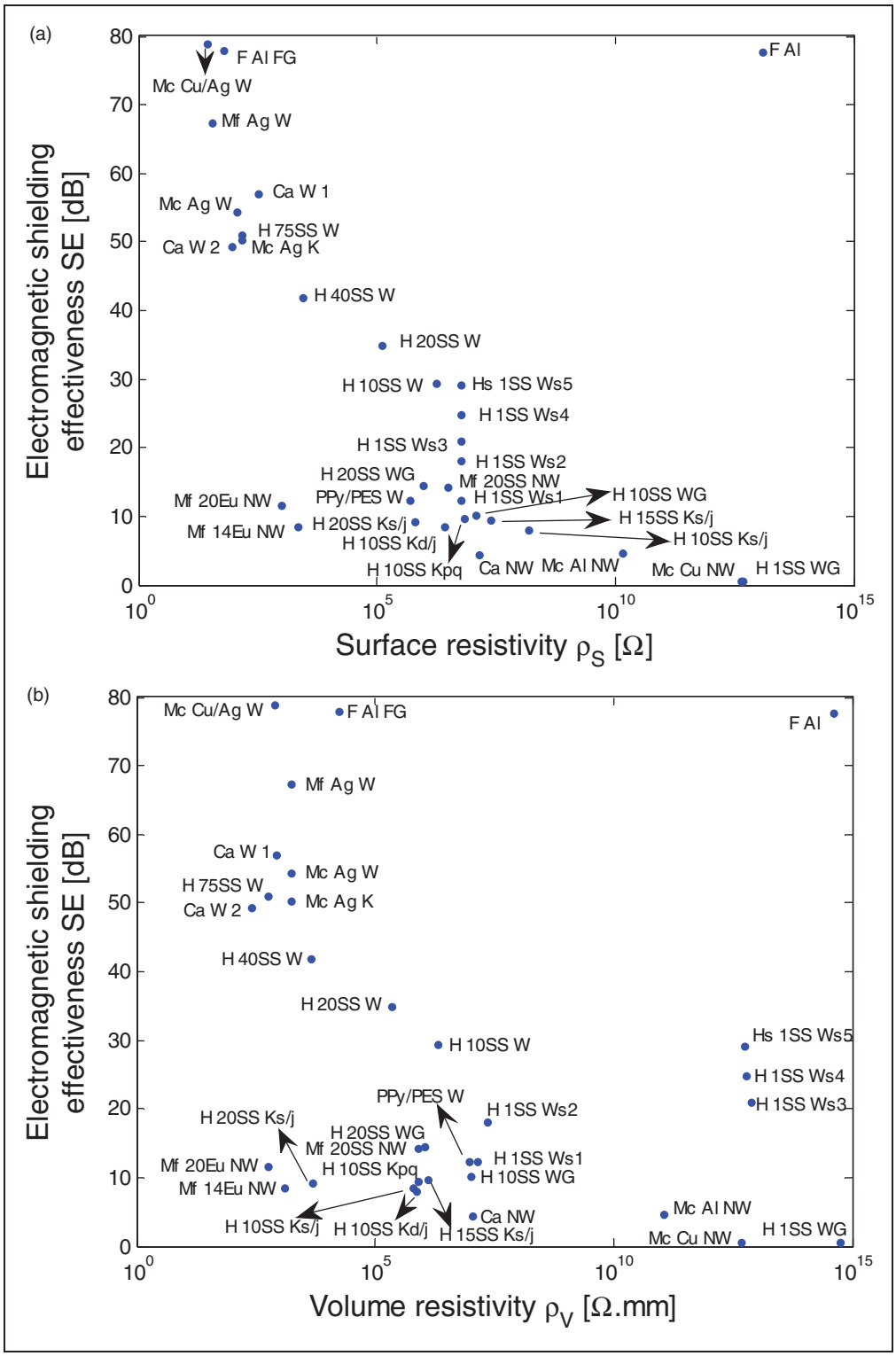

Figure 10. Scatter diagram of (a) surface resistivity [Ω] and (b) volume resistivity [Ω. mm] versus electromagnetic shielding effectiveness [dB] of the electro-conductive samples.

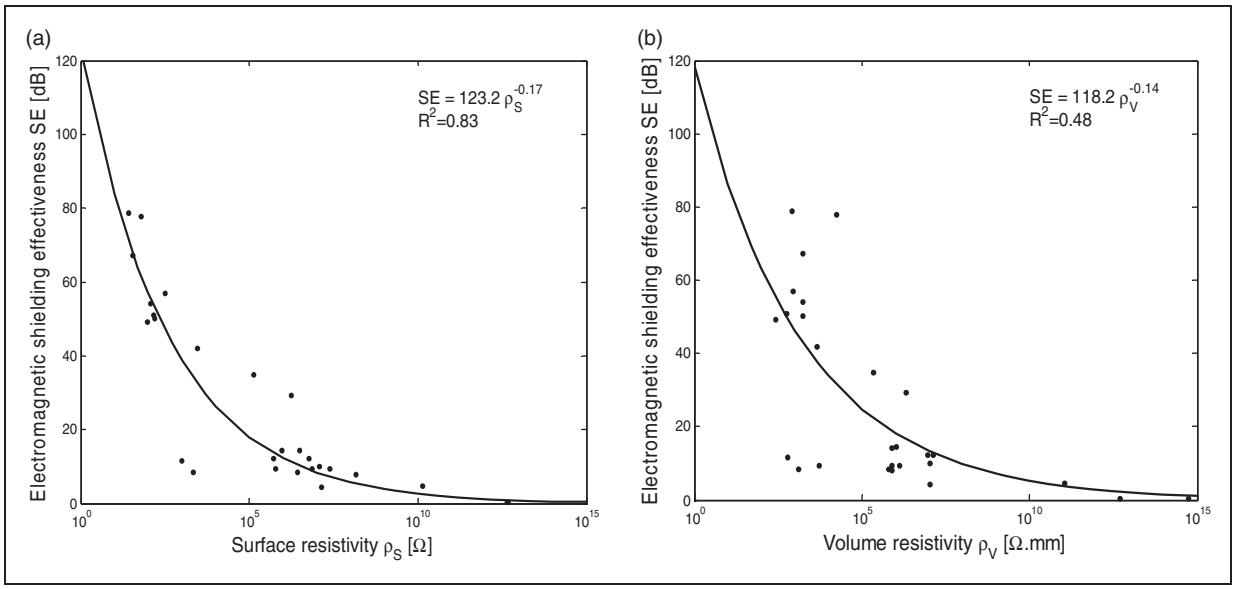

Figure 11. Scatter diagram with statistical analysis of electrical resistivity on the electromagnetic shielding effectiveness (EM SE) [dB] of the electro-conductive samples: (a) EM SE versus surface resistivity [Ω]; (b) EM SE versus volume resistivity [Ω.mm].

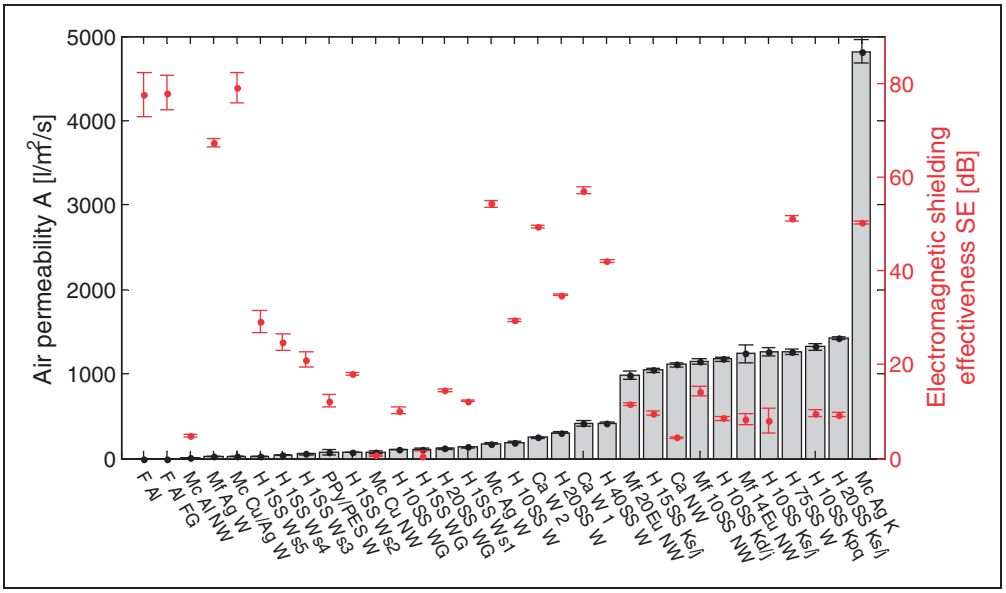

Figure 12. Combined graph of the air permeability and the electromagnetic interference shielding effectiveness of the electro-conductive samples.

the metal fiber incorporated nonwoven samples ("Mf 20Eu NW", "Mf 14Eu NW" and "Mf 10SS NW"), where $A \sim 1000\,\mathrm{l/m^2/s}$. The metal particle paint coating on the surface of the nonwovens fills the pores of the sample and, therefore, the paste-coated samples become less permeable to air. The metal-coated yarn knitted sample ("Mc Ag K") shows the highest air permeability value ($A = 4820\,\mathrm{l/m^2/s}$) of all the samples, because of its low thickness, more open structure and the fact that the metal coating is applied on to the yarn surface, which is does not significantly reduce the porosity of the sample. As expected, with an increasing number of layers of the sandwich samples (H 1SS Ws1, H 1SS Ws2, H 1SS Ws3, H 1SS Ws4 and H 1SS Ws5), the air permeability decreases because of the higher thickness and also the fact that one layer above the other can cover the pores of the preceding layer and block the direct path of the air.

Conclusions

In this study, 32 different electro-conductive samples having different structures and containing different types and portions of conductive components were chosen to introduce the present state of fiber-based EM shield production. This extensive sample set was taken for an analysis of EM SE, electrical conductivity and air permeability to enable the comparison and evaluation of different material approaches by a uniform methodology. In addition, seven non-conductive samples made of different traditional fibers were included in this study.

It was confirmed that textile structures made of conventional fibers are transparent to the EM field. The EM SE of the non-conductive samples is less than 0.1 dB in the frequency range from 200 to 1500 MHz, regardless of the material composition. This statement was supported by very high measured electrical resistance values of the traditional fabrics lying in the range of the insulators.

On the other hand, the EM SE of the textile structures containing different contents and different types of conductive component ranges from 1 to 79 dB at the high-frequency range. The ability of the material to shield the EM field can be controlled by a proper choice of the conductive component type, its content and placement. That is why the best results are provided by the samples made of metal-coated yarns or fibers (even if the GSM and the air permeability is taken into account) having SE in the range of 50–80 dB, which means a ''Very good'' grade even for professional use according to the specific requirements for EM shielding textiles.[37] The frequency-independent SE of metal-coated textile structures is also very favorable, which guarantees constant shielding for the given frequency range. The only drawback is their metallic appearance and touch. The aluminum foils offer very good shielding ability having 78 dB, but zero air permeability and their touch and mechanical properties are very restrictive for many applications. The samples made of hybrid yarns (containing the staple SS fiber), especially the woven fabrics, represent a promising approach. The EM SE of these hybrid fabrics varies between 10 and 50 dB, depending on their structure and metal fiber content, which ranks them up to the ''Good'' grade for professional use.[37] The advantage of mixing conductive fibers with non-conductive ones is a nice touch for the final fabric and other properties, including appearance, which is not different from traditional textiles. The woven fabrics made of carbon roving also show a very good performance and sufficient air permeability, but they are not at all appropriate for usage as traditional fabrics. Their usability can be seen as reinforcement for composites.

Other material approaches, such as coatings of non-conductive substrates with conductive polymers; treatment of non-conductive substrates by metal particle filled pastes; the incorporation of carbon particles in nonwoven structures; or the incorporation of conductive fibers in the bulky nonwoven structures, does not seem promising, especially in light of their lower functionality (EM SE). Another disadvantage of conductive polymer usage as a coating for non-conductive textile substrates is that their stability in different environmental conditions (high humidity, high temperature) together with washing resistance is expected to be low.

For example, the hybrid woven fabric containing about 10% of SS fiber mixed with the traditional fiber (cotton, PES) made of yarns with the fineness about 30 tex with weft and warp density of about $30\,cm^{-1}$ could be used in the production of protective clothing for pregnant women, because the fabric of this material composition and the structure satisfies the requirements of functionality (SE $\sim$ 29 dB for frequencies higher than 1 GHz), visual appearance (it can be dyed or printed), washing durability,[42] transport properties and other comfort properties (drape, handle, low flexural rigidity).

As another example, for the lining of cabin sidewalls in aircraft where a very high functionality and low weight are the main requirements, metal-coated woven fabrics (preferably with silver or copper) with a very high SE could be used, although they have a metallic appearance and low air permeability.

The shielding ability results of the examined materials were supported by measuring the ability of a material to conduct an electric current. It was found that the surface resistivity can be used to predict the EM shielding ability of a sample, due to the strong inverse relationship ($R^2 = 0.83$) between these two parameters. The power function model can be used for prediction of the EM SE of a newly developed material based on the knowledge of its surface resistivity. The prediction ability of this model is restricted to samples without an insulating layer on their surface.

Declaration of conflicting interests

The authors declared no potential conflicts of interest with respect to the research, authorship and/or publication of this article.

Funding

The authors disclosed receipt of the following financial support for the research, authorship, and/or publication of this article: This work was supported in part by a research project of the Technology Agency of the Czech Republic (Grant No. TG01010117 PROSYKO).

References

1. Das A, Kothari VK, Kothari A, et al. Effect of various parameters on electromagnetic shielding effectiveness of textile fabrics. *Indian J Fibre Text* 2009; 34: 144–148.
2. Roh JS, Chi YS, Kang TJ, et al. Electromagnetic shielding effectiveness of multifunctional metal composite fabrics. *Text Res J* 2012; 78: 825–835.
3. Su CI and Chern JT. Effect of stainless steel containing fabrics on electromagnetic shielding effectiveness. *Text Res J* 2004; 74: 51–54.
4. Safarova V and Militky J. Electromagnetic field shielding fabrics with increased comfort properties. *Adv Mat Res* 2013; 677: 161–168.
5. Eddy current. http://en.wikipedia.org/wiki/Eddy current (accessed 28 October 2016).
6. Duran D and Kadoglu H. Electromagnetic shielding characterization of conductive woven fabrics produced with silver-containing yarns. *Text Res J* 2015; 85: 1009–1021.
7. Cheng L, Zhang T, Guo M, et al. Electromagnetic shielding effectiveness and mathematical model of stainless steel composite fabric. *J Text Inst* 2014; 106: 577–586.
8. Cheng KB, Cheng TW, Nadaraj RN, et al. Electromagnetic shielding effectiveness of the twill copper woven fabrics. *J Reinf Plast Compos* 2006; 25: 699–708.
9. Ortlek HG, Alpyildiz T and Kilic G. Determination of electromagnetic shielding performance of hybrid yarn knitted fabrics with anechoic chamber method. *Text Res J* 2013; 83: 90–99.
10. Park SH, Theilmann P and Bandarau PR. Enhanced electromagnetic interference shielding through the use of functionalized carbon nanotube-reactive polymer composites. *IEEE Trans Nanotechnol* 2010; 9: 464–469.
11. Lin SC, Ma CCM, Hsiao ST, et al. Electromagnetic interference shielding performance of water borne polyurethane composites filled with silver nanoparticles deposited on functionalized graphene. *Appl Surf Sci* 2016; 385: 436–444.
12. Tunakova V, Gregr J, Tunak M, et al. Functional polyester fabric/polypyrrole polymer composites for electromagnetic shielding: optimization of process parameters. *J Ind Text* 2018; 47: 686–711.
13. Yildiz Z, Usta I and Gungor A. Investigation of the electrical properties and electromagnetic shielding effectiveness of polypyrrole coated cotton yarns. *Fibres Text East Eur* 2013; 21: 32–37.
14. Amol JP and Pandey AK. A novel approach for in situ polymerization of polypyrrole on cotton substrates. *Indian J Fibre Text* 2012; 37: 107–113.
15. Muthukumar N and Thilagavathi G. Development and characterization of electrically conductive polyaniline coated fabrics. *Indian J Chem Technol* 2012; 19: 434–441.
16. Luo X and Chung DDL. Electromagnetic interference shielding using continuous carbon-fiber carbon-matrix and polymer-matrix composites. *Composites Part B* 1999; 30: 227–231.
17. Kim T and Chung DDL. Mats and fabrics for electromagnetic interference shielding. *J Mater Eng Perform* 2006; 15: 295–298.
18. Liu X, Zhang L, Yin X, et al. Flexible thin SiC fiber fabrics using carbon nanotube modification for improving electromagnetic shielding properties. *Mater Des* 2016; 104: 68–75.
19. Bonaldi RR, Siores E and Shah T. Electromagnetic shielding characterisation of several conductive fabrics for medical applications. *J Fiber Bioeng Inf* 2010; 2: 237–245.
20. Lu L, Xing D, Xie Y, et al. Electrical conductivity investigation of a nonwoven fabric composed of carbon fibers and polypropylene/polyethylene core/sheath bicomponent fibers. *Mater Des* 2016; 112: 383–391.
21. Sano E and Akiba E. Electromagnetic absorbing materials using nonwoven fabrics coated with multi-walled carbon nanotubes. *Carbon* 2014; 78: 463–468.
22. Cheng KB, Ramakrishna S and Lee KC. Electromagnetic shielding effectiveness of copper/glass fiber knitted fabric reinforced polypropylene composites. *Composites Part A* 2000; 31: 1039–1045.
23. Yu ZC, Zhang JF, Lou CW, et al. Determination of electromagnetic shielding and antibacterial properties of multifunctional warp knitted fabrics. *J Text Inst* 2015; 106: 1203–1211.
24. Jagatheesan K, Ramasamy A, Das A, et al. Fabrics and their composites for electromagnetic shielding applications. *Text Prog* 2015; 47: 87–161.
25. Ozen MS. Investigation of the electromagnetic shielding effectiveness of carded and needle bonded nonwoven fabrics produced at different ratios with conductive steel fibers. *J Eng Fibers Fabr* 2015; 10: 140–151.
26. Safarova V and Militky J. Electromagnetic shielding properties of woven fabrics made from high-performance fibers. *Text Res J* 2014; 84: 1255–1267.
27. Safarova V and Militky J. Multifunctional metal composite textile shields against electromagnetic radiation—effect of various parameters on electromagnetic shielding effectiveness. *Polym Compos* 2017; 38: 309–323.
28. Lin JH, Huang YT, Li TT, et al. Manufacture technique and performance evaluation of electromagnetic-shielding/far infrared elastic warp-knitted composite fabrics. *J Text Inst* 2015; 107: 493–503.
29. Perumalraj R and Dhasarathan BS. Electromagnetic shielding effectiveness of copper core yarn knitted fabric. *Indian J Fibre Text* 2009; 34: 149–154.
30. Morari C and Balan I. Methods for determining shielding effectiveness of materials. *EEA – Electro tehnica Electronica Automatica* 2016; 64: 134–140.
31. ASTM D257. Standard test methods for DC resistance or conductance of insulating materials, 2007.
32. ASTM D4935. Standard test method for measuring the electromagnetic shielding effectiveness of planar materials, 2010.
33. ASTM D3776. Standard test method for mass per unit area (weight) of fabric, 2013.
34. ISO 9237. Textiles - determination of the permeability of fabrics to air, 1995.

35. Hersh SP and Montgomery DJ. Electrical resistance measurements on fibers and fiber assemblies. *Text Res J* 1952; 22: 805–818.
36. Kaiser KL. *Electromagnetic shielding*. Boca Raton, FL: CRC Press, Taylor & Francis Group, 2006.
37. Committee for conformity assessment on accreditation and certification of functional and technical textiles. Specified requirements of electromagnetic shielding textiles, http://www.ftts.org.tw/images/fa003E.pdf (2010, accessed 16 November 2016).
38. Tong XC. *Advanced materials and design for electromagnetic interference shielding*. Boca Raton, FL: CRC Press, Taylor & Francis Group, 2009.
39. ASTM D1909. Standard tables of commercial moisture regains and commercial allowances for textile fibers, 2013.
40. Clingerman ML, King JA, Schulz KH, et al. Evaluation of electrical conductivity models for conductive polymer composites. *J Appl Polym Sci* 2002; 83: 1341–1356.
41. Ott HW. *Electromagnetic compatibility engineering*. Hoboken, NJ: John Wiley & Sons, 2009.
42. Tunakova V, Technikova L and Militky J. Influence of washing/drying cycles on fundamental properties of metal fiber containing fabrics. *Text Res J* 2017; 87: 175–192.

Appendix 4

V. Tunakova, Z. Hrubosova, M. Tunak, M. Kasparova, and J. Mullerova, "Laser surface modification of electrically conductive fabrics: Material performance improvement and design effects," Opt. Laser Technol., vol. 98, pp. 178–189, 2018.

Optics and Laser Technology 98 (2018) 178–189

Contents lists available at ScienceDirect

Optics and Laser Technology

journal homepage: www.elsevier.com/locate/optlastec

Full length article

Laser surface modification of electrically conductive fabrics: Material performance improvement and design effects

Veronika Tunakova [a,*], Zuzana Hrubosova [a], Maros Tunak [a], Marie Kasparova [a], Jana Mullerova [b]

[a] Faculty of Textile Engineering, Technical University of Liberec, Czech Republic
[b] Institute for Nanomaterials, Advanced Technologies and Innovation, Technical University of Liberec, Czech Republic

ARTICLE INFO

Article history:
Received 17 February 2017
Received in revised form 15 May 2017
Accepted 14 July 2017
Available online 12 August 2017

Keywords:
Conductive fabrics
Laser
Electromagnetic shielding effectiveness
Appearance
Design
Mechanical properties

ABSTRACT

Development of lightweight flexible materials for electromagnetic interference shielding has obtained increased attention in recent years particularly for clothing, textiles in-house use and technical applications especially in areas of aircraft, aerospace, automobiles and flexible electronics such as portable electronics and wearable devices. There are many references in the literature concerning development and investigation of electromagnetic shielding lightweight flexible materials especially textile based with different electrically conductive additives. However, only little attention is paid to designing and enhancing the properties of these special fabrics by textile finishing processes. Laser technology applied as a physical treatment method is becoming very popular and can be used in different applications to make improvement and even overcome drawbacks of some of the traditional processes. The main purpose of this study is firstly to analyze the possibilities of transferring design onto the surface of electrically conductive fabrics by laser beam and secondly to study of effect of surface modification degree on performance of conductive fabric including electromagnetic shielding ability and mechanical properties. Woven fabric made of yarns containing 10% of extremely thin stainless steel fiber was used as a conductive substrate.

1. Introduction

Electrically conductive fabrics have obtained increased attention for electromagnetic shielding and anti-electrostatic purposes, mainly because of their desirable flexibility and low weight. There are many references in the literature concerning development and investigation of electromagnetic shielding lightweight flexible materials especially textile based with different electrically conductive additives.

One way to create conductive fabrics is using minute electrically conductive fibers (metal, carbon, conductive polymer fibers). They can be produced in filament or staple lengths and can be incorporated with traditional non-conductive fibers to create yarns that possess varying degrees of conductivity [1–7]. Another way represents conductive coatings on fibers or yarns by metals [8–11] or conductive polymers [12–15]. Fibers containing therein carbon black or other conductive particles can be also used [16,17].

Large amount of literature on preparation and investigation of properties of fabrics in which extremely thin stainless steel staple fiber is incorporated can be found. For example, electromagnetic shielding of woven fabric made of 40 tex PET yarn containing different portion of stainless steel short fibers (d = 12 μm) was reported in [18]. The transmissibility of electromagnetic wave power of the fabrics with 10 wt%, 20 wt%, and 30 wt% stainless steel fiber was close to 0% at a frequency ranging from 500 MHz to 1500 MHz. The electromagnetic shielding of the fabrics shows an absorption-dominant mechanism while a shift from absorption to reflection was observed with a decrease in metal fiber percentage as well as with an increased frequency.

In this article [2], similar type of conductive component, i.e. stainless steel short fiber (d = 8 μm), was used for production of yarns, and woven and knitted structures were prepared. An effect of metal fiber content, a placement of conductive yarn, geometry of the textile structure, number of layers, material of the nonconductive component, moisture content and correlation with frequencies were studied. It was found that electromagnetic field shielding ability of fabric can be controlled by: (a) content of conductive component in hybrid yarn, (b) hybrid yarn density, (c) thickness of fabric using e.g. multilayered system, (d) moister con-

* Corresponding author at: Faculty of Textile Engineering, Technical University of Liberec, Studentska 2, Liberec 463 17, Czech Republic.
E-mail address: veronika.tunakova@tul.cz (V. Tunakova).

http://dx.doi.org/10.1016/j.optlastec.2017.07.017
0030-3992/

tent, (e) type of nonconductive component and (f) compactness of structure.

Influence of washing and drying cycles on the electromagnetic shielding ability was studied in [19]. In this case, hybrid yarns were composed of conventional polypropylene fiber (85 wt%) and staple Bekinox stainless steel metal fiber (15 wt%). Despite the relatively significant increase of electric resistivity after washing, the samples did not totally lose their electromagnetic shielding ability. After applying 20 cycles of wet processing, electromagnetic shielding effectiveness at frequency 1.5 GHz dropped by 9.5% to 29.4 dB for the woven sample compared to reference (unwashed) samples. Electromagnetic shielding ability remained almost the same for the knitted sample at frequency 1.5 GHz after 20 cycles of washing/drying.

Despite many published papers dealing with development and characterization of electrically conductive fabrics containing extremely thin stainless steel fibers as a conductive component, only little attention is paid to designing and enhancing visual characteristics of these special textiles by textile finishing processes.

Changing appearance and visual characteristics of fabrics by applying certain designs to the texture and surface of textiles according to expectations of consumers and therefore increasing their added value is a desired effect in the textile industry [20]. Patterning during weaving and knitting processing using input material of different properties (color, fineness, etc.) represents one way how to get certain design. However, this method is not flexible enough (especially using special conductive yarns). It is time consuming due to problems in work flow and it is unable to apply the original forms, writings and designs on the product. Usage of design-oriented finishing represents another way how to get special design on to the fabric which is already prepared. The color and pattern of textile materials in a particular design can be achieved by dyeing, printing, and other finishing techniques.

In the last decade, laser technology has been used to enhance visual and tactile characteristics of fabrics to create new structures and surfaces, often by combining conventional textile techniques with laser processing [21] as laser technology is a low-energy, dry and efficient approach that does not involve chemicals and is therefore considered environmentally friendly.

The use of laser beam enables to cause controlled deformation on textile surfaces and thus create new designs by making use of the polymeric and heat-sensitive materials in the structure of the fabric [20]. Certain adjustment of laser beam (power, wavelength) is possible according to the nature of substrate and various adaptations of patterns can be created by means of certain adjustment. Another effect represents visual features of textile surfaces which becomes wrinkled and three-dimensional by means of deformation as well as designing on leather. The same mechanism can also be used for the purpose of cutting and creating designs through cutting [20].

In this study, electrically conductive and electromagnetically shielding woven fabric was modified with CO_2 laser technology to engineer pattern on to the fabric with high-resolution graphics. Laser patterns were generated by CO_2 laser technology involving preparation of design in graphical software. The work considers the aesthetic possibilities, production opportunities and also effect of degree of surface modification connected with various laser treatment parameters on performance of patterned conductive fabric including mainly electromagnetic shielding ability and mechanical properties. Furthermore morphology and color change of modified samples was studied by the help of SEM and image processing. An understanding of levels of color of modified samples was used to define the optimum laser energy for application. Material changes of laser irradiated samples were explored using infrared spectroscopy. Woven fabric with twill 2/2 weave made of conductive yarn containing 10 wt% stainless steel staple fibers was used as a substrate.

2. Experimental

2.1. Materials

2.1.1. Hybrid yarns

Hybrid yarns were composed of conventional polyester (PET) fiber (59 wt%) and cotton (CO) fiber (31 wt%). Both nonconductive fibers had white color. As a conductive component staple BEKINOX stainless steel (SS) metal fibers (10 wt%) were used. This particular percentage of conductive fiber was chosen with respect to previous studies [2,3]. Usage of 10% metal fiber guarantees electrical conductivity close to the percolation threshold of conductive component and achieves satisfactory electromagnetic shielding performance of fabrics made of these metal fiber containing yarns. On the other hand, this particular content of conductive fiber does not change significantly process ability of the yarns and fabrics made of. Also physiological properties, roughness and appearance of fabrics made of these yarns are comparable with traditional fabrics used in the textile area. The aspect ratio (length/diameter ratio, l/d) of the SS used in this study is 5625, since the diameter of the SS is 8 μm and the average fiber length of the SS is 45 mm. These three components were mixed at the drawing frame and a ring spinning system was used to produce blended single yarns with linear density 30 tex.

2.1.2. Hybrid fabric

Metal fiber containing fabric for patterning was created using hybrid yarns described above. Hybrid fabric has twill 2/1 weave made of 100% of conductive yarn (warp sett 39 1/cm, weft sett 22 1/cm). The characteristics of the hybrid fabric are shown in Table 1.

2.2. Methods

2.2.1. Laser irradiation

Irradiation of conductive sample was carried out by commercial pulsed CO_2 laser (Marcatex 150 Flexi, Easy-Laser) under atmospheric condition in the air [22]. The laser is used for cutting and marking textiles and produces laser beam of wavelength of 10.6 μm. The samples were irradiated by the laser beam directly on one side of the fabric. The duty cycle and pixel time was set constant to 50% and 100 μs. Laser power was 100 W at duty cycle 50% and frequency 5 kHz. Threshold color as well as threshold pointer were set to 220.

2.2.2. Laser patterning method

Digital laser patterns were formed with multiple tones generating a tonal spectrum. High-resolution capability of the laser beam spot when modifying textile fabric enabled patterning likened to "dots-per-inch", as in digital printing processes. Raster beam scanning method was used for patterning, Adobe Photoshop was used to create files and laser software was used for laser processing.

A grayscale design approach was used for laser image depiction and variable modification levels of the textile surface in the form of percentages of black (gray scale GS) [%] – e.g. 30%, 60%, etc. which represent intensity of an input image pixels within given range between minimum and maximum. This range is from 0 (total absence of intensity, white) to 1 (total presence, black), with any fractional values between. Different percentages of black influence energy density of laser and therefore variable power output is controlled. When combined with special laser parameters, this system

Table 1
Characteristics of hybrid fabric used as substrate for laser modification.

Composition	Warp/weft count [tex]	Hybrid yarn placement	Fabric structure	Fabric thickness [mm]	Mass per unit area [g/m^2]
10% SS/59% PET/31% CO	30/30	100%	2/1 twill	0.36	190

determined differential visual effect based on variable fiber modification linked to grey data.

Two approaches were explored in this study. At first, 15 × 15 cm samples were homogenously irradiated by different energy of density expressed by 12 different percentages of black, ranging from 0% (untreated) to 57% (see Fig. 1, where input images designated for laser engraving are shown). The main goal of this part was to study the effect of surface degree modification on performance of conductive fabrics including electromagnetic shielding ability and mechanical properties together with visual effect.

Based on this, appropriate laser energy density was chosen to achieve required color effect and favorable mechanical properties in patterned areas of textile surface and set of designs was prepared in second step. The main goal of the second step was to present aesthetic possibilities and production opportunities of digital laser patterning of electrically hybrid textiles containing stainless steel metal fiber.

2.2.3. Statistical analysis of small samples

For the small sample sizes available for electromagnetic shielding evaluation process and fabric mechanical properties evaluation, a procedure based on order statistics introduced by Horn [23] was used. This methodology is used for sample sizes where $4 \leq n \leq 20$ and it is based on the depths which correspond to the sample quartiles.

2.2.4. Electromagnetic shielding effectiveness evaluation

Electromagnetic shielding effectiveness (SE) of irradiated fabrics was measured according to ASTM D 4935-10 for planar materials using a plane-wave, far-field EM wave. SE of samples was measured over frequency range of 30 MHz to 1.5 GHz. The set-up consisted of a sample holder with its input and output connected to the network analyzer. A shielding effectiveness test fixture (Electro-Metrics, Inc., model EM-2107A) was used to hold the sample. The design and dimension of sample holder follows the ASTM method mentioned above. Network analyzer Rohde & Schwarz ZN3 was used to generate and receive the electromagnetic signals. The standard mentioned above determines the electromagnetic shielding effectiveness of the fabric using the insertion-loss method. A reference measurement for the empty cell was required for the shielding effectiveness assessment. A "through" calibration by the help of the reference sample was made first. A load measurement was performed on a solid disk shape sample subsequently. The reference (doughnut shape) and load (round shape) specimens must be of the same material and thickness. Samples were air conditioned before testing (T = 22 °C ± 3, RH = 50% ± 10%). The measurement was carried out at 5 different places of textile samples because of subsequent statistical analysis (significance level α = 0.05, $t_{L,0.95}(5)$ = 1.37). The mean values estimator (pivot half sums) together with 95% confidence intervals of means for SE for frequency 600 MHz, 1 GHz and 1.5 GHz and are summarized in Table 2.

2.2.5. Mechanical properties evaluation

The testing of tensile properties of the samples in warp direction was carried out using TIRAtest 2300 tensile tester according to ISO 13934-1 standard. The specimen length under test was taken as 100 mm and the testing speed was maintained at 100 mm/min. Initial width of sample was 20 mm. Five samples were measured for each laser treated fabric because of subsequent statistical analysis. Mechanical testing was done under standard laboratory conditions (T = 22 °C ± 3, RH = 50% ± 10%) with a view to ultimate mechanic characteristics of the material. The mean values estimator (pivot half sums) together with 95% confidence intervals of means for tensile strength in warp direction (ultimate strength) and elongation at break are summarized in Table 3.

2.2.6. Evaluation of sample color

Color information and intensity of the irradiated samples was estimated with the aid of image processing using MATLAB® envi-

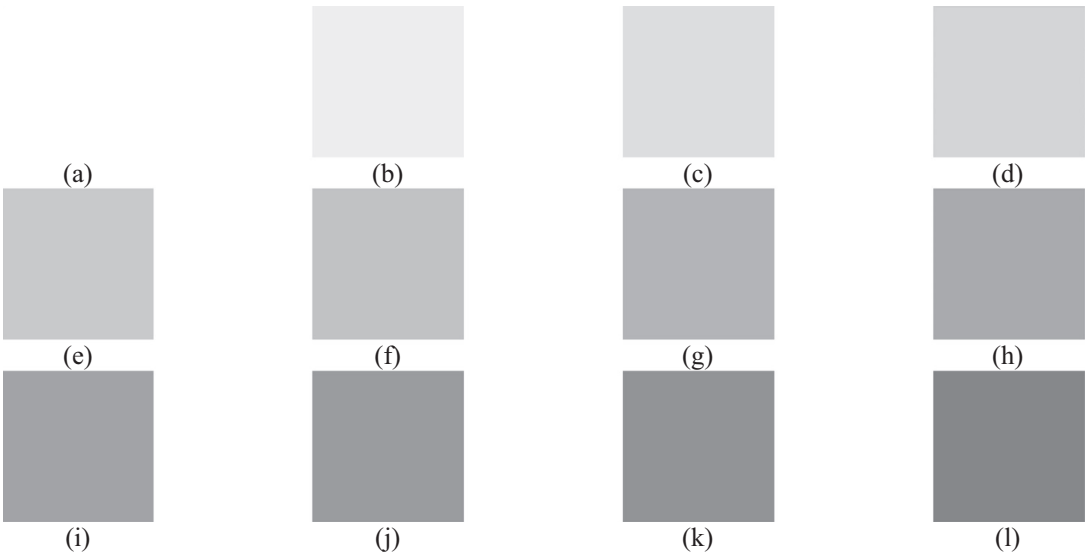

Fig. 1. Input images for laser irradiation of samples with different gray scale: (a) 0%, (b) 7.5%, (c) 14.9%, (d) 19.2%, (e) 24.3%, (f) 27.8%, (g) 34.5%, (h) 39.2%, (i) 42.7%, (j) 46.7%, (k) 51.0%, (l) 56.9%.

Table 2
Mean values and 95% confidence intervals of means for SE of laser treated samples.

Gray scale [%]	Electromagnetic shielding effectiveness [dB]		
	f = 600 MHz	f = 1 GHz	f = 1.5 GHz
0	25.44 ± 0.38	28.44 ± 0.39	31.42 ± 0.32
7.5	24.62 ± 0.42	28.22 ± 0.71	31.28 ± 0.59
14.9	25.12 ± 0.73	28.09 ± 0.28	31.50 ± 0.49
19.2	25.04 ± 0.93	28.35 ± 0.51	31.58 ± 0.38
24.3	26.49 ± 0.99	29.26 ± 0.32	32.35 ± 0.58
27.8	26.48 ± 0.53	29.39 ± 0.84	32.65 ± 0.62
34.5	27.80 ± 0.41	30.52 ± 0.27	33.02 ± 0.74
39.2	29.76 ± 1.05	31.89 ± 0.90	34.26 ± 0.95
42.7	31.57 ± 0.33	33.90 ± 0.40	35.82 ± 1.49
46.7	31.24 ± 2.40	33.20 ± 0.95	35.52 ± 0.06
51.0	31.85 ± 1.07	33.81 ± 0.49	35.43 ± 1.15
56.9	29.45 ± 0.59	31.46 ± 0.57	33.90 ± 0.42

Table 3
Mechanical properties (average ultimate tensile strength and ultimate elongation) of irradiated samples.

Gray scale [%]	Ultimate tensile strength [N]	Ultimate elongation [%]
0	351.22 ± 22.81	17.44 ± 0.74
7.5	331.57 ± 9.71	16.63 ± 0.72
14.9	318.49 ± 17.55	17.36 ± 1.63
19.2	274.50 ± 5.12	15.58 ± 0.79
24.3	174.51 ± 43.61	12.27 ± 2.41
27.8	152.78 ± 6.12	9.80 ± 0.27
34.5	90.61 ± 18.16	6.16 ± 0.76
39.2	58.32 ± 0.80	3.93 ± 0.78
42.7	48.89 ± 15.62	2.23 ± 0.87
46.7	38.55 ± 4.05	2.20 ± 0.57
51.0	22.26 ± 11.30	1.44 ± 0.89
56.9	28.20 ± 2.12	1.92 ± 0.60

ronment with Image Processing Toolbox by MathWorks®, Inc. in this study. Images of the samples were captured using HP Scanjet 5590 digital flatbed scanner (homogenous illumination of samples) in resolution 200 dpi. Images were captured as RGB (24-bit) image matrices of size $M = 950 \times N = 300$ pixels, real size of sample was 114.3×44.5 mm (1 px = 0.127 mm). Captured images were not preprocessed, individual components of sample RGB triplet were analyzed directly after capturing and gray level intensity of images was also studied. Average color component intensities $(\overline{R}, \overline{G}, \overline{B})$ were estimated according to

$$\overline{R} = \frac{1}{MN}\sum_{i=1}^{M}\sum_{j=1}^{N} R_{ij}, \qquad \overline{G} = \frac{1}{MN}\sum_{i=1}^{M}\sum_{j=1}^{N} G_{ij}, \qquad \overline{B} = \frac{1}{MN}\sum_{i=1}^{M}\sum_{j=1}^{N} B_{ij} \quad (1)$$

for $i = 1, 2, \ldots, M$ and $j = 1, 2, \ldots, N$. MN is total number of pixels in image and R_{ij}, G_{ij} and B_{ij} are intensities of pixels in Red, Green and Blue channel. Grey level images were obtained from RGB image after transformation

$$GL_{ij} = 0.30R_{ij} + 0.59B_{ij} + 0.11B_{ij}. \quad (2)$$

Average gray levels of images of irradiated samples $(\overline{GL})$ together with coefficient of variation of grey levels (cv_{GL}) were also estimated using following equations

$$\overline{GL} = \frac{1}{MN}\sum_{i=1}^{M}\sum_{j=1}^{N} GL_{ij}, \quad (3)$$

$$s_{GL} = \sqrt{\frac{1}{MN-1}\sum_{i=1}^{M}\sum_{j=1}^{N}\left(GL_{ij} - \overline{GL}\right)^2}, \quad (4)$$

$$cv_{GL} = \frac{s_{GL}}{\overline{GL}}100, \quad (5)$$

where s_{GL} is standard deviation of grey levels. Results are shown in Table 4.

2.2.7. Material composition evaluation

Material composition of samples was tested using infrared spectroscopy, more precisely FT-IR spectrometer Nicolet iZ10 (Thermo Fisher, USA), measured by ATR technique with ZnSe crystal. Spectrum of unknown material was compared for "best matches" with libraries of spectra cataloged for known materials.

2.2.8. Surface morphology evaluation

Scanning electron microscopy (SEM) was used for investigation of fiber morphology. SEM images of patterned fabrics were recorded at magnification of 100× and 500× by using Vega Tescan TS 5130 instrument. Samples were coated by gold prior to the SEM examination.

3. Results and discussion

3.1. Effect of laser irradiation on electromagnetic shielding effectiveness

Main aim of this subchapter was to find out whether laser treatment has some influence on functionality of hybrid fabric, especially on its ability to shield electromagnetic field. Fig. 2 shows the variation in electromagnetic shielding effectiveness (SE) for woven fabrics after laser treatment with incident frequency in the range 30–1500 MHz. It can be seen that the untreated sample (black line) reaches one of the lowest values of electromagnetic shielding efficiency throughout the whole frequency band ($SE \sim 31$ dB for $f = 1.5$ GHz). It seems that with increasing intensity of laser treatment (expressed by increasing gray scale of input image GS [%]), the shielding effectiveness of the material slightly

Table 4
Average RGB component intensities and average grey levels together with coefficients of variations for images of irradiated samples.

Gray scale [%]	Red intensity [–]	Green intensity [–]	Blue intensity [–]	Gray level [–]	Coefficient of variation [%]
0	220.5	218.1	220.1	220.5	4.0
7.5	226.8	224.3	226.4	226.8	3.6
14.9	227.3	224.7	226.8	227.3	3.7
19.2	224.3	222.6	224.0	224.3	4.1
24.3	220.9	224.1	220.1	220.9	3.9
27.8	212.8	219.7	211.7	212.8	3.9
34.5	191.6	201.4	190.0	191.6	4.0
39.2	152.2	164.4	150.0	152.2	5.9
42.7	149.7	163.4	147.2	149.7	5.8
46.7	135.8	151.6	132.7	135.8	6.1
51.0	124.6	141.5	120.6	124.6	7.4
56.9	148.1	160.9	145.4	148.1	5.4

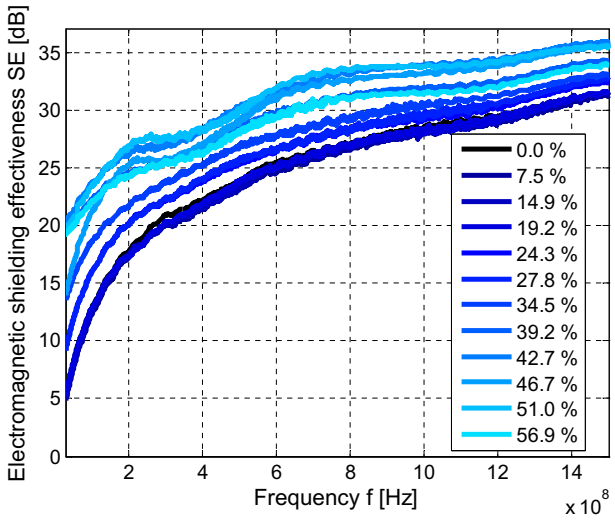

Fig. 2. The dependence of electromagnetic shielding effectiveness on frequency for samples with different laser modification levels expressed by gray scale GS [%].

increases proportionally for all frequencies up to gray scale 51% ($SE \sim 35$ dB for $f = 1.5$ GHz). It is assumed that this behavior is connected with increasing partial degradation of textile fibers (especially cotton fibers) accompanied by increasing amount of carbon phase in sample structure which was irradiated by laser, whereas carbon materials have quite good electrical conductivity and they have great ability to absorb electromagnetic wave [24]. With further increase of laser treatment intensity of ($GS > 51\%$), ability of sample to shield electromagnetic field decreases. This phenomenon is caused by total degradation of the sample, accompanied by cracks in its structure which leads to limitation of its barrier ability. It is possible to observe that the relationship between electromagnetic shielding effectiveness and frequency for all samples (untreated and irradiated) can be approached by generalized logarithmic function adapted from [19]

$$SE = a + b\log(f) + c\sqrt{f}, \tag{6}$$

where a, b, c are constants depending on characteristic impedance of shield material and characteristic impedance of medium surrounding the shield, f is frequency.

In Fig. 3a–c, there are shown dependences of electromagnetic shielding effectiveness of samples on different intensity of laser irradiation (expressed by GS [%]) for the frequency 600 MHz,

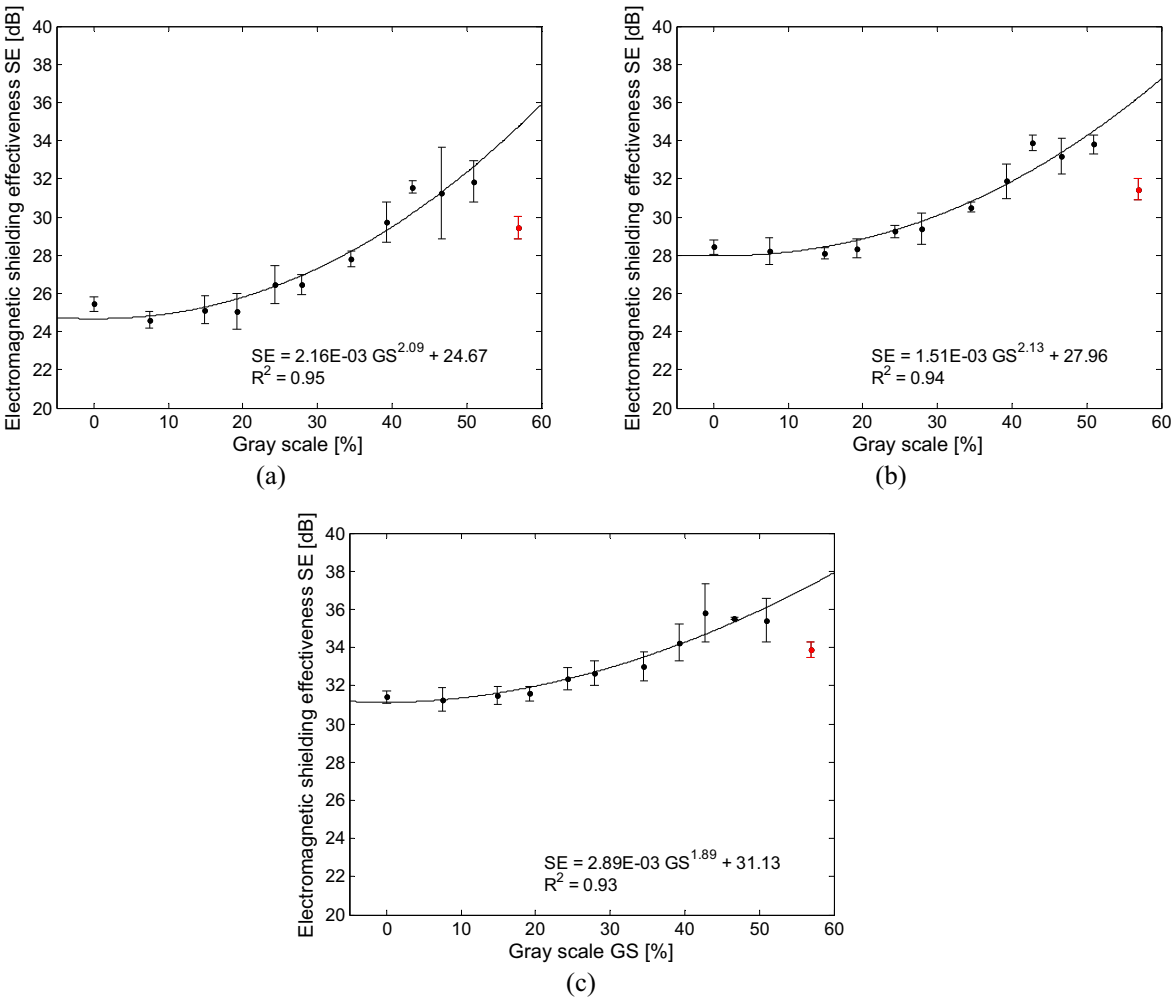

Fig. 3. The dependence of electromagnetic shielding effectiveness on different laser modification levels expressed by gray scale for following frequencies: (b) 600 MHz, (c) 1 GHz, (d) 1.5 GHz.

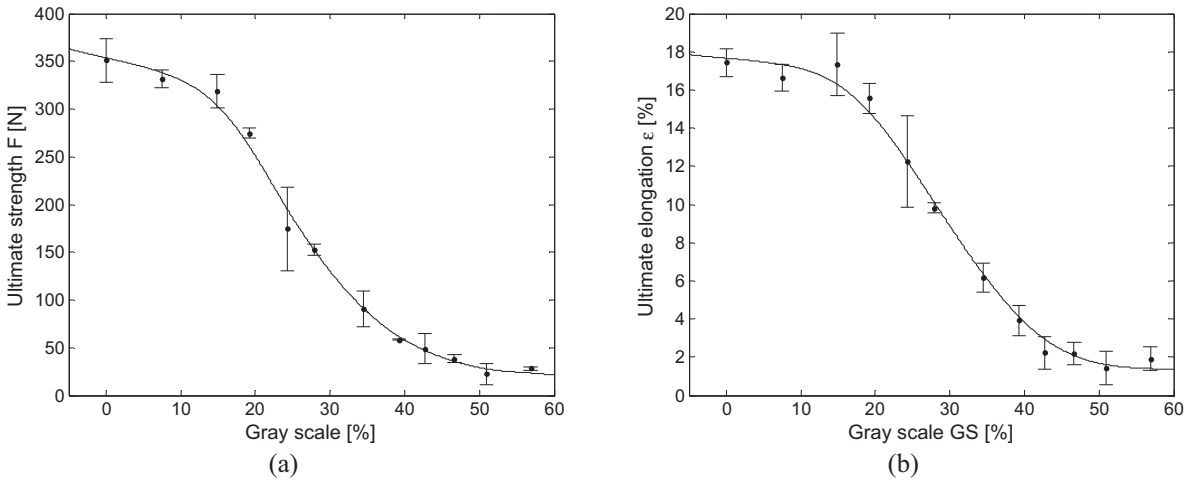

Fig. 4. The dependence of (a) ultimate strength [N] and (b) ultimate elongation [%] of sample measured in warp direction on different laser modification levels expressed by gray scale [%].

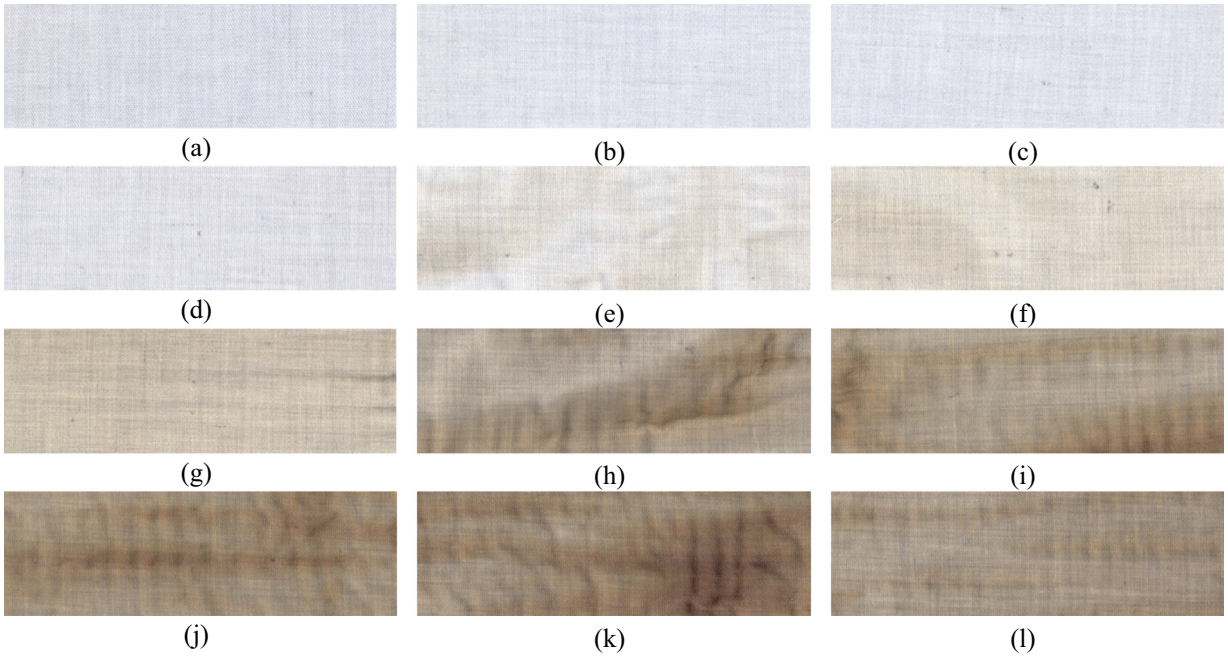

Fig. 5. Scanned images of samples irradiated by different intensity expressed by gray scale [%]: (a) 0%, (b) 7.5%, (c) 14.9%, (d) 19.2%, (e) 24.3%, (f) 27.8%, (g) 34.5%, (h) 39.2%, (i) 42.7%, (j) 46.7%, (k) 51.0, (l) 56.9%.

1 GHz and 1.5 GHz. These particular frequencies were chosen because they represent whole measured frequency range and they are close to working frequency of communication networks including GPS navigation devices ($f \sim 1.5$ GHz), cell phones ($f \sim 900$ MHz, $f \sim 1.8$ GHz) and radars ($f = 300$ MHz–1 GHz). It is visible that laser irradiation having intensity lower than GS 20% has not statistically significant effect on electromagnetic shielding effectiveness (95% confidence intervals of means are overlapping). With further increase of laser irradiation intensity, SE slightly increases up to 51% gray scale for all frequencies. Electromagnetic shielding effectiveness lifts at GS 24% and GS 51% of about 1 dB, resp. 4 dB compared to the original SE value of untreated sample (which means increase of about 2.8%, resp. 12.7% of base line for all studied frequencies). With regards to 95% confidence intervals of sample means, it is obvious that there is a statistically significant increase of electromagnetic shielding ability connected with laser irradiation above GS 20%.

After getting over this gray scale "critical value" ($GS > 51\%$), the sample becomes fragile, cracks appear and therefore sample's shielding ability is fading because of easier penetration of electromagnetic wave through the sample. Electromagnetic shielding of this sample is displayed in red color. Dependence of electromagnetic shielding effectiveness (SE) on gray scale (GS) below the "critical value" can be approximated using power function. The solid lines in this graph correspond to the regression models with parameters obtained by the minimizing sum of squared errors. Corresponding coefficient of determination $R^2 = 0.95$ indicates the good quality of fit.

3.2. Effect of laser irradiation on tensile strength and elongation

In previous text, functionality expressed by ability of sample act as a barrier to electromagnetic field was studied. It was found that laser irradiation of sample by specific intensity can enhance mate-

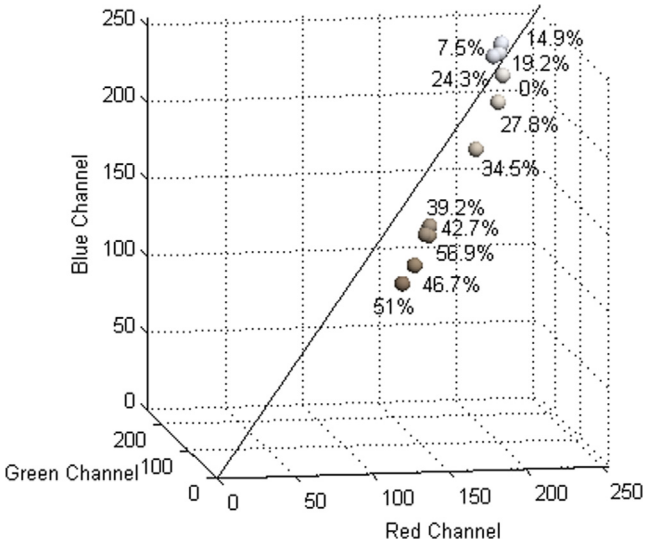

Fig. 6. RGB color cube showing color shade of samples irradiated by different laser intensity.

rial performance (electromagnetic shielding ability). On the other hand, after some limit of laser intensity, treated sample becomes fragile and crack appears during handling. On this account tensile testing of treated samples was carried out to find out whether the laser treatment has significant effect on the mechanical properties and eventually whether the laser modification restricts the usage of laser treated samples.

Fig. 4a displays the dependence of ultimate strength of sample measured in warp direction (sample width was 2 cm) on different laser modification levels expressed by gray scale [%]. It is visible, that strength of sample is decreasing with increasing gray scale. At very low laser treatment intensities ($GS < 15\%$) the strength remains almost the same to that of the untreated sample ($F > 300$ N). Then, at a point called percolation threshold of gray scale (analogically with electrical percolation threshold), the strength of the sample decreases dramatically over a quite narrow range of laser intensities. In this case percolation threshold occurs about GS 15–35%. This is important information showing at which laser intensity is material losing significantly its strength. Strength of sample irradiated by GS 19.2%, resp. GS 34.5% decreases to 78% (274 N), resp. to 26% (91 N) of its original value (untreated sample). Strength of samples irradiated by laser at intensity higher than GS 35% is very poor, lower than 50 N which means decline up to 8% of the strength of untreated sample. Strength behavior of laser treated samples is in good accordance with behavior of ultimate elongation of samples (see Fig. 4b) saying that the lower the ultimate strength of sample is, the lower ultimate elongation sample has. With regards to these findings, intensity of laser higher than GS 35% should not be used for treatment of samples because of its significant degradation.

3.3. Effect of laser irradiation on color

Main aim of this subchapter was to analyze color change of laser irradiated sample depending on different laser modification levels expressed by gray scale [%]. Color shade of irradiated samples was changed from light gray (untreated sample) to brown with increasing laser modification level; see Fig. 5, where scanned images of samples are shown. Light gray color of untreated sample (Fig. 5a) is caused by presence of stainless steel fibers in the structure of yarns. Brown color of the fabric surface is a consequence of carbonization of the fibers treated by the laser beam. It is also noticeable from images, that irradiation of samples is not homogenous especially at higher levels of laser intensity ($GS > 39\%$). This phenomenon can be expressed by variation coefficient of measured grey level pixels of sample images showed in Table 4. Samples with intensity of laser irradiation lower than GS 39.2% has not variation coefficient exceeding 4%. Variation coefficient of samples irradiated by higher laser intensity ($GS > 39.2\%$) is from 5.8% to 7.4%. It seems that irradiation of large sample areas by continuous pattern at higher laser intensity is not feasible homogenously. Further, wrinkling and three-dimensional effects are noticeable at samples irradiated by higher laser intensity ($GS > 39.2\%$).

Average RGB components (average red, green and blue) from all pixels of samples were counted (see Table 4) and plotted into RGB color cube (Fig. 6). It can be seen that with increasing laser treatment intensity, average color of sample is darker. Color of samples with low laser irradiation intensity ($GS < 27.8\%$) is similar to the color of untreated sample and therefore color markers (balls) are clustered in the RGB color cube. With further increase of irradiation intensity, color of samples is getting darker approaching dark brown color. It is observable that markers are almost following the line (corresponding to gray levels of image) joining black and white color.

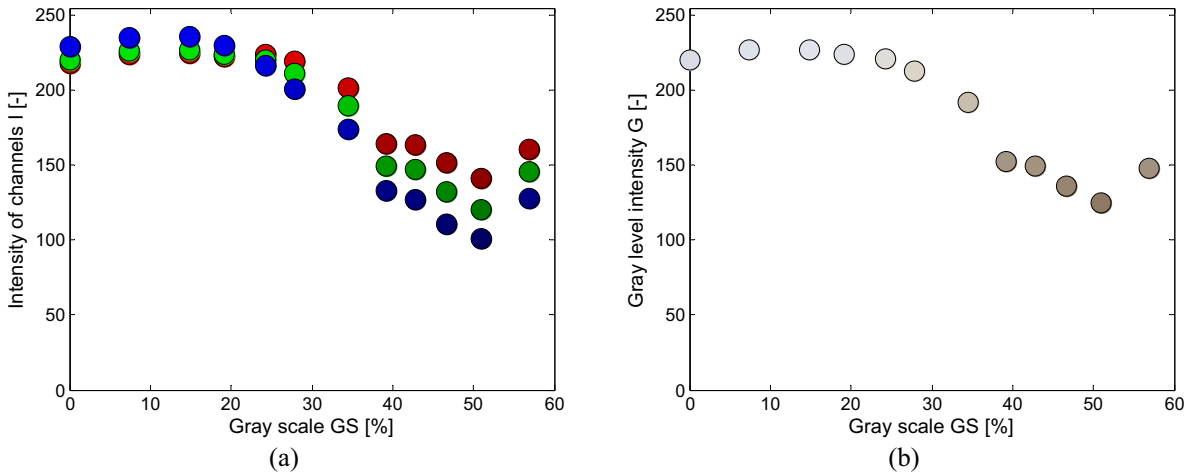

Fig. 7. The dependence of (a) average intensity of each triplet color [–] and (b) average gray level intensity [–] on different laser modification levels expressed by gray scale [%]. (For interpretation of the references to colour in this figure legend, the reader is referred to the web version of this article.)

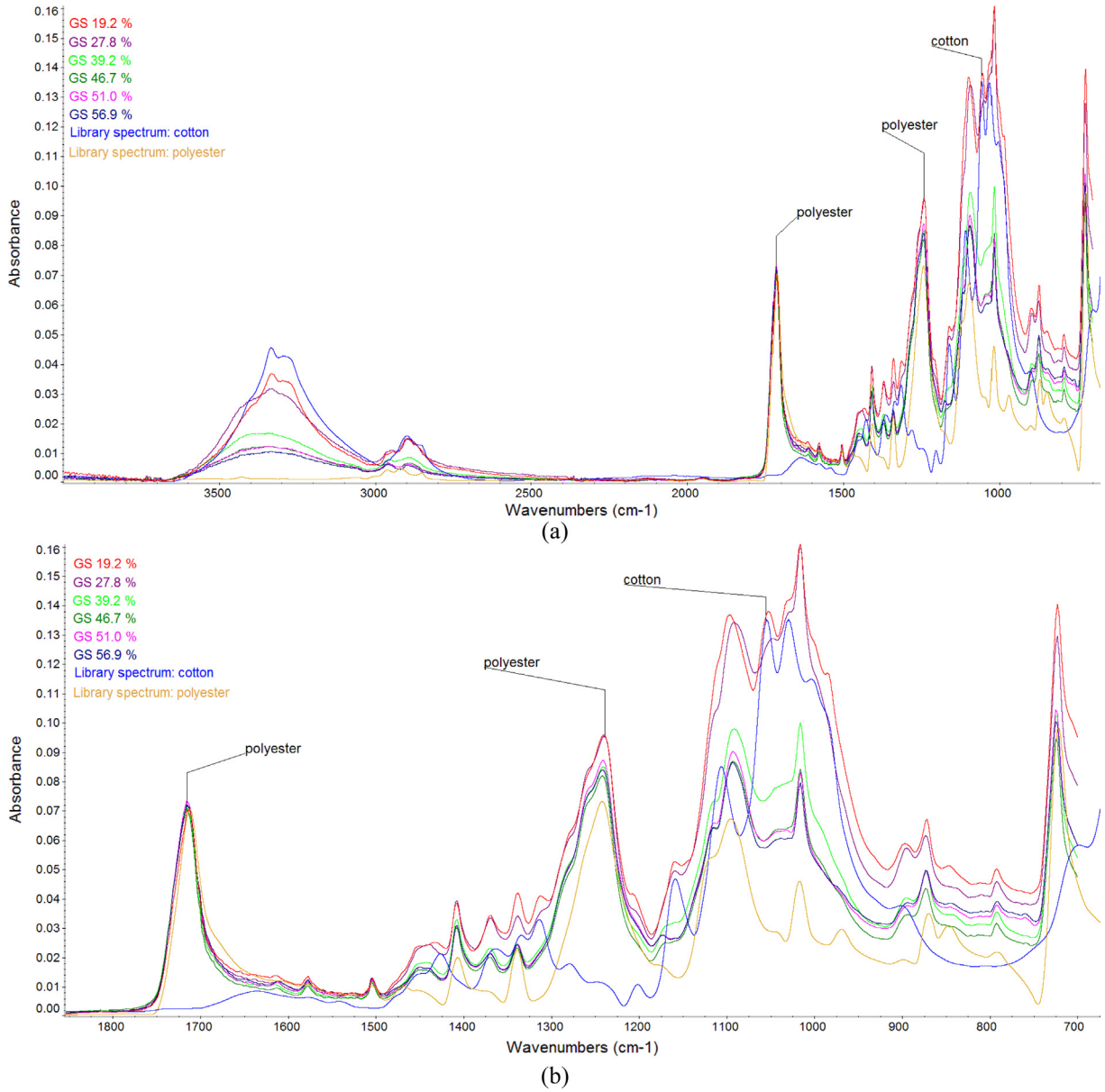

Fig. 8. FT-IR transmission spectra of samples irradiated by different laser intensity expressed by gray scale [%]: (a) whole band of measured wavenumbers, (b) detailed spectra in the region from 700 to 1900 cm^{-1}.

Similar behavior can be seen in Fig. 7; where Fig. 7a shows dependence of average intensity of individual color component and Fig. 7b displays average gray level intensity (face color of circles represents average real color of sample). In both cases, the independent variable is gray scale [%] representing intensity of laser irradiation. When exploring Fig. 7a, it is visible that all three color components of image (red, blue, green) of first four samples with the lowest intensity of irradiation behave similarly, close to the color components of the untreated sample ($I \sim 220$). The intensity of all color channels is almost the same in this region of irradiation corresponding to grey appearance of sample. It means that irradiation of sample by laser intensity to the GS 20% is not causing change in the color appearance. With increasing intensity of sample irradiation, overall intensity of color channels is decreasing indicating darkening of sample color, whereas the lowest intensity has blue channel, green color component has intermediate intensity and red color component intensity is highest for all samples with laser irradiation intensity higher than 20% (expressed in gray scale). Because the intensities of all color channels are not the same with predominant red channel intensity, the appearance of samples is brown. Critical behavior is possible to observe in the area ranging from GS 20% to GS 40% where smooth change over from the color of the untreated material to the color of totally destroyed sample occurs. Similar behavior is possible to observe from Fig. 7b where mean grey levels intensities of samples irradiated by different levels are shown. It can be summarized, that for visual patterning purposes the laser intensity should be higher than GS 20%.

3.4. Effect of laser irradiation on sample material composition

To check material composition of samples and sample partial degradation during laser modification, infrared (IR) spectroscopy was employed. It was supposed that increase of electromagnetic shielding ability of laser irradiated sample is caused by increasing content of carbon (providing high electrical conductivity) in the structure of the sample which is formed during degradation of

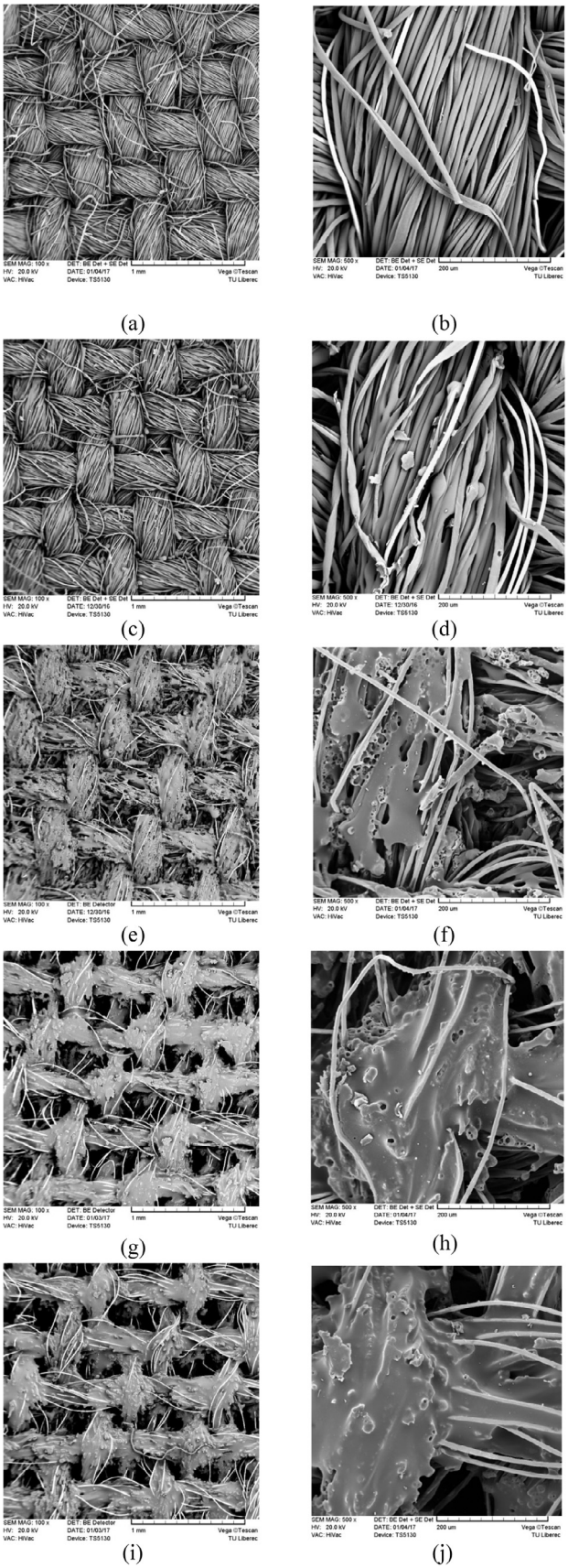

Fig. 9. SEM images of: (a and b) untreated sample and laser treated samples with different intensities expressed by gray scale [%]: (c and d) GS 19.2%, (e and f) GS 34.5%, (g and h) 46.7%, (i and j) 56.9%.

fibers. It was assumed that degradation of cotton fibers take place first, because cotton fibers decomposes about 200 °C, polyester fibers decomposes at $T > 350$ °C and stainless steel melts even at 1500 °C. Unfortunately, IR spectra of carbon materials are difficult to obtain because of problems in its poor transmission and uneven light scattering. Spectra interpretation of carbon materials is also not definite and moreover, the electronic structure of carbon materials results in a complete absorption band through the visible region to the infrared [25]. On this account, change in IR spectra of laser irradiated samples was explored with a view to polyester and cotton peak changes. Fig. 8 shows the IR spectra of chosen samples irradiated by different laser intensity expressed by gray scale [%] as follows: 19.2%, 27.8%, 39.2%, 46.7%, 51.0% and 56.9% together with library spectra of cotton and polyester and notation of peaks corresponding to polyester and cotton, where Fig. 8a shows IR spectra in whole measured region of wavenumbers and Fig. 8b shows detail of the spectra in the region from 700 to 1900 cm^{-1}. Intensity decline of absorbance peaks around wavenumber 3500 cm^{-1} and 2900 cm^{-1} in Fig. 8a indicates reduction of cotton with increasing laser irradiation intensity. Similar reduction of cotton with laser irradiation appears from 1030 to 1100 cm^{-1} (Fig. 8b). When inspecting polyester characteristic peaks, absorbance intensity peak is not changed with increasing laser irradiation intensity at 1720 cm^{-1} but slight decrease of absorbance intensity peak is observable at 1240 cm^{-1} and slightly more decrease of polyester intensity peak is apparent 1020 cm^{-1}. This behavior confirms presumption that especially cotton fibers are carbonized accompanied by increase of sample electrical conductivity and therefore ability to shield electromagnetic field is improved.

3.5. Effect of laser irradiation on sample morphology

Fig. 8 shows scanning electron micrographs of untreated and laser treated samples with chosen intensities at two different magnifications 100× and 500×. When exploring Fig. 9a and b where images of untreated sample are shown, cotton fibers (twisted ribbon appearance), polyester fibers (circular cross-section) and stainless steel fibers (lighter one) are recognizable. Fig. 9c and d present the SEM images of sample irradiated by GS 19.2%. It is clear that stainless steel fibers were unaffected still having smooth surface while it seems that cotton fibers are partially destroyed creating unfixed fragments and polyester fibers start to melt. Fig. 9e and f show the SEM images of sample irradiated by GS 34.5%. Using this laser intensity, various sizes of pores on the cotton fibers are created resulting in a sponge-like structure (which has been already described in [26]), melting of polyester fibers is more remarkable and at the same time stainless steel fibers stay in pristine condition. Fig. 9g and h illustrate the SEM images of sample irradiated by GS 46.7%. It is visible that melted area of polyester fibers increases compared to lower laser intensity and at the same time there is a noticeable amount of sponge-like areas. Fig. 9i and j illustrate the SEM images of sample irradiated by the highest laser intensity, namely GS 56.9%. Using this laser intensity, fiber structure was totally decomposed with prevailing part of fragile melted places adhered on durable stainless steel fibers. It is also possible to observe, that with increasing laser intensity, a cover factor of fabric is decreasing accompanied with creation of larger pores between decomposed yarns which can positively influence air permeability of fabric.

3.6. Patterning of electrically conductive samples

Previous subchapters of this paper described physical and aesthetic properties of laser modified electrically conductive samples with different laser setting. In this subchapter practical realization

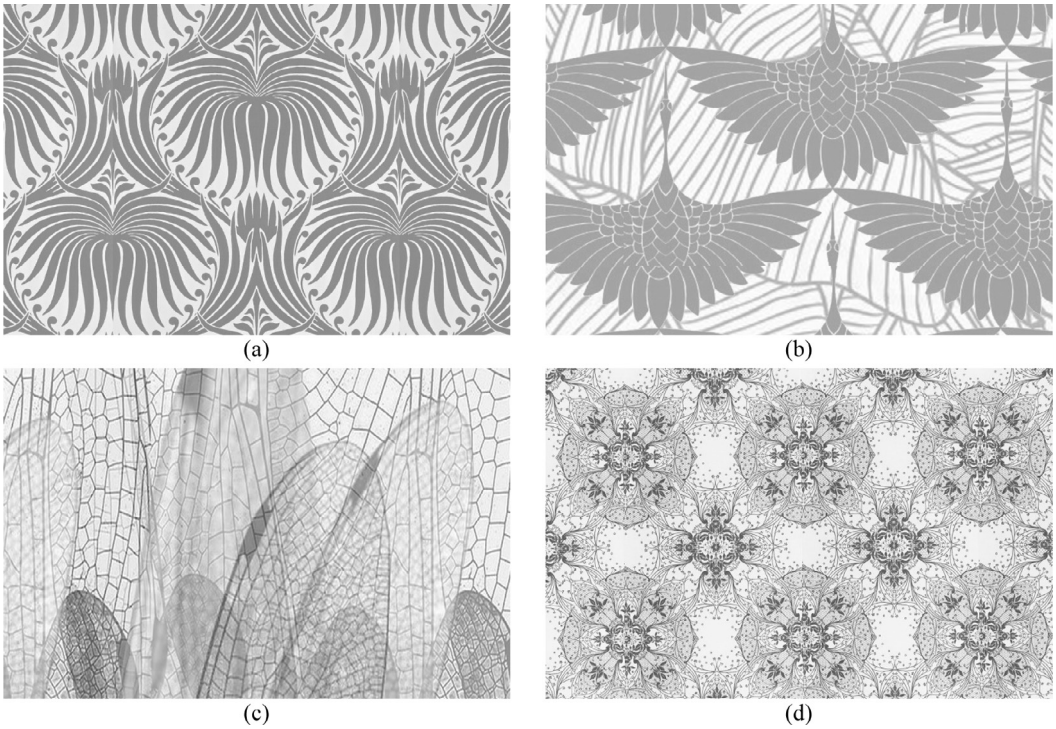

Fig. 10. Digital design image files as an input for laser patterning: (a) pattern A, (b) pattern B, (c) pattern C, (d) pattern D.

Table 5
Minimum and maximum GS together with mean GS and median of GS of all pixels of input images.

Pattern	Minimum GS [%]	Maximum GS [%]	Mean GS [%]	Median of GS [%]
A	0	54.9	29.6	42.7
B	0	38.4	22.3	27.5
C	0	81.9	20.6	18.4
D	0	75.7	22.1	15.7

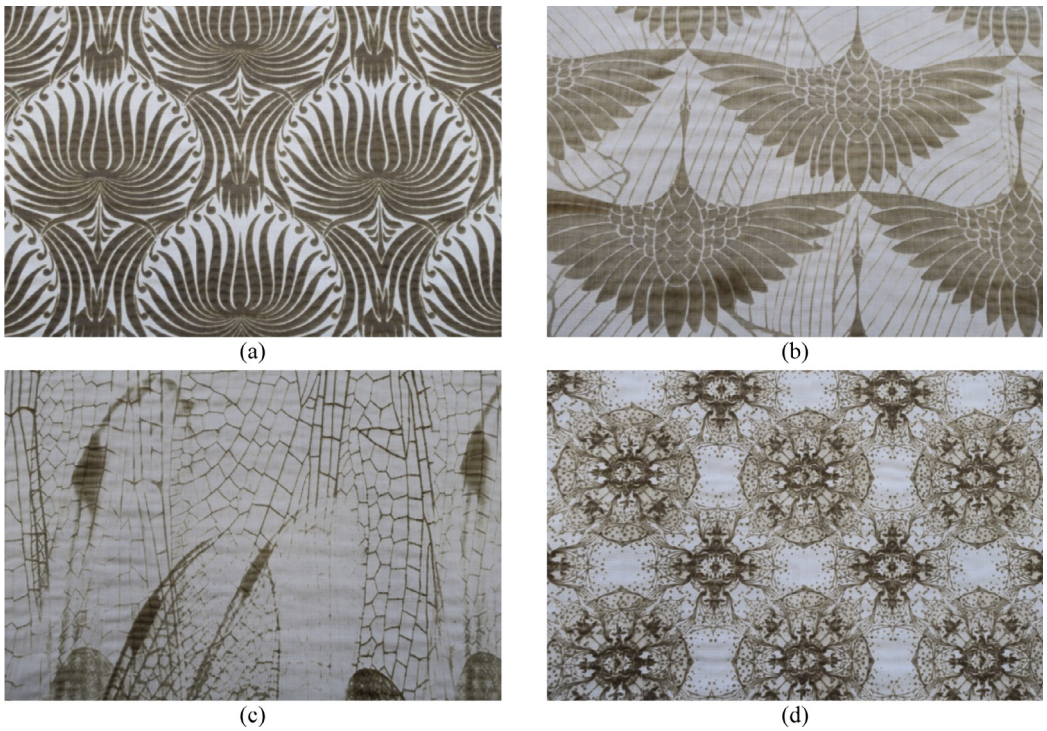

Fig. 11. Laser engraved functional (electrically conductive) samples: (a) pattern A, (b) pattern B, (c) pattern C, (d) pattern D.

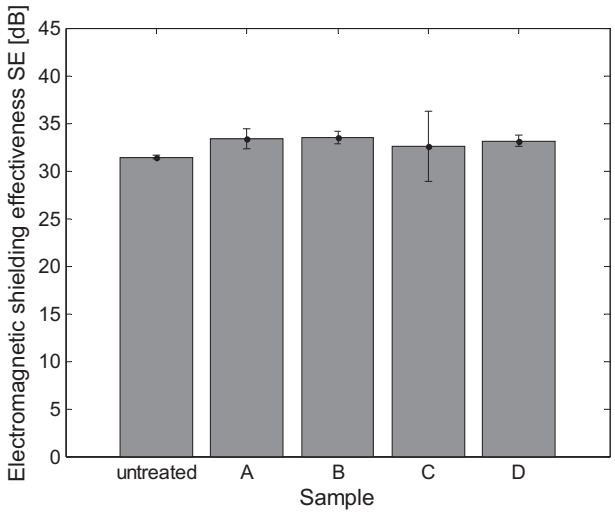

Fig. 12. Comparison of electromagnetic shielding effectiveness at frequency 1.5 GHz of patterned samples.

of patterning connected with changing appearance and visual characteristics of functional fabrics by applying certain designs to the texture and surface of textiles is presented. Main goal of this part was to present aesthetic possibilities and production opportunities of digital laser patterning of electrically hybrid textiles containing stainless steel metal fiber.

Four different digital image files (marked A, B, C, D) in bitmap format containing design for laser patterning were prepared first and are shown in Fig. 10. Grey levels of individual pixels in the image determine the laser energy density required to achieve specific tonal and visual effect. Samples were irradiated by the laser beam directly on one side of the fabric. The duty cycle and pixel time was set constant to 50% and 100 μs. Grey level of individual pixels of patterns was selected on the basis of previous investigation with a view to visual effect and mechanical properties of laser engraved fabric. Table 5 shows details of gray levels of input digital images (minimum, maximum, mean and median). In case of patterned fabrics, laser is applied only to the designated parts of fabric; it is not applied over its entire surface and therefore it is assumed that tenacity of the patterned fabric will be better than in case of fabric full-area engraving.

Fig. 11 illustrates images of real electro-conductive fabric engraved by patterns shown in Fig. 10. Images of real fabrics were captured using HP Scanjet 5590 digital flatbed scanner (because of homogenous illumination of samples) in resolution 200 dpi. It is visible, that desired pattern was achieved and therefore laser engraving represents one of promising techniques for changing appearance of functional fabrics according to expectations of consumers.

At the same time it was confirmed that shielding ability of samples was increased using laser patterning, see Fig. 12, where electromagnetic shielding effectiveness of untreated and laser treated samples by different design measured at frequency 1.5 GHz is shown. When exploring mechanical properties, patterned sample B–D embodies very good mechanical properties and pleasant touch. It seems that places irradiated by higher intensity at patterned sample A are relatively brittle, which limits usage of fabric patterned by this design. This behavior is consistent with previous analysis saying that certain range of laser intensities expressed by gray scale should be used to obtain electrically conductive fabric with desired properties.

4. Conclusions

In this paper, some common textile properties together with evaluation of functionality of special electrically conductive fabric were studied after laser surface treatment with different intensity. Woven fabric with twill 2/1 weave made of conductive yarn containing 10 wt% stainless steel staple fibers was used as a substrate. Commercial pulsed CO_2 laser (Marcatex 150 Flexi, Easy-Laser) under atmospheric condition in air was used for irradiation of samples. Laser beam energy density was controlled by gray scale information of individual pixels in the input image.

It was found that some properties are influenced positively with increasing intensity of laser treatment (visual effect, electromagnetic shielding effectiveness) while change in other properties was undesirable (mechanical properties). Influence of laser engraving on physical and esthetic properties was also confirmed by studying morphological changes and infrared spectra of material. Increase of electromagnetic shielding ability is dedicated to increase of sample electrical conductivity caused by carbonization of sample during laser irradiation accompanied by color change (from light grey to brown). Visual effect and mechanical properties can be controlled by laser intensity. As an optimum laser intensity expressed by gray scale in percentages for this specific type of fabric (determined by material composition and geometrical characteristics) is in the area from 20% to 35%. Laser intensity below GS 20% is not causing desired visual effect and at the same time laser intensity above GS 35% is too high initiating too large degradation of the sample accompanied with loss of mechanical properties and functionality (electromagnetic shielding ability) restricting its practical usage.

It has been shown that the use of laser patterning upon special electrically conductive hybrid woven fabric is valuable tool to modify appearance and visual characteristics according to expectations of consumers and therefore increasing its added value. Because of significance decrease of mechanical properties, laser patterned fabrics are not appropriate for using as traditional textile fabric for clothing. This procedure of patterning seems to be suitable especially for preparation of interior textiles, furnishing textiles or technical textiles, e.g. with respect to electromagnetic shielding effectiveness it can be used as textile wallpapers or interior textile screens (using paper or fabric backing to improve their mechanical properties) in living or working places. Usage of this patterned shielding textile as a lining of cabin sidewalls (using lamination to increase mechanical properties and provide washability of its surface) in the aircrafts appears as other possible application.

Acknowledgements

This work was supported by the partial research project of TG01010117 PROSYKO granted by Technology Agency of the Czech Republic.

References

[1] A.L. Apreutesei, A. Curteza, V. David, et al., Investigation of the textile structures with different design used in electromagnetic shielding, in: Proceedings of the 2014 International Conference of Exposition on Electrical and Power Engineering. Iasi, Romania, 16–18 October 2014, pp. 596–601.
[2] V. Safarova, J. Militky, Multifunctional metal composite textile shields against electromagnetic radiation – effect of various parameters on electromagnetic shielding effectiveness, Polym. Compos. Epub ahead of print 15 May 2015. doi: 10.1002/pc.23588.
[3] V. Safarova, J. Militky, Electromagnetic shielding properties of woven fabrics made from high-performance fibers, Textile Res. J. 84 (12) (2014) 1255–1267.

[4] H.G. Ortlek, T. Alpyildiz, G. Kilic, Determination of electromagnetic shielding performance of hybrid yarn knitted fabrics with anechoic chamber method, Textile Res. J. 83 (1) (2013) 90–99.
[5] S. Palamuctu, A. Ozek, C. Karpuz, et al., Electrically conductive textile surfaces and their electromagnetic shielding efficiency measurement, Textil ve Konfeksiyon 20 (3) (2010) 199–207.
[6] M.S. Hong, W.K. Choi, K.H. An, et al., Electromagnetic interference shielding behaviors of carbon fibers-reinforced polypropylene matrix composites: II. Effects of filler length control, J. Indust. Eng. Chem. 20 (5) (2014) 3901–3904.
[7] V. Safarova, J. Militky, Lightweight and flexible structures for electromagnetic interference shielding – present state, in: Proceedings of 38th International Conference on Telecommunications and Signal Processing, TSP 2015, Praha, Czech Republic, 9–11 July 2015, pp. 257–261.
[8] L. Vojtech, M. Neruda, Design of radiofrequency protective clothing containing silver nanoparticles, Fibres Textiles Eastern Europe 21 (5) (2013) 141–147.
[9] D. Duran, H. Kadoglu, Electromagnetic shielding characterization of conductive woven fabrics produced with silver-containing yarns, Textile Res. J. 85 (10) (2015) 1009–1021.
[10] L. Vojtech, J. Hajek, M. Neruda, et al., Monometallic textile electrodes for "green" batteries, Elektronika ir Elektrotechnika 20 (9) (2014) 25–28.
[11] B. Li, D. Li, J. Wang, Copper deposition on textiles via an automated dispensing process for flexible microstrip antennas, Textile Res. J. 84 (19) (2014) 2026–2035.
[12] N.V. Bhat, D.T. Seshadri, S. Radhakrishan, Preparation, characterization and performance of conductive fabrics: cotton + PANi, Textile Res. J. 74 (2) (2004) 155–166.
[13] Y. Wang, X. Jing, Intrinsically conductive polymers for electromagnetic interference shielding, Polym. Adv. Technol. 16 (4) (2005) 344–351.
[14] C. Merlini, S.D.A.S. Ramoa, G.M.O. Barra, Conducting polypyrrole-coated banana fiber composites: preparation and characterization, Polym. Compos. 34 (4) (2013) 537–543.
[15] V. Tunakova, J. Gregr, M. Tunak, G. Dohal, Functional polyester fabric/polypyrrole polymer composite for electromagnetic shielding: optimization of process parameters. J. Indust. Textiles, Epub ahead of print 31 August 2016. doi: https://doi.org/10.1177/1528083716667262.
[16] S. Naeem, V. Baheti, V. Tunaova, et al., Development of porous and electrically conductive activated carbon web for effective EMI shielding applications, Carbon 111 (2017) 439–447.
[17] P. Xue, X.M. Tao, K.H. Park, Electrically conductive fibers/yarns with sensing behavior prom PVA and carbon black, Key Eng. Mater. 462–463 (2011) 18–23.
[18] T.W. Shyr, J.W. Shie, Electromagnetic shielding mechanism using soft magnetic stainless steel fiber enabled polyester textiles, J. Magn. Magn. Mater. 324 (23) (2012) 4127–4132.
[19] V. Tunakova, L. Technikova, J. Militky, Influence of washing/drying cycles on fundamental properties of metal fiber-containing fabrics designed for electromagnetic shielding purposes, Textile Res. J. 87 (2) (2017) 175–192.
[20] Z. Ondogan, O. Pamuk, N.E. Ondogan, A. Ozguney, Improving the appearance of all textile products from clothing to home textile using laser technology, Optics Laser Technol. 37 (8) (2005) 631–637.
[21] K. Akiwowo, F. Kane, J. Tyrer, et al., Digital laser-dyeing for polyester fabrics, J. Textile Des. Res. Practice 2 (2) (2014) 133–152.
[22] M. Stepankova, J. Wiener, J. Dembicky, Properties of cotton fabric after irradiation with infrared CO_2 laser, Fibers Polym. 15 (10) (2014) 2072–2076.
[23] P.S. Horn, Some easy t statistics, J. Am. Statist. Assoc. 78 (1983) 930–936.
[24] T. Zhao, C. Hou, H. Zhang, et al., Electromagnetic wave absorbing properties of amorphous carbon nanotubes, Sci. Rep. 4 (4519) (2014) 1–7.
[25] E. Fuente, J.A. Menendez, M.A. Diez, et al., Infrared spectroscopy of carbon materials: a quantum chemical study of model compounds, J. Phys. Chem. B 107 (2003) 6350–6359.
[26] Y.L. Chow, C.K. Chan, C.W. Kan, SEM analysis of CO2 laser treated cotton grey fabric, Microsc.: Sci., Technol., Appl. Educat. (2010) 1860–1867.

Appendix 5

V. Tunakova, J. Gregr, M. Tunak, and G. Dohnal, "Functional polyester fabric/polypyrrole polymer composites for electromagnetic shielding: Optimization of process parameters," J. Ind. Tex., vol. 47, no. 5, pp. 686–711, 2018.

Article

Journal of Industrial Textiles

2018, Vol. 47(5) 686–711

DOI: 10.1177/1528083716667262
journals.sagepub.com/home/jit

SAGE

Functional polyester fabric/polypyrrole polymer composites for electromagnetic shielding: Optimization of process parameters

Veronika Tunáková[1], Jan Grégr[2], Maroš Tunák[1] and Gejza Dohnal[3]

Abstract

Intrinsically conducting polymer polypyrrole/polyester textile composites were prepared by in situ chemical oxidative polymerization of polypyrrole on a polyester fabric. As an oxidizing agent ferric chloride was used, *p*-toluenesulfonic acid was used as a dopant. Polymerization conditions (concentration of monomer, polymerization time and temperature) were investigated and optimized by the help of Design of experiment methodology to obtain fabric with electromagnetic shielding efficiency at least 12 dB for frequency 1.5 GHz. Moreover, weight increase, macroscopic color shade of images and scanning electron microscopy images of samples were evaluated. It was found that all selected factors and their interactions have statistically significant effect on resulting electromagnetic shielding effectiveness, whereas monomer concentration has the highest positive influence. Experimental data were used to derive an empirical model linking the output and inputs. Optimized parameters (polymerization temperature 6.7°C, polymerization time 10 h and monomer concentration 5.8 g/l) for creating polypyrrole/polyester textile composite with electromagnetic shielding ability higher than 12 dB were successfully verified.

[1]Faculty of Textile Engineering, Technical University of Liberec, Czech Republic
[2]Faculty of Science, Humanities and Education, Technical University of Liberec, Czech Republic
[3]Faculty of Mechanical Engineering, Czech Technical University of Prague, Czech Republic

Corresponding author:
Veronika Tunáková, Faculty of Textile Engineering, Technical University of Liberec, Studentská 2, Liberec 463 17, Czech Republic.
Email: veronika.tunakova@tul.cz

Keywords
Conductive fabrics, Design of experiment, electromagnetic shielding effectiveness, polyester, polypyrrole

Introduction

Numerous sources of electromagnetic emission in our environment produce electromagnetic (EM) waves that can cause interference in electronic and electrical devices. Sources of such emissions could include generation and transmission of electricity, domestic appliances and industrial equipment, telecommunications and broadcasting. Over the last few years, there has been mounting concern about the possibility of adverse health effects resulting from exposure to radiofrequency EM fields, such as those emitted by wireless communication devices. In 2011, the World Health Organization/International Agency for Research on Cancer (IARC) has classified radiofrequency electromagnetic fields as possibly carcinogenic to humans (Group 2B), based on an increased risk for glioma, a malignant type of brain cancer, and associated it with wireless phone use [1]. One the other hand, despite many studies, the evidence for biological effects of electromagnetic fields on human body when exposed to levels that are below the official threshold values [2] was not unambiguously confirmed. Nevertheless, electromagnetic emissions have to be reduced as possible and simultaneously there is a growing need for suitable materials, which can act as barrier against electromagnetic waves. Actually, shields such as copper or other metallic compounds are used as electromagnetic screens. However, recently electromagnetic shields based on flexible materials have been developed for many applications, especially for protective clothing.

Conductive textile structures have obtained increased attention for electromagnetic shielding and anti-electrostatic purposes in recent years. This is mainly due to their desirable flexibility and lightweight. Conductive fabrics based on use of metallic materials in form of bulk sheets, meshes, plating coatings, powders in filled polymer composites and fibers (filaments) embody excellent shielding effectiveness [3–7], but possess high weight, corrosion, and oxidation problems. Carbons are also used in EM shielding applications, mainly as fibers, particles, powders, filament, and tubes due to their electrical conductivity, chemical resistance, and low density [8–10], but the conductivity and EM shielding performance of carbon-based materials in not good enough.

Intrinsically conducting polymers (ICPs) are attractive alternative for EM shielding. Since the discovery of ICPs in late 1970s, textile structures integrating ICPs for EMI shielding, as well as electrostatic discharge have been developed and evaluated by many papers [11–17]. These materials combine high electrical conductivity (as compared with carbons), ease processability, low density (e.g. density of polypyrrole (PPy) is 1.5 g/cm^3 far less than that of metals, such as 8.9 g/cm^3 for copper), and corrosion resistance together with absorption shielding mechanism (differing from the reflection one for metals). One of the most widely used approaches to fabrication of electrically conductive textiles from inherently

conductive polymers is to use a submicron thick coating of an ICP onto an existing textile substrate. While a lot of research papers describe development of ICPs/textile composites with different set-up of input parameters (different types of oxidizing agents, dopants and their concentrations, polymerization time and temperature, monomer concentration, material of substrate), little attention has been dedicated to investigation of coating formulation that is sufficiently robust for all various input parameters and disposed for particular product.

In this paper, the process for the preparation of conductive fabrics composed of 100% polyester (PET) yarns coated with conducting polypyrrole is described. Polyester was chosen as a substrate because it has been one of the most popular fibers measured by production quantity in recent years. Polyester fibers have many desirable properties, such as relatively high tenacity, low creep, good resistance to strain and deformation, high glass transition temperature, and good resistance to acids and oxidizing agents. On the other hand, hydrophobic nature of polyester fibers makes them difficult to dye and to finish in aqueous media. This creates challenge to investigate and develop methods of surface modifications of polyester-based textile structures. The key process parameters for the preparation of PET/PPy composites through oxidative polymerization in aqueous solution were studied by the help of Design of experiment (DoE) methodology to develop textile composite with electromagnetic shielding efficiency 15 ± 3 dB for frequency 1.5 GHz. It means that electromagnetic shielding effectiveness (SE) cannot be lower than 12 dB, but excess of upper limit is not forbidden. This requirement has arisen from the statement that for personal shielding (general use), electromagnetic SE value should be in the range from 10 dB to 20 dB in the frequency spectrum of 0.8–2.5 GHz [18]. As an oxidizing agent, ferric chloride ($FeCl_3$) was used, and as a dopant *p*-toluenesulfonic acid (PTSA) was used in fixed amount. As input parameters, polymerization temperature, time, and monomer concentration were chosen. The key, main, and interaction effects of the input variables on the output variable (electromagnetic SE) were analyzed and the settings for acceptable performance were introduced. Moreover, weight increase, macroscopic color shade of PPy-coated samples, and scanning electron microscopy images of samples were evaluated. Optimized input parameters for creating PET/PPy textile composite with at least 12 dB electromagnetic SE were successfully verified.

Polypyrrole-coated fibers

As stated in this paper [15], ICPs are termed as organic polymers that possess electrical, electronic, magnetic, and optical properties of a metal while retaining the mechanical properties, processability, and so on commonly associated with a conventional polymer, and more commonly known as "synthetic metals". In 1977, Hideki Shirakawa, Alan MacDiarmid, and Alan Heeger published their discovery that led to the 2000 Nobel Prize in chemistry. Since the early 1980s, development has been great and today the inherently conductive polymers, such as polyaniline (PANI), polypyrrole (PPy), polythiophene (PT), and poly(perinaphtalene) (PPN) have achieved a level where

many industrial applications have become reality [19]. The level of conductivity achieved in ICPs depends on the molecular structure of the polymer backbone, the degree of doping, and the nature of the counter ion species incorporated [19]. Today, a wide variety of conducting polymers is available. Of all of the known conducting polymers, polypyrrole is the most frequently used in commercial applications, due to the long-term stability of its conductivity and the possibility of forming homopolymers or copolymers with improved mechanical properties [20].

One of the most widely used approaches for fabricating electrically conductive textiles from intractable inherently conductive polymers is to use a submicron thick coating of an ICP onto an existing textile substrate [21]. Usually, electrically conducting textiles are prepared through oxidative polymerization of monomer on the surface of various textile materials. Conducting polymer-based textile structures can be fabricated by in-situ polymerization and a two-step process.

In-situ polymerization consists of adsorption of monomer on the surface of the substrate followed by oxidation polymerization. This process is industrially applicable because it can be performed using standard textile dyeing equipment using aqueous solution for both aniline and pyrrole. The in situ polymerization of pyrrole to form an electrically conductive textile was first reported by Kuhn [17]. The process for forming the polypyrrole-coated textiles is based on the immersion of a fabric into an aqueous solution containing pyrrole and oxidative polymerization conducted by adding an oxidant agent solution. In the extensive literature on the polymerization of pyrrole, the influence of the counter ion on the electrical conductivity has been widely discussed. Oxidants such as iron (III) chloride ($FeCl_3$) [22–24] or ammonium peroxydisulfate (APS) are often used. Usually, aromatic sulfonic acids such as *p*-toleunesulfonic acid (PTSA) or anthraquinon-2-sulfonic acid (AQSA) [22,23] are used as dopants, see Figure 1. The selection of the dopant anion affects both the surface resistivity and thermal stability of the polypyrrole-coated textiles. The literature indicates that the ratio of monomer units to oxidant agent to dopant is varied between 1:9:3.5 and 1:1.2:0.3 [22,24–35]. Using dilute solutions of pyrrole (0.004–30 M [24,25,30,33,35]), the polymerization reaction occurs on the surface of the fiber

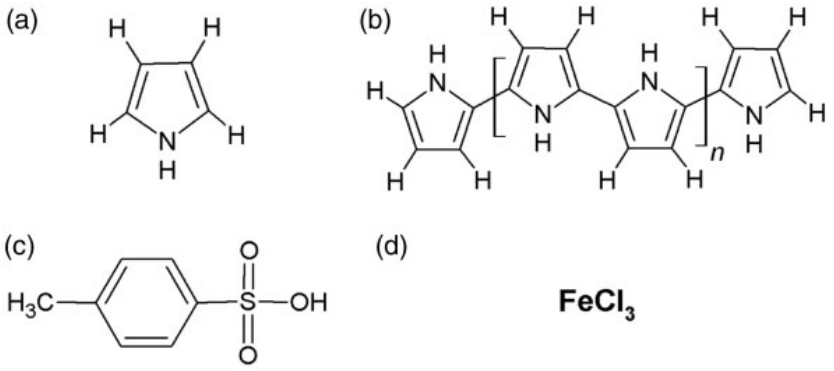

Figure 1. Chemical structure of: (a) pyrrole (Py), (b) polypyrrole (PPy), (c) *p*-toluenesulfonic acid (PTSA), and (d) ferric chloride ($FeCl_3$).

and leads to the formation of a precipitate in the bulk liquid phase. The influence of the polymerization temperature and the solvent used has also been investigated. For practical reasons, water is more often used as a solvent [34]. Lower temperatures are the most appropriate for obtaining the best conductivities in aqueous solutions of ferric salts. As a substrate, synthetic [8,11,23,26–28], semi-synthetic [25], and natural [24,29,32,33] textile structures were successfully used. The conductivity of these PPy-coated textiles could be varied from 10^{-1} to 10^{-4} S/cm and the electromagnetic shielding efficiency could be varied from 5 to 30 dB for frequency of around 1.5 GHz by controlling the polymerization time, number of repeating polymerizations, the concentration of the reactants in the polymerization bath, and the type of anion used to dope the PPy coating. In general, polymer conductivity is a function of monomer and oxidant agent concentrations, solvent, time of synthesis, and temperature of the synthesis.

Besides using an in-situ polymerization of conductive polymer to form an electrically conductive textile substrate, other researchers have adopted a two-step process. The major advantage of this procedure is that it can be easily adapted into a continuous process for industrial applications. Several variations to the two-step process include first immersing the textile support in a solution containing the oxidant and desired dopant anion and then exposing the impregnated textile structure to either conductive polymer vapor or polymer dissolved in an aliphatic solvent to initiate the polymerization reaction. Alternately, the textile support may be first exposed to polymer vapor and then immersed into an aqueous solution containing the oxidant and desired dopant anion [22].

Experimental

Materials

Polyester, more precisely polyethylene terephthalate (PET) fabric (white color, 100 % PET, weight: 176 g/m^2, thickness: 0.5 mm, weft and warp fineness 35 tex, warp sett 25 cm^{-1}, weft sett 22 cm^{-1} and plain weave), was used as a substrate. Samples of uniform dimensions 13.5 × 14.5 cm were cut using laser system Marcatex 150 Flexi to prevent fraying of sample edges. All samples were washed at 40°C using any detergent, thus minimizing impurities on the surface of these fabrics.

Reagent grade pyrrole (≥98%) and *p*-toluenesulfonic acid monohydrate (≥98.5%) were purchased from Sigma Aldrich (Germany), and iron (III) chloride anhydrous was purchased from Lach-Ner (Czech Republic). All chemicals including pyrrole were used without further purification as received. Deionized water was used in all reactions.

Design of experiment

Our experience has shown that the process operating conditions of in-situ polymerization of pyrrole on textile substrate significantly affect coating quality and

performance (e.g. electric conductivity, electromagnetic SE). In many cases, these effects are not strictly additive – process parameters can interact both synergistically and antagonistically. Although successive experiments can yield incremental improvement in quality or performance, the data from these experiments do not usually enable the researcher to identify and qualify interaction effects. Further, in trial and error experiments, full randomization is not possible. Also, studying several process parameters by trial and error is extremely inefficient.

The correct approach to dealing with several factors is to conduct a factorial experiment. This is an experimental strategy in which factors are varied together, instead of one at a time [36]. DoE methods include the factorial experiments, overcome the limitations of trial and error method described above, and quickly give the kind of understanding and results that are needed. The primary goal is usually to show the statistical significance of an effect that a particular factor exerts on the dependent variable and to find the optimum setting of factors to get desired level, small variability of dependent variable, or to minimize uncontrollable variables.

Full factorial design was chosen to completely and systematically study interaction between factors in addition to identifying significant factors. The variable of interest while in-situ polymerization of pyrrole on textile substrate was applied is the desired level of electromagnetic SE, namely > 12 dB measured at frequency 1.5 GHz. We next identified three controllable process parameters based on our experience and literature review: the polymerization temperature (A), the polymerization time (B) and the monomer concentration (C). The 3^3 factorial experiment was preferred to 3^2 one, because the nonlinear relation between inputs (Py concentration, polymerization time) and output (weight increase) is supposed as stated in this paper [24]. The factor's levels are given in Table 1. In our case, 27 treatment combinations had three replications; therefore 81 samples were prepared overall and these combinations had 80 total degrees of freedom and 54 degrees of freedom for error [36]. Runs were fully randomized.

Polymerization of Py

For chemical oxidative polymerization of Py on textile substrate, the sample dyeing instrument with dying pots (stainless steel tubes of capacity 300 ml) was used.

Table 1. Input variables, units, and levels.

Variable name	Variable units	Levels		
Polymerization temperature (A)	°C	5	15	25
Polymerization time (B)	h	1	8	15
Monomer concentration (C)	g/l	0.64	3.22	5.80

Tubes were placed in the water system of the internal bath in which temperature was controlled. The prepared samples were first placed into the dying tube together with the plastic grid to separate the sample by an empty space from the tube side so that the solution can circulate and to support the stability of the plain sample in the tube. Each sample was then soaked in aqueous solution (of about 250 ml) of very low concentration (<0.01%v/v) of Spolion 8 wetting agent to improve wetting of fabric substrate. After this, iron (III) chloride hexahydrate (oxidant) and *p*-toluenesulfonic acid monohydrate (dopant) were dissolved in 30 ml of distilled water and poured into the dying tube. After 5 min of diffusion, pyrrol monomer (0.2, 1 and 1.8 ml corresponding to 0.64, 3.22 and 5.80 g/l) was added to the tube. Finally, distilled water was added in to the tube up to volume of 300 ml and then the tube was closed, stirred, and placed into the dyeing instrument. The weight ratio of the monomer, oxidizing agent, and dopant was 1:5:3. Polymerization was carried out between 5 and 25°C and between 1 and 15 h, see Table 1. After polymerization process finished, samples were cleaned in large amounts of water, dried at room temperature and stored flat in an air conditioned laboratory at 20 ± 2°C and 40 ± 2% RH. Residual PPy which was polymerized onto smooth walls of dying pots was removed mechanically using detergent before next usage of pots.

Evaluation of electromagnetic SE

Electromagnetic SE of the PET/PPy textile composites was measured according to ASTM D 4935-10 [37], for planar materials using a plane-wave, far-field EM wave. SE of samples was measured in the frequency range of 30 MHz to 1.5 GHz. The set-up consisted of a sample holder with its input and output connected to the network analyzer. A shielding effectiveness test fixture (Electro-Metrics, Inc., model EM-2107A) was used to hold the sample. The design and dimension of sample holder follows the ASTM method mentioned above. Network analyzer Rohde & Schwarz ZN3 was used to generate and receive the electromagnetic signals. The standard mentioned above determines the SE of the fabric using the insertion–loss method. A reference measurement for the empty cell was required for the shielding-effectiveness assessment. A ''through'' calibration by the help of the reference sample was made first. A load measurement was performed on a solid disk shape sample subsequently. The reference and load specimens must be of the same material and thickness. Sample (both reference and load) geometries according to ASTM D 4935-10 are shown in Figure 2. One measurement was made at each sample. Three replicates of sample prepared at unique setting of input parameters were prepared; therefore, the sample mean values and 95% confidence intervals of *SE* for frequency 1.5 GHz are summarized in Table 2.

Weight increase

The amount of PPy deposited on the polyester fabric was determined by weighting the polyester samples before and after polymerization under standard conditions

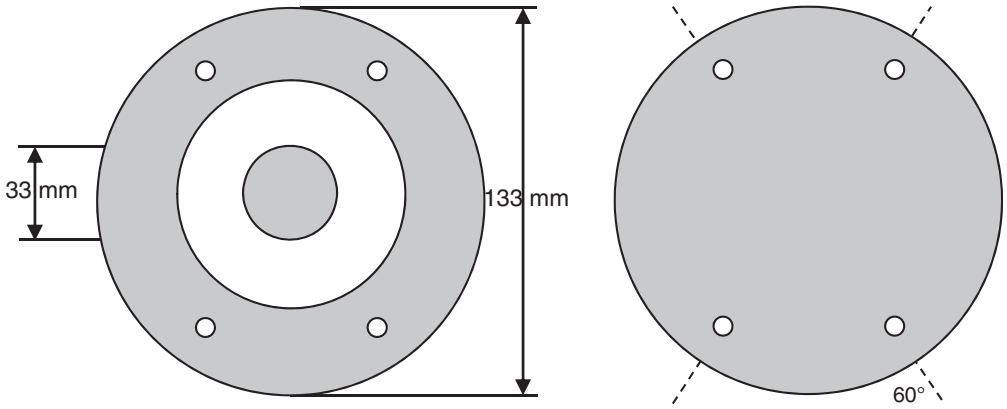

Figure 2. Illustrations of (a) reference and (b) load sample for measurement of electromagnetic shielding effectiveness.

($T = 22°C$, $RH = 40\%$). The percentage of weight increase W (%) was calculated as follows

$$W = \frac{W_f - W_i}{W_i} 100 \tag{1}$$

where W_i and W_f are the initial and final weights, respectively. The sample mean values of weight increase W together with 95% confidence intervals of means are summarized in Table 3.

Estimation of gray level from images of PPy coated samples

Mean gray level of the PET/PPy textile composites images was estimated with the aid of image processing in this study. Images of the PET/PPy textile composites were captured using HP Scanjet 5590 digital flatbed scanner. Images were stored as RGB image matrices of size $1680 \times 1588 \times 3$ pixels for both sides of samples (front-side and backside). Basic tools for digital image processing were used to prepare images for the following analysis. All PET/PPy textile composites samples have different levels of gray shades, and therefore no other color information is significant for subsequent processing. Images $f(x,y)$ were transformed to 8-bit grey-level range by the help of this formula

$$f(x, y) = 0.2989R + 0.5870G + 0.1140B \tag{2}$$

where R is red channel, G is green channel, and B is blue channel intensity. Now the image is grayscale and each pixel carries intensity information varying from black (the weakest intensity 0) to white (the strongest intensity 256). After that, images were cropped to size of 1481×1009 to remove labeling of the sample and uneven edges of sample. Gray level unevenness on the edges was caused by unintentional closing the edge of the sample by the lid of the dying tube during polymerization, and therefore the solution was not able to wet the caught edge. After cropping,

Table 2. Sample means and 95% confidence intervals (in parentheses) for electromagnetic shielding effectiveness measured at frequency 1.5 GHz [dB].

Monomer concentration (C) [g/l]		Polymerization temperature (A) [°C]								
		5			15			25		
		Polymerization time (B) [h]								
		1	8	15	1	8	15	1	8	15
0.64	$\bar{x}$	0.09	1.66	2.14	0.60	1.14	2.20	0.75	1.22	1.86
	95% CI	(0.04, 0.14)	(1.50, 1.82)	(1.89, 2.39)	(0.48, 0.72)	(0.97, 1.31)	(1.88, 2.52)	(0.66, 0.84)	(1.08, 1.36)	(0.62, 3.10)
3.22	$\bar{x}$	4.12	9.43	13.25	6.56	10.86	10.12	4.97	5.66	7.22
	95% CI	(3.84, 4.40)	(8.25, 10.61)	(12.47, 14.03)	(5.88, 7.24)	(9.84, 11.88)	(9.7, 10.54)	(4.16, 5.78)	(4.18, 7.14)	(5.92, 8.52)
5.80	$\bar{x}$	9.42	12.90	13.44	10.25	16.66	14.78	8.30	8.49	8.09
	95% CI	(7.84, 11.00)	(10.35, 15.45)	(11.54, 15.34)	(9.72, 10.78)	(14.15, 19.17)	(13.98, 15.58)	(6.23, 10.37)	(8.28, 8.70)	(6.86, 9.32)

Table 3. Sample means and 95% confidence intervals (in parentheses) for weight increase (%).

Monomer concentration (*C*) [g/l]		Polymerization temperature (*A*) (°C)								
		5			15			25		
		Polymerization time (*B*) [h]								
		1	8	15	1	8	15	1	8	15
0.64	$\bar{x}$	1.61	2.01	2.01	1.81	1.91	5.88	1.81	3.30	4.78
	95% CI	(0.76, 2.46)	(1.16, 2.86)	(0.83, 3.19)	(0.34, 3.28)	(0.73, 3.09)	(4.60, 7.16)	(1.47, 2.15)	(1.96, 4.65)	(3.00, 6.56)
3.22	$\bar{x}$	2.40	4.68	5.97	4.09	4.98	6.07	3.99	4.09	7.26
	95% CI	(1.23, 3.57)	(3.50, 5.86)	(4.76, 7.18)	(2.81, 5.37)	(3.95, 6.01)	(4.71, 7.43)	(2.59, 5.39)	(2.23, 5.95)	(6.56, 7.96)
5.80	$\bar{x}$	1.61	8.06	5.97	4.78	11.13	9.45	3.79	7.07	6.47
	95% CI	(1.42, 1.80)	(6.01, 10.11)	(4.50, 7.44)	(3.61, 5.95)	(9.95, 12.31)	(8.75, 10.15)	(2.82, 4.76)	(6.88, 7.26)	(5.69, 7.25)

mean value of gray level L [–] and 95% confidence interval of mean were calculated, based on knowledge of all pixel intensity information of both sides of each sample. The mean values of the sample and 95% confidence intervals of L are summarized in Table 4.

Results and discussion

Frequency dependent analysis of electromagnetic shielding efficiency

It is clear (see Table 2) that PET/PPy textile composites with electromagnetic SE ranging from almost 0 to 17 dB at frequency 1.5 GHz were prepared by the help of different settings of input parameters (polymerization temperature, polymerization time, and monomer concentration). Frequency of 1.5 GHz (maximum point of measured range) was found interesting as compared to lower frequencies because it is close to working frequency of particular electric devices (for example many GSM phones support 1.8 GHz band). This particular frequency (1.5 GHz) was used for further analysis of factorial design and correlations.

Figure 3 shows the variation in SE for three representatives of PET/PPy textile composites with low, intermediate, and the highest SE for incident frequency in the range of 30–1500 MHz. Electromagnetic SE increased logarithmically with the increasing frequency for samples with higher SE (SE > 2 dB), while dependence of SE on frequency for samples with very low SE (SE < 1 dB) was possible to approximate by negative exponential function. Crimped lines represent measured values of SE, while smooth lines show approximation of measured values by the models described above. Parameters of these models were obtained by minimizing the sum of squared errors.

Factorial design analysis

The analysis of variance (ANOVA) of the factorial design can be found in Table 5. It can be seen that all factors, A, B, and C, were statistically significant, because all of the p-values are below the significance level ($\alpha = 0.05$). All three two-factor interactions and one three-factor interaction were also significant. The main effect of C dominated this process, accounting for over 70% of the total variability, whereas the main effect of A and B accounted for about 7% and 8%, respectively. Percentage contribution of all interactions was lower than 4%. A normal probability plot of the residuals and the other usual diagnostics showed that both normality and constant variance assumptions were met.

The effects of three main factors are plotted in Figure 4. The main effect plots show that both variables Time (B) and Concentration (C) have positive main effects, i.e. increasing the variable moves the electromagnetic SE upward. The main effect of Concentration is much higher than that of Time.

Figure 5 shows the interaction plots to visualize interaction between two factors. The parallel lines indicate no interaction; out of parallel lines indicate interaction; and

Table 4. Sample means and 95% confidence intervals (in parentheses) for gray level obtained from sample images [–].

Monomer concentration (*C*) [g/l]		Polymerization temperature (*A*) (°C)								
		5			15			25		
		Polymerization time (*B*) [h]								
		1	8	15	1	8	15	1	8	15
0.64	$\bar{x}$	141.94	58.28	57.40	74.19	54.84	36.12	60.83	40.64	33.70
	95% CI	(141.93, 141.95)	(58.27, 28.29)	(57.39, 57.41)	(74.18, 74.20)	(54.83, 54.85)	(36.12, 36.13)	(60.82, 60.84)	(40.63, 40.65)	(33.70, 33.71)
3.22	$\bar{x}$	66.26	45.85	37.29	54.11	40.13	39.09	44.94	42.85	37.37
	95% CI	(66.25, 66.27)	(45.84, 45.86)	(37.29, 37.30)	(54.10, 54.12)	(40.12, 40.14)	(39.08, 39.10)	(44.93, 44.95)	(42.84, 42.86)	(37.37, 37.38)
5.80	$\bar{x}$	50.90	38.41	36.95	45.32	32.84	30.56	46.29	36.99	37.91
	95% CI	(50.89, 50.91)	(38.41, 38.42)	(36.95, 36.96)	(45.31, 45.33)	(32.84, 32.85)	(30.56, 30.56)	(46.28, 46.30)	(36.99, 37.00)	(37.91, 37.92)

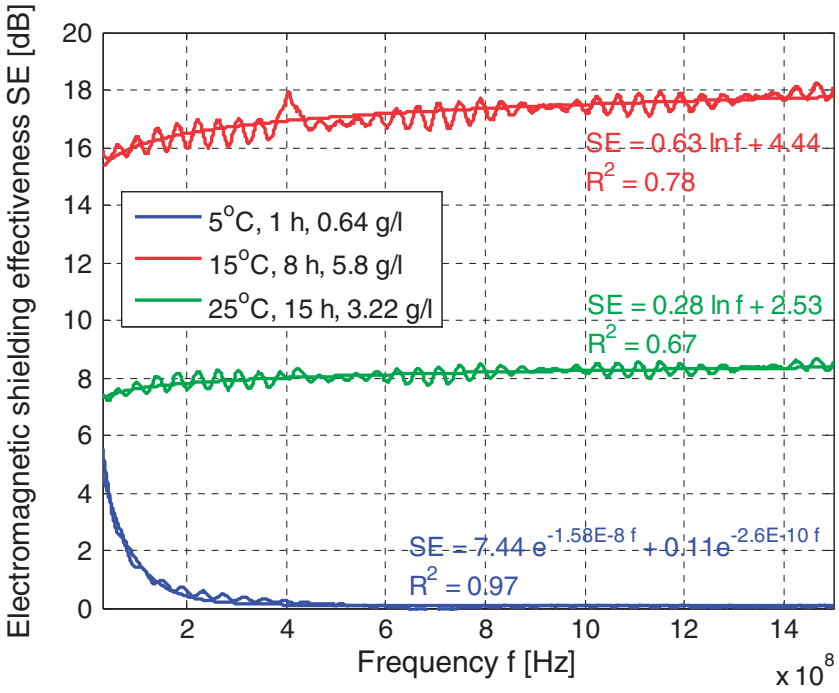

Figure 3. The dependence of shielding effectiveness on frequency for three representatives of PET/PPy textile composites: sample with low SE (polymerization temperature 5°C, polymerization time 1 h and monomer concentration 0.64 g/l); sample with intermediate SE (polymerization temperature 25°C, polymerization time 15 h and monomer concentration 3.22 g/l), and sample with the highest SE (polymerization temperature 15°C, polymerization time 8 h and monomer concentration 5.8 g/l).

Table 5. Analysis of variance for the factorial design.

Source	Sum Sq.	Percent contribution	d. f.	Mean Sq.	*F*	*Prob* > *F*
A	127.37	6.52	2	63.68	61.36	0
B	147.10	7.53	2	73.55	70.87	0
C	1424.9	72.95	2	712.45	686.5	0
*A***B*	49.99	2.56	4	12.49	12.04	0
*A***C*	75.94	3.89	4	18.98	18.29	0
*B***C*	37.88	1.94	4	9.47	9.13	0
*A***B***C*	34.06	1.74	8	4.26	4.10	0.0007
Error	56.04		54			
Total	1953.28		80			
S	1.02		R^2	97.13 %	*Adj* R^2	95.75 %

crossing lines indicate strong interaction between the two factors. The plot in Figure 5(a) shows that the effect of polymerization time on the SE depends on the polymerization temperature for low temperatures only. At a high temperature (25°C), the effect of time is negligible. A similar result can be seen from Figure 5(c). Moreover,

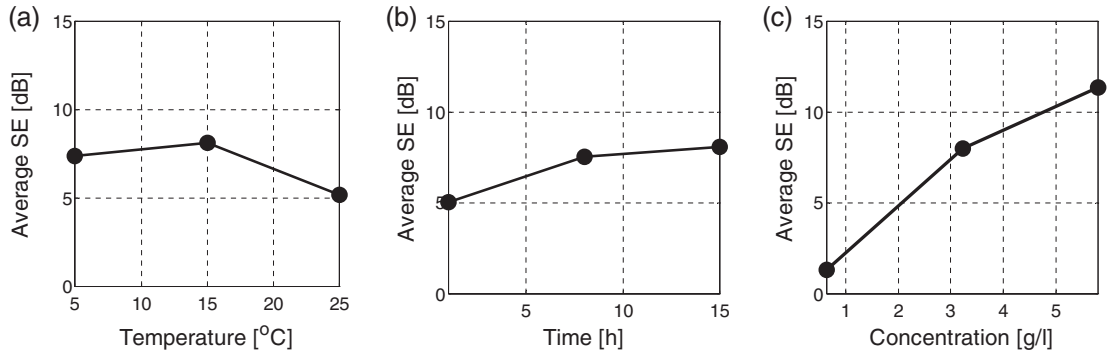

Figure 4. Main effect of: (a) temperature (*A*), (b) time (*B*), and (c) concentration (*C*) on average electromagnetic shielding effectiveness [dB] measured at frequency $f = 1.5$ GHz.

the SE differs for lower temperature and longer times. The polymerization temperature has a very small effect in a short time (1 h). The effect of monomer concentration on SE is increasing for any value of polymerization temperature. Figure 5(b) shows that the increase is most steep for the middle level of temperature (15°C) and less steep for the higher temperature (25°C). The interaction is not linear. The same results are shown in Figure 5(c). The higher differences between values of SE were observed for the middle level of temperature, while at high temperature these differences are lesser. The effect of monomer concentration on SE is increasing independently on polymerization time (Figure 5(d)). The interactions seem to be weak in these cases. Nevertheless, at higher polymerization times (8, 15 h), SE increases a little steeply than at short time (1 h). The weakness of interaction between concentration and polymerization time can be seen also in Figure 5(f).

Electromagnetic SE of the PET/PPy textile composites, which ranged from 0 to almost 17 dB at frequency 1.5 GHz, successfully covered the target range of the experimental region 15 ± 3 dB. Several mathematical approximation models were used to construct the fitted response surface. Akaike Information Criteria (AIC) [38], along with traditional null-hypothesis testing during regression analysis was used in order to determine the model that best describes the factors that influence the electromagnetic SE of the sample. The main aim was to choose a model which would be able to capture the true relationship between the variables of interest while not losing generality from overfitting the data [38]. The best model is then the model with the lowest AIC score

$$AIC = n \ \ln(RSS/n) + 2k \tag{3}$$

where n is sample size, k is number of model parameters, and RSS is the residual of sum of squares obtained by the regression analysis. The following models were estimated

$$\mathrm{M}_0 : SE(A, B, C) = \beta_0 + \beta_1 A + \beta_2 B + \beta_3 C + e \tag{4}$$

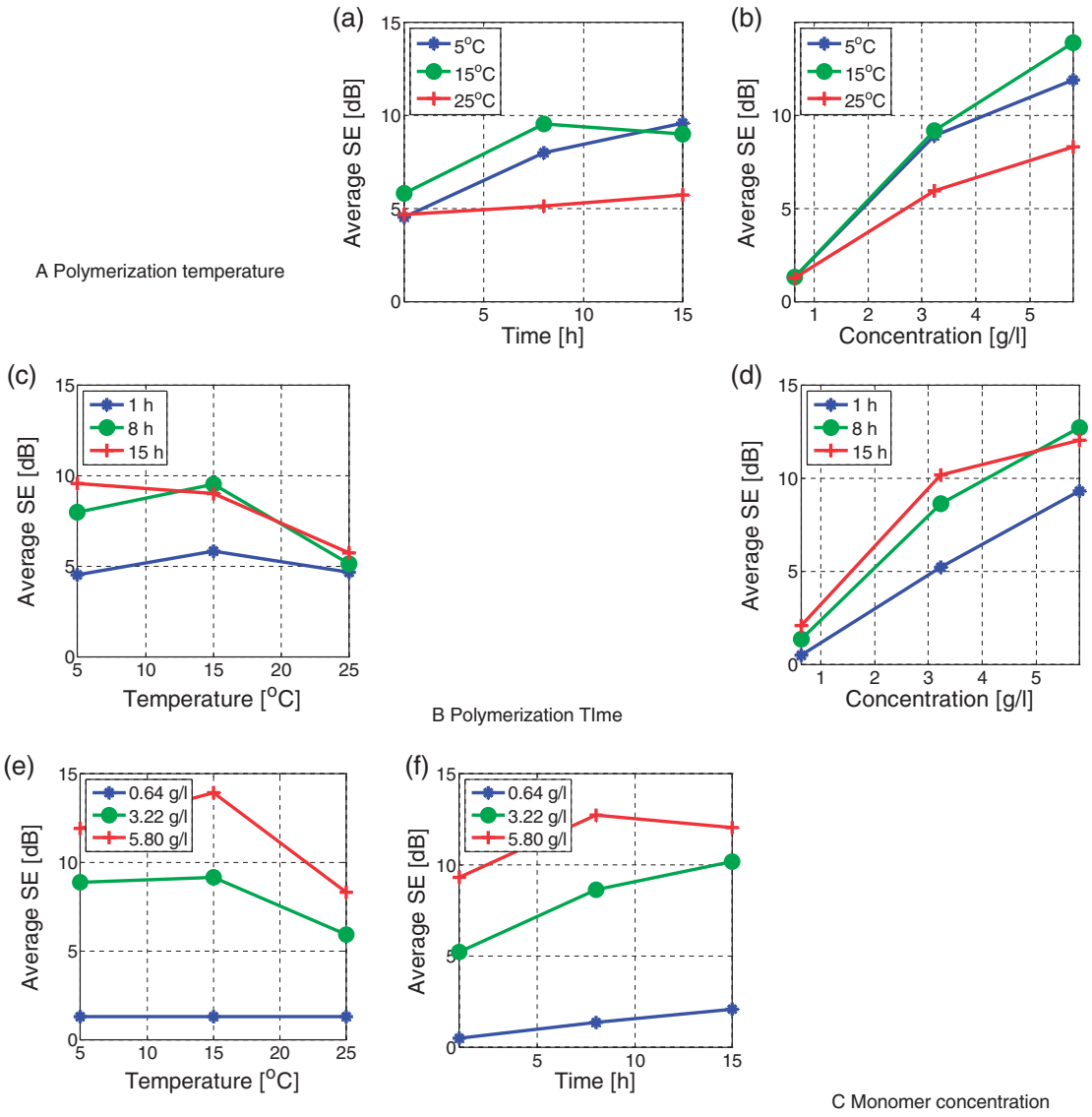

Figure 5. Interaction plots displaying interaction effects on average electromagnetic shielding effectiveness [dB] (f = 1.5 GHz) for all combinations of factors.

$$\mathrm{M}_1 : SE(A,B,C) = \beta_0 + \beta_1 A + \beta_2 B + \beta_3 C + \beta_{12} AB + \beta_{13} AC + \beta_{23} BC + e \tag{5}$$

$$\mathrm{M}_2 : SE(A,B,C) = \beta_0 + \beta_1 A + \beta_2 B + \beta_3 C + \beta_{11} A^2 + \beta_{22} B^2 + \beta_{33} C^2 + e \tag{6}$$

$$\mathrm{M}_3 : SE(A,B,C) = \beta_0 + \beta_1 A + \beta_2 B + \beta_3 C + \beta_{13} AC + \beta_{11} A^2 + \beta_{33} C^2 + e \tag{7}$$

$$\mathrm{M}_4 : SE(A,B,C) = \beta_0 + \beta_1 A + \beta_2 B + \beta_3 C + \beta_{13} AC + \beta_{11} A^2 + \beta_{22} B^2 + \beta_{33} C^2 + e \tag{8}$$

$$\mathrm{M}_5 : SE(A,B,C) = \beta_0 + \beta_1 A + \beta_2 B + \beta_3 C + \beta_{12} AB + \beta_{13} AC + \beta_{11} A^2 + \beta_{22} B^2 + \beta_{33} C^2 + e \tag{9}$$

$$\mathrm{M}_6 : SE(A,B,C) = \beta_0 + \beta_1 A + \beta_2 B + \beta_3 C + \beta_{12} AB + \beta_{13} AC + \beta_{23} BC + \beta_{11} A^2 + \beta_{22} B^2 + \beta_{33} C^2 + e \tag{10}$$

where SE [dB] is the function fit to a response, β is the regression coefficient to be estimated, A, B, and C are the factors, and e is the residual.

The models presented above had different numbers of coefficients to estimate, so k was different. These seven models were specifically chosen to highlight the effects of having different values for k and the difference between linear and quadratic polynomial models. The summary of ANOVA for regression analysis and AIC results for models relating the SE of samples and control variables is shown in Table 6.

Model 5 received the lowest AIC score ($AIC = 86.81$), indicating that this model is the most parsimonious model for given data. There is decisive evidence in favor of quadratic polynomial models to the linear polynomial models based on higher R^2 and lower AIC score. The final equation has the form

$$SE = -7.986 + 0.675A + 0.761B + 4.092C - 0.014AB - 0.035AC - 0.019A^2 - 0.020B^2 - 0.251C^2 + e \tag{11}$$

P-value of all regression coefficients (A, B, C, A^2, C^2, AB, AC) is lower than 0.001 with the exception of coefficient B^2 ($p \sim 0.01$), which means that all regression coefficients in equatuon (11) are statistically significant at the level $\alpha = 0.05$.

Table 6. Summary of ANOVA for regression analysis and AIC results.

Model	k	RSS	R^2 (%)	$Adj\ R^2$ (%)	AIC
M_0	4	384.73	80.30	79.54	134.21
M_1	7	317.28	83.76	82.44	124.59
M_2	7	253.91	87.00	85.95	106.55
M_3	7	243.12	87.55	86.54	103.03
M_4	8	225.05	88.48	87.37	98.77
M_5	9	189.41	90.30	89.23	86.81
M_6	10	186.47	90.45	89.24	87.54

Obtained model (11) can be also used for graphical representation of the experimental region. The response-surface plot (Figure 6) shows how response relates to two continuous design variables, while holding multiple variables in the model at specified levels. It is visible that higher SE ($SE > 14$ dB) can be reached using higher time ($B > 10$ h) and higher concentration at a relatively low temperature (see Figure 6(a) and (c)). To get higher SE, temperature of about 5–12°C and high concentration of monomer (5.8 g/l) at intermediate polymerization time (10 h) is favorable (Figure 6(b)). To obtain PET/PPy textile composites with electromagnetic shielding efficiency with at least 12 dB for frequency 1.5 GHz, optimizer tool available, e.g., in Minitab (optimization for target value) was used. Globally determined optimized parameters for PET/PPy textile composite with SE mentioned above are shown in Table 7.

Experimental verification of proposed model

Optimized input parameters for creating PET/PPy textile composite with at least 12 dB electromagnetic SE at frequency of 1.5 GHz were verified using subsequent

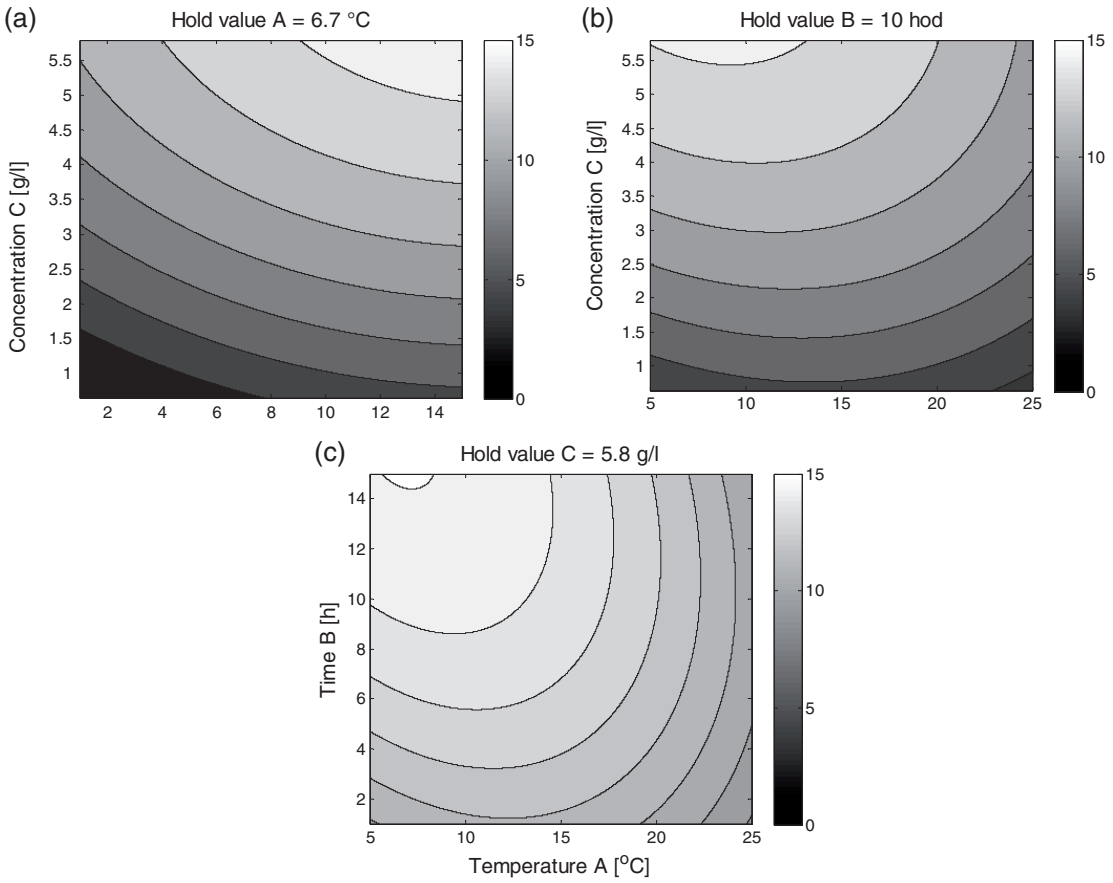

Figure 6. A response surface plot showing the quantitated effects of (a) polymerization time and monomer concentration, (b) polymerization temperature and monomer concentration, (c) polymerization temperature and time on electromagnetic shielding efficiency.

Table 7. The optimized parameters and the corresponding results.

Parameters			Performance
Polymerization temperature *A* (°C)	Polymerization time *B* (h)	Monomer concentration *C* (g/l)	SE (dB) according to (11)
6.7	10	5.8	14.26

experiment. PET substrate was prepared in the same way as in the previous experiments and chemical oxidative polymerization of Py on textile substrate was repeated according to the procedure described above. In this experiment, pyrrol concentration was 5.8 g/l, polymerization temperature was 6.7°C, and polymerization time was 10 h. The weight ratio among monomer, oxidizing agent, and dopant retains 1:5:3. Overall, 18 PET/PPy textile composite samples were prepared by application of the polymerization process with this particular setting and were evaluated according to their electromagnetic shielding ability. Table 7 presents the mean values and basic statistic evaluation of electromagnetic SE of PET/PPy textile composites at frequency of 1.5 GHz. Figure 7(a) presents the box plot for the electromagnetic SE. This box plot indicates that the distribution of SE is fairly symmetric around the central value and there are no outliers. The normal probability plot of the data in Figure 7(b) confirms the assumption that the electromagnetic SE is normally distributed (supported by Lilliefors test). The objective of this experiment was to demonstrate that the electromagnetic shielding of PET/PPy textile composite sample exceeds 12 dB, and therefore one-sided confidence interval was calculated. Consequently, the condition that SE > 12 dB was satisfied, as 95% lower bound was 12.81 dB (see Table 8).

Relation between weight increase and electromagnetic SE

Polymerization of Py resulted in black PET fabrics, meaning that the conductive polymer completely coated the surface of the fibers. The amount of polymer was evaluated by measuring the weight increase of PET/PPy textile composites compared to uncoated PET sample. The aim of this section is to find out if there is some relation between weight increase and electromagnetic SE. The dependence of electromagnetic SE (measured at frequency 1.5 GHz) on weight increase of PET/PPy textile composites is shown in Figure 8(a). The solid line in this graph corresponds to the linear regression model with parameters obtained by the minimizing sum of squared errors. Corresponding coefficient of determination $R^2 = 0.60$ indicates the good quality of fit. It is clear that SE increases with increasing weight increase of PET/PPy samples and therefore weight increase can be used as an indirect indicator of required electromagnetic SE or electric conductivity.

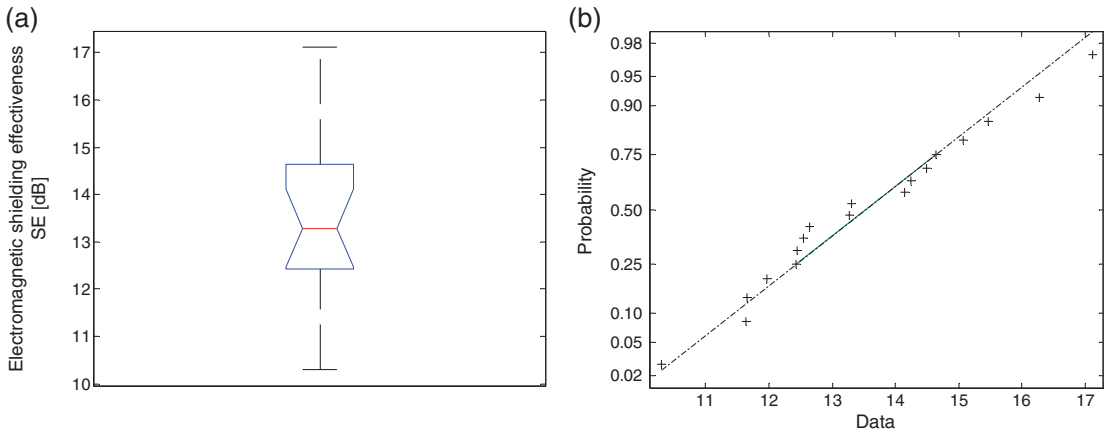

Figure 7. (a) Box plot and (b) normal probability plot for electromagnetic shielding effectiveness [dB] (f = 1.5 GHz) measured on 18 PET/PPy textile composites prepared during verification of proposed model.

Table 8. Descriptive statistics and results of one-sample t-test of SE measurement.

	Electromagnetic shielding effectiveness SE (dB)				
	N	Mean	SD	Var.	95% CI lower bound
PET/PPY textile composite	18	13.53	1.78	3.17	12.81

Relation between grayscale shades and electromagnetic SE

Originally, PET substrate was in white color (mean value of gray level $L = 250$). As mentioned above, polymerization of Py resulted in gray/black PET fabrics. It seemed that the darker color was achieved, and the sample with the higher electromagnetic SE of samples was prepared. On this account, the relation between electromagnetic SE (measured at frequency 1.5 GHz) and mean gray level of pixels of PET/PPy textile composites images was studied (see Figure 8(b)). It is visible from Figure 8(b) that when increasing the mean value of gray level (sample is lighter), the electromagnetic SE of the sample starts decreasing. This dependence can be approached by power function displayed by the solid line. Corresponding coefficient of determination $R^2 = 0.61$ indicates the sufficient quality of fit. On that ground, mean value of gray level can be also used as an indirect indicator of the required electromagnetic SE or electric conductivity. This phenomenon is limited for usage of light color fabrics as a substrate for the polymerization of PPy. Images of samples with different electromagnetic shielding ability and different mean value of gray level (for better visualization PPy coated sample with the highest, intermediate and the lowest mean value of gray level was chosen) are shown in Figure 9.

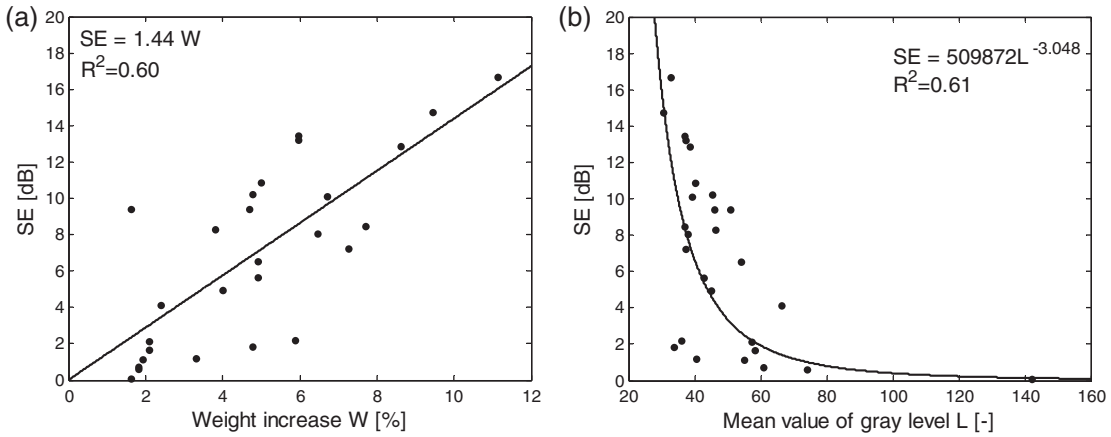

Figure 8. The dependence of electromagnetic shielding effectiveness (SE) on: (a) weight increase *W* [%], (b) mean value of gray level *L* [–].

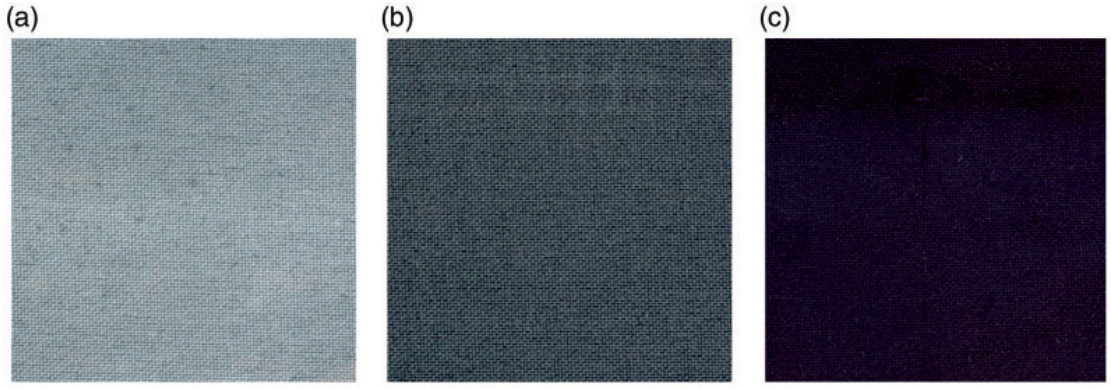

Figure 9. Images of PET/PPy textile composite samples with different electromagnetic shielding ability and different mean value of gray level prepared with the following process parameters: (a) 5°C, 1 h, 0.64 g/l (*L* = 142, *SE* = 0.09 dB), (b) 15°C, 1 h, 0.64 g/l (*L* = 74.2, *SE* = 0.6 dB), (c) 15°C, 15 h, 5.8 g/l (*L* = 30.6, *SE* = 15 dB).

Morphology of PPy coated PET fabrics

Morphological analysis of PPy-coated PET fabrics was performed by means of scanning electron microscopy (SEM). SEM pictures of PET/PPy textile composites surface prepared with different inputs (Py concentration, polymerization time and temperature) are shown in Figure 10. For better representation, the sample with low amount of PPy (prepared by following adjustment: 5°C, 1 h, 0.64 g/l, accompanied by low SE) and high amount of PPy (prepared by following adjustment: 15°C, 15 h, 5.8 g/l, accompanied by high SE) was chosen. Untreated PET fibers are characterized by an extremely smooth surface without any pore to the inside. After Py polymerization, fibers appeared homogenously coated with a film of PPy (Figure 10). Dendrite-like structure of PPy attached to the PET substrate can be

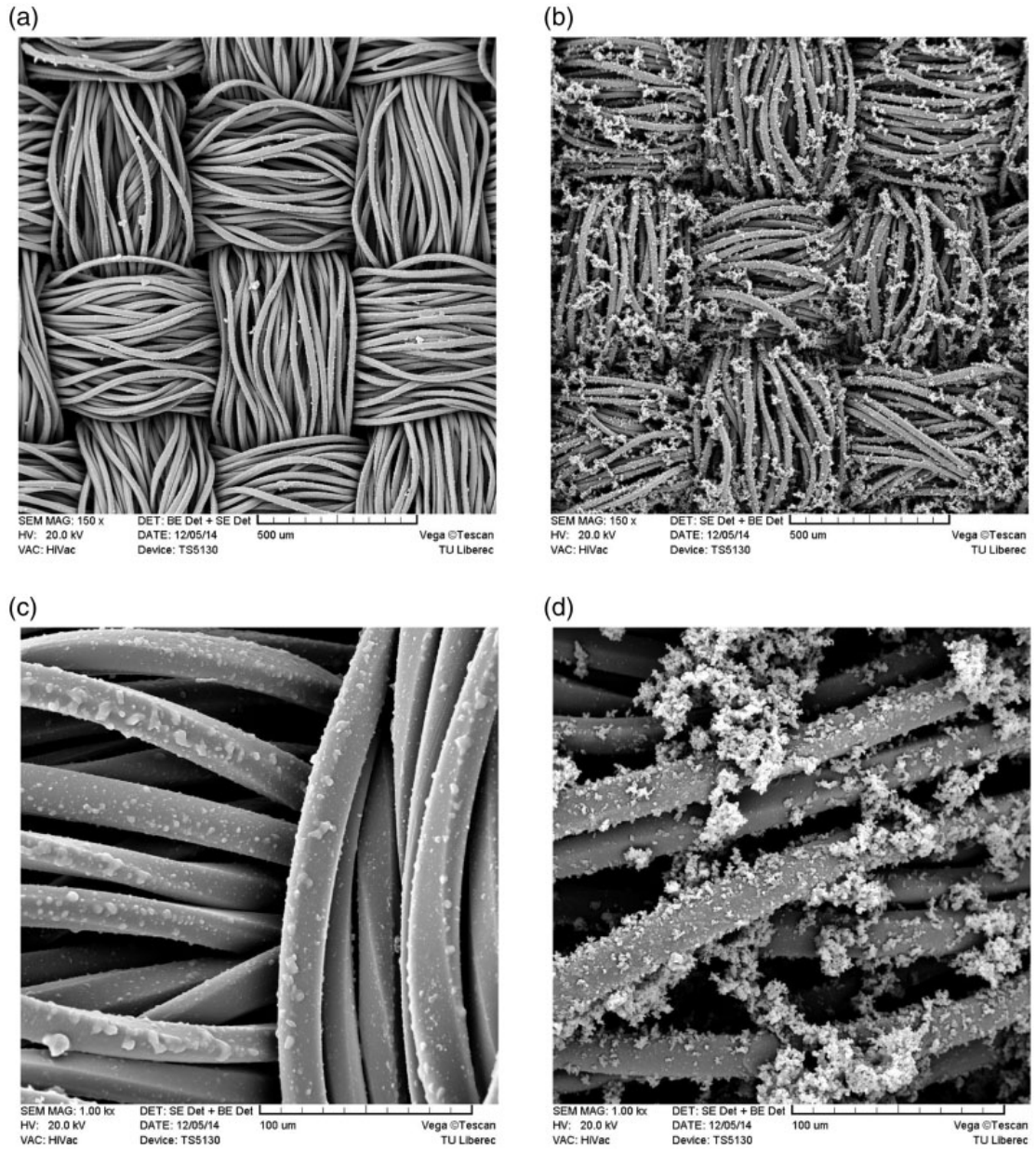

Figure 10. SEM pictures of PET/PPy textile composites prepared by following adjustments: (a),(c) 5°C, 1 h, 0.64 g/l, (b),(d) 15°C, 15 h, 5.8 g/l. Two different magnitudes were used: 150× and 1000×.

observed especially at the crossover of warp and weft polyester yarns. Their amount seemed to slightly increase with increasing monomer concentration in solution. It is expected that these loosely incorporated clusters of PPy on the surface of the substrate can be probably removed by mechanical stress or stronger washing cycles. The described phenomenon is also visible from cross sections (Figure 11). As the amount of Py in solution increased, the film texture became more compact and polymer aggregates grew into larger size and higher density. The thickness of the PPy layer increased as function of input parameters discussed above, especially of the monomer concentration in solution, which is in good agreement with the kinetics of weight increase. It is supposed that monomer did

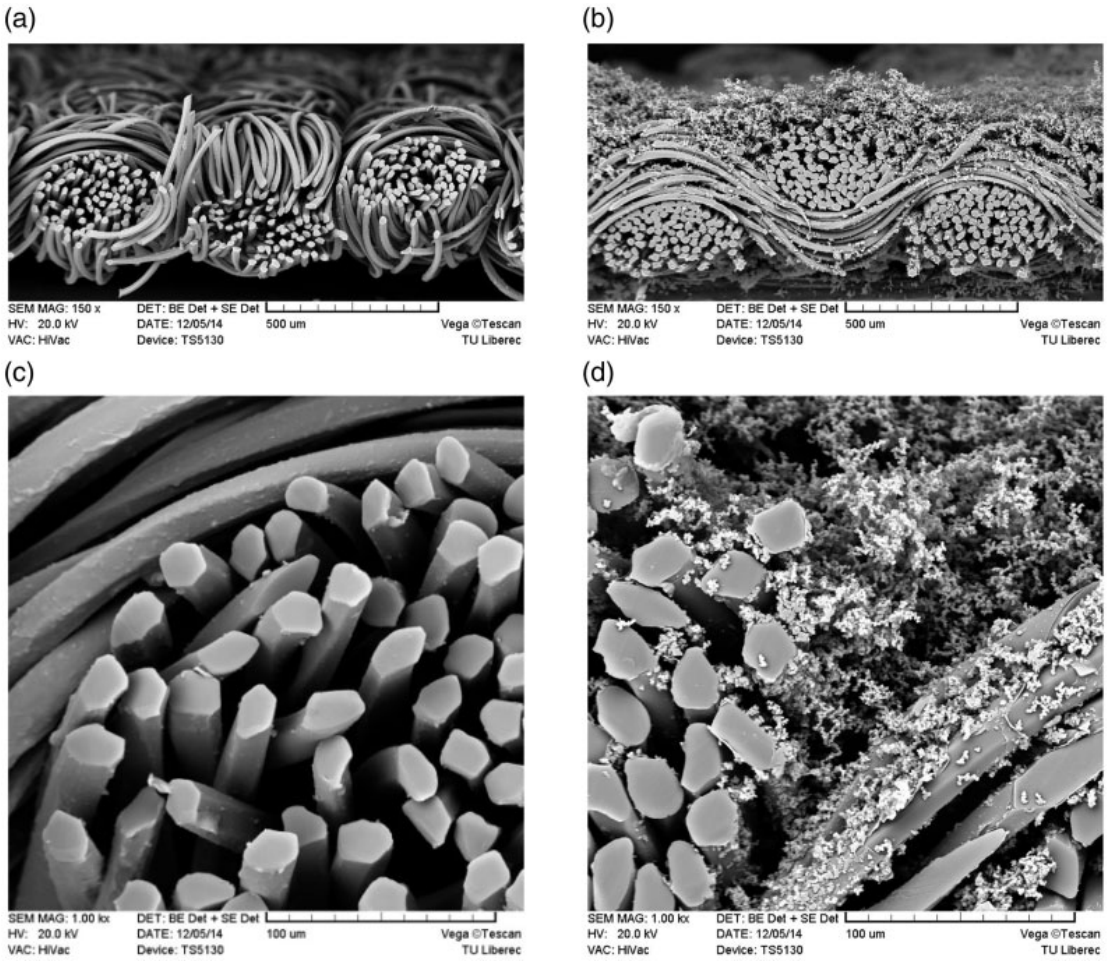

Figure 11. Cross section SEM pictures of PET/PPy textile composites prepared by following adjustments: (a),(c) 5°C, 1 h, 0.64 g/l, (b),(d) 15°C, 15 h, 5.8 g/l. Two different magnitudes were used: 150× and 1000×.

not penetrate and diffuse into the polyester fiber matrix because of the substrate nature, but rather formed a PPy/PET composite with a skin-core structure. In all PET/PPy textile composites, individual fibers did not stick to each other but stay well separated.

Conclusion

In-situ chemical oxidative polymerization of polypyrrole on a polyester fabric was performed in order to obtain relatively high conductive textiles for electromagnetic shielding purposes. As an oxidizing agent, $FeCl_3$ was used, and as a dopant PTSA was used. Statistical optimization of process parameters (concentration of monomer, polymerization time and temperature) using DoE was performed to achieve fabric with electromagnetic shielding efficiency of at least 12 dB for frequency 1.5 GHz. The macroscopic color shade and scanning electron microscopy images of samples were also evaluated.

It can be summarized that electromagnetic SE of PET/PPy textile composites ranged from 0 to 17 dB at frequency 1.5 GHz depending on process parameters of polymerization. The highest electromagnetic SE (16.7 dB at frequency 1.5 GHz) was exhibited by a sample prepared with the following input parameters: 15°C polymerization temperature, 8 h polymerization time, 5.8 g/l monomer concentration. It was also found that all selected factors and their interactions have statistically significant effect on resulting electromagnetic SE, whereas monomer concentration has the highest positive influence. Higher SE can be reached using higher polymerization time (> 8 h), high monomer concentration (5.8 g/l), and relatively low temperature (5–12°C). Experimental data were used to derive an empirical model linking the outputs and inputs. The proposed model can be used for prediction of electromagnetic SE of PET/PPy textile composites at specific settings of input parameters. By the help of this model, optimized parameters for creating polypyrrole/polyester textile composite with SE > 12 dB were found (polymerization temperature 6.7°C, polymerization time 10 h and monomer concentration 5.8 g/l) and successfully experimentally verified.

Evaluation of weight increase and color of coated samples confirmed that there is a relation between these two parameters and electromagnetic SE of samples. The highest weight increase (11%) was achieved by a sample prepared by following setting of input parameters at 15°C polymerization temperature, 8 h polymerization time, and 5.8 g/l monomer concentration. The darker the sample, the more PPy is deposited on the sample (higher weight increase) and therefore the higher the electromagnetic shielding ability of the sample. These findings were also supported by morphological analysis of PET/PPy textile composites SEM pictures. Weight increase and color of the PET/PPy textile composites therefore appear as a suitable simple indirect predictor of electromagnetic shielding ability, instead of direct evaluation of electromagnetic SE, which needs to use special devices.

For future, it is also necessary to explore stability of this surface modification applied to nonconductive textile substrate by monitoring changes of electromagnetic shielding ability and electric conductivity after rubbing, abrasion, or washing/drying cycles. Also, time stability accompanied by increased relative humidity and temperature of air and/or UV stability should be revised. These requirements could play significant role when preparing final application.

The described results and proposed models are limited to the certain polymeric systems, but the introduced concept should be applicable for other synthetic substrates and inherently conductive polymers. It seems that in-situ chemical oxidative polymerization of conducting polymer onto a textile structure can be easily applicable to obtain conductive textile structures, because the manufacturing method is simple and there is no necessity of special equipment. Moreover, the mechanical properties of the substrate remained.

Acknowledgement

This paper is original and has not been presented or published till now.

Declaration of Conflicting Interests

The author(s) declared no potential conflicts of interest with respect to the research, authorship, and/or publication of this article.

Funding

The author(s) disclosed receipt of the following financial support for the research, authorship, and/or publication of this article: This work was supported by the research project FR-TI1/122 ''Electromagnetic field protective textiles with improved comfort'' of Czech Ministry of Industry.

References

[1] International Agency for Research on Cancer. *IARC Classifies Radiofrequency electromagnetic fields as possibly carcinogenic to humans*. Press Release no. 208. Lyon: WHO/IARC, 2011.
[2] Ahlbom A, Bergqvist U, Bernhardt JH, et al. ICNIRP guidelines for limiting exposure to time-varying electric, magnetic and electromagnetic fields (up to 300 GHz). *Health Phys* 1998; 74: 4.
[3] Vojtech L and Neruda M. Design of radiofrequency protective clothing containing silver nanoparticles. *Fibres Text East Eur* 2013; 21: 5.
[4] Duran D and Kadoglu H. Electromagnetic shielding characterization of conductive woven fabrics produced with silver-containing yarns. *Text Res J* 2015; 85: 10.
[5] Safarova V and Militky J. Electromagnetic shielding properties of woven fabrics made from high-performance fibers. *Text Res J* 2014; 84: 12.
[6] Lu Y and Xue L. Electromagnetic interference shielding, mechanical properties and water absorption of copper/bamboo fabric (Cu/BF) composites. *Compos Sci Technol* 2012; 72: 7.
[7] Ozen MS, Sancak E and Akalin M. The effect of needle-punched nonwoven fabric thickness on electromagnetic shielding effectiveness. *Text Res J* 2014; 85: 8.
[8] Vojtech L and Neruda M. Application of shielding textiles for increasing safety airbone systems: limitations of GSM interference. In: *9th International conference on network*, France, Los Alamitos, 11–16 April 2010.
[9] Apreutesei AL, Curteza A, David V, et al. Investigation of the textile structures with different design used in electromagnetic shielding. In: *Proceedings of the 2014 international conference of exposition on electrical and power engineering*, Iasi, Romania, 16–18 October 2014.
[10] Gultekin ND and Usta I. The effect of multiwalled carbon nanotube (MWCNT) ration on electrical properties and electromagnetic shielding effectiveness of PA6/MWCNT-coated cotton fabrics. *J Text I* 2014; 105: 7.
[11] Li Y, Cheng XY, Leung MY, et al. A flexible strain sensor from polypyrrole-coated fabrics. *Synthetic Met* 2005; 155: 1.
[12] Trindale IG, Matos J, Lucas J, et al. Synthesis of poly(3, 4-ethylenedioxythiophene) coating on textiles by the vapor phase polymerization method. *Text Res J* 2015; 85: 3.
[13] Bhat NV, Seshadri DT and Radhakrishan S. Preparation, characterization and performance of conductive fabrics: Cotton + PANi. *Text Res J* 2004; 74: 2.
[14] Odhiambo SA, Mey GD, Hertleer C, et al. Discharge characteristics of poly(3,4-ethylene dioxythiophene): poly(styrenesulfonate) (PEDOT:PSS) textile batteries;

comparison of silver coated yarn electrode device and pure stainless steel filament yarn electrode device. *Text Res J* 2014; 84: 4.
[15] Wang Y and Jing X. Intrinsically conductive polymers for electromagnetic interference shielding. *Polym Adv Technol* 2005; 16: 4.
[16] Stempien Z, Rybicki T, Rybicky E, et al. In-situ deposition of polyaniline and polypyrrole electroconductive layers on textile surfaces by the reactive ink-jet printing technique. *Synth Met* 2015; 202. http://www.sciencedirect.com/science/article/pii/S0379677915000399.
[17] Kuhn HH, Child AD and Kimbrel WC. Toward real application of conductive polymers. *Synth Met* 1995; 71: 1–3.
[18] Committee for Conformity Assessment on Accreditation and Certification of Functional and Technical Textiles. Specified requirements of electromagnetic shielding textiles, http://www.ftts.org.tw/images/fa003E.pdf
[19] Harlin A and Ferenets M. *Book Intelligent textiles and clothing*. Boca Raton, FL: CRC Press, 2006.
[20] Kiebooms R, Menon R and Kwanghee L. *Handbook of advanced electronic and photonic materials and devices*. San Diego, CA: Academic Press, 2001.
[21] Heisey CL, Wightman JP, Pittman EH, et al. Surface and adhesion properties of polypyrrole-coated textiles. *Text Res J* 1993; 63: 5.
[22] Kuhn HH, Kimbrell WC, Fowler JE, et al. Properties and application of conductive textiles. *Synth Met* 1993; 57: 1.
[23] Yildiz Z, Usta I and Gungor A. Electrical properties and electromagnetic shielding effectiveness of polyester yarns with polypyrrole deposition. *Text Res J* 2012; 82: 20.
[24] Cuchi I, Boschi A, Arosio C, et al. Bio-based conductive composites: Preparation and properties of polypyrrole (PPy)-coated silk fabric. *Synth Met* 2009; 159: 3–4.
[25] Dall' Acqua L, Tonin C, Peila R, et al. Performance and properties of intrinsic conductive cellulose-polypyrrole textiles. *Synth Met* 2004; 146: 2.
[26] Safarova V, Gregr J and Martinek M. Preparation of functional PET fabric/polypyrrole composite. *Scientific papers of the University of Pardubice – Series A* 2012; 18.
[27] Avloni J, Ouyang M, Florio L, et al. Shielding effectiveness evaluation of metallized and polypyrrole-coated fabrics. *J Thermoplast Compos* 2007; 20: 3.
[28] Kaynak A, Hakansson E and Emiet A. The influence of polymerization time and dopant concentration on the absorption of microwave radiation in conducting polypyrrole coated textiles. *Synth Met* 2009; 159: 13.
[29] Varesano A, Dall'Acqua L and Tonin C. A study on the electrical conductivity decay of polypyrrole coated wool textiles. *Polym Degrad Stabil* 2005; 89: 1.
[30] Hakansson E, Amiet A, Nahavandi S, et al. Electromagnetic interference shielding and radiation absorption in thin polypyrrole films. *Eur Polym J* 2007; 43: 1.
[31] Huang CY, Wu JT, Tsano KY, et al. The manufacture and investigation of multiwalled carbon nanotube/polypyrrole/EVA nano-polymeric composite for electromagnetic interference shielding. *Thin Solid Films* 2011; 519: 15.
[32] Merlini C, Ramoa SDAS and Barra GMO. Conducting polypyrrole-coated banana fiber composites: Preparation and characterization. *Polym Compos* 2013; 34: 4.
[33] Babu KF, Senthilkumar R, Noel M, et al. Polypyrrole microstructure deposited by chemical and electrochemical methods on cotton fabrics. *Synth Met* 2009; 159: 13.
[34] Boutrois JP, Jolly R and Petrescu C. Process of polypyrrole deposit on textile – Products and applications. *Synth Met* 1997; 85: 1–3.

[35] Macasaquilt AC and Binag CA. Preparation of conducting polyester textile by in situ polymerization of pyrrole. *Philipp J Sci* 2010; 139: 2.
[36] Kenett RS, Zack S and Amberti D. *Modern industrial statistics: with applications in R, MINITAB and JMP*. Hoboken: Wiley, 2014.
[37] ASTM D4935-10. *Standard test method for measuring the electromagnetic shielding effectiveness of planar materials*. West Conshohocken: ASTM, 2010.
[38] Snipes M and Taylor DC. Model selection and Akaike Information Criteria: An example from wine ratings and prices. *Wine Econom Pol* 2014; 3: 1.

Appendix 6

S. Naeem, V. Baheti, **V. Tunakova**, et al., "Development of porous and electrically conductive activated carbon web for effective EMI shielding applications," Carbon, vol. 111, pp. 439-447, 2017.

Carbon 111 (2017) 439–447

Contents lists available at ScienceDirect

Carbon

journal homepage: www.elsevier.com/locate/carbon

Development of porous and electrically conductive activated carbon web for effective EMI shielding applications

Salman Naeem, Vijay Baheti*, Veronika Tunakova, Jiri Militky, Daniel Karthik, Blanka Tomkova

Department of Material Engineering, Faculty of Textile Engineering, Technical University of Liberec, Studentska 2, Liberec 46117, Czechia

ARTICLE INFO

Article history:
Received 21 August 2016
Received in revised form
10 October 2016
Accepted 12 October 2016
Available online 13 October 2016

Keywords:
Textile recycling
Acrylic fibrous wastes
Activated carbon
Electrical conductivity
Electromagnetic shielding
Physical activation
Specific surface area

ABSTRACT

In present work, porous and electrically conductive activated carbon needle punched nonwoven web was produced by heating acrylic fibrous wastes under the layer of charcoal using novel single stage carbonization and physical activation. The influence of 800 °C, 1000 °C and 1200 °C carbonization temperature on physical and morphological properties of activated carbon web was studied from EDX, X-ray diffraction, SEM, X-ray tomography and BET analysis. Additionally, the electrical conductivity was also measured. At the end, the utility of prepared activated carbon web was investigated for electromagnetic shielding ability in high frequency (i.e. at 2.45 GHz) and low frequency regions (i.e. below 1.5 GHz) using waveguide method and coaxial transmission line method, respectively. The activated carbon web produced at 1200 °C showed maximum shielding effectiveness in both high and low frequency regions. For single layers of 1200 °C web, the electromagnetic shielding effectiveness of 63.26 dB, 66.75 dB, and 75.44 dB was found for respective frequencies of 600 MHz, 1 GHz, and 1.5 GHz. This behavior was attributed to the increased multiple internal reflections and stronger absorption of electromagnetic radiations in 1200 °C activated carbon web.

1. Introduction

In recent years, research on electromagnetic interference (EMI) shielding materials has attracted significant attention due to increase in electromagnetic population from widespread applications of computer and telecommunication technologies [1,2]. Electromagnetic interference refers to the radiant electromagnetic signals emitted by electrical instruments during their operation. The emitted electromagnetic radiations are concerns since they interfere with the working of other appliances as well as cause serious health risks to the human [3]. The EMI shielding efficiency of materials is governed by reflection, absorption and multiple internal reflections of incident electromagnetic radiations [4–6]. Reflection is commonly used shielding mechanism by high electrically conductive materials such as metals and their nanoparticles. However, high density, lack of flexibility, easy corrosion, costly processing and weak microwave absorption are main drawbacks of metals [7]. Recently, the carbon nanostructures and graphene are reported as promising alternatives to metal-based shielding materials [3,8].

For eco-friendly advancements in EMI shielding effectiveness, the development of new light weight shielding materials having strong absorption and weak secondary reflection is necessary [9,10]. This can be achieved by porous morphology, large specific surface area and higher electrical conductivity of shielding materials [11]. For instance, carbon-based shielding foams are considered predominant in effective shielding mechanism due to their light weight and the synergetic effect of electrical conductivity and multiple reflections. As a result, many lightweight polymer foams with graphene, CNTs, or carbon nano-fibers were produced [11–15]. Nevertheless, the addition of high concentration of electrically conductive nanofillers was found to cause undesirable effects on the foam ability of the polymers for formation of porous structure [16]. Therefore, the numbers of studies in recent years focused on the development of lightweight EMI shielding materials using various new approaches. Yan et al. proposed a combination of high-pressure compression molding plus salt-leaching method to fabricate porous graphene/polystyrene composites [17]. In addition, the chemical vapor deposition and self assembly of highly aligned graphene sheets into 3D graphene porous structures was

* Corresponding author.
E-mail address: vijaykumar.baheti@gmail.com (V. Baheti).

http://dx.doi.org/10.1016/j.carbon.2016.10.026
0008-6223/

found to be efficient in improving the EMI shielding properties [18]. The development of carbon aerogels was attempted by some researchers to get maximum electromagnetic shielding due to their ultra-low density, ultra-high specific surface area, and large open pores [19].

Although number of research studies focused on development of porous carbon based EMI shielding materials, the construction of lightweight structures with excellent EMI shielding properties by simple and affordable method is still a big challenge. This work presented the simple and novel method for preparation of porous and electrically conductive activated carbon nonwoven web from acrylic fibrous wastes. The prepared activated carbon is advantageous over carbon made from other materials because of low cost, high density, better purity, and virtually dust-free nature of acrylic fibers [20]. The activated carbon web was prepared by sequential action of carding, needle punching and physical activation of acrylic fibrous wastes in presence of air. The carbonization was performed under the layer of charcoal at 800 °C, 1000 °C and 1200 °C with the heating rate of 300 °C h^{-1} and without any holding time. Further, electrical conductivity, EDX, X-ray diffraction, SEM, X-ray tomography and BET analysis was carried out to study the effect of carbonization temperature on physical and morphological properties of activated carbon web. At the end, the electromagnetic shielding ability of the produced three webs was investigated with respect to change in carbonization temperature and thickness of material using two different measurement approaches (i.e. waveguide method and coaxial transmission line method). In this way, the present study served to utilize large quantity of acrylic fibrous wastes for development of effective electromagnetic shielding materials.

2. Experimental methods

2.1. Materials

The acrylic fibrous waste was obtained from Grund Industries, Czech Republic in form of short lengths generated during mechanical processing of bath mats. The acrylic fibers are anionic copolymers containing 85–89% of acrylonitrile. Table 1 shows the physical properties of acrylic fibrous wastes.

2.2. Preparation of activated carbon nonwoven web

The short segments of acrylic fibers were removed from bath mats using mechanical cutting method. The compact dense structure of nonwoven web having thickness 11.6 mm and density 2.78 g/cm^3 was prepared by opening of short fibers on Carding Machine (Laboratory Roller Card, Befama, Poland) with subsequent action of Needle Punching Machine (Hansa, Germany). The predetermined size of acrylic nonwoven web was cut and transferred to high temperature furnace (Elektrické Pece Svoboda, Czech Republic) for carbonization in two stages. The sample was initially stabilized at 250 °C with heating rate of 35 °C h^{-1} and under predetermined tension. Further, the stabilized web was carbonized at 800 °C, 1000 °C and 1200 °C with heating rate of 300 °C h^{-1} and without any holding time. The controlled physical activation was carried out by carbonization under the layer of charcoal. The novel part of this study is single stage carbonization and physical activation in presence of air. The schematic of synthesis of activated carbon web from acrylic short fiber waste is shown in Fig. 1.

Table 1
Physical properties of acrylic short fiber wastes.

Physical properties	
Fineness (Denier)	13
Tenacity (GPD)	2.7
Elongation (%)	45
Shrinkage (%)	2.5

2.3. Characterization of activated carbon web

The physical properties of acrylic fibrous and activated carbon nonwoven web were determined in terms of shrinkage, flexibility and dusting tendency. The shrinkage measurement was performed as per ASTM D 2259 standard available for testing textile fibers. The shrinkage was evaluated from change in length of acrylic fiber web before and after carbonization. The flexibility or stiffness was evaluated from bending length by employing the principle of cantilever bending of the web under its own weight as per ASTM D 1388 standard. The dusting tendency was evaluated from amount of generated dust particles after rubbing the surface of web on Taber wear and abrasion tester as per ASTM D 3884 standard. The rotary rubbing action was performed for 30 cycles under controlled conditions of pressure and abrasive action.

2.3.1. Energy dispersive x-ray (EDX) analysis

It was performed on Oxford Instruments, LZ 5 EDX detector, UK to know the change in relative proportion of different elements with respect to change in carbonization temperature.

2.3.2. X-ray diffraction (XRD) analysis

It was carried out on a PANalytical X′ Pert PRO MPD diffraction system. The development of crystalline and amorphous regions in prepared activated carbon web was investigated with respect to change in carbonization temperature.

2.3.3. SEM analysis

The field emission scanning electron microscope Sigma, Zeiss, Germany was employed to investigate the morphology of acrylic fibrous web and prepared activated carbon web of 800 °C, 1000 °C and 1200 °C carbonization temperature. This helped to understand the development of porosity characteristics of activated carbon web with change in carbonization temperature. The micrographs were taken at 2 kV accelerated voltage and 1000× magnification. As prepared activated carbon web was electrically conductive, so it was not metalized before test. However, the acrylic fibrous nonwoven web was metalized by sputter coating.

2.3.4. X-ray micro-computed tomography

In order to observe the three dimensional view of prepared activated carbon, the X-ray micro computerized tomography was performed on SKYSCAN 1272 of BRUKER. The micro graph of 1200 °C activated carbon web was compared with acrylic fibrous web at a pixel resolution of 1.60 μm. The scanned images of 5 mm length sample size were reconstructed using NRecon into three dimensional object, which was further analyzed for structural properties using CTan. A suitable thresholding was applied to remove the back ground noise. DE speckling function was operated to remove noise and to fill small holes within the fibers structure. Shrink-wrap technique was used to limit the region of interest boundaries as per the fiber spread contours. The CTvox and Data Viewer tools were utilized for visualization and measurement of image database.

2.3.5. BET surface area

The specific surface area of 1200 °C activated carbon web was measured from N_2 adsorption–desorption isotherms at 77.35 K using Autosorb iQ, Quantachrome Instruments, USA. The adsorption/desorption isotherm measurements were collected in the

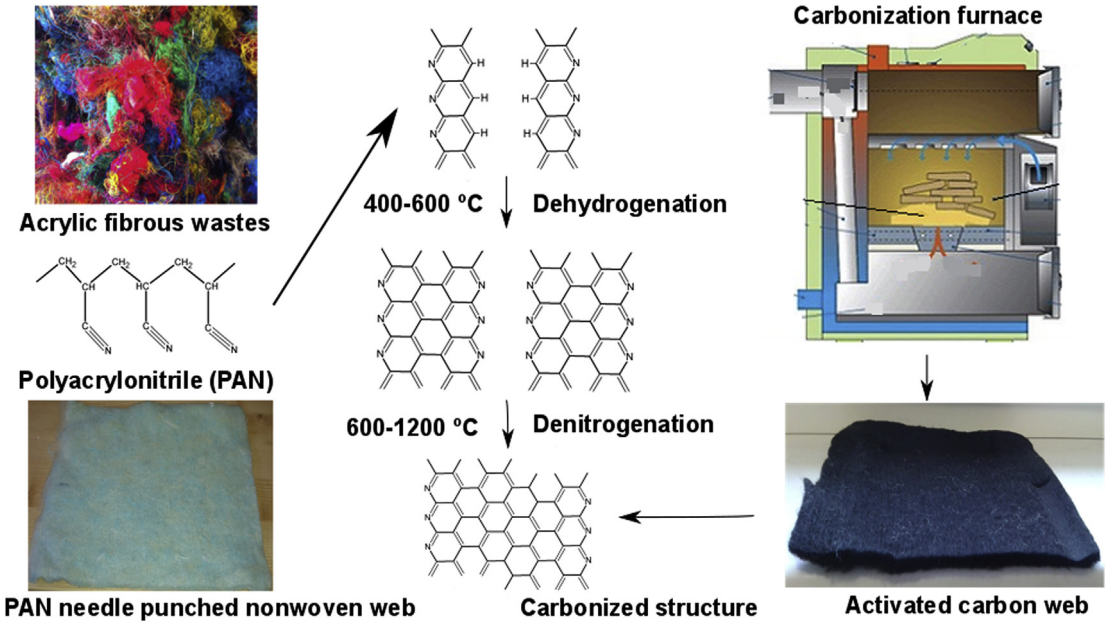

Fig. 1. Schematic of preparation of activated carbon from acrylic fibrous wastes. (A colour version of this figure can be viewed online.)

relative pressure range P/P_0 from 0.02 to 1, where P_0 is saturated pressure of nitrogen gas at 77.35 K temperature (i.e. 1 Atm). The samples were pre-treated in an oven at 45 °C in dry-room for at least 5 h and then out gassed overnight at 300 °C prior to the adsorption analysis. Both adsorption and desorption isotherms were obtained and the specific surface area was determined.

2.3.6. Electrical conductivity

Hewlett Packard 4339 B high resistance meter was used to measure the volume electrical resistivity of activated carbon web samples according to ASTM D257-14 at temperature 22 °C and relative humidity 40%. The specific voltage potential of 100 ± 5 V using direct current was applied across opposite ends of activated carbon web and resultant current flowing across the sample was measured after 15 ± 1 s.

2.4. Electromagnetic shielding effectiveness of activated carbon web

The electromagnetic shielding effectiveness of prepared activated carbon web was determined from two different measurement principles (i.e. waveguide method and coaxial transmission line method).

2.4.1. Waveguide method

The waveguide method examined the electromagnetic shielding ability at 2.45 GHz. This device consisted of a rectangular hollow waveguide having electrically conductive walls. A receiving antenna was placed inside of this waveguide, while a sample was placed at the entrance to the waveguide. A network analyzer Agilent E 4991A was used to generate, and a high frequency analyzer HF-38B (Gigahertz Solutions) was used to receive the electromagnetic signals. More details of this measurement method can be found in [21]. The electromagnetic shielding effectiveness *SE* [dB] was calculated based on Equation (1).

$$SE = 10 \log \frac{P_t}{P_i} \quad (1)$$

where P_t and P_i is power density (W/m^2) measured in presence of sample (transmitted), and without the sample (incident) respectively.

2.4.2. Coaxial transmission line method

The coaxial transmission line method examined the electromagnetic shielding ability in frequency range of 600 MHz to 1.5 GHz. This device determined electromagnetic shielding effectiveness using the insertion-loss method according to ASTM D 4935-10 standard [21]. The measurement set-up consisted of a sample holder with its input and output connected to the network analyzer. A shielding effectiveness test fixture (Electro-Metrics, Inc., model EM-2107A) was used to hold the sample. The network analyzer (Rohde & Schwarz ZN3) was used to generate and receive the electromagnetic signals.

3. Results and discussions

3.1. Effect of carbonization parameters on properties of activated carbon web

3.1.1. Effect of carbonization temperature

The physical characteristics of activated carbon webs prepared at 800 °C, 1000 °C and 1200 °C of temperature, under 300 °C h^{-1} heating rate and without any holding time are shown in Table 2. The stabilization of acrylic fibers at 250 °C leads to cyclization, dehydrogenation, and oxidation of polyacrylonitrile structure (Fig. 1) [22]. During this stage, nitrile groups form non-meltable ladder structure, which further enhances mechanical properties and final carbon yield. During subsequent carbonization of stabilized web, the ladder polymer further cross links to form turbostatic carbon structure and the orientation of basal planes leads

Table 2
Effect of carbonization temperature on physical properties of activated carbon web.

Temperature (°C)	Yield (%)	Shrinkage	Flexibility	Dusting
800	61.7	Good	Good	Good
1000	57.12	Good	Average	Average
1200	45	Average	Poor	Poor

to graphite like structure.

From Fig. 2, the specific surface area of prepared activated carbon web was found to increase with increase in carbonization temperature. The activated carbon web prepared at 1200 °C, 1000 °C and 800 °C exhibited the specific surface area of 278 m^2/g, 190 m^2/g and 120 m^2/g respectively. This behavior was attributed to gradual reaction of atmospheric oxygen with carbonized acrylic fibrous waste, which resulted into the opening of previously inaccessible pores through the removal of tars and disorganized carbon [20]. Therefore, the increased surface area at high temperature was indication of increase in porosity due to free spaces created by decomposition of organic matter.

3.1.2. Effect of pre-tension during stabilization

The pre-tension applied on the web during stabilization was found to affect the shrinkage, flexibility and dusting behavior of prepared activated carbon web. Fig. 3 shows the significant amount of shrinkage exhibited by carbonized sample (1200 °C temperature, 300 °C h^{-1} of heating rate and no holding time) when there was no pre-tension applied during the stabilization. This behavior can be explained from higher entropic and chemical shrinkage occurred in absence of pre-tension. The entropic shrinkage resulted from strain relaxation of molecular chains, whereas chemical shrinkage resulted from formation of cyclized ladder structure. The rate and magnitude of this shrinkage depends on various factors such as surrounding atmosphere, applied load and heating rate etc [22].

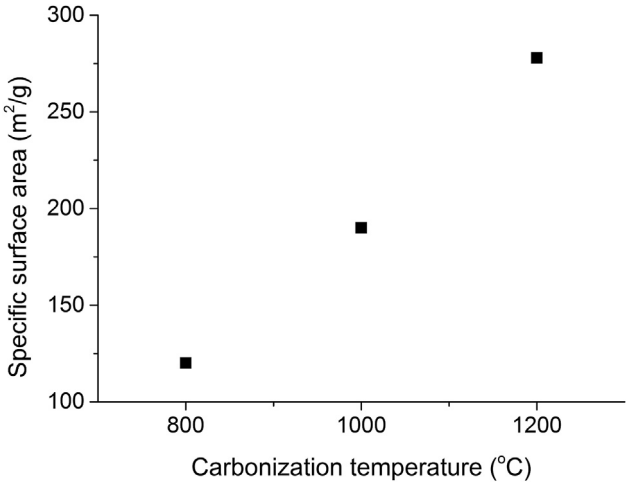

Fig. 2. Effect of carbonization temperature on specific surface area of activated carbon web.

3.2. Characterization of activated carbon web

3.2.1. EDX analysis

Energy disperse x-ray spectroscopy was performed to know the relative proportion of different elements present in the activated carbon webs. From Table 3, the increase in carbon content and reduction in oxygen content was found with increase in carbonization temperature from 800 °C to 1200 °C. The activated carbon web produced at 1200 °C exhibited 92.49% carbon content and 6.61% oxygen content. This behavior was attributed to removal of hydrogen, sulfur, nitrogen and other elements due to decomposition at higher temperature [23].

3.2.2. XRD analysis

In order to know the development of crystallinity with increase in carbonization temperature, the XRD analysis was carried out. Fig. 4 shows the XRD pattern of different activated carbon samples produced at 800 °C, 1000 °C and 1200 °C temperature. The crystallinity of material can be identified from nature of peaks present in the XRD pattern. The intensity and sharpness of peak was found to increase with increase in carbonization temperature. This confirmed the development of higher crystallinity in activated carbon samples produced at higher temperature. The strongest diffraction peak was found at 25.5°, which confirmed the presence of hexagonal graphitic structure due to C (002) reflection [10]. The other diffraction peaks found at 43° and 52.5° were associated with C (100) and C (004) diffraction of graphitic structure. The presence of sharp and intense peak for 1200 °C activated carbon sample showed more transformation of amorphous structure into graphitized structure. This is useful observation to support the results of increased electrical conductivity of activated carbon samples described in further sections.

3.2.3. SEM morphology

In order to know the development of porosity after carbonization of acrylic fibrous wastes, the surface morphology of acrylic fibers before and after carbonization was studied from SEM images. Fig. 5(a–d) show the SEM images of acrylic fibrous web and activated carbon web produced at temperature of 800 °C, 1000 °C and 1200 °C respectively. The activated carbon web showed noticeable rough surface as compared to acrylic fibrous web. The surface roughness was found to increase with increase in carbonization

Fig. 3. Activated carbon from stabilization (a) without any pre-tension, (b) with applied pre-tension. (A colour version of this figure can be viewed online.)

Table 3
Effect of carbonization temperature on elemental composition of activated carbon web.

Element	App conc.	Intensity	Weight %	Atomic %
800 °C				
C K	0.26	2.12	0.13	91.76
O K	0.01	0.761	0.01	8.24
1000 °C				
C K	0.37	2.12	0.18	91.87
O K	0.02	0.760	0.02	8.13
1200 °C				
C K	0.18	2.10	0.09	92.49
O K	0.01	0.744	0.01	6.61
Ca K	0.00	0.902	0.00	0.90

temperature, which indicated the development of more porous structure after physical activation of acrylic fibrous wastes.

3.2.4. Three dimensional morphology

The three dimensional morphology of acrylic fibrous and 1200 °C activated carbon web can be seen from Fig. 6 (a) and (b) respectively. The diameter of individual fibers in the web was found to become thinner after carbonization. For measurement of diameter distribution, the obtained images were processed and analyzed using image analysis software. The background noise was removed and morphological operations were performed using DE speckling function. After careful thresholding of images, the number of fibers for particular range of fiber diameter was examined. Fig. 7 shows the diameter distribution of fibers for acrylic fibrous and activated carbon web. The number of smaller diameter fibers in activated carbon web was found in higher quantity than the acrylic fibrous web. This further justified the development of higher surface area after controlled carbonization of acrylic fibers.

3.2.5. BET analysis

For electromagnetic shielding effectiveness to be achieved through absorption of radiations, the knowledge of pore characteristics and specific surface area of samples is necessary. Fig. 8 shows the nitrogen adsorption/desorption isotherm of activated carbon web prepared at 1200 °C of carbonization temperature, 300 °C h^{-1} of heating rate and no holding time. A rapid rise in the adsorption–desorption isotherm was found at low relative pressures, which was followed by a horizontal plateau at higher relative pressures. This behavior indicated type I isotherm based on the classification of the International Union of Pure and Applied Chemistry (IUPAC) [24,25]. The type I isotherm confirmed that

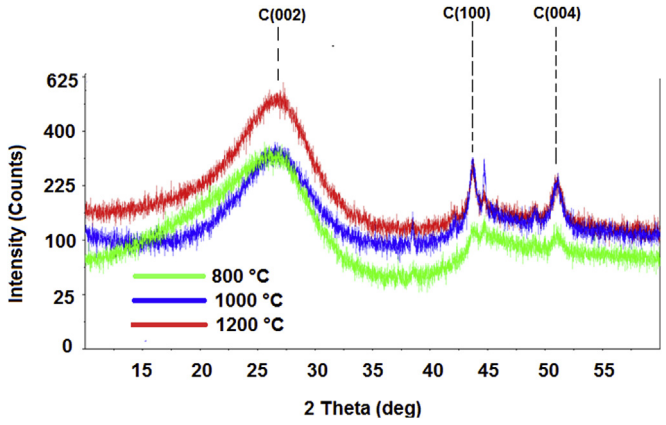

Fig. 4. Effect of carbonization temperature on crystallinity of activated carbon web. (A colour version of this figure can be viewed online.)

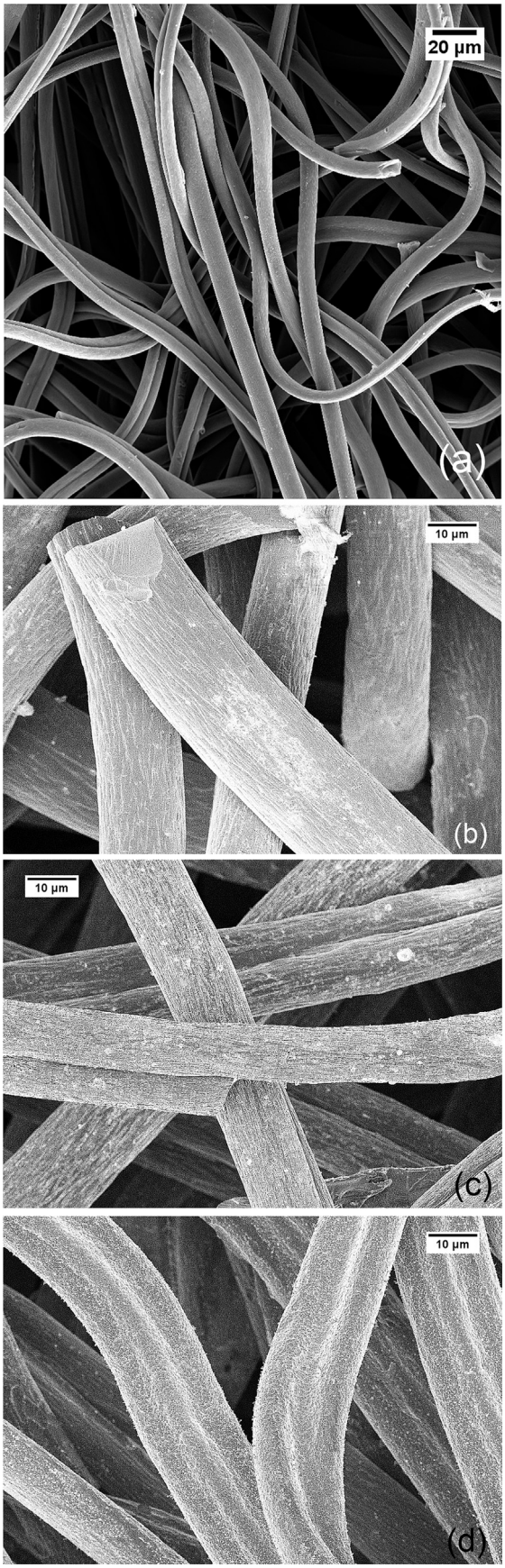

Fig. 5. SEM image of (a) acrylic fibrous web (b) 800 °C activated carbon web (c) 1000 °C activated carbon web (d) 1200 °C activated carbon web.

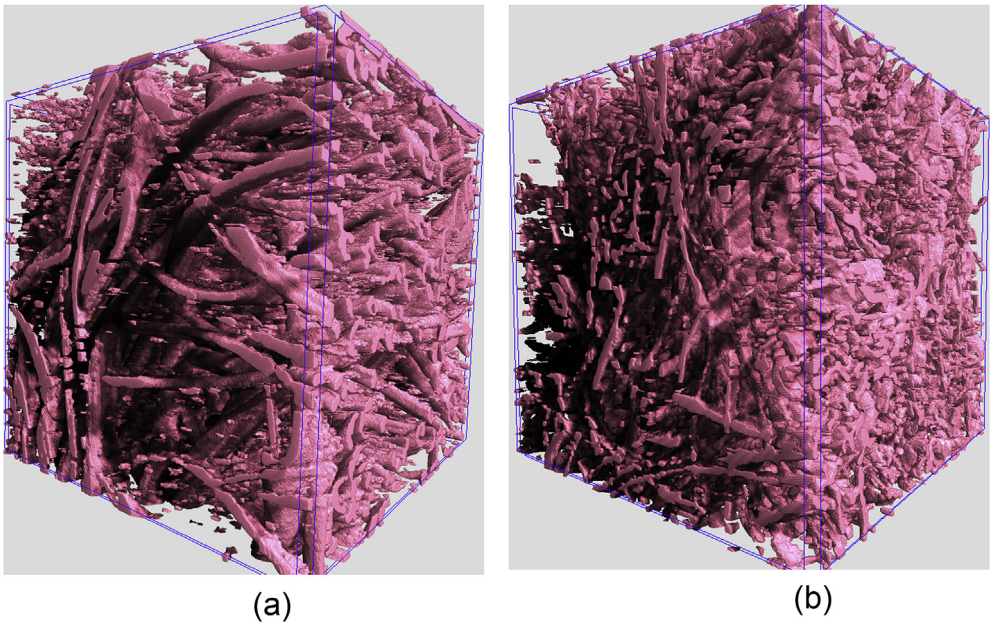

Fig. 6. Three dimensional view at 500 μm scale for (a) acrylic fibrous web (b) 1200 °C activated carbon web. (A colour version of this figure can be viewed online.)

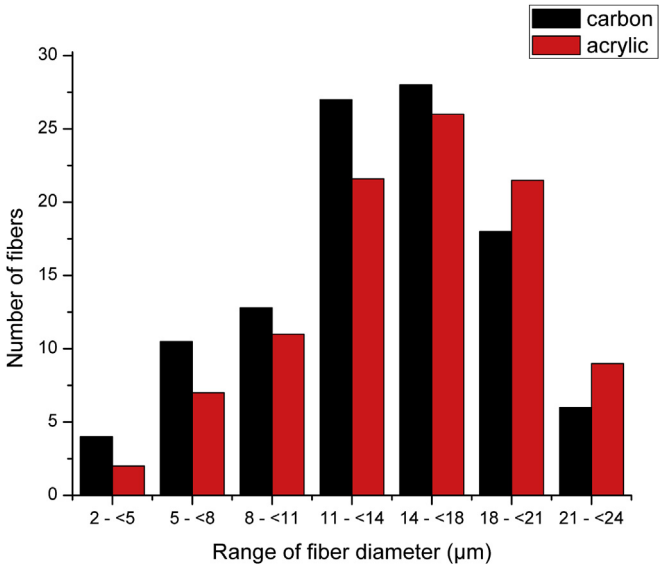

Fig. 7. Distribution of fiber diameter evaluated from computed tomography images. (A colour version of this figure can be viewed online.)

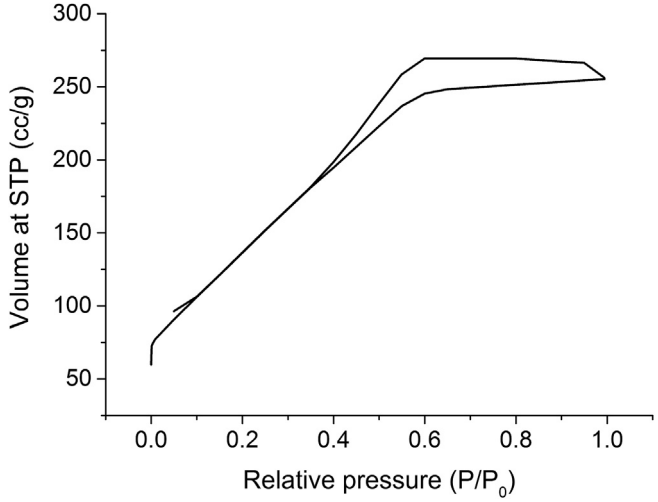

Fig. 8. Nitrogen adsorption-desorption isotherm of 1200 °C activated carbon web.

micropore was developed in the activated carbon web produced at 1200 °C. The pore volume and pore diameter of this activated carbon web was found 0.437 cc/g and 3.062 nm, respectively from BJH analysis. In accordance to IUPAC classification, the adsorbent pores are classified into three groups: micropore (diameter < 2 nm), mesopore (2–50 nm), and macropore (>50 nm) [26]. Therefore, the prepared activated carbon at 1200 °C predominantly exhibited mesoporous nature.

3.2.6. Electrical conductivity

For electromagnetic shielding effectiveness to be achieved through reflection of EM radiations, the knowledge of electrical conductivity of samples is necessary. Fig. 9 shows the average values in 95% confidence interval for electrical resistivity of activated carbon web samples. The electrical resistivity was found to decrease with increase in carbonization temperature. The linear regression model was applied and 76.15% coefficient of determination was found between carbonization temperature and achieved electrical resistivity. The 1200 °C activated carbon sample exhibited 1000 times reduction in electrical resistivity over 800 °C activated carbon sample. The higher electrical conductivity of 1200 °C activated carbon sample was attributed to more graphitization, which was confirmed from presence of sharp diffraction peak observed in XRD spectra (Fig. 4).

3.2.7. Mechanism of charge transport

Fig. 10(a–c) show the two possible modes of electron transport (i.e., migration and hopping) in the activated carbon web produced at 800, 1000 and 1200 °C, respectively. The development of electrical conductivity can be explained from the migration of electrons in one graphite layer or their jumping across the defects/interfaces

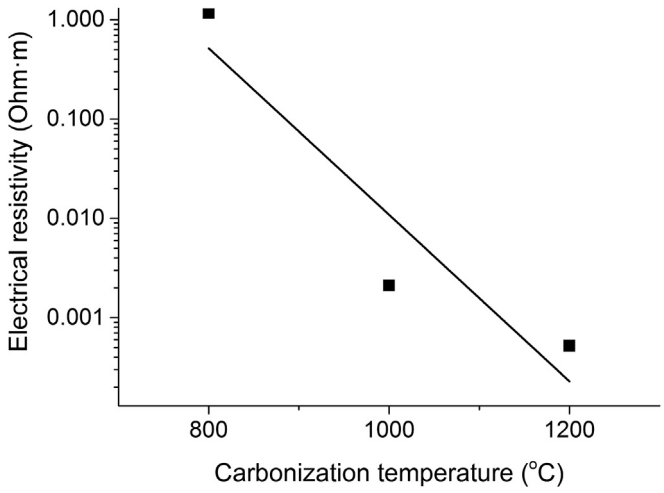

Fig. 9. Effect of carbonization temperature on electrical conductivity of activated carbon web.

between disordered graphite layers [27–29]. The higher electrical conductivity indicated relatively easier migration and hopping of electrons in case of 1200 °C activated carbon than 800 and 1000 °C activated carbon samples. This behavior can be attributed to their higher graphite content, uniform distribution of graphite layers, reduced fiber diameter, etc shown in Fig. 10, which ultimately resulted into the formation of dense micro-current network in 1200 °C activated carbon structure [30,6].

3.3. Electromagnetic shielding ability

3.3.1. Waveguide method

Fig. 11 (a–b) show the average values in 95% confidence interval for electromagnetic shielding effectiveness of prepared activated carbon web in single and double layers measured at 2.45 GHz frequency. The electromagnetic shielding effectiveness was found to increase with increase in number of layers and increase in carbonization temperature. The electromagnetic shielding effectiveness of 28.29 dB, 26.06 dB and 3.34 dB was exhibited by single layers of activated carbon web produced at 1200 °C, 1000 °C and 800 °C, respectively. At very low carbonization temperature, the shielding effectiveness remained similar to that of non-carbonized

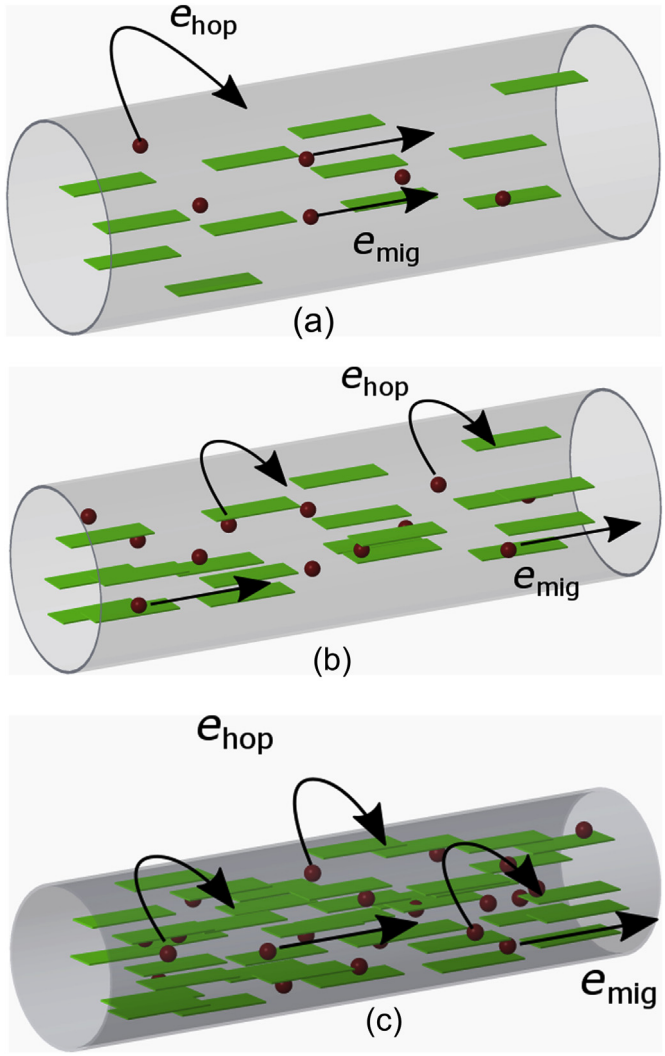

Fig. 10. Mechanism of charge transport in (a) 800 °C activated carbon (b) 1000 °C activated carbon (c) 1200 °C activated carbon. (A colour version of this figure can be viewed online.)

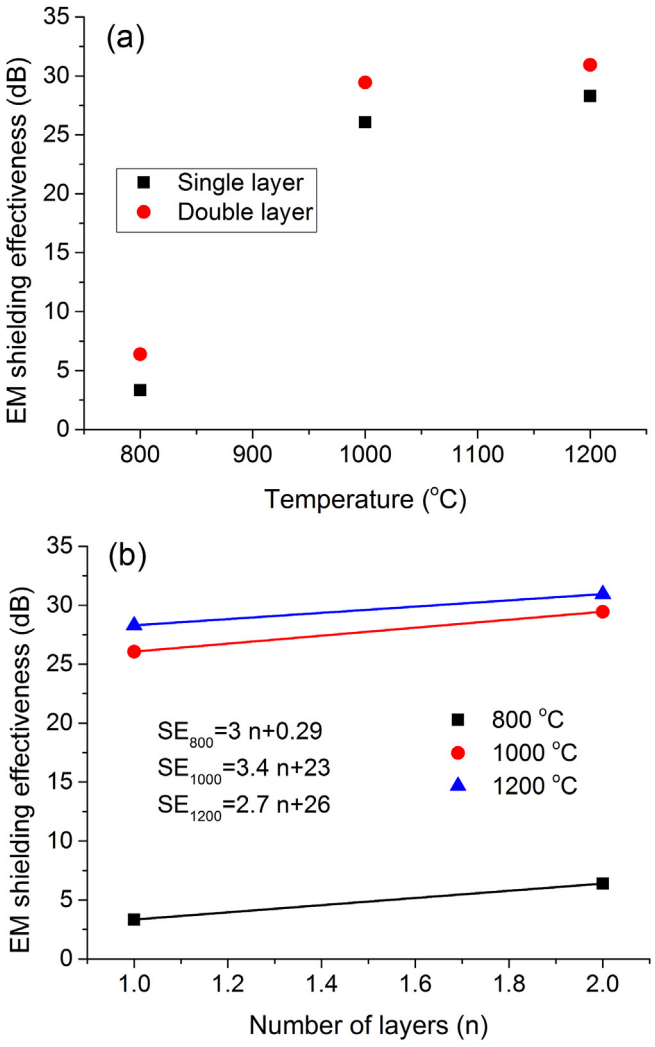

Fig. 11. (a). Effect of carbonization temperature on electromagnetic shielding effectiveness at 2.45 GHz (b). Effect of number of layers on electromagnetic shielding effectiveness at 2.45 GHz. (A colour version of this figure can be viewed online.)

polyacrylonitrile substrate (i.e. zero). Then, the shielding effectiveness was found to increase dramatically over a very narrow range of carbonization temperature, which was connected to the amount of carbon/graphite phase present in the structure. This point is called the percolation threshold, which showed minimum carbonization temperature required for maximum increase in conductivity for higher shielding effectiveness. In present study, the percolation threshold was found between the range of 800 °C and 900 °C carbonization temperature. The maximum shielding effectiveness in this range was attributed to increased multiple internal reflections and stronger absorption of electromagnetic radiations due to higher electrical conductivity, higher porosity and higher surface area [4]. The dramatic increase of shielding ability could not be expected with further increase of carbonization temperature ($T > 1100$ °C). Therefore, the usage of 1000 °C carbonization temperature was considered optimal with regard to its relatively high electromagnetic shielding ability and satisfactory mechanical properties. The similar trend was found for double layers of activated carbon, where shielding effectiveness was increased by 13% in case of 1000 °C activated carbon web. This behavior was attributed to increase in thickness with increase in number of layers.

3.3.2. Coaxial transmission line method

Fig. 12 (a–b) show the mean values of electromagnetic shielding effectiveness for single layers of activated carbon samples in frequencies of 600 MHz, 1 GHz and 1.5 GHz. The increase in shielding effectiveness with increase in carbonization temperature was observed. The single layer of 800 °C activated carbon web revealed the lowest electromagnetic shielding effectiveness of about 5 dB in frequency range of 600 MHz–1.5 GHz. On the other hand, the 1200 °C activated carbon web exhibited the shielding ability of 63.26 dB, 66.75 dB and 75.44 dB for respective frequencies of 600 MHz, 1 GHz and 1.5 GHz.

3.3.3. Mechanism of EMI shielding

The phenomena of reflection, absorption and multiple internal reflections of electromagnetic radiations contribute to the EMI shielding efficiency. The reflection is related to the impedance mismatch between air and absorber. The presence of surface nomadic charges or mobile charge carriers (electrons or holes) is considered as the most important factor for the reflection mechanism [27,6]. Absorption is the second important mechanism and it depends on the thickness of the shield. Absorption arises from Ohmic loss and polarization loss [30]. Ohmic loss comes from the dissipation of energy by nomadic charges through conduction, hopping and tunneling mechanisms, whereas polarization loss originates from the energy required for overcoming the momentum to reorient the dipoles in each half cycle of the EM wave. The polarization is derived from functional groups, defects and interfaces within the material. The third mechanism is multiple internal reflections which represent scattering effect within the shielding material due to its inhomogeneity and huge interfacial area [4].

The 1200 °C activated carbon web exhibited higher EMI shielding properties due to increased multiple internal reflection and stronger absorption of EM waves. This behavior was attributed to the development of heterogeneous surface with increased electrical conductivity and porosity at higher carbonization temperature. This can be explained further from Figs. 4, 7, 10 (c), where 1200 °C activated carbon web showed increased graphite content, uniform dispersion of graphite layers, reduced fiber diameter, etc. The greater number of nomadic charges (from increased graphite content in Fig. 4) coupled with their uniform state of dispersion led to elongated electrons' mean free paths and enhanced conductive network which consequently dissipated more electrical energy and thus higher Ohmic loss [5]. The reduced fiber diameter in Fig. 7 provided larger conductive surface area for dissipation of incident EM wave. Moreover, non-homogeneous surface characteristics of 1200 °C activated carbon web in Fig. 5 (d) could indicate enhanced EMI shielding further from higher polarization loss [31].

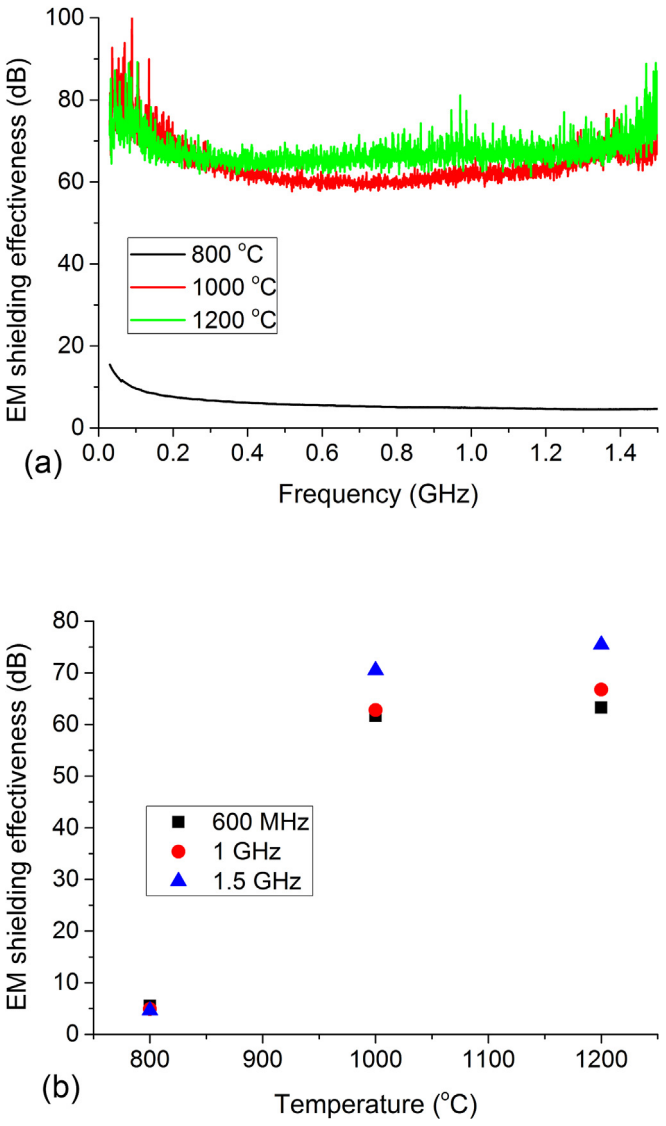

Fig. 12. (a). Effect of frequency on electromagnetic shielding effectiveness. (b). Effect of carbonization temperature on electromagnetic shielding effectiveness in low frequency region. (A colour version of this figure can be viewed online.)

4. Conclusions

The present study was focused on development of porous and electrically conductive activated carbon based electromagnetic shielding materials from acrylic fibrous wastes. The simple and novel approach was employed to introduce absorption and reflection properties of electromagnetic radiations into the shielding materials. This was achieved by physical activation of needle punched nonwoven web of acrylic fibers. The carbonization was performed under the layer of charcoal at 800 °C, 1000 °C and 1200 °C with the heating rate of 300 °C h^{-1} and without any holding time. Further, the influence of carbonization temperature on physical and morphological properties of activated carbon web

was studied from EDX, X-ray diffraction, SEM, X-ray tomography and BET analysis. In the end, the utility of prepared activated carbon web was investigated for electromagnetic shielding ability in high frequency (i.e. 2.45 GHz) and low frequency regions (i.e. below 1.5 GHz) using waveguide method and coaxial transmission line method, respectively. At 2.45 GHz, the electromagnetic shielding effectiveness of 28.29 dB, 26.06 dB and 3.34 dB was exhibited by single layers of activated carbon web produced at 1200 °C, 1000 °C and 800 °C, respectively. On the other hand, for low frequency regions, the 1200 °C activated carbon web exhibited the shielding ability of 63.26 dB, 66.75 dB and 75.44 dB for respective frequencies of 600 MHz, 1 GHz and 1.5 GHz. This behavior was attributed to increased multiple internal reflections and stronger absorption of electromagnetic radiations, which resulted from greater number of nomadic charges (i.e. graphite content), uniform dispersion of graphite layers, reduced fiber diameter, elongated electrons' mean free paths, larger surface area, higher porosity and enhanced conductive network formation in 1200 °C activated carbon.

Acknowledgement

This study was supported under the student grant scheme (SGS-21044) by Technical University of Liberec, Czech Republic.

References

[1] V. Šafářová, M. Tunák, J. Militký, Prediction of hybrid woven fabric electromagnetic shielding effectiveness, Text. Res. J. 85 (2015) 673–686, http://dx.doi.org/10.1177/0040517514555802.
[2] V. Šafářová, J. Militký, Electromagnetic shielding properties of woven fabrics made from high-performance fibers, Text. Res. J. 84 (2014) 1255–1267, http://dx.doi.org/10.1177/0040517514521118.
[3] D.D.L. Chung, Electromagnetic interference shielding effectiveness of carbon materials, Carbon N Y 39 (2001) 279–285, http://dx.doi.org/10.1016/S0008-6223(00)00184-6.
[4] E. Sano, E. Akiba, Electromagnetic absorbing materials using nonwoven fabrics coated with multi-walled carbon nanotubes, Carbon N Y 78 (2014) 463–468, http://dx.doi.org/10.1016/j.carbon.2014.07.027.
[5] M.-S. Cao, X.-X. Wang, W.-Q. Cao, J. Yuan, Ultrathin graphene: electrical properties and highly efficient electromagnetic interference shielding, J. Mater Chem. C Mater Opt. Electron Devices 3 (2015), http://dx.doi.org/10.1039/C5TC01354B. Ahead of Print.
[6] M. Arjmand, U. Sundararaj, Electromagnetic interference shielding of Nitrogen-doped and Undoped carbon nanotube/polyvinylidene fluoride nanocomposites: a comparative study, Compos Sci. Technol. 118 (2015) 257–263, http://dx.doi.org/10.1016/j.compscitech.2015.09.012.
[7] V. Rubežiene, J. Baltušnikaite, S. Varnaite-Žuravliova, A. Sankauskaite, A. Abraitiene, J. Matuzas, Development and investigation of electromagnetic shielding fabrics with different electrically conductive additives, J. Electrostat. 75 (2015) 90–98, http://dx.doi.org/10.1016/j.elstat.2015.03.009.
[8] L.L. Wang, B.K. Tay, K.Y. See, Z. Sun, L.K. Tan, D. Lua, Electromagnetic interference shielding effectiveness of carbon-based materials prepared by screen printing, Carbon N Y 47 (2009) 1905–1910, http://dx.doi.org/10.1016/j.carbon.2009.03.033.
[9] M. Inagaki, J. Qiu, Q. Guo, Carbon foam: preparation and application, Carbon N Y 87 (2015) 128–152, http://dx.doi.org/10.1016/j.carbon.2015.02.021.
[10] J.H. Kim, E. Jeong, Y.S. Lee, Preparation and characterization of graphite foams, J. Ind. Eng. Chem. 32 (2015) 21–33, http://dx.doi.org/10.1016/j.jiec.2015.09.003.
[11] Y. Li, B. Shen, X. Pei, Y. Zhang, D. Yi, W. Zhai, et al., Ultrathin carbon foams for effective electromagnetic interference shielding, Carbon N Y 100 (2016) 375–385, http://dx.doi.org/10.1016/j.carbon.2016.01.030.
[12] S. Farhan, R. Wang, K. Li, Electromagnetic interference shielding effectiveness of carbon foam containing in situ grown silicon carbide nanowires, Ceram. Int. 42 (2016) 11330–11340, http://dx.doi.org/10.1016/j.ceramint.2016.04.054.
[13] A. Fletcher, M.C. Gupta, K.L. Dudley, E. Vedeler, Elastomer foam nanocomposites for electromagnetic dissipation and shielding applications, Compos Sci. Technol. 70 (2010) 953–958, http://dx.doi.org/10.1016/j.compscitech.2010.02.011.
[14] B. Shen, Y. Li, D. Yi, W. Zhai, X. Wei, W. Zheng, Microcellular graphene foam for improved broadband electromagnetic interference shielding, Carbon N Y 102 (2016) 154–160, http://dx.doi.org/10.1016/j.carbon.2016.02.040.
[15] X. Sun, X. Liu, X. Shen, Y. Wu, Z. Wang, J.K. Kim, Graphene foam/carbon nanotube/poly(dimethyl siloxane) composites for exceptional microwave shielding, Compos Part A Appl. Sci. Manuf. 85 (2015) 199–206, http://dx.doi.org/10.1016/j.compositesa.2016.03.009.
[16] H. Wang, K. Zheng, X. Zhang, X. Ding, Z. Zhang, C. Bao, et al., 3D network porous polymeric composites with outstanding electromagnetic interference shielding, Compos Sci. Technol. 125 (2016) 22–29, http://dx.doi.org/10.1016/j.compscitech.2016.01.007.
[17] D.-X. Yan, P.-G. Ren, H. Pang, Q. Fu, M.-B. Yang, Z.-M. Li, Efficient electromagnetic interference shielding of lightweight graphene/polystyrene composite, J. Mater Chem. 22 (2012) 18772, http://dx.doi.org/10.1039/c2jm32692b.
[18] Z. Chen, W. Ren, L. Gao, B. Liu, S. Pei, H.-M. Cheng, Three-dimensional flexible and conductive interconnected graphene networks grown by chemical vapour deposition, Nat. Mater 10 (2011) 424–428, http://dx.doi.org/10.1038/nmat3001.
[19] W.-L. Song, X.-T. Guan, L.-Z. Fan, W.-Q. Cao, C.-Y. Wang, M.-S. Cao, Tuning three-dimensional textures with graphene aerogels for ultra-light flexible graphene/texture composites of effective electromagnetic shielding, Carbon N Y 93 (2015) 151–160, http://dx.doi.org/10.1016/j.carbon.2015.05.033.
[20] V. Baheti, S. Naeem, J. Militky, M. Okrasa, B. Tomkova, Optimized preparation of activated carbon nanoparticles from acrylic fibrous wastes, Fibers Polym. 16 (2015) 2193–2201, http://dx.doi.org/10.1007/s12221-015-5364-0.
[21] V. Safarova, M. Tunak, M. Truhlar, J. Militky, A new method and apparatus for evaluating the electromagnetic shielding effectiveness of textiles, Text. Res. J. 86 (2016) 44–56, http://dx.doi.org/10.1177/0040517515581587.
[22] Y. Liu, Y.H. Choi, H.G. Chae, P. Gulgunje, S. Kumar, Temperature dependent tensile behavior of gel-spun polyacrylonitrile and polyacrylonitrile/carbon nanotube composite fibers, Polym. Guildf. 54 (2013) 4003–4009, http://dx.doi.org/10.1016/j.polymer.2013.05.051.
[23] Y. MA, X. YIN, Q. LI, Effects of heat treatment temperature on microstructure and electromagnetic properties of ordered mesoporous carbon, Trans. Nonferrous Met. Soc. China 23 (2013) 1652–1660, http://dx.doi.org/10.1016/S1003-6326(13)62644-8.
[24] H. Ghorbani, H. Tavanai, M. Morshed, Fabrication of activated carbon nanoparticles from PAN precursor, J. Anal. Appl. Pyrolysis 110 (2014) 12–17, http://dx.doi.org/10.1016/j.jaap.2014.07.008.
[25] Q. Jiang, Y. Zhao, Effects of activation conditions on BET specific surface area of activated carbon nanotubes, Microporous Mesoporous Mater 76 (2004) 215–219, http://dx.doi.org/10.1016/j.micromeso.2004.08.020.
[26] B.D. Zdravkov, J.J. Čermák, M. Šefara, J. Janků, Pore classification in the characterization of porous materials: a perspective, Cent. Eur. J. Chem. 5 (2007), http://dx.doi.org/10.2478/s11532-007-0039-3, 1158–1158.
[27] M.S. Cao, W.L. Song, Z.L. Hou, B. Wen, J. Yuan, The effects of temperature and frequency on the dielectric properties, electromagnetic interference shielding and microwave-absorption of short carbon fiber/silica composites, Carbon N Y 48 (2010) 788–796, http://dx.doi.org/10.1016/j.carbon.2009.10.028.
[28] W.L. Song, M.S. Cao, Z.L. Hou, X.Y. Fang, X.L. Shi, J. Yuan, High dielectric loss and its monotonic dependence of conducting-dominated multiwalled carbon nanotubes/silica nanocomposite on temperature ranging from 373 to 873 K in X -band, Appl. Phys. Lett. 94 (2009) 1–4, http://dx.doi.org/10.1063/1.3152764.
[29] B. Wen, M.S. Cao, Z.L. Hou, W.L. Song, L. Zhang, M.M. Lu, et al., Temperature dependent microwave attenuation behavior for carbon-nanotube/silica composites, Carbon N Y 65 (2013) 124–139, http://dx.doi.org/10.1016/j.carbon.2013.07.110.
[30] M. Arjmand, K. Chizari, B. Krause, P. Pötschke, U. Sundararaj, Effect of synthesis catalyst on structure of nitrogen-doped carbon nanotubes and electrical conductivity and electromagnetic interference shielding of their polymeric nanocomposites, Carbon N Y 98 (2016) 358–372, http://dx.doi.org/10.1016/j.carbon.2015.11.024.
[31] K.L. Kaiser, Electromagnetic Shielding, CRC Press, Boca Raton, 2006, pp. 1–52.

Appendix 7

V. Safarova and J. Militky, "Multifunctional metal composite textile shields against electromagnetic radiation - effect of various parameters on electromagnetic shielding effectiveness," Polymer Composites, vol. 38, no. 2, pp. 309–323, 2017.

Multifunctional Metal Composite Textile Shields Against Electromagnetic Radiation—Effect of Various Parameters on Electromagnetic Shielding Effectiveness

Veronika Šafářová, Jiří Militký
Faculty of Textile Engineering, Technical University of Liberec, Czech Republic

Over the last few years, there has been mounting concern about the possibility of adverse health effects resulting from exposure to radiofrequency electromagnetic fields, such as those emitted by wireless communication devices. For the reason given above, a demand for protection of human beings against influence of electromagnetic signals and troublesome charges, has been increasing. Therefore textile structures with increased electromagnetic shielding ability, which satisfy the requirements for casual dress or preserve air circulation at workplace, is suitable. This article presents the present state of fabrication and characterization of multifunctional light weight flexible fabrics with increased resistance to electromagnetic radiation while preserving basic properties of textile structures designated for clothing or technical purposes. In this article, an effect of metal content, a placement of conductive yarn, geometry, moisture content and correlation with frequencies is studied. In addition, percolation thresholds are identified and a form of relation between conductive component and total shielding effectiveness is proposed. POLYM. COMPOS., 38:309–323, 2017. © 2015 Society of Plastics Engineers

INTRODUCTION

According to World Health Organization [1], exposure to electromagnetic (EM) fields is not a new phenomenon. However, during the 21th century, environmental exposure to man-made EM fields has been steadily increasing as growing electricity demand, ever-advancing technologies, and changes in social behavior.

Hence, everyone is exposed to a complex mix of weak electric and magnetic fields, both at home and at work. Sources of such emissions could include generation and transmission of electricity, domestic appliances and industrial equipment, telecommunications, and broadcasting. While electrical and EM fields in certain frequency bands have wholly beneficial effects which are applied in medicine, other nonionizing frequencies, sourced from extremely low frequencies, power lines, or certain high frequency waves used in the fields of radar, telecommunications, and mobile telephony, appear to have more or less potentially harmful, non-thermal, biological effects on plants, insects and animals as well as the human body [2, 3].

Mobile telephony has become commonplace around the world. This wireless technology relies upon an extensive network of fixed antennas, or base stations, relaying information with radio frequency signals. Over 1.4 million base stations exist worldwide and the number is increasing significantly with the introduction of third-generation technology. Other wireless networks that allow high-speed internet access and services, such as wireless local area networks, are also increasingly common in homes, offices, and many public areas (airports, schools, residential, and urban areas). As the number of base stations and local wireless networks increases, so does the radio frequency exposure of the population [2].

Over the last few years, there has been mounting concern about the possibility of adverse health effects resulting from exposure to radiofrequency EM fields, such as those emitted by wireless communication devices. In 2011, the World Health Organization/International Agency for Research on Cancer (IARC) has classified radiofrequency electromagnetic fields as possibly carcinogenic to humans (Group 2B), based on an increased risk for glioma, a malignant type of brain cancer, associated with wireless phone use [1]. One the other hand, despite many studies the evidence for biological effects of electromagnetic fields on human body when exposed to levels that are below the official threshold values was not confirmed. For the reasons given above, a demand for protection of human beings against undesirable influence EM signals and troublesome charges (especially for professional use), has been increasing.

The best material for shielding or absorption of EM wave must have both high electric conductivity (imparts higher reflection of EM wave especially at lower

Correspondence to: V. Šafářová; e-mail: veronika.safarova@tul.cz
Contract grant sponsor: TIP–MPO VaV 2009 "Electromagnetic field protective textiles with improved comfort" of Czech Ministry of Industry.
DOI 10.1002/pc.23588
Published online in Wiley Online Library (wileyonlinelibrary.com).

frequencies) and high magnetic permeability (provides higher absorption of EM wave especially at lower frequencies) and therefore shields based on the use of metals and magnetic alloys are the best ones. The materials used for shielding radio-frequency fields are usually copper, aluminum, or silver based (in the form of wires, metal plating, or conductive fillers). These shields work by reflecting the waves, because these metals have a high electric conductivity. To shield magnetic field, materials must have a high magnetic permeability to be able then absorb the fields [4]. In contrast, most synthetic fabrics are electrically insulating and transparent to EM radiation [5].

In recent years, conductive fabrics have obtained increased attention for electromagnetic shielding and antielectrostatic purposes. This is mainly due to their desirable flexibility and lightweight. One way how conductive fabrics can be created is by using minute electrically conductive fibers. They can be produced in filament or staple lengths and can be incorporate with traditional nonconductive fibers to create yarns that possess varying degrees of conductivity [6–11]. Another way represents conductive coatings which can transform substrates into electrically conductive materials without significantly altering the existing substrate properties. They can be applied to the surface of fibers, yarns or fabrics. The most common are metals [12, 13] and conductive polymer coatings [14, 15]. Main disadvantages are that plated metal or conductive polymer coating can be easily peeled of the fiber during processing and use and their poor durability in use. Their color (metallic or conductive polymer color—e.g., polypyrrole is black) is also sometimes undesirable for textile use. Fibers containing therein carbon black or other conductive particles can be also used [16]. To gain proper conductivity of conductive fiber it is necessary use a large amount of at least 15 wt% conductive particles. This large amount of conductive particles causes the fiber-producing process to be difficult, complex and expensive. Also, it is impossible to contain the carbon black in the inside of the natural fibers.

However, there are some general difficulties in creating electrically conductive fabrics for clothing. Conductive component have to be embedded in textiles in such a way that the flexibility and comfort of the fabrics are retained. Fibers and fabrics have to meet special requirements concerning not only conductivity but also processability and wearability: (a) the fibers have to be able to withstand handling that is typical for textiles, for example weaving, washing and wrinkling, without damaging functionality, (b) fibers that are used for clothing have to be fine and somewhat elastic in order to be comfortable to wear, (c) fabrics need to have a low mechanical resistance to bending and shearing so that they can be easily deformed and draped. The closer the textiles are to the body, the more flexible and lightweight they have to be. Fabrics have to be light weight (preferable not more than 250 g/m^2), permeable to air and water vapor and washable like other cloths without impairment of the electromagnetic shielding effectiveness. Moreover fabrics should be dyeable such that pleasing and fashionable articles of clothing can be made of it.

There are many references in the literature concerning adding a varying amount of single conductive filler to a polymer matrix in order to produce an electrically conductive, shielding material. For example, carbon black, carbon fibers, conductive polymer and metal particles or nickel-coated carbon fibers have been used [6, 10, 12, 14, 16, 17]. Conductive textiles made with the aid of conductive particles mentioned above were found unsuitable for clothing purposes. The diameters of the metal fibers utilized in previous studies for electromagnetic shielding fabric were too large (0.08–0.15 mm) to be flexible enough to be applied for certain applications [9, 10, 18]. In addition, costs arising from consumption of metals and demand on continuous competitiveness of manufactures focusing on modern shielding materials require an optimization of shielding structure and a minimization of metal materials consumption, as mentioned in Ref. 19. To the authors' knowledge, there is not enough research on shielding properties of conductive fabrics designated for protective clothing produced directly from conductive fibers and optimization of their structure mainly regarding metal fiber consumption.

This article presents the present state of fabrication and characterization of multifunctional light weight flexible fabrics with increased resistance to electromagnetic radiation while preserving basic properties of textile structures designated for clothing or special technical purposes. For purpose of this study, extremely thin stainless steel staple fibers were incorporated to yarn structure as conductive fillers. Stainless steel was selected mainly because of its high magnetic permeability and considering that it does not readily corrode, rust, or stain with water. In this article, an effect of metal content, a placement of conductive yarn, geometry, moisture, and correlation with frequencies is studied. In addition, percolation thresholds are identified and predictor models are proposed to be able to optimize the fabric structure with a view to final application of product. These hybrid fabrics have many possible applications such as radiofrequency protective suits, tents, curtains or tapestry, smart clothing with incorporated conductive paths, electrostatic dissipative material for clothing or equipment, clean room working clothes, etc.

MECHANISM OF ELECTROMAGNETIC SHIELDING

An electromagnetic field is built up from various electric E and magnetic field H components. An electric field is created by a voltage difference and magnetic field is created by a moving charge, i.e., by a current. Every current is thus accompanied by both an electric and a magnetic field.

Electromagnetic (EM) interference shielding consists of two regions, the near field shielding region and far field shielding region. Two types of loss are encountered by an incident electromagnetic wave to a shield. The wave is partially reflected from the surface, and the transmitted (no reflected) portion of the wave is partially or totally

 DOI 10.1002/pc

attenuated as it passes through the shield. This latter effect, called absorption or penetration loss, is the same in either the near or the far field and for electric or magnetic fields [20].

The total shielding of a solid material with no apertures is equal to the sum of the absorption loss (A) plus the reflection loss (R) plus a correction factor (B) to account for multiple reflections in thin shields. Total electromagnetic shielding effectiveness therefore can be written as [20]:

$$\mathrm{SE} = A + R + B\,[\mathrm{dB}]. \tag{1}$$

The reflection is usually the primary mechanism of electromagnetic interference shielding. The wave, which is incident to the boundary with the second medium is partially reflected back and partially transmitted to second medium. The same situation occurs at the interface between second and third material. The reflection loss at the interface between two media is related to the difference in characteristic impedance between the media and also subjected to have mobile charge carriers (electrons and holes), which can interact with the electromagnetic field in the radiation. As a result, the shield tends to be electrically conducting, although a high conductivity is not required. For example, a volume resistivity of the order of 1 Ω cm is typically sufficient. Metals are the most common materials for EM shielding. Reflection loss for plane waves is greater at low frequencies and for high conductivity materials [21].

Secondary mechanism of EMI shielding is usually absorption. When an electromagnetic wave passes through a medium, its amplitude decreases exponentially. This decay occurs because currents induced in the shield produce ohmic losses and heating of material. General expression for absorption loss can be written as [20]:

$$A = 0.0848\, t\sqrt{f\,\mu_r\sigma_r}\,[\mathrm{dB}], \tag{2}$$

where t is thickness of the shield in meters. For significant absorption of the radiation by the shield, the shield should have electric and/or magnetic dipoles, which interact with the electromagnetic fields in the radiation. The electric dipoles may be provided by materials having a high value of the dielectric constant. The magnetic dipoles may be provided by materials having a high value of the magnetic permeability.

The absorption loss is a function of the product $\sigma_r.\mu_r$, whereas the reflection loss is a function of the ratio σ_r/μ_r, where σ_r is the electrical conductivity relative to copper and μ_r is the relative magnetic permeability. Table 1 shows these factors for various materials. Silver, copper, gold, and aluminum are excellent for reflection, due to their high conductivity. Supermalloy and mummetal are excellent for absorption, due to their high magnetic permeability. The reflection loss decreases with increasing frequency, whereas absorption loss increases with increasing frequency [20].

Other than reflection and absorption, a mechanism of shielding is multiple reflections (B), which refer to the reflections at various surfaces or interfaces in the shield. This mechanism requires the presence of a large surface area or interface area in the shield. An example of a shield with a large surface area is a porous or foam material. The loss due to multiple reflections can be neglected when the distance between the reflecting surfaces or interfaces is large compared with the skin depth.

TABLE 1. Relative conductivity and permeability of various materials [20].

Material	σ_r	μ_r	$\sigma_r.\mu_r$	σ_r/μ_r
Silver	1.05	1	1.05	1.05
Copper	1	1	1	1
Gold	0.7	1	0.7	0.7
Aluminum	0.61	1	0.61	0.61
Brass	0.26	1	0.26	0.26
Bronze	0.18	1	0.18	0.18
Nickel	0.2	100	20	2.10^{-3}
Stainless steel	0.02	500	10	4.10^{-5}

Operation of the electromagnetic shield is possible to be characterized by so called shielding attenuation coefficient (dimensionless) defined as a ratio between electromagnetic field density in a specific place of shielded space P_t and incident electromagnetic field density P_i:

$$\mathrm{ES} = \frac{P_t}{P_i}\,[-]. \tag{3}$$

Logarithmic size of this coefficient called electromagnetic shielding effectiveness (SE) is used more frequently:

$$\mathrm{SE} = 10\log\frac{P_t}{P_i} = 20\log\frac{E_t}{E_i} = 20\log\frac{H_t}{H_i}\,[\mathrm{dB}], \tag{4}$$

where H_t, E_t, P_t are the electric field strength, magnetic field strength and electromagnetic field density values measured in the presence of the textile material, H_i, E_i, P_i are the same values measured without the textile material.

The electromagnetic shielding effectiveness of element is characterized by its electric conductivity, permittivity, and permeability, parameters of source and properties of ambient surrounding. Basic proposed numerical models of fabrics SE are based either on electrical properties (especially volume conductivity) of element [16, 22–24] or on analysis of leakage through of opening in textile [25, 26].

Determining the level of attenuation of an EMI shield can be complex and the methods often vary according to the particular shield application. The more common techniques for testing shielding strength include Open Field Test, Coaxial Transmission Line Test, Shielded Box Test, and Shielded Room Test [27].

EXPERIMENTAL

Hybrid Yarns

Hybrid yarns were composed of conventional polypropylene (PP) fiber and different content of staple

TABLE 2. Properties of fibers used for this study.

Fiber	Linear density (tex)	Length (mm)	Tensile strength (cN/tex)	Elongation (%)	Young's modulus (cN/dtex)
Stainless steel fiber (SS)	3.85	50	14.35	1.29	111.56
Polypropylene fiber (PP)	2.20	50	34.83	57.57	24.95

BEKINOX stainless steel (SS) metal fibers (1–75%). The aspect ratio (length/diameter ratio, *l*/*d*) of the SS used in this study is 6,250, since the diameter of the SS is 8 μm and the fiber length of the SS is 50 mm. In this study, TREVON polypropylene fiber with a fineness 2.2 dtex and 50 mm length was used as a nonconductive component. Properties of these fibers are given in Table 2. The two components were mixed at the drawing frame and a ring spinning system was used to produce blended yarns. Hybrid yarns were prepared in two different linear densities: (a) single yarn (fineness of yarns was 25 tex), (b) two ply yarns (fineness of yarns was 2 × 25 tex). Figure 1 presents microscopic images of hybrid yarns with different content of conductive component.

Hybrid Fabrics

Four groups of fabrics were made using hybrid yarns described above. First three groups (18 samples) represents woven fabrics with the same structure (weft and warp fineness 50 tex, warp sett 20 1/cm, weft sett 19 1/cm and twill weave). The first group, nine samples (W1–W75), were made of 100% hybrid yarn containing different portion of conductive phase. Second group is represented by three cotton twill weaves (W5-3, W5-4, W5-5) in which hybrid yarns were inserted in certain intervals (3, 4, 5 mm) to obtain different open grid structure. In this case, yarns with identical metal content (5% of SS) were used. Polypropylene twill weaves with identical grid structure (W1-5–W20-5) form third group of samples. In this case, warp and weft opening is identical (5 × 5 mm) and metal component content in hybrid yarn varies (1–20%). Fourth group, six knitted samples (K1–K20) with the same structure (single jersey knit, yarn fineness 25 tex, 12 wales/cm in wale direction, 16 courses/cm in the course direction), were made of 100% hybrid yarn containing different portion of conductive phase. The characteristics of the hybrid fabrics are shown in Table 3. Schematic structure of the hybrid fabrics is represented in

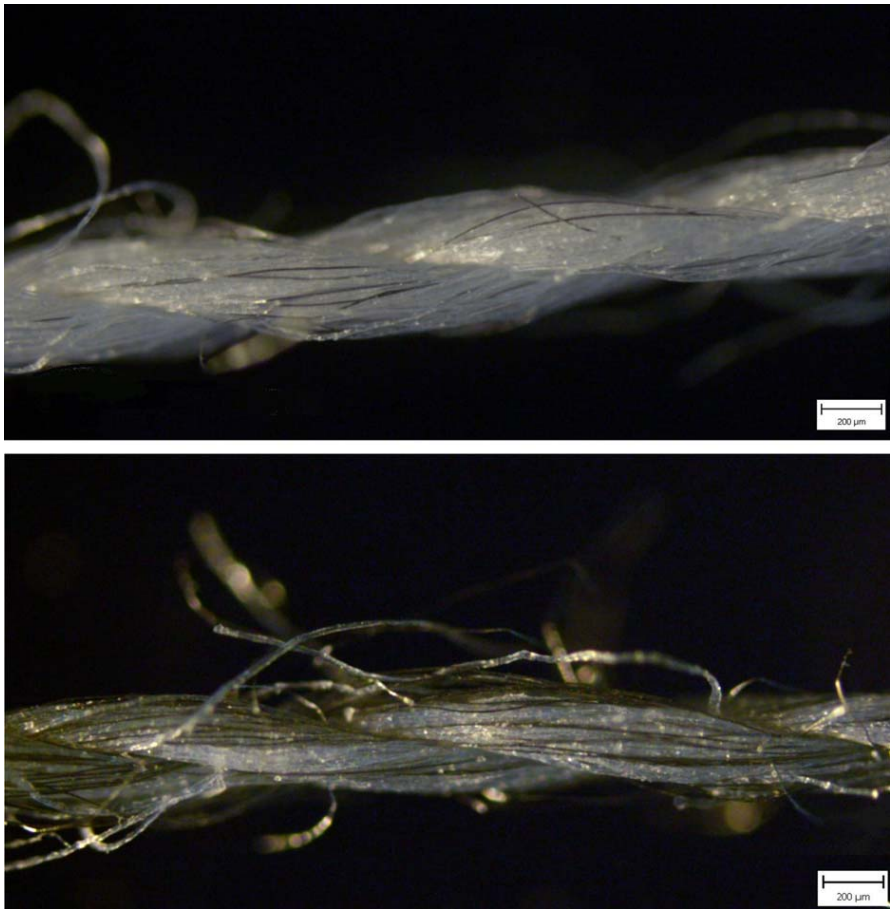

FIG. 1. Microscopic images of two ply hybrid yarns containing (a) 15 %, (b) 60 % of conductive component. [Color figure can be viewed at wileyonlinelibrary.com]

 DOI 10.1002/pc

TABLE 3. Characteristics of hybrid fabrics.

Sample	Composition	Warp/weft count (tex)	Hybrid yarn placement	Fabric structure	Fabric thickness (mm)	Mass per unit area (g/m^2)
W1	1% SS/99% PP	25 × 2/25 × 2	100%	2/2 twill	0.78	233.5
W3	3% SS/97% PP				0.75	225.1
W5	5% SS/95% PP				0.77	209.0
W10	10% SS/80% PP				0.75	221.0
W15	15% SS/75% PP				0.73	217.7
W20	20% SS/80% PP				0.71	208.8
W40	40% SS/60% PP				0.70	206.5
W60	60% SS/40% PP				0.63	183.0
W75	75% SS/25% PP				0.57	159.4
W5-3	5% SS/95% PP + 100% CO	25 × 2/25 × 2	3 × 3 mm	2/2 twill	0.66	220.0
W5-4	5% SS/95% PP + 100% CO		4 × 4 mm		0.67	220.0
W5-5	5% SS/95% PP + 100% CO		5 × 5 mm		0.65	220.0
W1-5	1% SS/99% PP + 100% PP	25 × 2/25 × 2	5 × 5 mm	2/2 twill	0.83	221.9
W3-5	3% SS/97% PP + 100% PP				0.83	216.2
W5-5	5% SS/95% PP + 100% PP				0.83	225.3
W10-5	10% SS/80% PP + 100% PP				0.83	221.3
W15-5	15% SS/75% PP + 100% PP				0.83	222.7
W20-5	20% SS/80% PP + 100% PP				0.83	222.9
K1	1% SS/99% PP	25	100%	single jersey knit	0.67	157.7
K3	3% SS/97% PP				0.66	154.3
K5	5% SS/95% PP				0.64	151.9
K10	10% SS/80% PP				0.64	153.4
K15	15% SS/75% PP				0.65	149.9
K20	20% SS/80% PP				0.64	156.2

Fig. 2. Microscopic images of hybrid fabrics are shown in Fig. 3.

Statistical Analysis of Small Samples

Due to the very small sample sizes $4 \leq n \leq 20$ available for evaluation process, a procedure based on order statistics introduced by Horn [28] was used. This is based on the depths which correspond to the sample quartiles. The pivot depth is expressed by

$$H_L = \text{int}[(n+\ l)/2]/2 \text{ or } H_L = \text{int}[(n+\ l)/2 + \ l]/2 \quad (5)$$

according to which of the H_L is an integer. The lower pivot is $x_L = x_{(H)}$ and the upper one is $x_U = x_{(n\ +\ 1\ -\ H)}$. Denote that the $x_{(i)}$ are ordered statistics i.e. $x_{(i)} \leq x_{(i\ +\ l)}$. The estimate of the parameter of location is then expressed by the *pivot half sum*

$$P_L = 0.5\,(x_L + x_U) \quad (6)$$

and the estimate of the parameter of spread is expressed by the *pivot range*

$$R_L = (x_U - x_L) \quad (7)$$

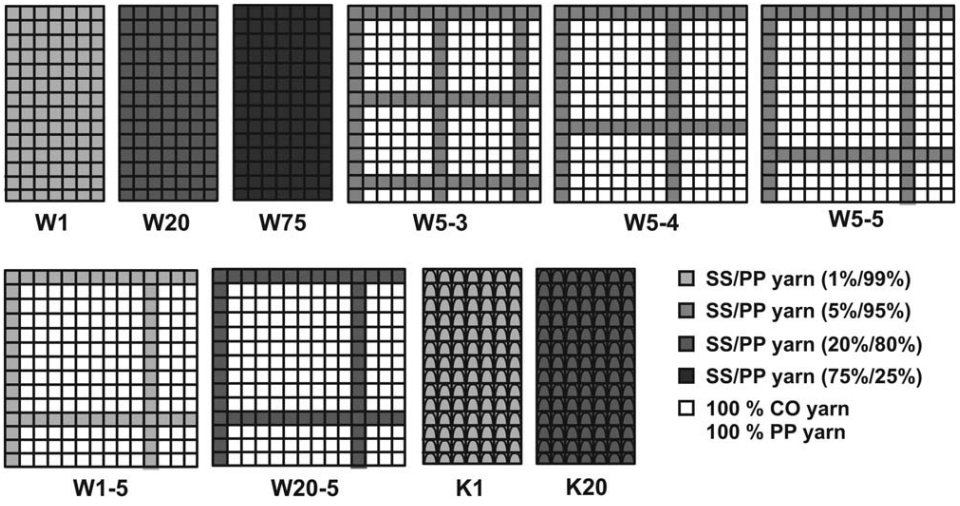

FIG. 2. Schematic diagram of hybrid fabric structure (grey squares: hybrid yarns, white squares: 100 % cotton yarns or 100% polyestere yarns).

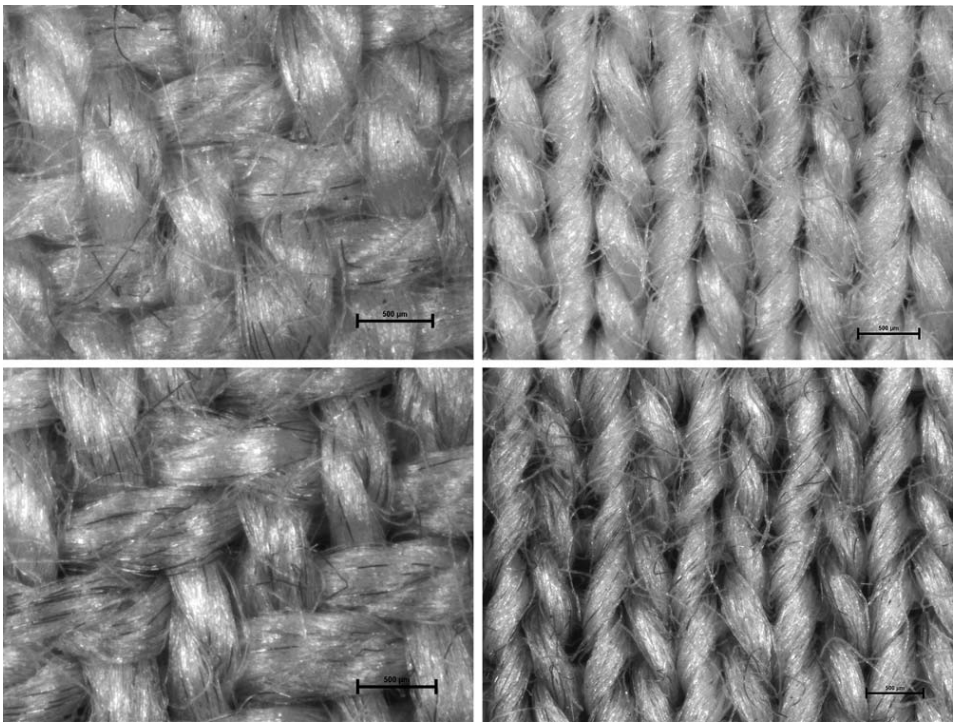

FIG. 3. Microscopic images of sample: (a) W5, (b) W20, (c) K1, (d) K20.

The random variable

$$T_L = \frac{P_L}{R_L} = \frac{x_L + x_U}{2\,(x_U - x_L)} \tag{8}$$

has approximately symmetric distribution and its quantiles are given in Ref. 28.

The 95% confidence interval of the mean is expressed by pivot statistics as

$$P_L - R_L t_{L,0.95}(n) \le \mu \le P_L + R_L t_{L,0,95}(n) \tag{9}$$

and analogously hypothesis testing may also be carried out. For small samples ($4 \le n \le 20$), the pivot statistics lead to more reliable results than the application of Student's F-test or robust t-tests.

Characterization

Electromagnetic Shielding Effectiveness Evaluation. SE of the high-performance hybrid fabrics was measured according to ASTM D 4935-10 [29], for planar materials using a plane-wave, far-field EM wave. SE of samples was measured over frequency range of 30 MHz to 1.5 GHz. The set-up consisted of a sample holder with its input and output connected to the network analyzer. A shielding effectiveness test fixture (Electro-Metrics, Inc., model EM-2107A) was used to hold the sample. The design and dimension of sample holder follows the ASTM method mentioned above. Network analyzer Rohde & Schwarz ZN3 was used to generate and receive the electromagnetic signals. The standard mentioned above determines the electromagnetic shielding effectiveness of the fabric using the insertion-loss method. A reference measurement for the empty cell was required for the shielding effectiveness assessment. A "through" calibration by the help of the reference sample was made first. A load measurement was performed on a solid disk shape sample subsequently. The reference and load specimens must be of the same material and thickness. Sample (both reference and load) geometries according to ASTM D 4935-10 are shown in Fig. 4.

On the basis of logarithmic relation between electromagnetic shielding effectiveness and frequency [20]

$$\mathrm{SE} = a + b\log(f) + c\sqrt{f}, \tag{10}$$

where a, b, c are constants depending on characteristic impedance of shield material and characteristic impedance of medium surrounding the shield, f is frequency, the values beyond the original observation range (e.g., for $f = 2.45$ GHz) were estimated by extrapolation process. Logarithmic relation (10) is valid only for woven fabrics, therefore SE values beyond the measured frequency range were determined only for first three groups of samples.

The measurement was carried out at five different places of textile samples because of subsequent statistical analysis, $\alpha = 0.05$, $t_{L,0.95}(5) = 1.37$. The mean values estimator (pivot half sums), pivot ranges, confidence intervals for means of SE for frequency 600 MHz, 1.5 GHz, and

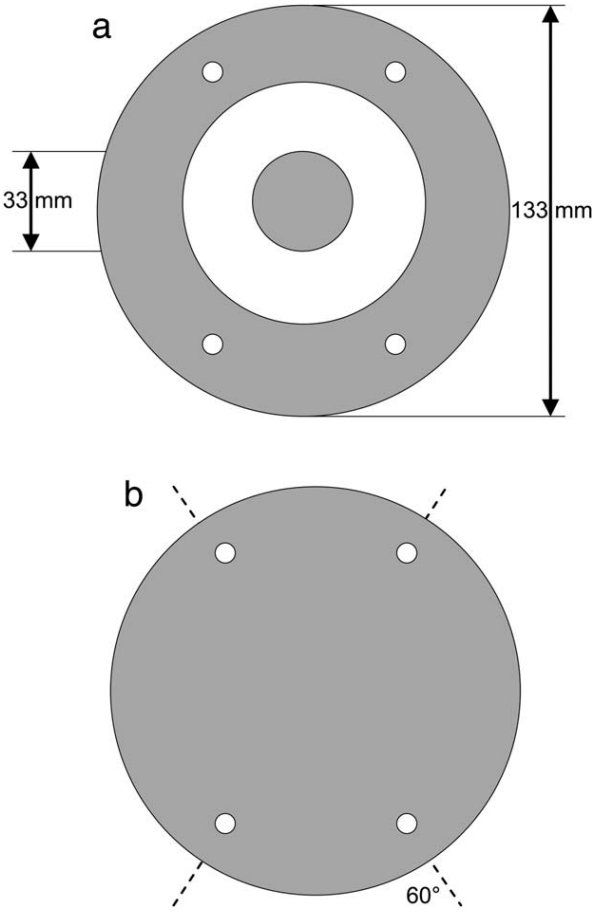

FIG. 4. Illustrations of (a) reference and (b) load sample.

2.45 GHz are summarized in Table 4. To study the effect of number of fabric layers on the total electromagnetic shielding effectiveness, 1, 2, 3, 4, and 5 layers of same fabrics (sample W1 with composition 1% SS/99% PP) were sandwiched before carrying out the test. These samples are marked W1 × 1 – W1 × 5. To study the effect of moisture content on the total electromagnetic shielding effectiveness, fabric W3 (sample with composition 3% SS/97%PP) was gradually moisten to get as much as 140% regain. These samples are marked W3-m0 – W3-m140. In this case only one sample of each regain was measured due to quick changes of moister content in fabric. To measure the moisture content of wet textile sample, procedure adopted form ASTM D 2654 [30] standard was used. This standard uses oven drying procedure, using ambient air heated to 105 ± 2°C (dry until change in sample mass <0.01% at 2 h intervals) to record the moisture regain percentage according to the following formula

$$m = \frac{L-W}{W} 100\,[\%], \tag{11}$$

where L is weight (g) of the wet specimen before drying and W is weight (g) of oven dried (ultra dry) specimen.

RESULTS AND DISCUSSION

Frequency Dependent Analysis of Electromagnetic Shielding Effectiveness

Figure 5 shows the variation in SE for all groups of fabrics with incident frequency in the range 30 to 1,500 MHz. It was confirmed that the electromagnetic shielding effectiveness increased logarithmically with the increasing frequency for woven sets of samples. Electromagnetic shielding effectiveness out of the measured range (1,500 MHz–2,450 MHz) was calculated by the extrapolation in terms of (10) for woven fabrics. It stands for woven fabrics, that SE is strongly increasing function of frequency below about 1,500 MHz, while the SE is more slowly increasing function of frequency in the range above 1,500 MHz. It seems that electromagnetic shielding effectiveness will not increase dramatically above 2,450 MHz. As frequency increases, the wavelength of the electromagnetic wave decreases and becomes closer to the size of the fiber. Wave length 0.2 m (0.12 m) corresponds to frequency 1,500 MHz (2,450 MHz), which is much lower compared with diameter of metal fiber (8 μm) or yarn diameter (∼0.5 mm). Thus, the higher frequency waves are more likely to encounter fiber embedded in the polymer matrix [16]. Hence, SE increases as the frequency increases. Dependence of SE on frequency for knitted group of samples behaves differently compared with woven samples. Frequency dependence of knitted samples SE was approximated by cubic spline function with smoothing parameter $p \rightarrow 0$, which possesses a sufficiently high degree of smoothness. The position of the SE global maximum is possible to observe about frequency 1.1 GHz for sample K15 and K20. In case of knitted samples, extrapolation out of the measured range is not suitable.

All studied woven fabrics have the same 2/2 twill structure. Warp and weft density of the fabrics and linear density of the warp and weft yarns were fixed. The differences in the woven fabrics were blend rations (therefore changes in mass per unit area of samples), hybrid yarn densities, number of fabric layers forming sandwich, and moister content. All studied knitted fabrics have also the same structure—single jersey knit. Number of wales and courses per cm of the fabrics and linear density of the yarns were fixed. The differences in the knitted fabrics were only blend rations (changes in mass per unit area of samples). Based on exploring Fig. 5 it is possible to summarize, that the fabric with the highest content of conductive component (metal fiber) along with the highest cover factor (W75) has the highest electromagnetic shielding effectiveness from all studied samples through studied frequency range. Knitted samples with identical content of metal fiber have lower SE compared with woven sample. This phenomenon is caused by lower weight and lower cover factor of knitted samples compared with woven ones. The results show that SE increases with

TABLE 4. Results of electromagnetic shielding effectiveness evaluation.

	Electromagnetic shielding effectiveness SE (dB)								
	$f = 600$ GHz			$f = 1.5$ GHz			$f = 2.45$ GHz		
Sample	Pivot half sum, P_L	Pivot range, R_L	95% CI	Pivot half sum, P_L	Pivot range, R_L	95% CI	Pivot half sum, P_L	Pivot range, R_L	95% CI
W1	7.19	0.31	±0.42	13.16	0.63	±0.86	17.82	0.55	±0.76
W3	14.04	0.45	±0.62	20.36	0.45	±0.62	24.34	0.71	±0.97
W5	17.11	0.52	±0.71	23.83	0.47	±0.64	27.91	0.53	±0.73
W10	23.16	0.35	±0.48	28.89	0.23	±0.32	31.79	0.46	±0.63
W15	27.41	0.10	±0.14	32.47	0.24	±0.33	34.70	0.43	±0.59
W20	30.04	0.32	±0.44	34.59	0.24	±0.33	36.43	0.49	±0.67
W40	38.99	0.36	±0.49	41.99	0.29	±0.40	43.12	0.71	±0.97
W60	41.95	0.19	±0.26	45.14	0.15	±0.20	46.42	0.84	±1.15
W75	45.90	0.18	±0.25	50.50	0.45	±0.62	53.36	1	±1.37
W1 × 1	7.19	0.31	±0.42	13.16	0.63	±0.86	17.82	0.55	±0.76
W1 × 2	12.98	0.28	±0.39	17.22	0.23	±0.32	19.07	0.45	±0.62
W1 × 3	18.73	0.48	±0.66	22.39	0.15	±0.21	23.60	0.38	±0.52
W1 × 4	24.83	0.61	±0.84	26.91	0.41	±0.56	26.19	0.43	±0.59
W1 × 5	29.66	0.50	±0.69	30.66	0.58	±0.80	28.69	0.55	±0.75
W3-m0	13.53	—	—	19.34	—	—	22.88	—	—
W3-m16	18.39	—	—	22.28	—	—	24.09	—	—
W3-m36	20.30	—	—	24.18	—	—	26.47	—	—
W3-m62	23.21	—	—	25.94	—	—	27.19	—	—
W3-m86	24.60	—	—	26.91	—	—	27.56	—	—
W3-m103	25.53	—	—	27.42	—	—	27.75	—	—
W3-m117	26.57	—	—	27.51	—	—	26.95	—	—
W3-m140	26.87	—	—	27.70	—	—	27.07	—	—
W5-3	5.40	0.32	±0.44	11.63	0.26	±0.35	16.56	0.28	±0.39
W5-4	4.33	0.29	±0.41	9.91	0.45	±0.62	14.61	0.31	±0.43
W5-5	3.32	0.44	±0.60	8.21	0.54	±0.74	12.58	0.27	±0.39
W1-5	0.28	0.15	±0.20	1.33	0.37	±0.51	2.14	0.9	±0.12
W3-5	1.62	0.29	±0.41	4.29	0.18	±0.24	5.67	0.18	±0.23
W5-5	3.16	0.74	±1.02	6.84	0.78	±1.07	8.01	0.22	±0.30
W10-5	5.10	0.29	±0.41	9.75	0.72	±0.98	11.06	0.24	±0.33
W15-5	7.82	0.27	±0.37	12.63	0.56	±0.79	13.34	0.28	±0.39
W20-5	11.00	0.13	±0.18	14.42	0.68	±0.93	14.13	0.29	±0.41
K1	0.34	0.04	±0.05	0.40	0.09	±0.12	—	—	—
K3	0.31	0.02	±0.03	0.76	0.19	±0.26	—	—	—
K5	0.44	0.09	±0.12	2.33	0.53	±0.73	—	—	—
K10	1.42	0.26	±0.35	7.63	0.66	±0.90	—	—	—
K15	4.29	0.97	±1.33	9.69	0.25	±0.35	—	—	—
K20	4.64	0.47	±0.65	9.51	0.26	±0.36	—	—	—

increase in number of fabric layers as well as moisture content. The higher the density of hybrid yarn (smaller opening), the higher SE.

Effect of Metal Content

The effect of metal content on the SE has been already well established (e.g., Refs. 10, 31, and 32). As expected, SS had a strong influence on the SE characteristics of fabrics. It was confirmed in this study that electromagnetic shielding effectiveness increases with increasing metal fiber content. Sample W75 with the highest content of metal fiber reaches the highest electromagnetic shielding effectiveness—50.5 dB for frequency 1,500 MHz, whereas sample W1 containing the lowest portion of conductive component displays the lowest electromagnetic SE (13.16 dB for frequency 1,500 MHz). Figure 6a shows the effect of metal content (P) on SE for the first groups of woven samples for frequency 1,500 MHz. This frequency was found interesting because it is included in the measured range and close to working frequency of particular electric devices. Many GSM phones support 1,800 MHz band. The overall SE increased according to power function with metal content (Fig. 6a). At very low conductive fiber loadings, the SE remains similar to that of the pure matrix material, i.e., almost zero. Then, at a point called the percolation threshold (analogically with electrical percolation threshold), the SE increases dramatically over a very narrow range of fiber concentration. In this material system, percolation threshold (P_0) occurred about 3 to 5 wt% of conductive component. It is an important phenomenon for the polymer matrix composites

 DOI 10.1002/pc

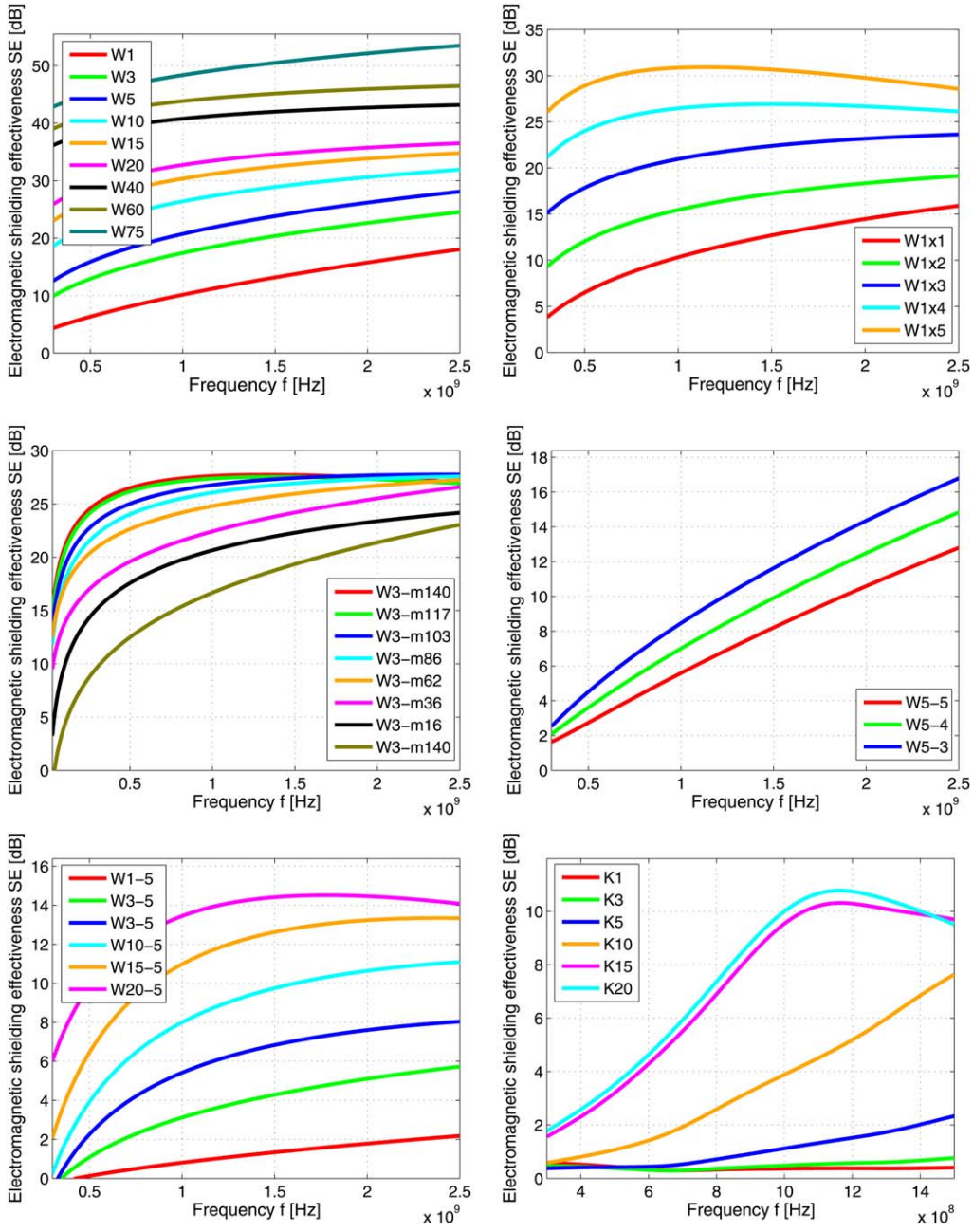

FIG. 5. The dependence of shielding effectiveness on frequency for (a) woven samples made of 100 % hybrid yarn, (b) sandwitched woven samples, (c) woven samples with different moisture content, (d) woven samples with open grid structure – constant content of metal fiber, different spacing, (e) woven samples with open grid structure – constant spacing, different metal fiber content, (f) knitted samples made of 100 % hybrid yarn. [Color figure can be viewed at wileyonlinelibrary.com.]

which shows at which minimum wt% of the filler (metal fiber) the conductivity of the polymer matrix composite increased. Generally at higher fiber amounts the SE begins to level out again at a value many orders of magnitude higher than that of the pure matrix material. The dependence of SE on P for the range above P_0 ($P > 10\%$) can be simply approximated by line (see Fig. 6b). The solid line in this graph corresponds to the linear regression model with parameters obtained by the minimizing sum of squared differences. This linear regression model can be used for prediction of the value of P for sufficient shielding. For example for samples W3–W75

$$P = \frac{\mathrm{SE} - 27.58}{0.31} \tag{12}$$

For example the SE = 35 dB can be obtained at conductive component concentration $P = 24\%$. The

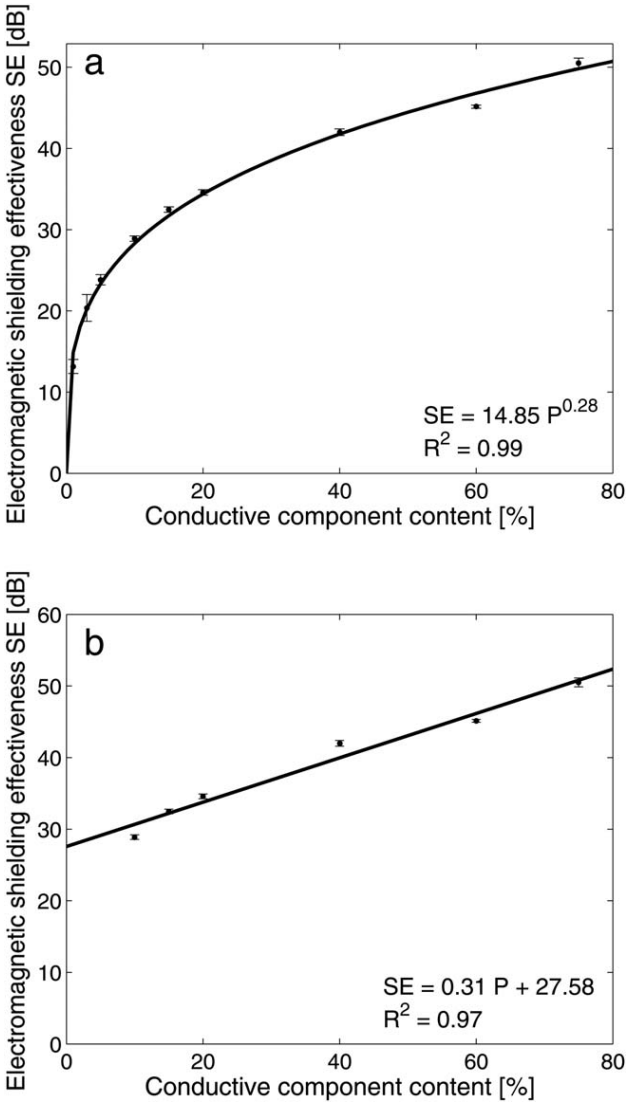

FIG. 6. The dependence of shielding effectiveness on metal fiber content for (a) samples: W1–W75, (b) samples with conductive component above percolation threshold: W10–W75.

prediction ability of this line model is restricted to the content of conductive component above percolation threshold P_o. Behavior of the dependence of SE on metal fiber content described above was also observed for group of samples containing grid structure (W1-5 – W20-5, see Fig. 7) and also for other frequencies.

Figure 8 shows dependence of SE on conductive component for group of knitted samples at frequency 1 GHz and 1.5 GHz. It was confirmed that electromagnetic shielding effectiveness increases with increasing metal fiber content. Sample without metal fiber embodies zero ability to shield electromagnetic radiation. Knitted structure containing 1% of metal fiber had SE lower than 1 dB, while knitted fabric made of hybrid yarn containing 20% of metal fiber had SE about 10 dB. This dependence was approximated by cubic spline function. Percolation threshold is about 10% of conductive component for knitted samples.

Effect of Number of Fabric Layers

One of the ways to increase electromagnetic shielding effectiveness is to increase the thickness of conductive material. Figure 9 illustrates the effect of the number of fabric layers (n) on the SE of woven fabrics. The results clearly show that SE increases linearly with the increase in the number of fabric layers. It is clear from *Eq. 2* that as the thickness (t) increases the absorption loss (A) also increases. According to the above equation, the SE of any material is directly proportional to the thickness of material apart from the other parameters that are related. Comparing SE of sample containing 5% of SS (W5, SE = 23.83 at $f = 1.5$ GHz) and sandwich composed of five layers of fabric W1 (W1 × 5, SE = 30.66 at $f = 1.5$ GHz) in Table 4, it can be examined that it is preferable to use sandwich system than plane single layer containing the same portion of conductive component in the term of conductive component content. This

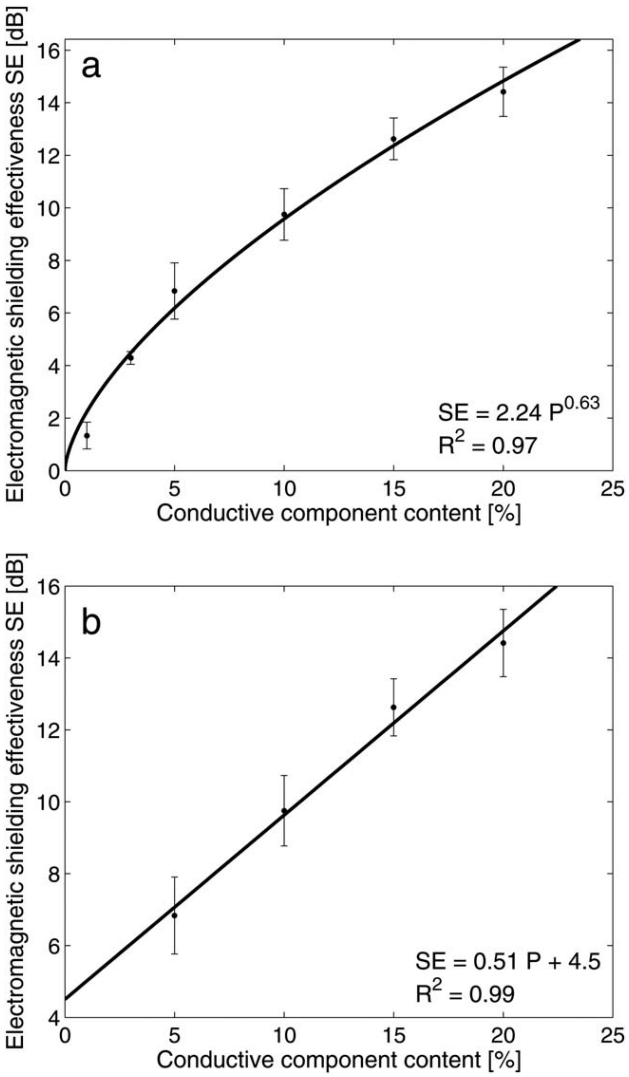

FIG. 7. The dependence of shielding effectiveness on metal fiber content for (a) samples: W1-5–W20-5, (b) samples with conductive component above percolation threshold: W5-5–W20-5.

 DOI 10.1002/pc

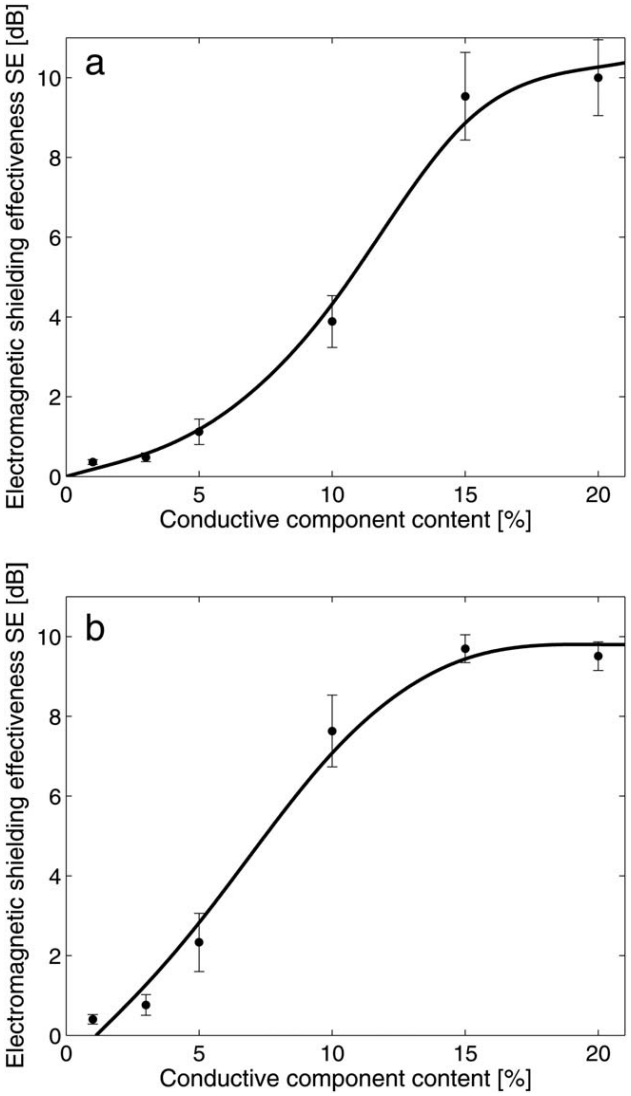

FIG. 8. The dependence of shielding effectiveness on metal fiber content for knitted samples at frequency (a) 1 GHz, (b) 1.5 GHz.

phenomenon is due to the fact that one layer above the other can cover the apertures of the preceding layer and blocks the direct path of electromagnetic wave.

Effect of Moisture Content

It is expected that the moisture content of material also has an important effect on their electrical properties and therefore on their electromagnetic shielding effectiveness. Generally, the resistance decreases (conductivity increases) with increasing moisture content. Figure 10 shows the change in electromagnetic shielding effectiveness with moisture content (m) for a sample W3. The dependence of SE on moisture content is possible to approximate by power function. The changes in electromagnetic shielding ability are large especially in the area of $0\% < m < 80\%$: there is approximately 2 dB increase in SE for every 15% increase in the fabric moisture content. The results show that after saturation of sample with water (about $m > 80\%$) the SE is almost constant. We can summarize that the SE is strongly dependent on water content, which is a caused by following phenomena. Water itself has a much higher permittivity ($\varepsilon_{\text{r-water}} = 80$) than the material making up the fiber/fabric ($\varepsilon_{\text{r-PP}} \sim 3$) and so as moisture is absorbed by the fiber/fabric the overall value of SE is influenced by this [33].

Effect of Hybrid Yarn Density

Figure 11 illustrates the effect of hybrid yarn density d on the SE of fabric for both chosen frequencies. In this case twill weave samples with fixed content of metal fiber (5%) in which hybrid yarns were inserted in certain intervals (3, 4, 5 mm) were used. Sample made totally of hybrid yarn containing 5% of metal fiber (W5) was also included to this part of the study. The results clearly show that SE increases logarithmically with the increase in the hybrid

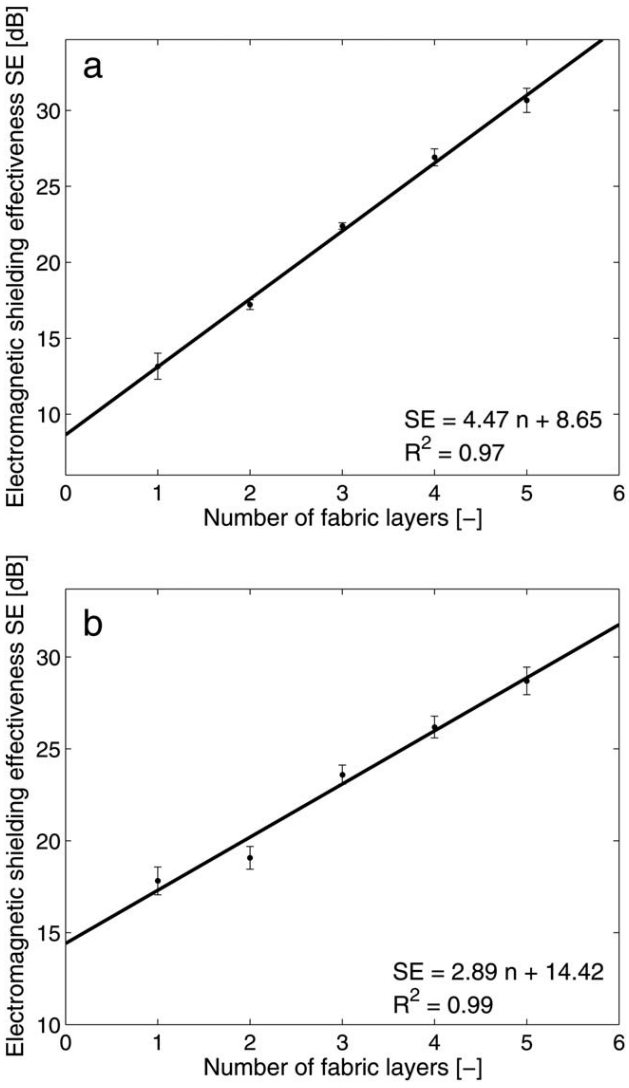

FIG. 9. The dependence of shielding effectiveness on number of fabric layers for frequency (a) 1.5 GHz, (b) 2.45 GHz.

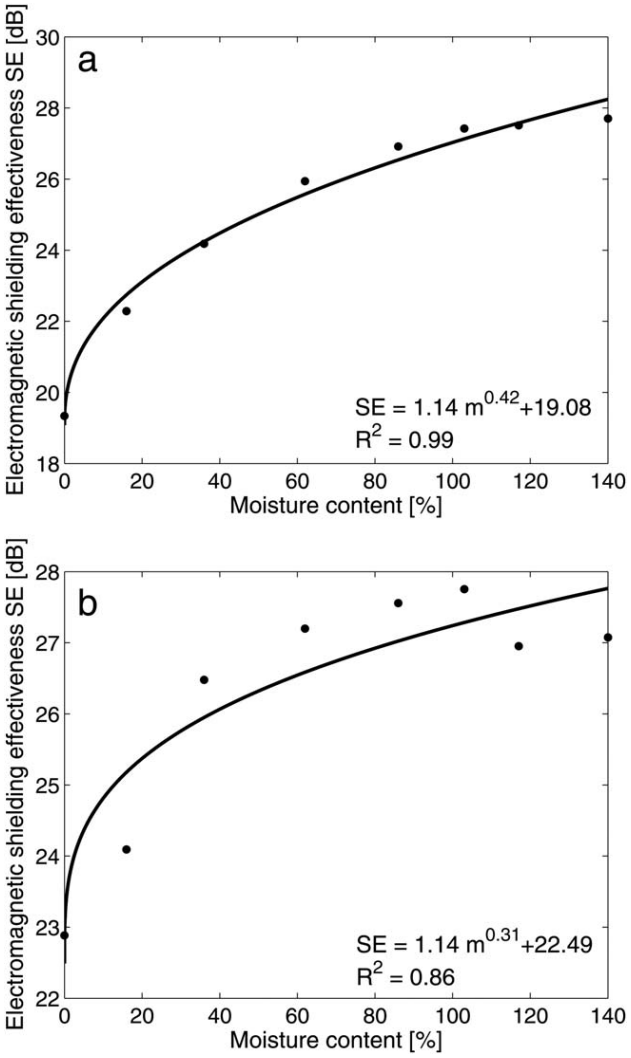

FIG. 10. The dependence of shielding effectiveness on moisture content of fabric at frequency (a) 1.5 GHz, (b) 2.45 GHz.

yarn density. This can be explained by the fact that fabric with smaller hybrid yarn spacing (higher density of hybrid yarn) has a larger amount of metal fiber than fabrics with larger hybrid yarn spacing. Again, the results confirm that the more conductive component content material contains, the higher electromagnetic shielding effectiveness is.

Effect of Nonconductive Matrix Material

In this section two samples having the same 2/2 twill structure, the same warp and weft density and the same density of hybrid yarn (the same openness) with fixed content of metal fiber (5%) was compared according to their electromagnetic shielding effectiveness at three different frequencies. The difference in these two samples (marked W5-5) was type of nonconductive matrix material. First nonconductive matrix in which hybrid yarn is making up conductive grid was made of 100% cotton yarn (CO), while second nonconductive matrix was made of 100% polypropylene yarn (PP). Results show (Fig. 12) that sample with cotton matrix reached higher SE at all studied frequencies. The total average difference between SE of both samples is 5.2 dB at whole frequency range. This can be explained by the fact, that polypropylene yarn has extremely high resistivity (R_{PP} ~3E + 12 Ω m at 65% RH and 20°C) in comparison with cotton (R_{CO} ~6E + 09 Ω m at 65% RH and 20°C) [32]. This effect is supported by the fact that natural fibers exhibit a relatively high hydrophilic property and this property causes the natural fibers to exhibit relatively high electric conductivity at a relatively high humidity due to a relatively high content of moisture absorbed in natural fibers. PP has also low wettability (v_p = 0–0.005% at 65% RH and 20°C) compared with CO (v_p = 7.6–8.6% at 65% RH and 20°C) [33].

Effect of Structure

In this section samples having identical metal fiber content and different structure were compared according

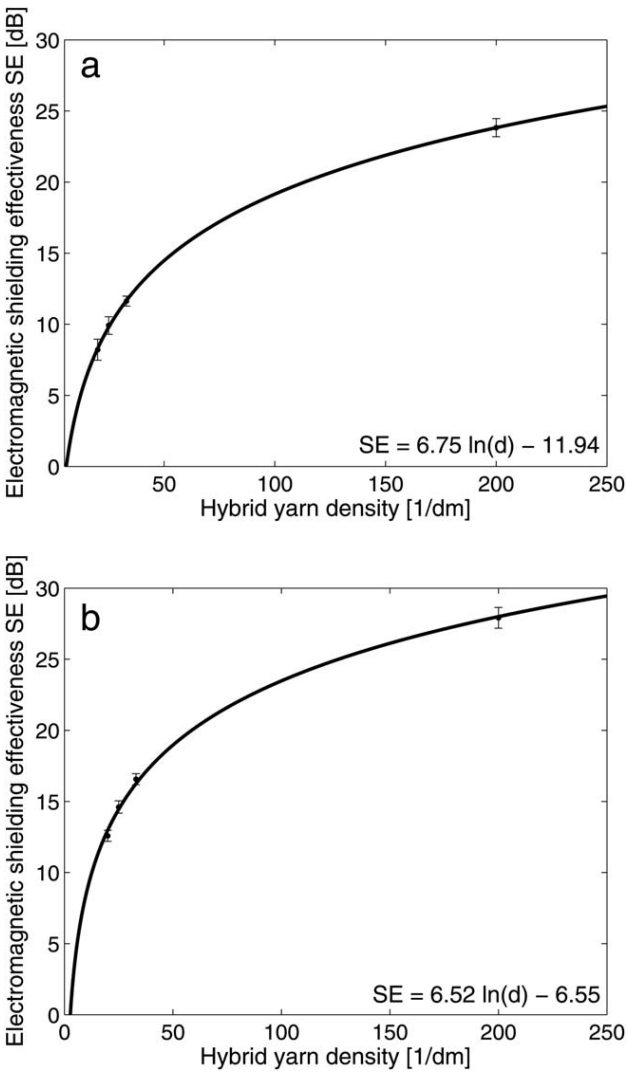

FIG. 11. The dependence of shielding effectiveness on hybrid yarn spacing at (a) 1.5 GHz, (b) 2.45 GHz.

 DOI 10.1002/pc

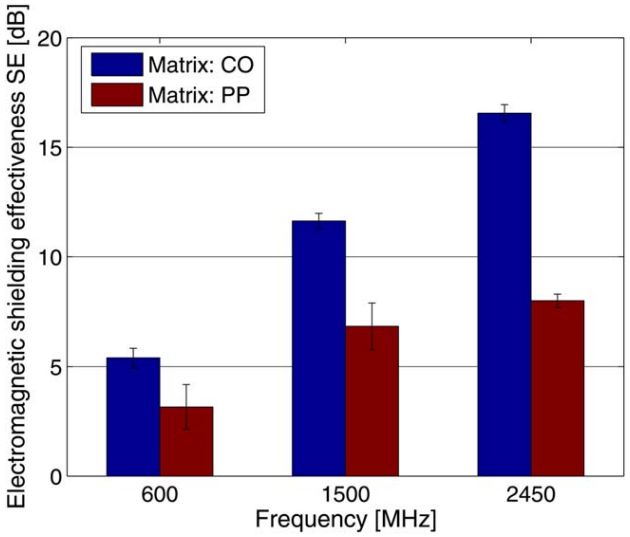

FIG. 12. Comparison of SE of samples with different matrix material (PP, CO) at different frequencies. [Color figure can be viewed at wileyonlinelibrary.com.]

to their electromagnetic shielding effectiveness at different frequencies. As shown in Fig. 13 and Table 4, electromagnetic shielding of the woven fabrics is generally higher compared with electromagnetic shielding of knitted samples. The difference between SE of both types of structures (woven, knitted) ranges from 7 to 25 dB. The higher the metal fibers content in the hybrid yarn the higher differences between SE. The total average difference between SE of both samples is about 19 dB at whole frequency range. These results were expected because the knitted fabrics were made of finer yarn (25 tex), had lower mass per unit area (154 g/m^2 on the average), and lower thickness (0.65 mm) and therefore higher porosity compared with woven fabrics ($T = 50$ tex, $m = 220$ g/m^2, $t = 0.75$ mm). Moreover, woven fabrics contain higher content of conductive component at specific unit of area or volume than knitted samples (due to utilization of thicker yarns and higher mass per unit area), which significantly influence total electromagnetic shielding effectiveness as already mentioned.

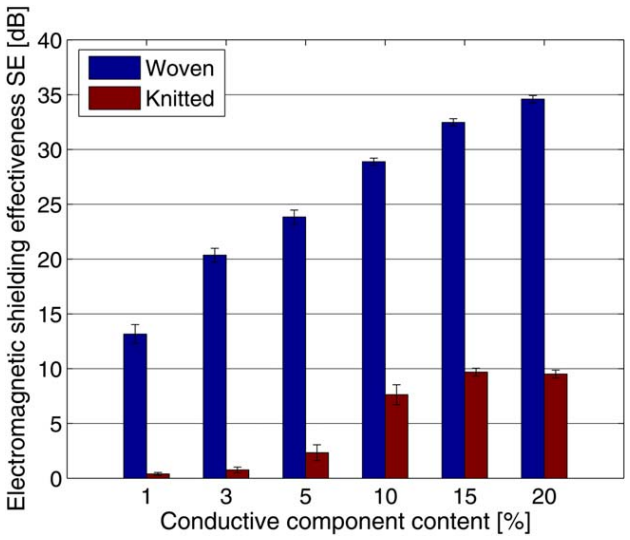

FIG. 13. Comparison of SE of samples with different structure (woven, knitted) at 1.5 GHz. [Color figure can be viewed at wileyonlinelibrary.com.]

Comparison of Different Types of Conductive Sheets

Table 5 shows the comparison of different types of conductive fabrics with metal composite fabrics developed during this study. Although some of the these materials have higher SE (aluminum foil, copper coated fabric, carbon fabric) than developed metal composite fabrics, not all of them are suitable for using like an ordinary fabric (e.g., flexibility, drapability, durability, comfort properties, sewing, washing, etc.). Lightweight metal composite fabrics described in this article in which extremely thin staple metal fibers used as a conductive component meet requirements mentioned above. The production of these yarns and fabrics is made by traditional techniques, they are flexible enough, have a nice drape, excellent comfort properties, they can be treated as ordinary fabrics (sewn, dyed, washed, etc.).

CONCLUSIONS

This article presents the present state of fabrication and characterization of multifunctional light weight flexible fabrics with increased resistance to electromagnetic radiation while preserving basic properties of textile structures designated for clothing or special technical purposes. For purpose of this study, extremely thin stainless steel staple fibers were incorporated to yarn structure as conductive fillers. Plane-wave shielding properties of the composite fabrics were measured between 30 and 1,500 MHz using coaxial transmission line method and the main parameters influencing electromagnetic shielding properties of the composite fabric were investigated.

As expected, SS has a strong influence on the SE characteristic of the fabrics. By controlling the amount of SS (through variations in blend ratio and through hybrid yarn

TABLE 5. Electromagnetic shielding effectiveness of chosen conductive planar materials measured according to ASTM D 4935-10 at frequency 1,500 MHz (metal composite fabrics developed in this study are emphasized using bold letters).

Material	SE (dB)
Woven fabric made of 100% cotton yarn	0
Hybrid knitted fabric—80% PP/20% SS	**10**
Hybrid woven fabric containing conductive mesh 5 × 5 mm, 80% PP/20% SS	**14**
Polypyrrole coated woven PES fabric	20
Hybrid woven fabric—25% PP/75% SS	**50**
100% carbon fiber fabric (190 g/m^2)	57
Copper coated woven PES fabric	67
100% aluminum foil (30 g/m^2)	80

density), the SE of the fabric can be easily adjusted. Sample with the highest content of metal fiber reaches the highest electromagnetic shielding effectiveness—50.5 dB for frequency 1,500 MHz, whereas sample containing the lowest portion of conductive component displays the lowest electromagnetic SE (13.16 dB for frequency 1,500 MHz). Percolation thresholds of conductive component were examined and linear regression model was proposed. This model can be used for prediction of the certain value of conductive component for sufficient shielding. Analogically, sample with the highest hybrid yarn density (200 yarns/dm) reaches the highest electromagnetic shielding effectiveness—23.8 dB for frequency 1,500 MHz, whereas sample with the lowest hybrid yarn density (20 yarns/dm) displays the lowest SE (8.2 dB for frequency 1,500 MHz) at fixed conductive component content (5 wt%).

Electromagnetic shielding effectiveness of the metal composite could be also tailored by modifying geometry of the structure. Sandwich with highest thickness (3.9 mm) has the highest shielding effectiveness—30.7 dB for frequency 1,500 MHz, whereas sample with the lowest thickness (0.78 mm) has the lowest SE (13.1 dB for frequency 1,500 MHz) at fixed conductive component content (1 wt%). Samples with lower porosity and more compact structure (woven fabrics) exhibit higher SE (even 35 dB for frequency 1,500 MHz) compared with knitted samples (SE only about 10 dB for frequency 1,500 MHz) at fixed conductive component content (20 wt%).

Moisture content and hydrophilic property of nonconductive component can also significantly affect the total electromagnetic shielding effectiveness of sample. Hydrophilic fibers are preferred ones, because the resistance decreases (conductivity increases) with increasing moisture content and therefore total shielding effectiveness also increases.

Generally, it is said that conductive materials with 40 to 50 dB of electromagnetic shielding effectiveness can prevent electromagnetic interference emitted from 90% of current commercial electronic devices [12]. Ability of textile structures containing stainless steel staple fibers to shield electromagnetic field can be controlled by following: (a) higher content of conductive component in hybrid yarn, respectively, smaller resistivity of textile structure gives higher electromagnetic shielding effectiveness, (b) higher hybrid yarn density, which corresponds with metal fiber content, (c) higher thickness using e.g., multilayered system which provides blocking of the direct path of electromagnetic wave, (d) higher moister content which increases electrical conductivity and therefore electromagnetic shielding ability, (e) nonconductive component should exhibit hydrophilic property according to preferable higher total moister content, (f) more compact structure—woven fabrics are preferred to single knitted fabrics.

When comparing different types of conductive fabric with metal composite fabrics developed during this study, it can be concluded, that even through chosen sheets have higher SE than developed metal composite fabrics, not all of them are suitable for using like an ordinary fabric. Described metal composite textile shields possess flexibility, drapability, durability, comfort properties, and they can be manufactured by traditional textile production techniques, they can be joined by sewing, they can be washed without loss of functionality, etc. Therefore they have many possible applications such as radiofrequency protective suits, tents, curtains or tapestry, smart clothing with incorporated conductive paths, electrostatic dissipative material for clothing or equipment, clean room working clothes, etc.

ACKNOWLEDGMENT

This article is original and has not been presented or published till now.

REFERENCES

1. World Health Organization, *Establishing a Dialogue on Risks from Electromagnetic Fields*, WHO, Geneva (2002).
2. Committee on the Environment, Agriculture and Local and Regional Affairs, *The Potential Dangers of Electromagnetic Fields and Their Effect on the Environment*, CE, Strasbourg (2011).
3. J.F.B. Bolte and M.J.M. Pruppers, Electromagnetic Fields in the Working Environment. Ministry of Social Affairs and Employment (SZW) Report, Netherlands (2006).
4. J. Avloni, R. Lau, M. Ouyang, L. Florio, A.R. Henn, and A. Sparavigna *J. Ind. Text*., **38**, 55 (2008).
5. L.E. Polisky, *Radiation Hazards Issues for Telecommunication Facility Professionals*, Comsearch, Ashburn (2005).
6. Z.C. Yu, J.F. Z.W. Lou, and J.H. Lin, *Text. Res. J*., **85**, 188 (2015).
7. K. B. Cheng, M. L. Lee, S. Ramakrishna, and T. H. Ueng, *Text. Res. J*., **71**, 42 (2001).
8. Ch. I. Su and J. T. Chern, *Text. Res. J*., **74**, 51 (2004).
9. H. G. Ortlek, T. Alpyildiz, and G. Kilic. *Text. Res. J*., **83**, 90 (2013).
10. D. Duran and H. Kadoglu, *J. Text. Apparel*, **22**, 354 (2012).
11. V. Safarova and J. Militky, *Text. Res. J*., **84**, 1255 (2014).
12. S. Shinagawa, Y. Kumagai, and K. Urabe, *J. Porous Mater*., **6**, 185 (1999).
13. Y. Lu and L. Xue, *Compos. Sci. Technol*., **72**, 828 (2012).
14. J. Avloni, M. Ouyang, L. Florio, A.N. Henn, and A. Sparavigna, *J. Thermoplas. Compos. Mat*., **20**, 241 (2007).
15. Z. Yidiz, I. Usta, and A. Gungor, *Text. Res. J*., **82**, 2137 (2012).
16. J.M. Keith, N.B. Janda, and J.A. King, *Polym. Compos*., **26**, 671 (2005).
17. L. Vojtech and M. Neruda, *Fibres Text. East. Eur*., **21**, 141 (2013).
18. T. Ramachandran and C. Vigneswaran, *J. Ind. Text*., **39**, 81 (2009).

19. L. Vojtech, M. Neruda, and J. Hajek, *Int. J. Commun. Antenna Propag*., **1**, 21 (2011).
20. H. W. Ott, Electromagnetic Compatibility Engineering, Wiley, New York (2009).
21. D. D. L. Chung, *J. Mater. Eng. Perform*., **9**, 350 (2000).
22. D. White, *A Handbook Series on Electromagnetic Interference and Compatibility*, Don White Consultants, Virginia (1971).
23. R. Simon, *Polym. Plast. Technol. Eng*., **17**, 1 (1981)
24. N. Colaneri and L. Shacklette, *IEEE Trans. Instrum. Meas*., **41**, 291 (1992).
25. R. Perumalraja, B. S. Dasaradan, A. Anbarasu, P. Arokiaraj, and L. Harish, *J. Text. Inst*., **100**, 512 (2009).
26. V. Safarova, M. Tunak, and J. Militky, *Text. Res. J*., **85**, 673 (2015).
27. S. Geetha, K.K.S. Kumar, Ch. R.K. Rao, M. Vijayan, and D.C. Trivedi, *J. Appl. Polym. Sci*., **112**, 2073 (2009).
28. P.S. Horn, *J. Am. Stat. Assoc*., **78**, 930 (1983).
29. ASTM D 4935-10, *Standard Test Method for Measuring the Electromagnetic Shielding Effectiveness of Planar Materials*, ASTM International, West Conshohocken, PA (2010).
30. ASTM D 2654, Test Methods for Moisture in Textiles, ASTM International, West Conshohocken, PA (1997).
31. K.B. Cheng. T.W. Cheng, K.C. Lee, T.H. Ueng, and W.H. Hsing, *Compos. A*, **34**, 971 (2003).
32. H.M. Kim, K. Kim, C.Y. Lee, J. Joo, S.J. Cho, H.S. Yoon, D.A. Pejakovic, J.W. Yoo, and A.J. Epstein, *Appl. Phys. Lett*., **84**, 589 (2004).
33. W.E. morton and J.W.S. Hearle, *Physical Properties of Textile Fibres*, CRC Press, Boca Raton (2008).

Appendix 8

V. Safarova, M. Tunak, M. Truhlar, and J. Militky, "A new method and apparatus for evaluating the electromagnetic shielding effectiveness of textiles," Textile Research Journal, vol. 86, no. 1, pp. 44–56, 2016.

Textile Research Journal

Original article

Textile Research Journal
2016, Vol. 86(1) 44–56

DOI: 10.1177/0040517515581587
trj.sagepub.com
SAGE

A new method and apparatus for evaluating the electromagnetic shielding effectiveness of textiles

Veronika Šafářová[1], Maroš Tunák[1], Martin Truhlář[2] and Jiří Militký[1]

Abstract

Textile structures with electromagnetic shielding ability are widely used to attenuate the strength of electromagnetic fields, and their functionality is evaluated through direct measurement of their electromagnetic shielding effectiveness. Depending on the size of the shield and measured frequency range, various test methods can be used. There is still a need for development of a rapid testing procedure designed for special materials where only small samples are accessible. The paper presents a new convenient shielding effectiveness measuring procedure based on the modified shielded box method. The design, construction, and testing results of a new device are described in this paper. The proposed method is primarily designed for rapid comparative measurements of newly fabricated samples of relatively small size. Replacement of existing measurement standards is not the goal of this proposal. The main advantages of the new device and methodology are a small required sample size, no necessity of sample preparation to special shapes or dimensions, rapid measurements, and simple and cheap equipment in comparison with standardized equipment. To prove usability of the proposed method the electromagnetic shielding effectiveness of a textile sample set was tested with the help of the new method and the obtained results were statistically compared with those gained by the coaxial transmission line method based on ASTM D 4935-10. The agreement between results from the proposed and comparative methods was verified for textile samples with low and intermediate electric conductivity. Suitability, scope of application, benefits, and limitations of proposed measuring system are discussed.

Keywords

electromagnetic shielding effectiveness, testing. textile materials

Materials with electromagnetic shielding efficiency are widely used to attenuate the strength of electromagnetic fields to increase susceptibility of electrotechnic devices and reduce interference of the devices.[1] One modern application is not only technical protection, but also protection of human beings while operating specific electric equipment. In these days, instead of metallic shields it is more common to use various types of textile materials due to their desirable flexibility and light weight.

Usage of minute electrically conductive fibers is one way how to create conductive fabrics. They can be produced in filament or staple lengths and can be incorporate with traditional non-conductive fibers to create yarns that possess varying degrees of conductivity.[2–7] Another way is conductive coatings, which can transform substrates into electrically conductive materials without significantly altering the existing substrate properties. They can be applied to the surface of fibers, yarns, or fabrics. The most common are metals[8–10] and conductive polymer coatings.[11,12] The main disadvantages are that plated metal or conductive polymer coatings can be easily peeled off the fiber during processing and use, and they consequently have a poor durability in use. Their color (metallic or

[1]Faculty of Textile Engineering, Technical University of Liberec, Czech Republic
[2]Faculty of Mechatronics, Informatics and Interdisciplinary Studies, Technical University of Liberec, Czech Republic

Corresponding author:
Veronika Šafářová, Faculty of Textile Engineering, Technical University of Liberec, Studentská 2, Liberec 463 17, Czech Republic.
Email: veronika.safarova@tul.cz

conductive polymer color—e.g. polypyrrole is black) is also sometimes undesirable for textile use. Fibers containing carbon black or other conductive particles can also be used.[13] To gain proper conductivity of conductive fiber it is necessary to use a large amount of at least 15 wt% conductive particles. This large amount of conductive particles causes the fiber-producing process to be difficult, complex, and expensive. Also, it is impossible to contain the carbon black in the inside of the natural fibers.

The total shielding, expressed as electromagnetic shielding effectiveness (SE) in dB, of a solid material with no apertures is equal to the sum of the absorption loss (A) plus the reflection loss (R) plus a correction factor (B). The reflection is usually the primary mechanism of electromagnetic interference shielding. The wave incident to the boundary with the second medium is partially reflected back and partially transmitted to the second medium. The same situation occurs at the interface between the second and third mediums. The reflection loss at the interface between two media is related to the difference in characteristic impedance between the media. Reflection loss for plane waves is greater at low frequencies and for high conductivity materials.[14] The secondary mechanism of EMI shielding is usually absorption. When an electromagnetic wave passes through a medium, its amplitude decreases exponentially. This decay occurs because currents induced in the shield produce ohmic losses resulting in a heating effect. As mentioned in Chung,[15] the absorption loss is a function of the product $\sigma_r \cdot \mu_r$, whereas the reflection loss is a function of the ratio σ_r/μ_r, where σ_r is the electrical conductivity relative to copper and μ_r is the relative magnetic permeability. Therefore, highly conductive materials such as silver, copper, gold, and aluminum are excellent for reflection, while materials with high magnetic permeability, such as supermalloy and mummetal, are excellent for absorption. The reflection loss decreases with increasing frequency, whereas absorption loss increases with increasing frequency.[15] Other than reflection and absorption, a mechanism of shielding is multiple reflection (B). This loss is due to the multiple reflections inside the shield. This mechanism requires the presence of a large surface area or interface area in the shield.[15] If the shield is electrically thick, then this term is close to zero and can be neglected.[16]

While we are able to determine electromagnetic shielding effectiveness for metal shield on the basis of their electromagnetic parameters, for samples with more complex structure, and often heterogeneous composition, such as textile materials, the electromagnetic shielding effectiveness can be precisely determined, particularly based on direct measurement.[17] Nevertheless, in recent years, several papers giving results of electromagnetic shielding modeling of inhomogeneous or porous structures have appeared.[18–21] There are several methods available for electromagnetic SE measurement. However, for thin planar structures, there is no global standard defining the evaluation of small samples of only several tens of centimeters in size. The following test methods are commonly used to measure electromagnetic shielding effectiveness of a given shielding material:[22]

1. coaxial transmission line method
2. shielded room method
3. open field or free space method (without shielded box or anechoic chamber)
4. shielded box (enclosure) method.

Each mentioned method has some advantages and limitations. For example, the coaxial transmission line method, according to the ASTM D 4935-10 or ASTM ES7-83 standard for planar materials using a plane-wave, far-field EM wave is now the preferred method. The measurement set-up consists of two coaxial adapters (sample holder) and a network analyzer, where signals are transmitted by coaxial cable line coupled with attenuators. The principle of the design of flanged coaxial line sample holder is based on transmission line theory. For the coaxial transmission line, the principal mode of propagation is the transverse electromagnetic (TEM) wave.[23] The material under the test is inserted between the parts of the holder and is exposed to electric fields in all directions over the full 360° within the coaxial holder. The flanges are fastened together by means of insulating screws to avoid direct electrical contact between two parts of the holder. In this way, the sample gets compressed when inserted between two flanges of the holder, which is more significant for nonwoven textiles. The measurements can be made at a specific frequency range (from 30 MHz to 1.5 GHz). The results obtained in different laboratories are comparable as confirmed by a round robin test described in ASTM D 4935-10:2010.[24] From the round robin results, the standard deviation for three different tested materials varied from 0.9 to 6 dB. Generally, tests are carried out on doughnut shaped samples, and a reference sample is also needed, so the preparation of samples is quite time consuming. Measurement uncertainty should fall within $\pm$ 5 dB.[17] This type of measurements presents several shortcomings that could generate different results among different laboratories; some of these differences may be associated with variations in the tester fabrication (sample holder has a complex shape and it is difficult to manufacture). Besides that, the mass of the ASTM D 4935-10 tester holder is about 18 kg, making it inconvenient for frequent handling during assembly and disassembly.[23] Variations of the scaled

sample holder for special purposes, like testing nano-designed materials, have appeared recently in the literature.[17,23,25–27]

The shielded box (enclosure) method is frequently used for comparative measurements of test samples made of different shield materials. The method comprises a metal box with a sample port in one wall, with a receiving antenna fitted inside the metal box. A transmitting antenna is placed outside the box and the intensity of signals received by the antenna is recorded both through the open port and with a sample fitted over the port.[22] The drawback of this method is that it is limited to range of frequency of about 500 MHz.[22] The shielded room method overcomes this limitation, but the sample size is greatly increased.

In many cases the results depend on the individual test arrangement, and it is difficult to separate these influences and assign an uncertainty to the results. Obtaining material-specific attenuation properties that are geometry-independent remains difficult. Therefore, there is a need for the development of an experimental method for the fast determination of the electromagnetic shielding effectiveness of textile samples of several centimeters in size and without the necessity of special preparation of test samples. In this paper we present a new measurement method and equipment which is based on a waveguide principle. It is similar to the arrangement with the shielded box method, but is easier to handle. The main advantages are: a small required sample size of only a few tens of cm^2, no necessity for sample preparation to special shapes or dimensions, rapid measurements, and simple and cheap equipment. However, it also has certain limitations; equipment (waveguide) with specific parameters is required for a particular narrow frequency range. The proposed method is designated especially for rapid comparative measurements of newly-fabricated samples of relatively small size. To prove usability of the proposed method the electromagnetic shielding effectiveness of a textile sample set was tested by the proposed method and the results obtained were compared with those gained by coaxial transmission line method based on the ASTM D 4935-10 standard.

This comparative measurement method was chosen because it is the most frequently used method for evaluation of electromagnetic shielding effectiveness of textile fabrics and composites in recent years, and the main aim was to develop a device which can replace the coaxial transmission line method when quick measurement of small newly-developed samples is required. This explains the selection of a comparative measurement method different from the proposed one, especially on account of the diverse propagation of electromagnetic waves inside the sample holder.

Measurement method

In this paper we present a newly developed modified shielded box method. Basic part of the device is a rectangular hollow waveguide with conducting walls. A receiving wire (antenna) is placed inside of this waveguide, while a textile sample is placed at the entrance to the waveguide. The end of the waveguide is filled with foam saturated with carbon particles, absorbing the electromagnetic field passed through the sample. The fabric sample is oriented perpendicularly to the electromagnetic waves. Transmitting antenna is placed in front of the waveguide input. The scheme, image of test configuration, and simulation of electromagnetic wave entering the waveguide are shown in Figure 1(a–c). A progressive wave passing from the entrance to the end is excited outside the waveguide. The electromagnetic field distribution within the wave guide is known, conserving the lengths of the inner sides of waveguide and considering frequency. It is possible to measure *S*-parameters (scattering parameters describing the input-output relationship between ports in an electrical system) with a vector analyzer, by which it is possible to determine transmitted and reflected electromagnetic waves. Great shielding of surrounding man-made noise is the main advantage of this approach. On the other hand, for a particular narrow frequency range a waveguide with specific dimensions is required.

We may assume that the lengths a,b of the inner sides satisfy $b \leq a$, as shown in Figure 2(a). In our case, the guide is filled with air (relative magnetic permeability $\mu_r \sim 1$ and relative permittivity $\varepsilon_r \sim 1$). Due to Maxwell's equations, the fields within the waveguide always have a specific form, called modes. The dimensions of a hollow metallic waveguide determine which wavelengths it can support, and in which modes. Typically, the waveguide is operated so that only a single mode is present. The lowest order mode possible is generally selected. Frequencies below the waveguide's cutoff frequency will not propagate.

Assume the wave guide is oriented such that the energy is to be transmitted along the waveguide axis, the z-axis. In summary, the electromagnetic field components are:[28]

$$E_x = 0 \tag{1}$$

$$E_y(x, y, z, t) = E_0 \sin k_c x e^{j\omega t - j\beta z} \tag{2}$$

$$E_z = 0 \tag{3}$$

$$H_x(x, y, z, t) = H_1 \sin k_c x e^{j\omega t - j\beta z} \tag{4}$$

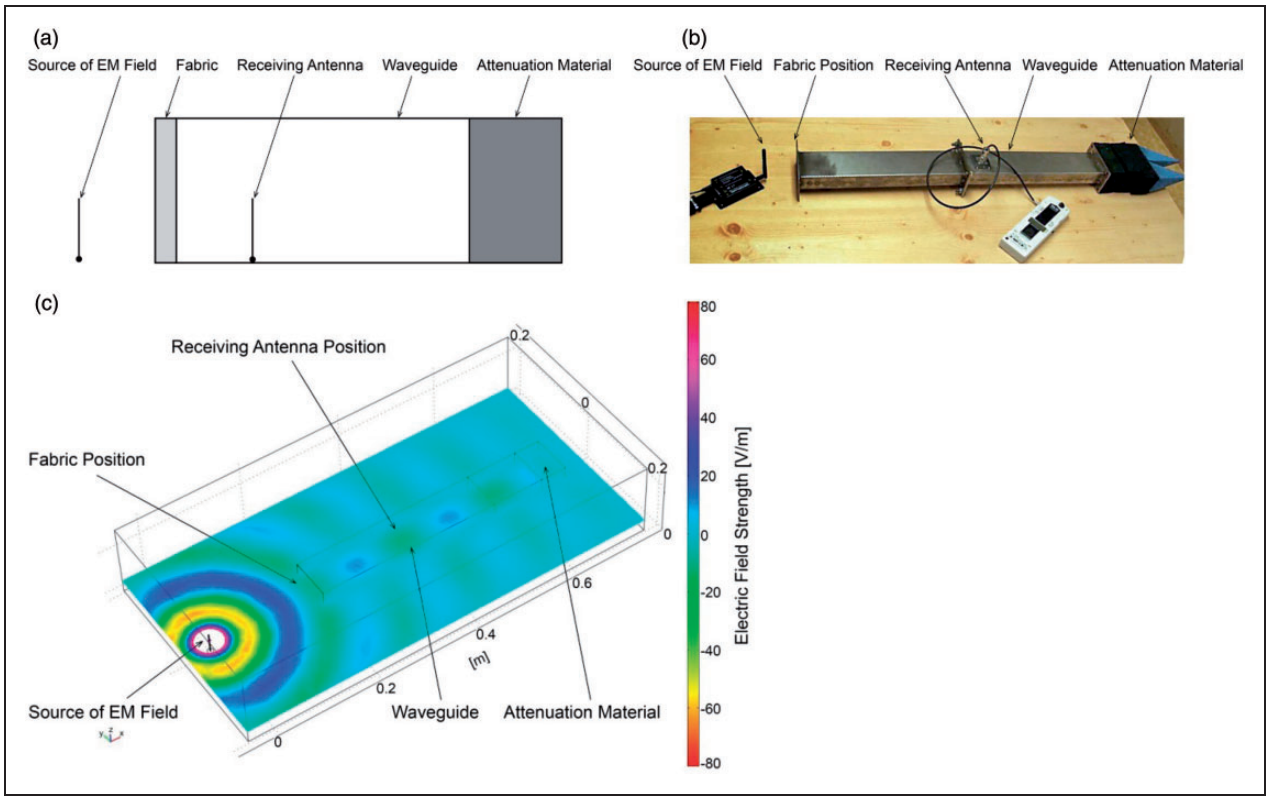

Figure 1. (a) The test set-up, (b) image of proposed rectangular waveguide, (c) simulation of electromagnetic wave entering the waveguide.

$$H_y = 0 \tag{5}$$

$$H_z(x, y, z, t) = H_0 \cos k_c x e^{j\omega t - j\beta z} \tag{6}$$

where $j = \sqrt{-1}$ is the imaginary unit, β is the propagation wave number along the guide direction, k_c is so-called cutoff wavenumber, H_0 is a (complex-valued) constant, and other constants are defined as:

$$H_1 = \frac{j\beta}{k_c} H_0 \tag{7}$$

$$E_0 = j\eta \frac{\omega}{\omega_c} H_0 \tag{8}$$

where η is medium impedance and ω, ω_c are angular frequency and cut-off angular frequency, respectively.

Assuming perfectly conducting walls and because the electric field is in the y-direction and it is normal to the top and bottom sides, the boundary conditions requires:[28]

$$E_y(a) = E_0 \sin k_c a = 0 \tag{9}$$

This requires that $k_c a$ is an integral n multiple of π:

$$k_c a = n\pi \tag{10}$$

In our case, the dominant mode of the waveguide is the transverse electric TE_{10} mode having $n = 1$ and a cutoff wavenumber is:

$$k_c = \frac{\pi}{a} \tag{11}$$

The cutoff frequency for this mode is:

$$f_c = \frac{c_0 k_c}{2\pi} = \frac{c_0}{2a} \tag{12}$$

where: c_0 is the speed of light within the waveguide. Figure 2(b) depicts the electric field $E_y(x) = E_0 \sin k_c x = E_0 \sin(\pi x/a)$ of this mode as a function of x.[28]

To achieve the widest possible usable bandwidth for the TE_{10} mode, the guide dimensions must satisfy $b \leq a/2$ so that the bandwidth is in the interval (f_c, $2f_c$). If the maximum power is required in addition to the widest bandwidth, the dimension b has to be chosen as large as possible, that is, $b = a/2$.[28] In general, standard waveguides are designed such as: (a) the lower edge of the band is approximately 30% higher than the waveguide's cutoff frequency, (b) the upper edge of

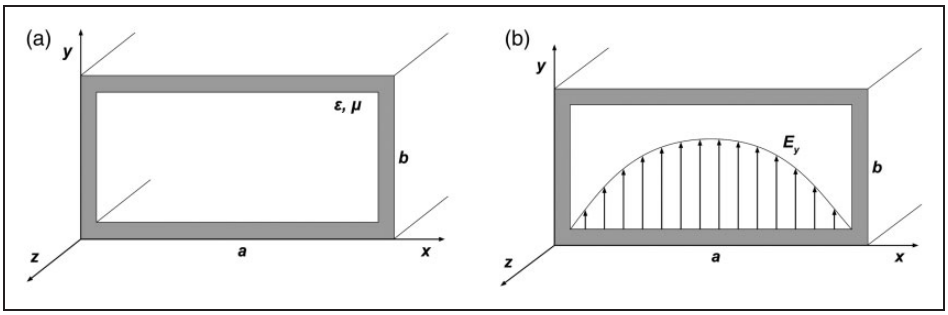

Figure 2. (a) Rectangular waveguide, (b) electric field inside the rectangular waveguide.

the band is approximately 5% lower than the cutoff frequency of the next higher order mode.

In practice waveguides for easy and fast measurements of electromagnetic shielding effectiveness on interesting frequencies can be prepared in following way. For example, the dimensions of the waveguide, in which TE_{10} mode will be excited for example for source frequency 1.8 GHz (frequency of GSM mobile used in most parts of the world: Europe, Middle East, Africa, Australia, Oceania and most of Asia is 1.8 GHz) were determined as: $a = 120$ mm a $b = 60$ mm. Corresponding cutoff frequency $f_c = 1.25$ GHz. Dimensions of a waveguide for source frequency 2.45 GHz (frequency of microwave oven, wi-fi broadcast), were determined as: $a = 90$ mm a $b = 45$ mm. Corresponding cutoff frequency $f_c = 1.67$ GHz. The cutoff frequency has to be lower than source frequency.

Measuring procedure

Electromagnetic shielding effectiveness of textile sample was characterized by the attenuation of electromagnetic field power density by using simple device described above. Efficiency of the electromagnetic shield is possible to characterize by so called shielding attenuation coefficient (dimensionless) defined as a ratio between energy flux density in a specific place of shielded space P_t and incident energy flux density P_i of electromagnetic field:

$$ES = \frac{P_t}{P_i} \tag{13}$$

Logarithmic size of this coefficient, called the electromagnetic shielding effectiveness (dB), is more common:

$$SE = 10\log\frac{P_t}{P_i} = 20\log\frac{E_t}{E_i} = 20\log\frac{H_t}{H_i} \tag{14}$$

where: H_t, E_t, P_t are the magnetic field strength, electric field strength and electromagnetic field density values measured in the presence of the textile material, H_i, E_i, P_i are the same physical values measured without the textile material.

Electromagnetic shielding effectiveness for specific frequency ranges can be calculated based on the following quantities:[16]

– for the frequency range up to 20 MHz:

$$SE\,[\mathrm{dB}] = 20\log\frac{H_t}{H_i} \tag{15}$$

– for the frequency range 20–300 MHz:

$$SE\,[\mathrm{dB}] = 20\log\frac{E_t}{E_i} \tag{16}$$

– for the frequency above 300 MHz:

$$SE\,[\mathrm{dB}] = 10\log\frac{P_t}{P_i} \tag{17}$$

To determine the electromagnetic shielding effectiveness, according to this definition, two measurements can be performed while maintaining the same measurement conditions:

– the reference measurement performed without the textile material

Table 1. Details of studied fabric samples

Sample no.	Composition	Mass per unit area ($g \cdot m^{-2}$)	Thickness (mm)	Volume resistivity ($\Omega \cdot cm$)
1	99% PP/ 1% SST	233.50	0.78	1.42 E+07 ± 8.41 E+06
2	97% PP/ 3% SST	225.10	0.75	7.34 E+06 ± 4.16 E+06
3	95% PP/ 5% SST	209.02	0.77	2.84 E+05 ± 1.36 E+05
4	90% PP/ 10% SST	221.02	0.75	7.75 E+04 ± 1.37 E+04
5	85% PP/ 15% SST	217.66	0.73	3.64 E+04 ± 8.48 E+03
6	80% PP/ 20% SST	208.78	0.71	1.79 E+04 ± 2.50 E+03
7	60% PP/ 40% SST	206.46	0.70	5.47 E+03 ± 1.49 E+03
8	40% PP/ 60% SST	182.98	0.63	1.56 E+03 ± 8.29 E+01

– the appropriate measurement performed for the material placed on the entrance of the waveguide.

Both measurements can be performed for the same measuring conditions so the research results can be accepted as representative. The position of both antennas must be exactly the same in both cases. A network analyzer was used both to generate and to receive signals.

Experimental verification of proposed method

Materials

Hybrid yarns were composed of conventional polypropylene (PP) fiber and different contents of staple BEKINOX® stainless steel (SST) metal fibers (1–75 %). The aspect ratio (length/diameter ratio, l/d) of the SST used in this study is 6250, since the diameter of the SST is 8 μm and the fiber length of the SST is 50 mm. In this study, TREVON® polypropylene fiber with a fineness 2.2 dtex and 50 mm length was used as a nonconductive component. The two components were mixed at the drawing frame, and a ring spinning system was used to produce blended yarns. Nine special textile samples were made of these yarns. Samples with the same structure (weft and warp fineness 51 tex, warp sett 20 cm^{-1}, weft sett 19 cm^{-1} and twill weave) and different content of conductive component (SST fiber) were chosen for this experiment. Details about studied fabrics are given in the Table 1. Volume resistivity (ρ_V) was measured according to the standard ASTM D257-07 using circular electrodes, at the temperature $T = 22.3°C$ and relative humidity $RH = 40.7\%$. The measurement was carried out at 20 different places of textile samples and mean values together with 95% confidence interval are stated in the Table 1. Microscopic images of samples containing 5%, 20%, and 75% of conductive component are shown in Figure 3. Stainless steel fiber (dark color) is observable in all images. Sample no. 3 in Figure 3(a) contains a lower amount of SST fibers than sample no. 6, while sample no. 9 contains a very high amount of SST fibers.

Characterization

In order to verify usability of the proposed method, the experimental results obtained by waveguide method were compared with those obtained by transmission line method based on ASTM D 4935-10, which is designated for planar materials using a plane-wave, far-field EM wave. SE of samples was measured by the comparative method over a frequency range of 30–1500 MHz. The set-up consisted of a sample holder with its input and output connected to the network analyzer, see Figure 4(a,b). The distribution of electric field (E) and magnetic field (H) in the coaxial transmission line is shown in Figure 4(c). An electromagnetic shielding effectiveness test fixture (Electro-Metrics, Inc., model EM-2107A) was used to hold the sample. The design and dimension of the sample holder follows the ASTM method mentioned above. A network analyzer Rohde & Schwarz model ZNC3 was used to generate and receive the electromagnetic signals. The standard mentioned above determines the electromagnetic shielding effectiveness of the fabric using the insertion-loss method. A reference measurement for the empty cell was required for the electromagnetic shielding effectiveness assessment. A 'through' calibration by the help of the reference sample was made first. A load measurement was performed on a solid disk-shaped sample subsequently. The reference and load specimens must be of the same material and thickness.

A rectangular waveguide with specific dimensions (inner dimensions of waveguide opening were 120 × 60 mm) prepared for measuring source frequency 1800 MHz was used. This frequency was found interesting because it is close to the working frequency of particular electric devices. Many mobile phones support 1800 MHz band, also radar and wireless computer network (WLans) use a frequency close to 1800 MHz.

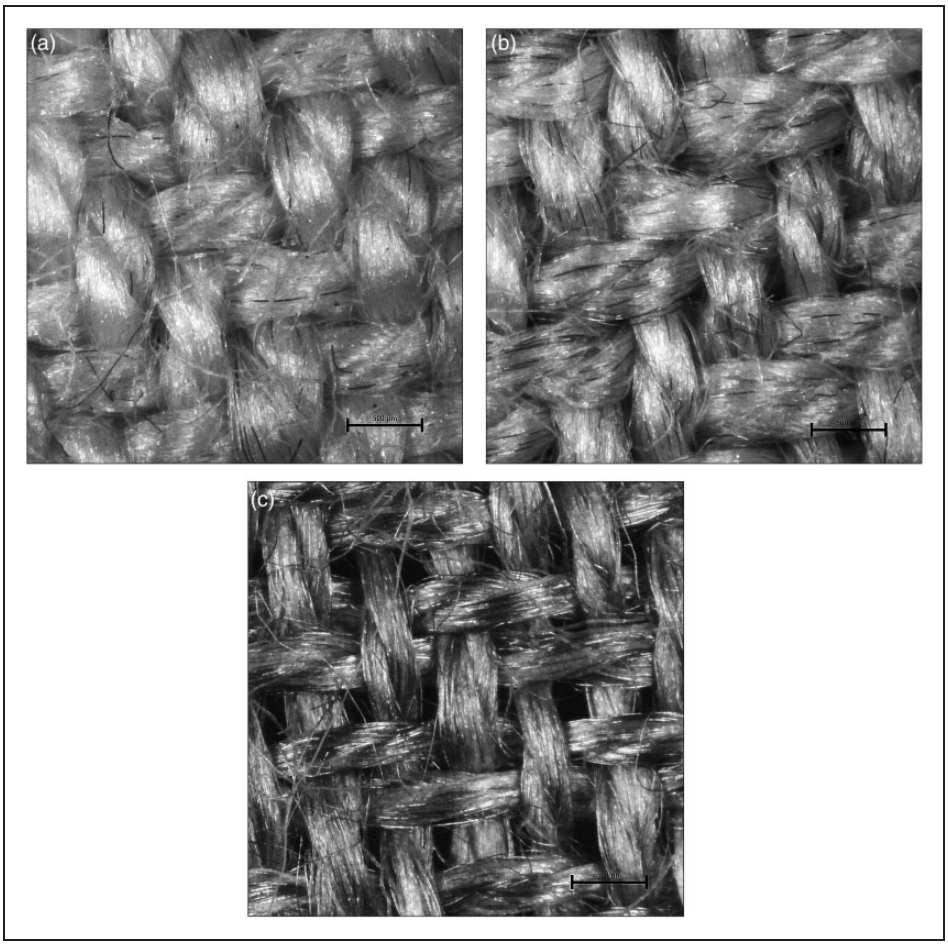

Figure 3. Microscopic image of chosen studied fabrics: (a) sample no. 3 (95% PP/ 5% SST), (b) sample no. 6 (80% PP/ 20% SST), (c) sample no. 9 (25% PP/75% SST).

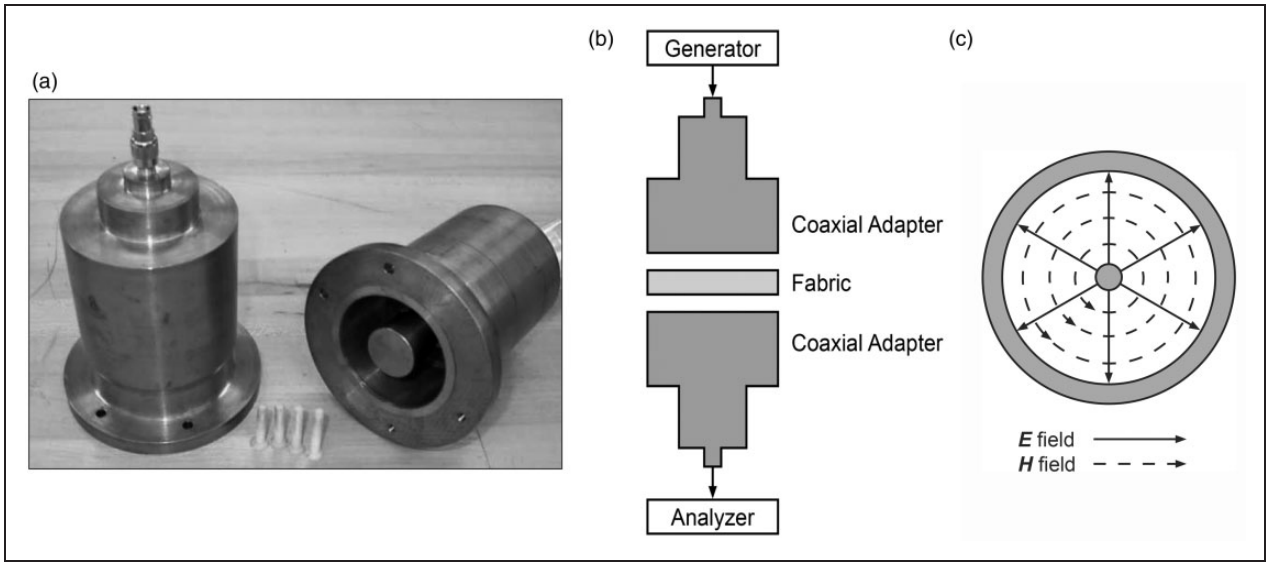

Figure 4. (a, b) Set-up with coaxial adapters, (c) electric and magnetic field distribution inside a coaxial line.

Table 2. Descriptive statistics of SE measurement

		Electromagnetic shielding effectiveness SE (dB)					
		Waveguide			Coaxial transmission line		
Sample no.	Content of SST (%)	Mean	Std.	95% CI	Mean	Std.	95% CI
1	1	17.03	4.57	± 2.90	14.57	0.61	± 0.39
2	3	24.74	4.51	± 2.87	22.61	0.69	± 0.44
3	5	27.29	3.55	± 2.26	25.07	0.75	± 0.48
4	10	31.32	4.56	± 2.90	29.95	0.24	± 0.15
5	15	36.54	4.26	± 3.05	33.69	0.55	± 0.35
6	20	37.59	3.89	± 2.47	35.67	0.54	± 0.34
7	40	39.29	3.97	± 3.05	42.37	0.29	± 0.19
8	60	39.54	5.89	± 5.45	46.11	0.46	± 0.29
9	75	39.77	2.75	± 2.54	51.64	0.25	± 0.16

A network analyzer Agilent E4991A was used to generate, and a high frequency analyzer HF-38B (Gigahertz Solutions) was used to receive the electromagnetic signals. It is possible to measure the SE at a maximum frequency of 1.5 GHz by the coaxial transmission line method. Therefore, to be able to compare outcomes of the two methods, results for the frequency 1.8 GHz measured by the coaxial transmission line method were obtained with the help of extrapolation of measured values at the frequency range 30–1500 MHz. Different places of textile samples were tested by means of coaxial transmission line method or waveguide method because of subsequent statistical analysis.

Statistical analysis

Twelve measurements (observations) of SE of each sample by means of both methods (proposed waveguide method and comparative coaxial transmission line method) were obtained. Before statistical testing, the methods of exploratory data analysis were applied to each sample measured by both methods, including testing for normality of sample distribution and sample homogeneity. For this purpose Lilliefors test (do samples come from a distribution in the normal family?) and notch box-and-whisker plots (homogeneity of sample set) were used. It was found, that data come from a normal distribution and data sets are homogeneous. Descriptive statistics, namely mean values, standard deviations, and confidence intervals for means of both methods are summarized in Table 2.

In order to compare whether the average difference between the two measuring methods (proposed and comparative) is really significant or if it is due to random chance, statistical analysis using a two-sample t-test was performed (significance level $\alpha = 0.05$). The null hypothesis in the t-test is given as:

$$H_0 : \mu_w = \mu_c \tag{18}$$

That is, the mean value of SE measured by waveguide method (μ_w) is equal to the mean value of SE measured by the coaxial transmission line method (μ_c) The alternative hypothesis, that the means are not equal, is defined as:

$$H_1 : \mu_w \neq \mu_c \tag{19}$$

The two-sample t-test and test statistic is performed under the assumption of equal or unequal samples variances, so, firstly, a two-sample F-test was carried out to determine if variances are equal or not. The null hypothesis is that the data comes from normal distributions with the same variance and the alternative hypothesis is that they come from normal distributions with different variances. Results of the two-sample F-tests and two-sample t-tests are presented in Table 3 by means of p-values. When the p-value is less then a predetermined significance level ($\alpha = 0.05$), the test rejects the null hypothesis. The F-test indicates rejection of the null hypothesis if the two data set variances are equal for all tested samples. The t-test confirms that there is not a significant difference between mean values of SE measured by the waveguide method and mean values of SE measured by the coaxial transmission line method for samples nos 1–6, whereas test statistics indicate a significant difference between the means measured by both methods for samples nos 7–9 (p-value < 0.05).

Table 3. Results of two-sample tests

	p-value	
Sample no.	two-sample *F*-test	two-sample *t*-test
1	<0.0001	0.09
2	<0.0001	0.13
3	<0.0001	0.06
4	<0.0001	0.32
5	<0.0001	0.06
6	<0.0001	0.12
7	<0.0001	0.048
8	<0.0001	0.025
9	<0.0001	<0.0001

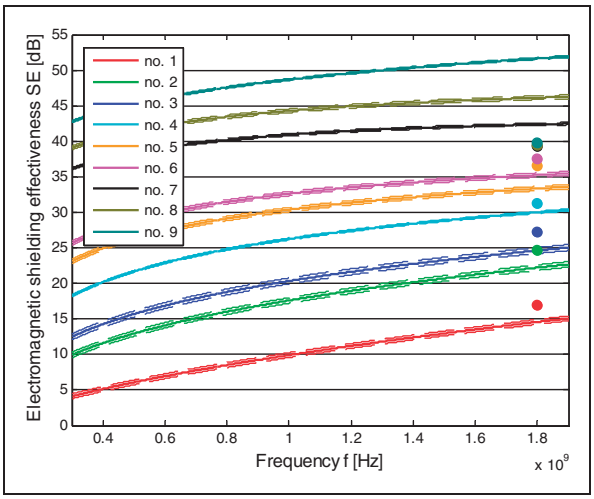

Figure 5. Frequency dependent electromagnetic shielding effectiveness measured by coaxial transmission line method (solid and dash line), points represent SE measured by waveguide method at frequency 1800 MHz.

Results and discussion

Figure 5 shows the electromagnetic shielding effectiveness measurement results gained by the coaxial transmission line method and it's approximation by the help of generalized logarithmic function:[14]

$$SE = a + b\log(f) + c\sqrt{f} \tag{20}$$

where: a,b,c are constants depending on the intrinsic impedance of the material/shield and the intrinsic impedance of the medium surrounding the shield, and f is frequency. Solid lines represent approximations of data means measured by coaxial transmission line method. Moreover, lower and upper limit of mean confidence intervals is displayed by dash line. By the help of extrapolation process (see equation (20)) a values of SE outside the measured range ($f > 1500$ MHz) were predicted and are also displayed. Points in this graph represent measurements performed by waveguide method at frequency 1800 MHz. By examining frequency dependent electromagnetic shielding effectiveness of samples it was confirmed that the electromagnetic shielding effectiveness is increasing logarithmically with the increasing frequency for whole sample set. As frequency increases, the wavelength of the electromagnetic wave decreases and becomes similar to the size of the fiber. Thus, the higher frequency waves are more likely to encounter fiber embedded in the polymer matrix.[13] Hence, SE increases as the frequency increases. We can distinguish two groups of samples—samples with lower metal fiber content and higher resistivity and at the same time tighter structure (samples nos 1–6), and samples with higher metal fiber content (lower resistivity) which causes more open structure (samples nos 7–9). Based on exploratory data analysis (Table 2, Figure 5) we can say that mean values of SE measured by the waveguide method are higher than those measured by the coaxial transmission line method for samples nos 1–6. On the other hand, mean values of SE measured by waveguide method are lower than those measured by coaxial transmission line method for samples nos 7–9.

Mean values and 95% confidence intervals for means of whole sample set measured by both measurement methods (waveguide and coaxial transmission line) at frequency 1800 MHz are shown in Figure 6 using bar plot where x-coordinate represents sample labeling. Blue bars in this graph represent waveguide method and red bars coaxial transmission line method. Again two groups of samples are distinguishable. For first group of samples with lower metal fiber content (nos 1–6), the two-sample t-test used as a classical test of significance of difference in the parameters of location and spread showed, that the mean values of SE measured by both methods are at good agreement. The p-value is the probability of obtaining a test statistic at least as extreme as the one that was actually observed, assuming that the null hypothesis is true, see Table 3. All the test statistics indicate a non-significant difference between the means of proposed and comparative method for this group of samples. For second group of samples with higher metal fiber content (nos 7–9) the two-sample t-test showed that the mean values of SE measured by both methods are not at good agreement. The p-value is less than a predetermined significance level ($\alpha = 0.05$) and therefore the null hypothesis is rejected. This phenomenon can be explained by fact that samples nos 7–9 containing high percentages of stainless steel fiber embody high electrical conductivity which is the cause of high reflection of electromagnetic wave in the entrance of the waveguide.

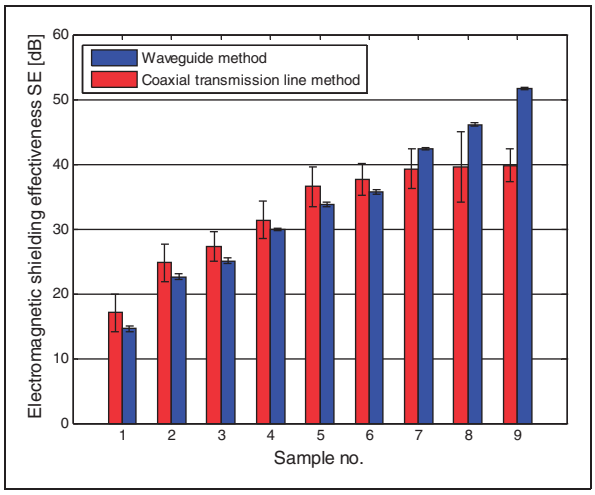

Figure 6. Comparison of mean values of SE measured by both methods along with 95 % confidence intervals for mean.

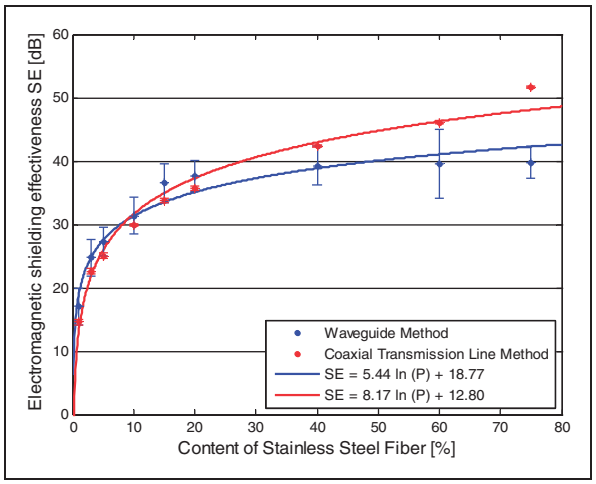

Figure 7. The dependence of electromagnetic shielding effectiveness at frequency 1800 MHz on metal fiber content for the whole sample set.

Examining the variance of the two sample sets by the Fisher–Snedecor test by the help of *p*-values in Table 3 we can see that the null hypothesis (variances are equal) can be rejected at the 5% significance level for whole sample set. It is clear that the variance, which is a measure of how far a set of numbers is spread out from the mean, is higher when applied waveguide method compared to coaxial transmission line method. This phenomenon is also visible exploring 95% confidence intervals for means in Figure 6. The roposed waveguide method is therefore less precise (has higher standard deviations) compared to the coaxial transmission line method. Nevertheless, total variability of the waveguide method is satisfactory (coefficient of variation is lower than 30 % for whole sample set[29]) and that is why the proposed waveguide method is useful, especially for rapid comparative measurements of newly fabricated samples of relatively small size, because a small sample size of only a few tens of cm^2 is required, sample preparation is very easy, measurement is fast, and the equipment itself is simple and cheap.

From Figure 7 the effect of metal content (P) can be studied, and it confirms that electromagnetic shielding effectiveness increases (according to logarithmic function) with increasing metal fiber content:

$$SE = a \ln P + b \tag{21}$$

where a, b are constants determined by the help of the least square method and P is metal fiber content (%). Usability of the logarithmic function model for approximation of SE on metal content dependence was verified during previous studies.[7,30] At very low conductive fiber loadings, the SE remains similar to that of the pure matrix material, i.e. almost zero. Then, at a point called the percolation threshold (analogical to electrical percolation threshold), the SE increases dramatically over a very narrow range of fiber concentration. In this material system, the percolation threshold (P_0) occurred at about 3–5 wt % of conductive component. It stands that SE is a strongly increasing function of metal fiber content below about 30%, while the SE is a more slowly increasing function of metal fiber content at further increases in conductive component content. It seems that electromagnetic shielding effectiveness will not increase dramatically above 40% of SS fiber content. Optimization of shielding structure and a minimization of metal materials consumption is necessary because costs from consumption of metals are arising. We can generally say that conductive materials with 30–40 dB of electromagnetic shielding effectiveness can prevent electro-magnetic interference emitted from 90% of current commercial electronic devices.[8,31] For the reason given above, woven fabrics with a conductive component lower than 25% are sufficient for very many applications.

The quantile–quantile plot is an effective display of the relationship between corresponding order statistics from two data samples (Figure 8). It was confirmed that both data sets come from the same distribution (more precisely from the normal family, as described above), because the points lie approximately on a straight line. When the whole sample set is studied via dependence of the SE of the coaxial transmission line method on the SE of the waveguide method, the linear regression line has a slope of 1.4, an intercept of -11.6, and a correlation coefficient of 0.94 (Figure 8(a)). This means that there is rough direct proportionality between both methods, and electromagnetic shielding effectiveness obtained by the waveguide method is shifted by approximately 11.6 dB against the SE

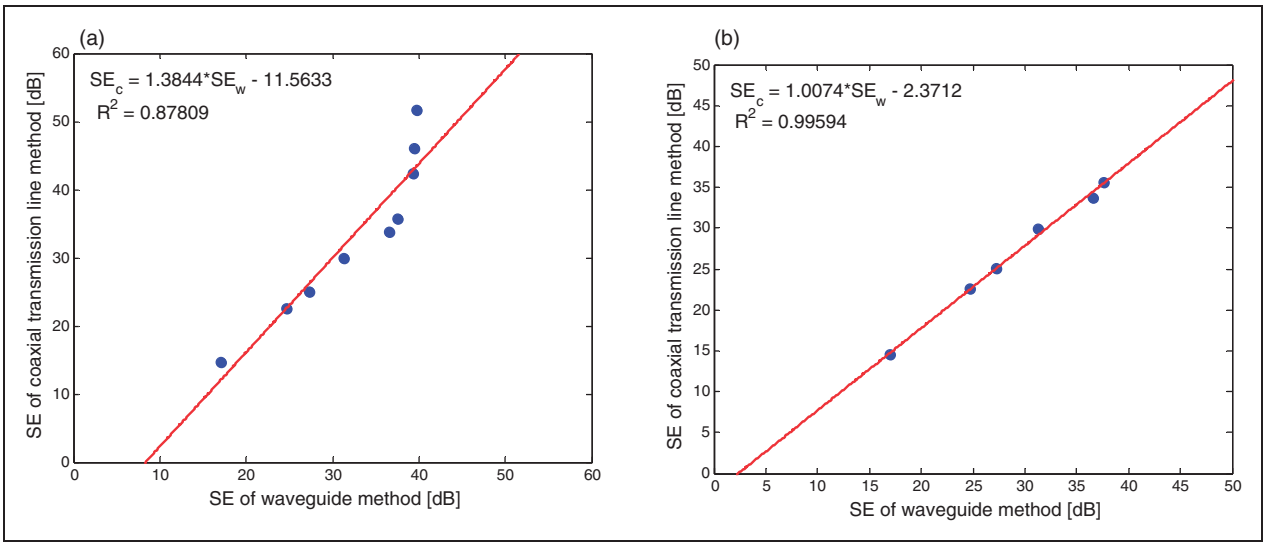

Figure 8. Quantile–quantile plot of SE data sets measured by the two measurement techniques (proposed waveguide method and comparative coaxial transmission line method) for (a) whole sample set, (b) sample set excluding samples with extremely high electrical conductivity.

obtained by the coaxial transmission line method. When the samples with extremely high metal fiber content and very high conductivities are excluded from this analysis (based on recommendations presented in the previous paragraph), the linear regression line has a slope 1, an intercept of 2.4, and a correlation coefficient of 0.99 (Figure 8(b)). In this case direct proportionality between both methods is clear, and electromagnetic shielding effectiveness obtained by the waveguide method is shifted by 2.4 dB against the SE obtained by the coaxial transmission line method. The correction formula below can be used for calculation of SE using the waveguide measurement method:

$$SE = SE_w - 2.37 \tag{22}$$

where SE_w is electromagnetic shielding effectiveness measured by the help of proposed waveguide method. Validity of this correction formula was proved for samples with electrical conductivity up to 6E-03 S.m^{-1}.

Conclusion

A new shielded box based equipment called a waveguide has been designed and fabricated to measure the electromagnetic shielding effectiveness of planar materials in the microwave frequency range. The measurement system is based on a rectangular metal waveguide with specific dimensions for the opening. A receiving antenna is placed inside the waveguide, while an electromagnetic wave is excited outside the waveguide. The tested material covers free entrance of the waveguide during load measurement. The tester was primarily designed to overcome several shortcomings of standard testers used at present, such as, for example, relatively large sample dimensions, complexity of sample test fixture, handling difficulty, tester costs, etc. Theoretically, the new tester could operate in the microwave frequency band, but it was experimentally tested at a frequency of 1800 mMHz. This frequency was found interesting because it is close to the working frequency of many electric devices, especially wireless communication systems.

Usability of the proposed method was confirmed by a two-sample *t*-test performed on nine samples differing in their electrical conductivity. For the intermediately conducting samples the measured SE using both the ASTM method and the new waveguide method are in good agreement, with only a small shift of results considered, and therefore a correction model was proposed. It was found that the waveguide method is not appropriate for samples with high conductivity (conductivity higher than 6E-03 S.m^{-1}), where reflection predominates. The new waveguide method embodies higher variability of measured SE values compared to the ASTM method, although total variability of the waveguide method is satisfactory (lower than 30%). When compared with the coaxial transmission line method, measurement using the proposed waveguide method is much faster, measured samples are relatively small (depending on source frequency), and there is no need of special preparation of test samples. Production of the waveguide itself is relatively inexpensive and easy. On the other hand, a waveguide with specific dimensions is required for the particular narrow frequency range. The proposed method is especially

suitable for testing the electromagnetic shielding effectiveness of different types of textile, polymeric materials, or special composites, where only small samples are accessible and quick testing is required. Aside from operational reasons and purchase costs, the ASTM method remains one of the most useful methods for evaluating electromagnetic shielding effectiveness of textile samples with satisfactory repeatability and reproducibility.

Acknowledgement

This work was supported by the research project TIP-MPO VaV 2009 "Electromagnetic field protective textiles with improved comfort" of Czech Ministry of Industry.

References

1. Vojtech L and Neruda M. Application of shielding textiles for increasing safety airborne systems – limitation of GSM interference. In: *Proceedings of the Ninth International Conference on Networks*, IEEE Computer Society, Los Alamitos, CA, USA, 11–16 April 2010, pp. 157–161.
2. Yu ZC, Zhang JF, Lou ChW, et al. Investigation and fabrication of multifunctional metal composite knitted fabrics. *Textile Res J* 2015; 85(2): 188–199.
3. Cheng KB, Lee ML, Rmakrshna S, et al. Electromagnetic shielding effectiveness of stainless steel/polyester woven fabrics. *Textile Res J* 2001; 71(1): 42–49.
4. Su CI and Chern FT. Effect of stainless steel-containing fabrics on electromagnetic shielding effectiveness. *Textile Res J* 2004; 74(1): 51–54.
5. Ortlek HG, Alpyildiz T and Kilic G. Determination of electromagnetic shielding performance of hybrid yarn knitted fabrics with anechoic chamber. *Textile Res J* 2013; 83(1): 90–99.
6. Duran D and Kadoglu H. A research on electromagnetic shielding with copper core yarns. *J Textile Apparel* 2012; 22(4): 354–359.
7. Safarova V and Militky J. Electromagnetic shielding properties of woven fabrics made from high-performance fibers. *Textile Res J* 2014; 84(12): 1255–1267.
8. Shinagawa S, Kumagai Y and Urabe K. Conductive papers containing metallized polyester fibers for electromagnetic interference shielding. *J Porous Mater* 1999; 6(3): 185–190.
9. Vojtech L and Neruda M. Design of radiofrequency protective clothing containing silver nanoparticles. *Fibers Textiles East Eur* 2013; 21(5): 141–147.
10. Lu Y and Xue L. Electromagnetic interference shielding, mechanical properties and water absorption of copper/bamboo fabric (Cu/BF) composites. *Composites Sci Technol* 2012; 72(7): 828–834.
11. Avloni J, Florio L, Henn AR, et al. Polypyrrole-coated nonwovens for electromagnetic shielding. *J Ind Textiles* 2008; 38(1): 55–68.
12. Yidiz Z, Usta I and Gungor A. Electrical properties and electromagnetic shielding effectiveness of polyester yarns with polypyrrole deposition. *Textile Res J* 2012; 82(20): 2137–2148.
13. Keith JM, Janda NB, King JA, et al. Shielding effectiveness density theory for carbon fiber/nylon 6,6 composites. *Polymer Comps* 2005; 26: 671–678.
14. Ott HW. *Electromagnetic Compatibility Engineering*. New York: John Wiley & Sons, 2009.
15. Chung DDL. Materials for electromagnetic interference shielding. *J Mater Engng Performance* 2000; 9(3): 350 – 354.
16. Kaiser KL. *Electromagnetic Shielding*. New York: Taylor & Francis, 2006.
17. Wieckowski TW and Janukiewicz JM. Methods for evaluating the shielding effectiveness of textiles. *Fibers Textiles East Eur* 2006; 14(5): 18–22.
18. Rybicki T, Brzezinski S, Lao M, et al. Modeling protective properties of textile shielding grids against electromagnetic radiation. *Fibers Textiles East Eur* 2013; 1(97): 78–82.
19. Liu Z, Yang Y, Wang X, et al. Prediction model of shielding effectiveness of electromagnetic shielding fabric with rectangular hole. *Progress Electromag Res C* 2014; 48: 151–157.
20. Lopez A, Vojtech L and Neruda M. Comparison among models to estimate the shielding effectiveness applied to conductive textiles. *Adv Electric Electronic Engng* 2013; 11(5): 387–391.
21. Safarova V, Tunak M and Militky J. Prediction of hybrid woven fabric electromagnetic shielding effectiveness. *Textile Res J* 2015; 85(7): 673–686. Epub ahead of print 7 November 2014.
22. Geetha S, Kumar KKS, Rao ChRK, et al. EMI shielding: Methods and materials—A review. *J Appl Polymer Sci* 2009; 112: 2073–2086.
23. Tezel S, Kavusturan Y, Vandenbosch GAE, et al. Comparison of electromagnetic shielding effectiveness of conductive single jersey fabrics with coaxial transmission line and free space measurement techniques. *Textile Res J* 2013; 84(5): 461–476.
24. ASTM D 4935-10:2010. *Standard Test Method for Measuring the Electromagnetic Effectiveness of Planar Materials*. West Conshohocken, PA: ASTM, 2010.
25. Vasquez H, Espinoza L, Lozano K, et al. Simple device for electromagnetic interference shielding effectiveness measurement. *IEEE Trans Electromag Compat* 2009; 220: 62–68.
26. Feher A, Nagy S and Mojzes I. Developing sample holders for measuring shielding effectiveness of thin layers on compound semiconductor substrates. In: *Progress in Electromagnetics Research Symposium*, The Electromagnetics Academy, Cambridge, MA, Moscow, 18–21 August 2009, pp. 1503–1507.
27. Hong YK, Lee CY, Jeong CK, et al. Method and apparatus to measure electromagnetic interference shielding efficiency and its shielding characteristics in broadband frequency ranges. *Rev Scientific Insts* 2003; 74(2): 1098–1102.
28. Orfanidis PJ. *Electromagnetic Waves and Antennas*. New Brunswick, NJ: Rutgers University, 2008.

29. Brown ChE. Coefficient of variation. *Applied Multivariate Statistics in Geohydrology and Related Sciences*. Berlin: Heidelberg: Springer, 1998, pp.155–157.
30. Militky J and Safarova V. Numerical and experimental study of the shielding effectiveness of hybrid fabrics. *Vlakna a Textil* 2012; 19(1): 21–27.
31. C*ommittee for Conformity Assessment on Accreditation and Certification of Functional and Technical Textiles. Specified Requirements of Electromagnetic Shielding Textiles*. Available at: http://www.ftts.org.tw/images/fa003E.pdf (2005, accessed 24 February 2015).

Appendix 9

V. Safarova, M. Tunak, and J. Militky, "Prediction of hybrid woven fabric electromagnetic shielding effectiveness," Textile Research Journal, vol. 85, no. 7, pp. 673–686, 2015.

Textile Research Journal

Original article

Textile Research Journal
2015, Vol. 85(7) 673–686

DOI: 10.1177/0040517514555802
trj.sagepub.com
SAGE

Prediction of hybrid woven fabric electromagnetic shielding effectiveness

Veronika Šafářová, Maroš Tunák and Jiří Militký

Abstract

This paper deals with experimental verification of numerical models of fabric shielding effectiveness especially via analysis of leakage through the apertures (pores) in the textile structure. Equations for both solid shield and non-compact material were adopted from the literature, whereas an aperture equation based on waveguide conception was used. The experimental sample set was woven fabrics made of hybrid yarns composed of polypropylene fibers with different contents of staple stainless steel metal fibers in their structure. Geometrical characteristics of the aperture structure used for prediction were estimated with the aid of image analysis. Electric conductivity of the hybrid fabric was determined by measuring volume resistivity and plane-wave electromagnetic shielding properties of the sample set were measured by means of the coaxial transmission line method. The effect of metal fiber content on geometrical characteristics (e.g. area of pores, number of pores, cover factor), volume resistivity and electromagnetic shielding effectiveness was investigated. Results obtained by modeling of sample shielding effectiveness and experimental results achieved by measuring of shielding effectiveness were compared and discussed. It was confirmed that electromagnetic shielding effectiveness increased with a higher amount of metal fibers in the hybrid yarn structure. It was verified that the proposed numerical model is usable for predicting electromagnetic shielding effectiveness based on knowledge of dimensions of the structure apertures (pores), thickness of the fabric and volume resistivity of the material.

Keywords

electric conductivity, electromagnetic propagation, electromagnetic propagation in non-homogeneous media, textile industry

According to the World Health Organization,[1] exposure to electromagnetic fields is not a new phenomenon; however, during the 20th century, environmental exposure to man-made electromagnetic fields has been steadily increasing due to growing electricity demand, ever-advancing technologies and changes in social behavior. Due to rapid development in commercial, military and scientific electronic devices and communication instruments, there has been an increased interest in developing materials that could shield against electromagnetic radiation in order to prevent interference. In recent years, conductive fabrics have obtained increased attention for electromagnetic shielding and anti-electrostatic purposes. This is mainly due to their desirable flexibility and lightweight properties.

The electromagnetic interference (EMI) shielding effectiveness (SE) measurement needs to use special devices, and results are dramatically affected by the applied measuring method in addition. In contrast, measurements of surface or volume resistivity are much simpler. It is known from theory that it is possible to measure characteristics of the electrical part of electromagnetic field only at sufficiently high frequencies and therefore there should be a mathematical relation between total SE and fabric resistivity or conductivity. One of the extraordinary features of textile materials with increased electromagnetic SE is not

Faculty of Textile Engineering, Technical University of Liberec, Czech Republic

Corresponding author:
Veronika Šafářová, Faculty of Textile Engineering, Technical University of Liberec, Studentská 2, Liberec 463 17, Czech Republic.
Email: veronika.safarova@tul.cz

only technical protection, but also protection of human beings while operating specific electrical equipments.

As stated by Cheng et al.[2] and Wieckowski and Jankukiewicz,[3] while we are able to determine SE easily for metal shields just by knowing the material's electromagnetic parameters, for materials containing inserted metallic or graphite yarns, metalized surfaces or composite materials, the easiest way how to determine the SE is by actually measuring it. There are available several methods that allow measurements of electromagnetic SE.[4–8] However, the EMISE measurements need to use special devices and results are dramatically affected by the applied measuring method.[9] Nevertheless, in recent years several papers giving results of electromagnetic shielding modeling of inhomogeneous or porous structures have been introduced.[10–15] For the reason given above, there is a need for a simple computational method to accurately determine the SE of such products (textile structures) based on knowledge of electrical properties (which can be easily determined) and geometrical characteristics.

The aim of this paper is to describe a straightforward, semi-empirical method for calculating the SE of hybrid woven fabrics based on the geometry of the fabric (pore size and thickness) and the measured volume resistivity. The object is to develop a simple and accurate model that can assist in optimizing the performance of hybrid fabrics for various applications.

Analysis of the shielding effectiveness of woven fabrics

The SE of any element varies with frequency, geometry of the shield, material of the shield, position within the shield where the shield is measured, type of the field being attenuated, angle of incidence and polarization.[16]

The total SE of a solid material with no apertures (SE_{sheet}) is equal to the sum of the absorption loss (A) plus the reflection loss (R) plus a correction factor to account for multiple reflections (B) in the shield. The multiple reflection factor can be neglected if the absorption loss is greater than 9 dB. From a practical point of view, multiple reflections can be neglected for electric fields and plane waves.[16]

$$SE_{sheet} = A_{sheet} + R_{sheet} + B_{sheet}. \quad (1)$$

The reflection is usually the primary mechanism of EMI shielding. The wave incident to the boundary with the second medium is partially reflected back and partially transmitted to the second medium. The same situation occurs at the interface between the second and third material. The reflection loss at the interface between two media is related to the difference in characteristic impedance between the media. Neglecting multiple reflections, a generalized equation for reflection loss of thin shields can be written as[16]

Table 1. Constants used in Equation (2)[16]

Type of field	C	n	m
Electric field	322	3	2
Plane wave	168	1	0
Magnetic field	14.6	−1	−2

$$R_{xheet} = C + 10\log\left(\frac{\sigma_r}{\mu_r}\right)\left(\frac{1}{f^n r^m}\right) \text{ [dB]}, \quad (2)$$

where the constants C, n and m are listed in Table 1 for plane waves, electric fields and magnetic fields, respectively. Parameter r is the distance from the source to the shield, μ_r is relative permeability and σ_r is relative conductivity.

For reflection of the radiation by the shield, the shield must have mobile charge carriers (electron and holes), which can interact with the electromagnetic field in the radiation. As a result, the shield tends to be electrically conducting, although a high conductivity is not required. For example, a volume resistivity of the order of 1 Ω.cm is typically sufficient. Metals are the most common materials for EMI shielding. Reflection loss for plane waves is greater at low frequencies and for high-conductivity materials.[17]

Secondary, the mechanism of EMI shielding is usually absorption. When an electromagnetic wave passes through a medium, its amplitude decreases exponentially. This decay occurs because currents induced in the shield produce ohmic losses and heating of material. The distance required for the wave to be attenuated to 1/e or 37% of its original value is defined as the shin depth, which is equal to[16,18]

$$\delta = \frac{1}{\sqrt{\pi f \mu \sigma}} \text{ [m]}, \quad (3)$$

where f is frequency [Hz]. Hence, the skin depth decreases with increasing frequency and with increasing conductivity and permeability.

The general expression for absorption loss can be written as[16]

$$A_{sheet} = 0.0848\, t\sqrt{f \mu_r \sigma_r} \text{ [dB]}, \quad (4)$$

where t is thickness of the shield in meters. For significant absorption of the radiation by the shield, the shield should have electric and/or magnetic dipoles, which interact with the electromagnetic fields in the radiation. The electric dipoles may be provided by materials having a high value of the dielectric constant.

The magnetic dipoles may be provided by materials having a high value of the magnetic permeability.

The absorption loss is a function of the product $\sigma_r.\mu_r$, whereas the reflection loss is a function of the ratio σ_r/μ_r, where σ_r is the electrical conductivity relative to copper and μ_r is the relative magnetic permeability. Silver, copper, gold and aluminum are excellent for reflection, due to their high conductivity. Supermalloy and mumetal are excellent for absorption, due to their high magnetic permeability. The reflection loss decreases with increasing frequency, whereas absorption loss increases with increasing frequency[16]

Other than reflection and absorption, a mechanism of shielding is multiple reflections (B), which refer to the reflections at various surfaces or interfaces in the shield. This mechanism requires the presence of a large surface area or interface area in the shield. An example of a shield with a large surface area is a porous or foam material. The loss due to multiple reflections can be neglected when the distance between the reflecting surfaces or interfaces is large compared to the skin depth.

The working of the electromagnetic shield is possible to characterize by the so-called shielding attenuation coefficient (dimensionless), defined as a ratio between electromagnetic field density in a specific place of shielded space P_t and incident electromagnetic field density P_i:

$$ES_{sheet} = \frac{P_t}{P_i}\ [-]. \tag{5}$$

The logarithmic size of this coefficient called SE is used further:

$$SE_{sheet} = 10\log\frac{P_t}{P_i} = 20\log\frac{E_t}{E_i} = 20\log\frac{H_t}{H_i}\ [\mathrm{dB}], \tag{6}$$

where H_t, E_t, P_t are the electric field strength, magnetic field strength and electromagnetic field density values, respectively, measured in the presence of the textile material, and H_i, E_i, P_i are the same values measured without the textile material.

The absorption loss and reflection loss at a shield with no apertures after simplification can be written as

$$A_{sheet} = 0.0848\, t\sqrt{\frac{K}{K_C}}f, \tag{7}$$

$$R_{sheet} = C + 10\log\left(\frac{K}{K_C f}\right), \tag{8}$$

where C is constant, K [S.cm^{-1}] is the volume conductivity and K_c is copper conductivity (5.82 10^5 S.cm^{-1}), f [MHz] is the frequency and t [m] is thickness of the shield. Thickness in inches from the original equation according to Ott[16] was converted to meters, relative magnetic permeability was neglected and relative conductivity was replaced by fraction (K/K_C) according to White[19] in Equation (7). The original form of Equation (8) was adapted from Ott[16] and Shinagawa et al.,[20] where the particular constant was replaced by general constant C, relative magnetic permeability was neglected according to Shinagawa et al.[20] and relative conductivity was replaced again by fraction (K/K_C) according to White.[19]

Many researches confirmed that the SE of the fabrics depends on the conductive filler content.[21–24] Equations describing the SE of conductive materials in the form of thin foils, wire meshes, perforated plates or materials with carbon filler have been already published.[20,25–29]

The previous formulations have assumed a solid shield with no apertures. In practice, however, most shields are not solid. There must be access covers, doors, holes for cables, ventilations, switches, displays and joints and seams.[16] In the case of fabrics, more precisely woven fabrics, the inter yarn pores represent the apertures. All of these apertures considerably reduce the effectiveness of the shield. As a practical matter, at high frequency, the intrinsic SE of the shield material is of less concern than the leakage through the apertures. Therefore, the SE of a fabric can be modeled as a combination of the attenuation due to a thin metal foil (if the wavelength of electromagnetic radiation incident on a fabric is significantly larger than the openings in the fabric) and an irregular mesh or panel, which will depend on the maximum pore size and fabric thickness.[14]

Analysis of shielding effectiveness of the fabric aperture

The amount of leakage from an aperture (SE_{aper}) depends mainly on the maximum linear dimension of the aperture, the wave impedance of the electromagnetic field and the frequency of the field. The amount of reduction depends on the number of apertures, the frequency and the spacing between the apertures.

The analysis of leakage through an opening in copper core yarn fabric shields based on transmission line theory is published in Perumalraja et al.[29] The electromagnetic SE is given by

$$SE_{aper} = A_a + R_a + B_a + K_1 + K_2 + K_3, \tag{9}$$

where A_a is attenuation introduced by a particular discontinuity [dB], R_a is fabric aperture with single reflection loss [dB], B_a is a multiple reflection correction

term [dB], K_1 is a correction term to account for the number of like discontinuities [dB], K_2 is a low-frequency correction term to account for skin depth [dB] and K_3 is a correction term to account for a coupling between adjacent holes [dB].

As Henn and Cribb[14] state, the apertures can be considered as a "subcritical" waveguide with dimensions L, s and t. The SE due to apertures of non-compact material can be calculated by taking into account the attenuation factor, operating wavelength and cut-off wavelength and geometric dimensions of apertures:

$$SE_{aper} = 100 - 20\log(Lf) + 20\log\left(1 + \ln\left(\frac{L}{s}\right)\right) + 30\frac{t}{L}, \quad (10)$$

where t is depth of the aperture or thickness of fabric [mm], L is the maximum pore dimension of the aperture [mm] (most frequently it is equivalent to the aperture diagonal, not its longest side), s is the minimum pore dimension [mm] and f is frequency [MHz]. The first two terms are due to reflection. The third term is a kind of polarization factor[19] and the last term describes the absorption term. The last term can have a significant contribution to the overall SE of an aperture when t/L is near to or greater than one.[14]

The total electromagnetic SE of fabric is a linear combination of the electromagnetic SE due to apertures (SE_{aper}) at high frequencies and the electromagnetic SE of compact materials at low frequencies (SE_{sheet}). This is because at low frequencies a sheet with apertures can be viewed as a compact sheet if the apertures are small enough:[14]

$$SE = f_1(d,\lambda)\, SE_{sheet} + f_2(d,\lambda)\, SE_{aper}. \quad (11)$$

Since the functions $f_1(d,\lambda)$ and $f_2(d,\lambda)$ must fulfill the equation $f_1(d,\lambda) + f_2(d,\lambda) = 1$, Equation (11) can be derived as

$$SE = f_1(d,\lambda)\, SE_{sheet} + (1 - f_1(d,\lambda))\, SE_{aper}. \quad (12)$$

According to Lopez et al.,[15] after performing the derivation of function $f_1(d,\lambda)$, Equation (13) is obtained:

$$f_1(d,\lambda) = \mathrm{e}^{-0.017d\sqrt{f}}. \quad (13)$$

The overall electromagnetic SE of textile can then be written as

$$SE = e^{-0.017d\sqrt{f}}\, SE_{sheet} + \left(1 - e^{-0.017d\sqrt{f}}\right) SE_{aper}. \quad (14)$$

Experimental details

Materials

Six woven fabrics with the same structure (weft and warp fineness 51 tex, warp sett 20/cm, weft sett 19/cm, twill weave) were used. Samples were made of 100% hybrid yarn containing different portions of conductive phase. Hybrid yarns were composed of polypropylene and different contents of staple stainless steel (SS) metal fiber (10, 15, 20, 40, 60, 75%). The aspect ratio (length/diameter ratio, l/d) of the SS used in this study is 6250, since the diameter of the SS is 8 μm and the fiber length of the SS is 50 mm. In this study, TREVON polypropylene fiber with a fineness 2.2 dtex and 50 mm length was used as a non-conductive component. The two components were mixed at the drawing frame and a ring spinning system was used to produce blended yarns. Hybrid yarns were prepared as two-ply yarns (fineness of yarns was 2×25 tex). Details of fabrics are given in the Table 2.

Statistical analysis of small samples

Due to the very small sample sizes $4 \le n \le 20$ of electrical properties and electromagnetic shielding evaluation available for evaluation process, a procedure based on order statistics introduced by Horn[30] was used. This is based on the depths that correspond to the sample quartiles. The pivot depth is expressed by

$$H_L = \mathrm{int}[(n+1)/2]/2 \,\mathrm{or}\, H_L = \mathrm{int}[(n+1)/2 + 1]/2, \quad (15)$$

according to which H_L is an integer. The lower pivot is $x_L = x_{(H)}$ and the upper one is $x_U = x_{(n+1-H)}$. Denote that the $x_{(i)}$ are ordered statistics, that is, $x_{(i)} \le x_{(i+1)}$. The estimate of the parameter of location is then expressed by the *pivot half sum*:

$$P_L = 0.5\,(x_L + x_U) \quad (16)$$

Table 2. Studied fabric details

Sample	Composition	Mass per unit area [g.m^{-2}]	Thickness [mm]
1	90% PP/ 10% SS	221.0	0.75
2	85% PP/ 15% SS	217.7	0.73
3	80% PP/ 20% SS	208.8	0.71
4	60% PP/ 40% SS	222.0	0.70
5	40% PP/ 60% SS	216.2	0.63
6	25% PP/ 75% SS	225.3	0.57

PP: polypropylene; SS: stainless steel.

and the estimate of the parameter of spread is expressed by the *pivot range*:

$$R_L = (x_U - x_L). \tag{17}$$

The random variable

$$T_L = \frac{P_L}{R_L} = \frac{x_L + x_U}{2(x_U - x_L)} \tag{18}$$

has approximately symmetric distribution and its quantiles are given by Horn.[30]

The 95% confidence interval of the mean is expressed by pivot statistics as

$$P_L - R_L t_{L,0.95}(n) \le \mu \le P_L + R_L t_{L,0,95}(n) \tag{19}$$

and analogously hypothesis testing may also be carried out. For small samples ($4 \le n \le 20$), the pivot statistics lead to more reliable results than the application of Student's *F*-test or robust *t*-tests.

Evaluation of electrical properties

Volume resistivity (ρ_V) was measured according to the standard ASTM D257-07,[31] at the temperature $T = 22.3°C$ and relative humidity (RH) = 40.7%. Volume resistivity is measured by applying a voltage potential across opposite sides of the sample and measuring the resultant electric current through the sample. The measurement was carried out at 20 different places of textile samples because of subsequent statistical analysis, $\alpha = 0.05$, $t_{L,0.95}(20) = 0.266$. The mean values estimator (pivot half sums), pivot ranges and confidence intervals for means of ρ_V are summarized in Table 3.

The dependence of ρ_V on conductive component content (P) for the range above the percolation threshold can be expressed by the simple power function as verified by extensive experiments:[32]

$$\rho_V = \rho_C \cdot P^E, \tag{20}$$

where ρ_C is volume resistivity for $P = 1\%$ of the conductive component in hybrid yarn and parameter E is dependent on the structure of the conductive component.

Table 3. Results of volume resistivity evaluation

		Volume resistivity ρ_V [Ω.cm]		
Sample	Composition	Pivot half sum P_L	Pivot range R_L	95% CI
1	90% PP/ 10% SS	7.75E + 04	5.15E + 04	1.37E + 04
2	85% PP/ 15% SS	3.64E + 04	3.19E + 04	8.48E + 03
3	80% PP/ 20% SS	1.79E + 04	9.40E + 03	2.50E + 03
4	60% PP/ 40% SS	5.47E + 03	5.60E + 03	1.49E + 03
5	40% PP/ 60% SS	1.56E + 03	3.12E + 01	8.29E + 01
6	25% PP/ 75% SS	1.51E + 03	3.91E + 01	1.04E + 02

PP: polypropylene; SS: stainless steel.

Electromagnetic shielding effectiveness test

Electromagnetic SE of the high-performance hybrid fabrics was measured according to ASTM D4935-99,[33] for planar materials using a plane-wave, far-field EM wave. SE of samples was measured over a frequency range of 30–1500 MHz. The set-up consisted of a sample holder with its input and output connected to the network analyzer. An electromagnetic SE test fixture (Electro-Metrics, Inc., model EM-2107A) was used to hold the sample. The design and dimension of the sample holder follows the ASTM method mentioned above. Network analyzer Rohde & Schwarz model ZNC3 was used to generate and receive the electromagnetic signals. The standard mentioned above determines the electromagnetic SE of the fabric using the insertion-loss method. A reference measurement for the empty cell was required for the electromagnetic SE assessment. A "through" calibration by the help of the reference sample was made first. A load measurement was performed on a solid disk shape sample subsequently. The reference and load specimens must be of the same material and thickness. Sample (both reference and load) geometries according to ASTM D4935-99 are shown in Figure 1.

On the basis of the logarithmic relation between electromagnetic SE and frequency[19]

$$SE = a + b\log(f) + c\sqrt{f}, \tag{21}$$

where a, b, c are constants depending on characteristic impedance of the shield material and characteristic impedance of the medium surrounding the shield and f is frequency; the values beyond the original observation range (e.g. for $f = 2450$ MHz) were estimated by the extrapolation process.

The measurement was carried out at five different places of textile samples because of subsequent statistical analysis, $\alpha = 0.05$, $t_{L,0.95}(5) = 1.37$. The mean values estimator (pivot half sums), pivot ranges and confidence intervals for means of *SE* for frequencies 600, 1500 and 2450 MHz are summarized in Table 4.

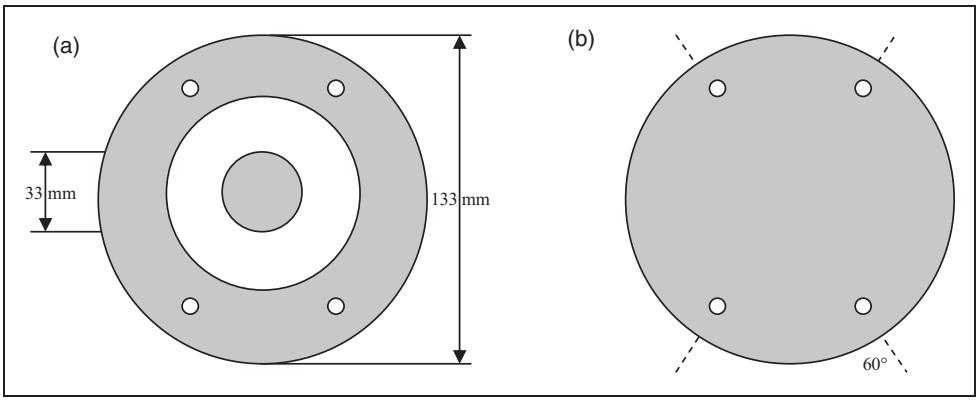

Figure 1. Illustrations of (a) reference and (b) load sample.

Table 4. Results of electromagnetic shielding effectiveness (SE) evaluation

	Electromagnetic shielding effectiveness SE [dB]								
	$f = 600$ MHz			$f = 1500$ MHz			$f = 2450$ MHz		
Sample	Pivot half sum P_L	Pivot range R_L	95% CI	Pivot half sum P_L	Pivot range R_L	95% CI	Pivot half sum P_L	Pivot range R_L	95% CI
1	23.16	0.35	0.48	28.89	0.23	0.32	31.79	0.46	0.63
2	27.41	0.10	0.14	32.47	0.24	0.33	34.70	0.43	0.59
3	30.04	0.32	0.44	34.59	0.24	0.33	36.43	0.49	0.67
4	38.99	0.36	0.49	41.99	0.29	0.40	43.12	0.71	0.97
5	41.95	0.19	0.26	45.14	0.15	0.20	46.42	0.84	1.15
6	45.90	0.18	0.25	50.50	0.45	0.62	53.36	1	1.37

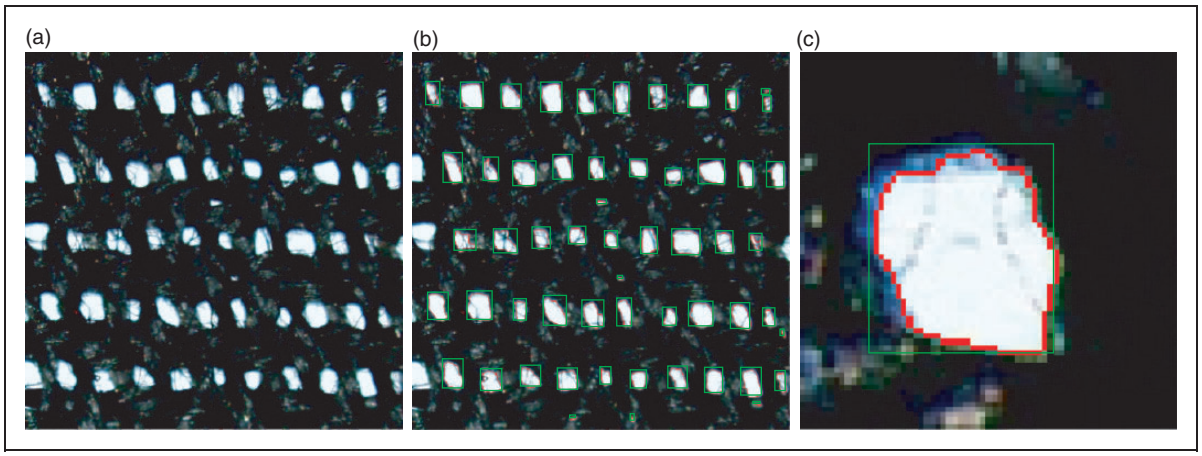

Figure 2. (a) original RGB image. (b), (c) resulting image where borders of objects plotted in red and the smallest rectangle containing objects is plotted in green.

Characterization of fabric apertures

Geometrical properties of fabric apertures were estimated with the aid of image processing in this study. Images of woven fabric were obtained by microscope Olympus BX51 by $5\times$ magnification in transmitted light. Images were captured as RGB image matrices of size 1360×1024 pixels (the real size of the sample is $14{,}021\ \mu m \times 10{,}557\ \mu m$). Figure 2(a) displays a crop

of sample No. 6 of size 500 × 500 for better visual representation. Tools of digital image processing are used for preparation of images for the following analysis.[34] Color information is not significant for subsequent processing, so images were transformed to eight-bit gray-level range, where warp and weft yarns are represented by dark gray levels and apertures between the yarns by light gray levels. The aim of image processing is determination of distribution of the area of apertures (pores) between the warp and weft yarns and length of sides of the smallest rectangle containing such apertures known as the Bounding Box. For this reason the binary image was converted from grayscale by using a global thresholding (thresh level = 0.5), where gaps as objects are displayed by white (level = 1) and the background represented by yarns is displayed by black (level = 0). Note that segmentation to a binary image simplifies subsequent image operations due to the application of binary logical operations. In such images it is easier to carry out following operations, such as measurement of shape characteristics of objects, since they have exactly defined borders in contrast to gray-level images (Figure 2(c)). Small objects may also be visible in binary images. These objects can be caused by random noise and it is necessary to remove these from binary images. Operation morphological opening is used to remove such small connected objects that consist of fewer than 20 pixels. Objects connected to the image border representing incomplete objects were also removed. Small holes, breaks and gulfs can be seen inside many objects; operation morphological closing with a disk structuring element of size 3 pixels was used for filling these types of defects. From such pre-processed images characteristics such as number of objects, area of objects and length of sides (a, b) of the smallest rectangle containing objects were extracted. Figure 2(c) shows borders of objects plotted in red and the smallest rectangle containing objects plotted in green. Figure 2(b) displays the result for only one object for better illustration.

Based on previous image analysis, characteristics of apertures (n is the number of pores, A is the area of pores, a, b are lengths of sides of the smallest rectangle containing pores) were extracted. As an estimation of mean and variance, robust estimators of μ and σ ($\widehat{\mu} = \tilde{x}_{0.5}$ and $\widehat{\sigma} = IQR/1.349$, where IQR is interquartile range) were taken.[35] Results for all samples obtained from prior analysis are summarized in Table 5, where robust estimators are given for all characteristics. Moreover, cover factor CF (ratio of the area covered by yarns to the total area) is stated in Table 5, where A_a represents total area of the pores (total area of samples was 1.4802E + 08 μm^2).

Results and discussion

Electrical properties

Figure 3 depicts the volume resistivity ρ_V concentration curve for the studied samples. A strong correlation was found; the resulting graph shows the rapid decrease in

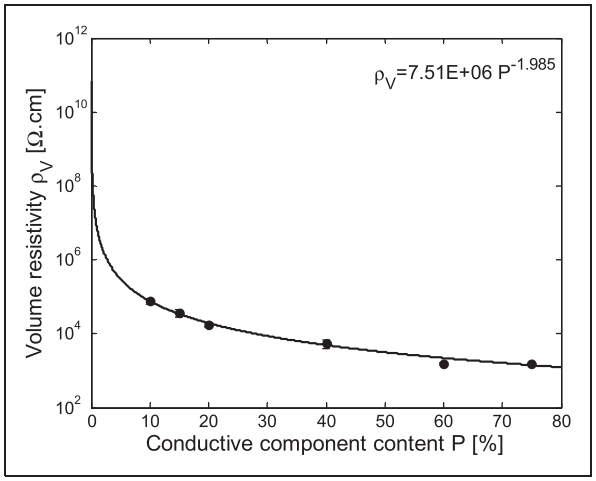

Figure 3. The dependence volume resistivity of samples on percentage of conductive component.

Table 5. Geometrical characteristics of apertures

		Area [μm^2]		a [μm]		b [μm]			
Sample	n	$\widehat{\mu}$	$\widehat{\sigma}$	$\widehat{\mu}$	$\widehat{\sigma}$	$\widehat{\mu}$	$\widehat{\sigma}$	A_a [μm^2]	CF [%]
1	30	3188.6	38.7	41.2	4.8	41.2	4.1	1.1585e + 005	99.92
2	48	3932.6	48.6	51.5	5.5	41.2	5.5	2.3734e + 005	99.84
3	43	3932.6	59.7	41.2	4.6	30.9	5.2	2.3160e + 005	99.84
4	104	6111.5	67.3	72.2	6.2	61.9	6.0	8.5349e + 005	99.42
5	180	10948.0	102.8	113.4	7.3	82.5	7.8	2.4877e + 006	98.32
6	329	30611.0	170.5	154.6	9.6	206.2	10.7	1.1295e + 007	92.37

volume resistivity about two orders of magnitude between 10% and 75% of metal fibers in the hybrid fabrics. A percolation threshold is not visible from this experiment. It can be expected at about a loading of 3% of conductive component based on previous studies.[32] Generally, the percolation threshold varies considerably with the shape and agglomeration of the conductive phase, as well as the type of non-conductive phase used. It is well known that the resistivity dependence on the amount of conductive component (P) is different for the range below and above the so-called percolation threshold P_o. The ρ_V is a strongly decreasing function of P below P_o. In our case, the ρ_V is a more slowly decreasing function of P in the range above P_o. It stands to reason that resistivity will not increase dramatically with additional increasing of the conductive component (above 75%). The dependence of ρ_V on conductive component content for the range above the percolation threshold can be expressed by the simple power function (20) adopted from Clingerman et al.,[36] correlation coefficient $r = 0.99$. It was found in previous research[32] that approximation of this dependence by the power function is suitable even for materials with a conductive component below 10% of SS.

Electromagnetic shielding effectiveness

Figure 4 shows the variation in SE for the six fabrics with incident frequency in the range 30–1500 MHz. Electromagnetic SE out of the measured range (1500–2450 MHz) was calculated by extrapolation in terms of (21). It was confirmed that the electromagnetic SE increased logarithmically with the increasing frequency for whole set of samples. The SE is a strongly increasing function of frequency below about 1500 MHz, while the SE is a more slowly increasing function of frequency in the range above 1500 MHz. It seems that electromagnetic SE will not increase dramatically above 2450 MHz. The fabric with the highest content of conductive component (metal fiber) has the highest electromagnetic SE through the studied frequency range. All studied fabrics have the same 2/2 twill structure. Warp and weft density of the fabrics and linear density of the warp and weft yarns were fixed. The differences in the fabrics were blend rations and therefore there were changes in mass per unit area of the samples. The effect of metal content on the SE has been already well established (e.g. Kirkpatrick,[22] Kim et al.[37] and Duran and Kadoglu[38]). As expected, SS had a strong influence on the SE characteristics of fabrics. It was confirmed in this study that electromagnetic SE increases with increasing metal fiber content. Sample No. 6, with the highest content of metal fiber, reaches the highest electromagnetic SE – 53 dB for frequency 2450 MHz, whereas sample No. 1, containing the lowest portion of conductive component, displays the lowest electromagnetic SE (32 dB for frequency 2450 MHz).

Figure 5 further illustrates the effect of fabric blend ratio on the SE at two particular frequencies, 1500 and

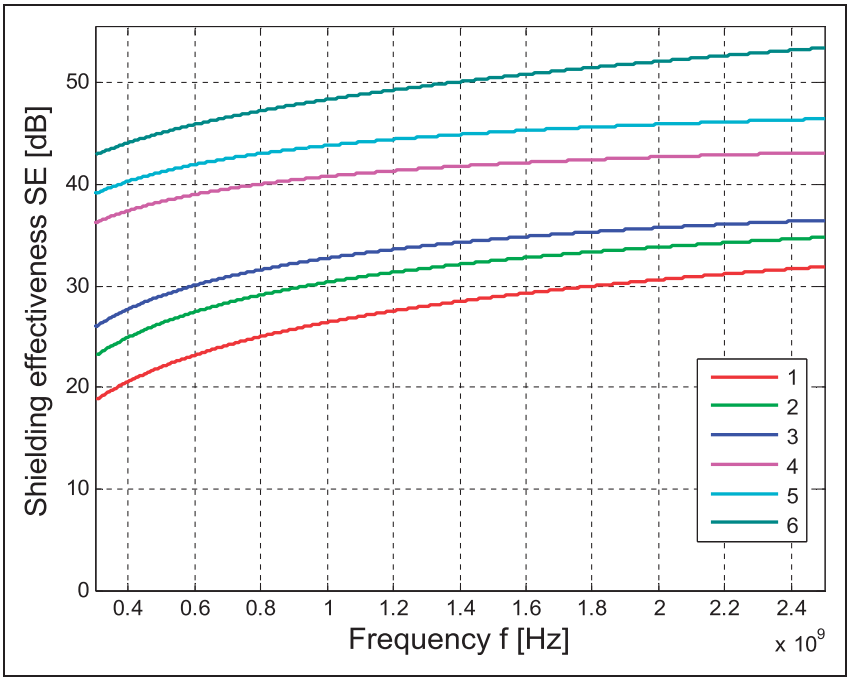

Figure 4. The dependence of measured electromagnetic shielding effectiveness on frequency for all samples.

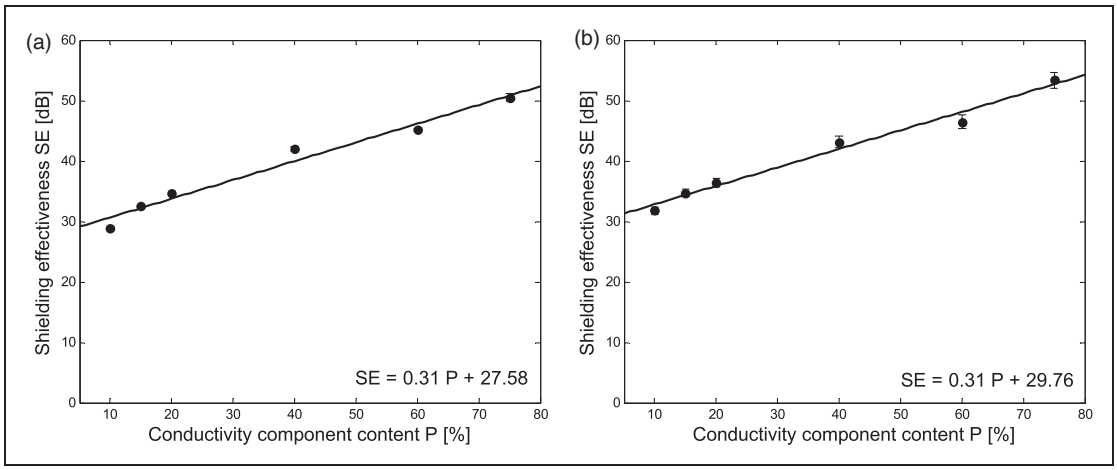

Figure 5. The dependence of shielding effectiveness on the conductivity component content for frequencies (a) 1500 MHz and (b) 2450 MHz.

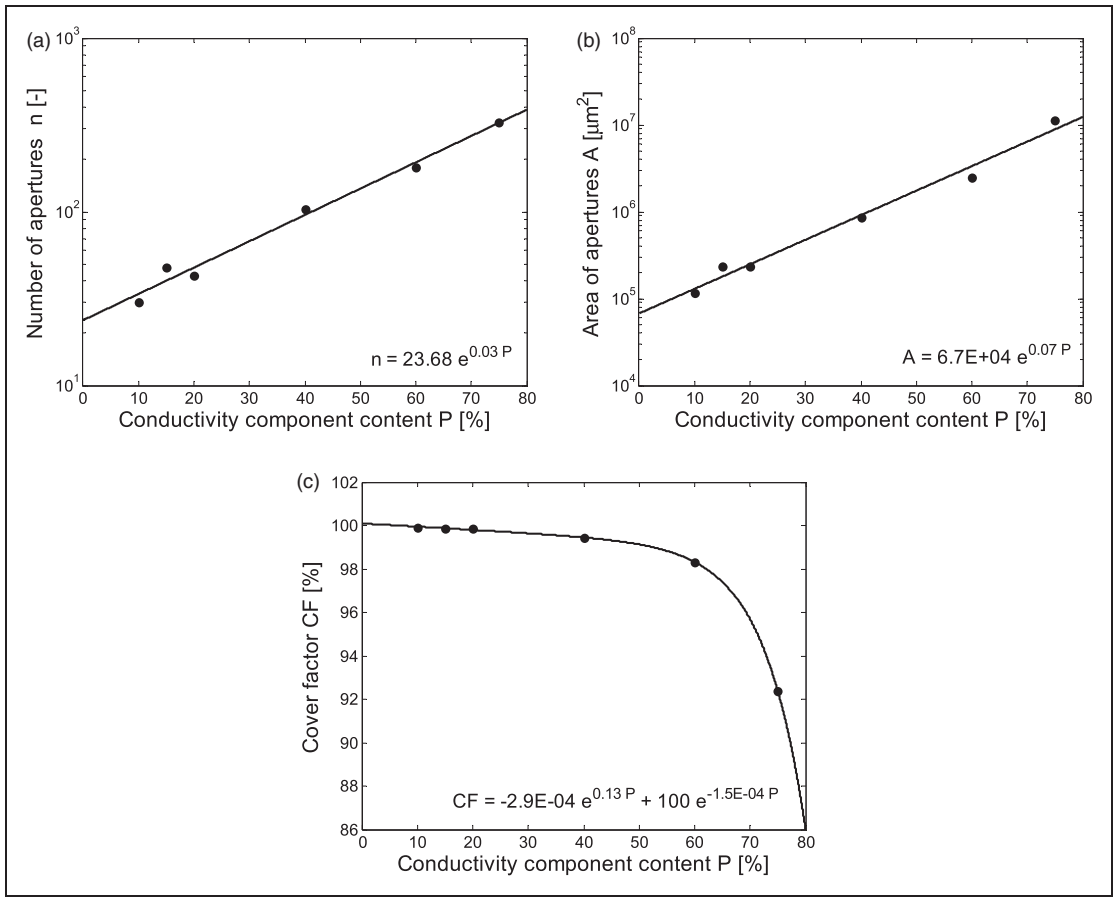

Figure 6. The dependence of (a) number of apertures, (b) area of apertures and (c) cover factor on the conductivity component content.

2450 MHz. A percolation threshold of the conductive component is not visible, because it is expected in the area below 10% of the conductive component. Even though the electromagnetic SE of samples was obviously frequency dependent, the electromagnetic SE increases linearly (in the area above percolation threshold) with metal content. The solid line in these graphs corresponds to the linear regression model with

parameters obtained by the minimizing sum of squared differences. It can be observed that a slope of the straight lines describing the dependence of SE on conductive component content P at two frequencies is almost identical, while an intercept of the line is higher for higher frequency dependence. The correlation coefficient (r) is 0.97 for both dependences. This linear regression model can be used for prediction of the value of P for sufficient shielding. For example, for frequency 1500 MHz:

$$P = \frac{SE - 27.58}{0.31}. \quad (22)$$

For example, $SE = 35$ dB can be obtained at conductive component concentration $P = 24.73\%$. The prediction ability of this line model is restricted to the content of the conductive component above the percolation threshold.

Geometrical structure of fabrics

Based on the analysis of geometrical parameters of apertures (pores), it is clear that with an increasing portion of metal fiber in yarn, the number of apertures becomes higher, the area of apertures is increases and the cover factor is decreases (see Figure 6). Dependence of number of apertures and area of apertures on conductivity component content is possible to describe by exponential function; the correlation coefficient (r) is 0.99 for both dependences. The exponential function also properly approximates the cover factor conductivity component content curve ($r = 1$). This phenomenon is caused by declining fineness of the yarn with increasing portion of the conductive component (see Figure 7), since the used metal fiber has dramatically lower diameter compared to the non-conductive component – polypropylene fiber. Yarn containing 75% of the conductive component has approximately a 30% decline of thickness compared with yarn containing 10% of metal fiber.

Prediction of hybrid woven fabric electromagnetic shielding effectiveness using image analysis

For prediction of hybrid woven fabric electromagnetic SE, the aperture equation based on waveguide conception was preferred because the aperture sizes and

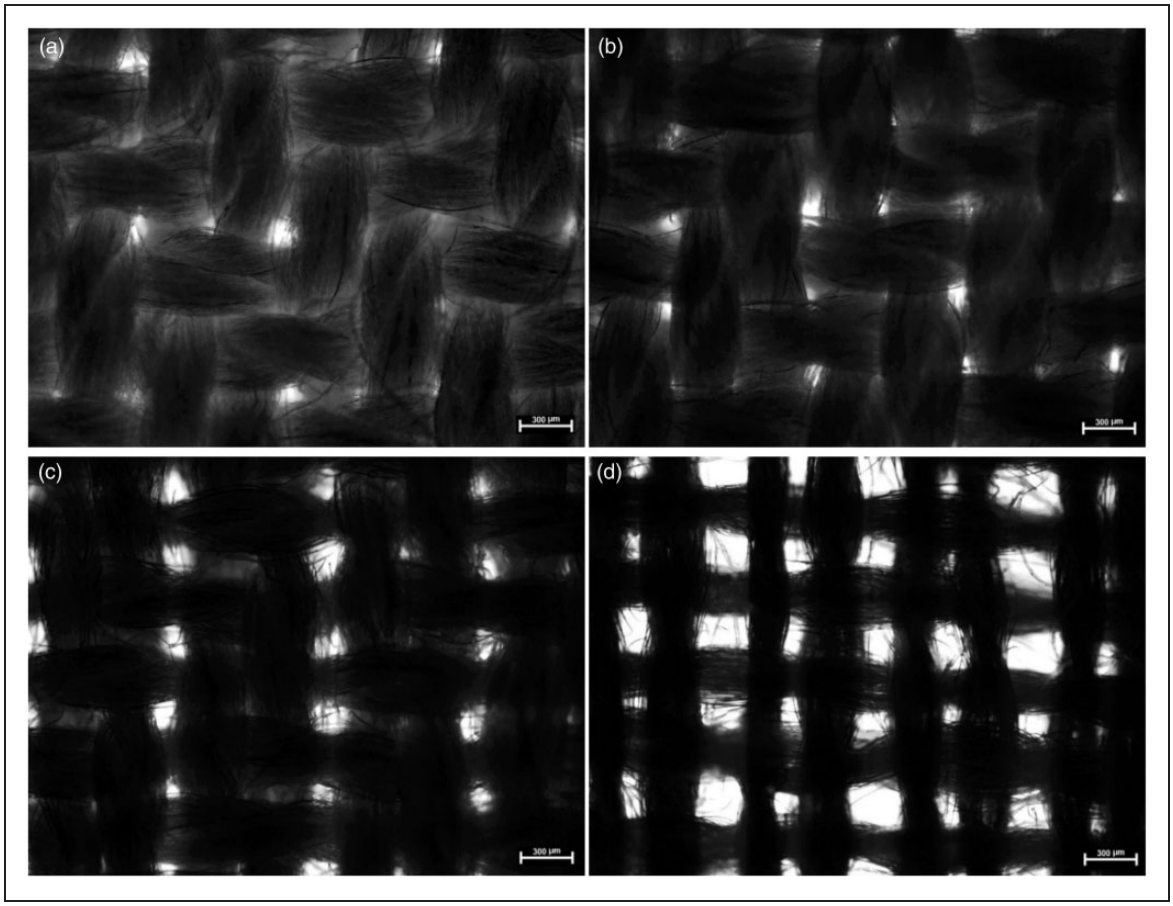

Figure 7. Microscopic images of studied samples: (a) sample No. 1; (b) sample No. 2; (c) sample No. 4; (d) sample No. 6.

shapes are irregular and the SE is predominantly determined by the largest aperture; fabrics are three-dimensional objects and the thickness can have a large impact on the shielding level. Using Equations (7), (8) and (14), it is possible to calculate the electromagnetic SE of hybrid woven fabrics containing different portions of conductive metal fiber if we know dimensions of the apertures (pores), thickness of the fabric and volume resistivity of the material. The thickness of fabric is taken equivalent to the depth of the aperture. The thickness was measured by standardized techniques (ASTM D1777[39]). A MATLAB script file was prepared to calculate and graph the electromagnetic SE of the hybrid fabric set using the listed input variables.

The plane-wave electromagnetic SE of six samples varying in electrical conductivity and geometrical structure was calculated according to Equation (14) as a function of frequency and plotted versus measured data. Constant C in Equation (8) was set to $C = 100$ with the help of the optimizing process. The measured data was obtained by the ASTM D4935-99 standard. The predicted and measured plane-wave attenuation is plotted in Figure 8. This figure confirms that the agreement between predicted and measured values occurs for fabric with a low content of SS (10–20%). Predicted values confirmed that electromagnetic SE of the studied samples increases with increasing conductive phase content, which means increasing electrical conductivity of the sample or, more precisely, decreasing volume resistivity of the sample. It was also confirmed that the electromagnetic SE increased logarithmically with the increasing frequency for the whole set of samples.

We can distinguish two groups of samples – samples with lower metal fiber content and at the same time tighter structure (sample Nos. 1–3) and samples with higher metal fiber content, which causes a more open structure (more apertures with larger diameter, lower cover factor, sample Nos. 4–6). The very good agreement between predicted and measured values can be observed for fabrics with lower metal fiber content (the difference is smaller than 1 dB for all frequency ranges). The difference between predicted and measured SE values of samples with higher metal fiber content (40–75%) at the low frequency range ($f < 500$ MHz) is satisfactory (not more than 5 dB), while the off-set between measured and predicted values is higher with increasing frequency (even 14 dB for $f = 2450$ MHz) for this group of samples. For the reasons given above, there is in practice a higher impact of apertures at higher frequencies ($f > 500$ MHz) for samples with higher metal fiber content than was found image analysis. It may be assumed that electromagnetic SE will not increase or decrease dramatically above a frequency of 2450 MHz for all samples.

In Table 6, there is a comparison of measured and predicted values of electromagnetic SE for all samples, especially for frequencies 1500 and 2450 MHz. These two frequencies were interesting because they are close to the working frequencies of particular electric devices. Many Global System for Mobile Communications (GSM) phones support the 1800 MHz band, while microwave ovens use 2450 MHz – a wavelength of 12.2 centimeters for heating. Wireless local area network (LAN) protocols, such

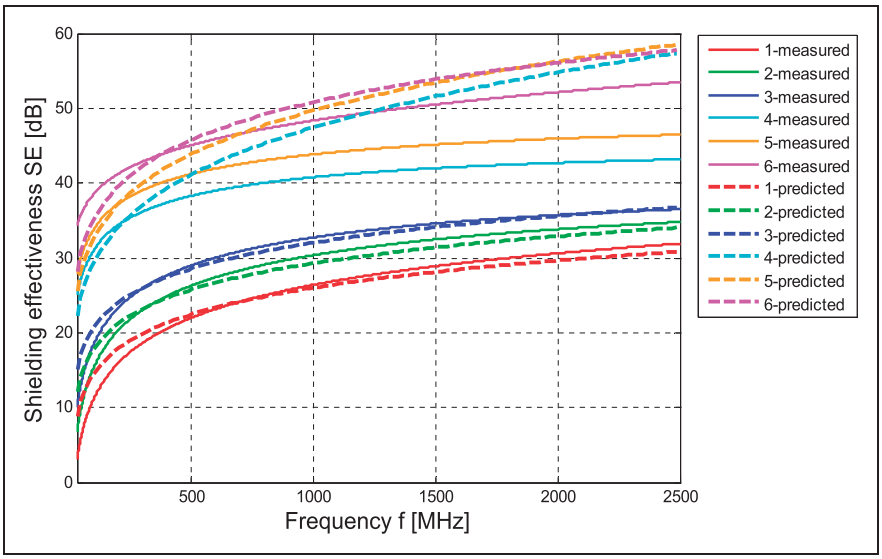

Figure 8. Frequency dependence of electromagnetic shielding effectiveness – comparison of predicted and measured values for all samples.

as Bluetooth and the IEEE 802.11 specifications, also use microwaves in the 2400 MHz frequency band. The agreement between measured and predicted electromagnetic shielding data for samples with different conductivity is visible. It is possible to observe an offset of 5.4 dB between all of them, on average at a frequency of 2450 MHz. However, due to the uncertainty of measurements, it can be considered that there is a minimum error of around 2 dB, which can be considered as satisfactory approximation.

Figure 9(a) compares results presented in Table 6 for frequency 2450 MHz. An empirical Q–Q plot of predicted and measured values of electromagnetic SE ($f = 2450$ MHz) is shown in Figure 9(b). The linear correlation coefficient (measuring the strength and direction of a linear relationship between two variables) is 0.92.

Table 6. Comparison of predicted and measured electromagnetic shielding effectiveness (SE)

	Electromagnetic shielding effectiveness SE [dB]			
	$f = 1500$ MHz		$f = 2450$ MHz	
Sample	Predicted	Measured	Predicted	Measured
1	28.14	28.89	30.81	31.79
2	31.41	32.47	34.04	34.70
3	34.13	34.59	36.74	36.43
4	51.63	41.99	57.38	43.12
5	53.47	45.14	58.51	46.42
6	53.90	50.50	57.75	53.36

Conclusions

A straightforward, simple model for predicting the electromagnetic SE of hybrid woven fabric containing extremely thin metal fibers in different concentrations was explored that incorporates fabric geometry and volume resistivity.

Fabric geometry was characterized by means of digital image processing. Dimensions of apertures (fabric pores), their quantity and other additional characteristics, for example the fabric cover factor, were evaluated. It was found that with increasing metal fiber content (from 10% to 75%), the number of pores increases and pores become larger (fabric with metal fiber content of 75% contains 10 times more pores and they are approximately 10 times larger than pores observed in the fabric with only 10% content of metal fiber). This phenomenon is caused by the decreasing diameter of the hybrid yarn with increasing conductive component content due to a higher amount of metal fibers, which are thinner (8 μm) than polypropylene fibers (17 μm). Yarn containing 75% of conductive component has a 30% decline of thickness compared with yarn containing 10% of metal fiber. In addition, the cover factor decreased from 99.9% (sample No. 1) to 92.4% (sample No. 6).

A rapid decrease of volume resistivity with increase metal fiber content (about two orders of magnitude between 10% and 75% content of metal fibers in the hybrid fabrics) was shown. The dependence of volume

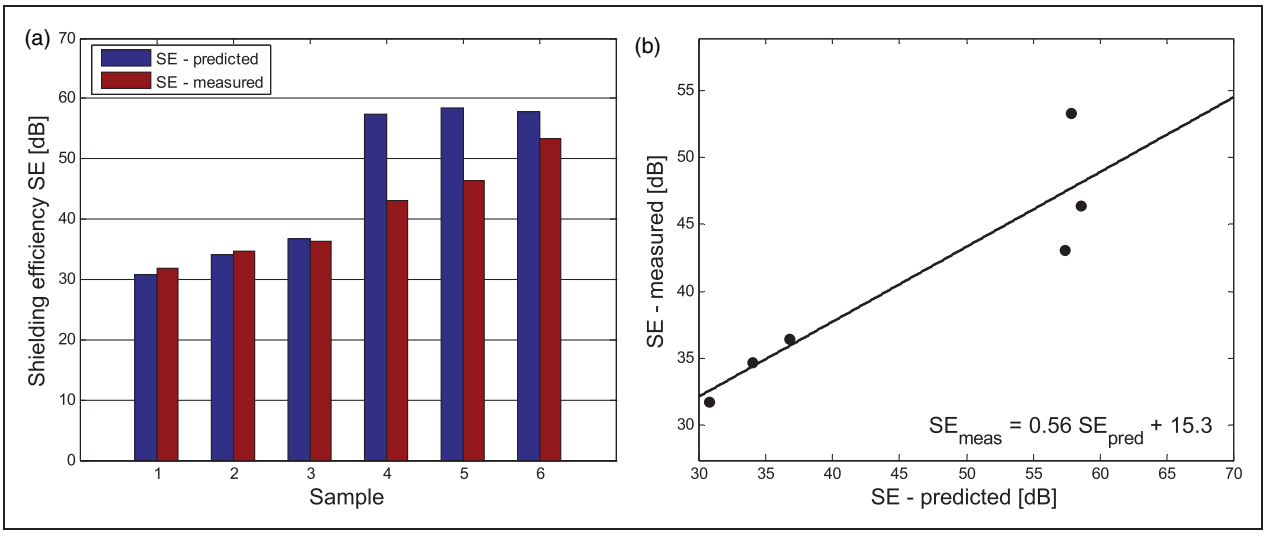

Figure 9. (a) comparison of predicted and measured electromagnetic shielding effectiveness for frequency 2450 MHz. (b) empirical Q–Q plot.

resistivity on the conductive component content for the range above the percolation threshold can be expressed by a simple power function adopted from the literature.

Plane-wave electromagnetic shielding properties (SE) of the sample set have been measured by means of the coaxial transmission line method according to standard ASTM D4935-99. It was found that the electromagnetic SE increased logarithmically with the increasing frequency for the whole set of samples. It was confirmed that SS fiber had a strong influence on the SE characteristics of fabrics and that electromagnetic SE increased with increased metal fiber content. Maximum electromagnetic SE (53 dB) at frequency 2450 MHz was reached by sample No. 6 with the highest content of metal fiber (75%). Fabric with the lowest conductive component content (10%) embodied SE of about 32 dB at frequency 2450 MHz. The dependence of electromagnetic SE on the conductive component content (P) for the range above the percolation threshold can be simply approximated by line. The proposed linear regression model can be used for prediction of the value of P for sufficient electromagnetic shielding.

Predicted data were examined and compared with measured ones. It was verified that the model is usable with a high success rate for predicting electromagnetic SE, especially for samples with a lower metal content and a higher cover factor. An offset of 5.4 dB between all of samples was observed, on average at a frequency of 2450 MHz. Usage of such prediction methods of electromagnetic shielding ability determination is favorable because direct EMISE measurement needs to use special expensive devices (e.g. a network analyzer and electromagnetic SE test fixture in the case of measurement according to ASTM D4935-99) and results are dramatically affected by the applied measuring method (it is expected that the test results obtained for the same material, tested at different laboratories by different methods, can vary even by as much as several tens of dB). Accuracy of the predictor model depends on the ability to determine the aperture dimension and measurement of electrical resistivity unloaded by errors. It seems that digital image processing presents a fast, easy and relatively precise way of analyzing geometrical and quantitative properties of fabric apertures (pores). Accuracy of aperture geometrical characteristic estimation depends on the quality of image capturing, especially image resolution and lightening conditions. The higher the resolution of the image, the more accurate estimation of geometrical characteristics of apertures will be obtained. The better lightening conditions at image capturing (e.g. homogenous lightening, sufficient contrast between the objects and background), the easier further image pre-processing and following segmentation will be acquired. The size of objects also influences accuracy of measurement. As the size of the object increases, geometrical characteristic estimation becomes more accurate.

Funding

This work was supported by the research project TIP–MPO VaV 2009 ''Electromagnetic field protective textiles with improved comfort'' of the Czech Ministry of Industry.

References

1. World Health Organization. *Establishing a dialogue on risks from electromagnetic fields*. Geneva: WHO, 2002.
2. Cheng KB, et al. Effects of yarn constitutions and fabrics specifications on electrical properties of hybrid woven fabrics. *Composites Part A* 2003; 34: 971–978.
3. Wieckowski TW and Jankukiewicz MJ. Methods for evaluating the shielding effectiveness of textiles. *Fibres Text East Eur* 2006; 14: 18–22.
4. Kodali V and IEEE Electromagnetic Compatibility Society. *Engineering electromagnetic compatability: principles, measurements, and technologies*. Hoboken: Wiley-IEEE Press, 1996.
5. Kleine-Ostmann T, Munter K and Schrader T. A new shielding effectiveness measurement method based on a skin-effect transmission line coupler. *Adv Radio Sci* 2007; 5: 37–42.
6. Geeha S, et al. EMI shielding: methods and materials – A review. *J Appl Polym Sci* 2009; 112: 2073–2086.
7. Vasquez H, Espinoze L and Lozano K. Simple device for electromagnetic interference shielding effectiveness measurement. In: *Proceedings of the IEEE Transactions on Electromagnetic Compatibility*, 2009, pp.62–68.
8. Hong Y, et al. Method and apparatus to measure electromagnetic interference shielding efficiency and its shielding characteristics in broadband frequency ranges. *Rev Sci Instrum* 2003; 2: 1–9.
9. Safarova V and Militky J. Comparison of methods for evaluating the shielding effectiveness of textiles. *Vlakna a Textil* 2012; 10: 50–56.
10. Rybicki T, et al. Modeling protective properties of textile shielding grids against electromagnetic radiation. *Fibres Text East Eur* 2013; 1: 78–82.
11. Volski V and Vandenbosch GAE. Full-wave electromagnetic modeling of fabrics and composites. *Compos Sci Technol* 2009; 69: 161–168.
12. Liu Z, et al. Prediction model of shielding effectiveness of electromagnetic shielding fabric with rectangular hole. *Prog Electromagn Res C* 2014; 48: 151–157.
13. Kendall C. Electromagnetic shielding behavior of wire-mesh screens. *IEEE Trans Electromagn Compat* 1988; 20: 298–306.
14. Henn A and Cribb R. Modeling the shielding effectiveness of metallized fabrics. In: *IEEE 1992 international symposium on electromagnetic compatibility, symposium record*, 1992, pp.283–286.
15. Lopez A, Vojtech L and Neruda M. Comparison among models to estimate the shielding effectiveness applied to conductive textiles. *Adv Electr Electron Eng* 2013; 11: 387–391.

16. Ott HW. *Electromagnetic compatibility engineering*. New York: John Wiley & Sons, 2009.
17. Chung DDL. Materials for electromagnetic interference shielding. *J Mater Eng Perform* 2000; 9: 350–354.
18. Vojtech L, Neruda M and Hajek J. Planar material electromagnetic shielding efficiency derivation. *Int J Commun Antenna Propag* 2011; 1: 21–28.
19. White D. *A handbook series on electromagnetic interference and compatibility*. Warrenton: Don White Consultants, 1971.
20. Shinagawa S, Kumagai Y and Urabe K. Conductive papers containing metallized polyester fibers for electromagnetic interference shielding. *J Porous Mater* 1999; 6: 185–190.
21. Keith JM, et al. Shielding effectiveness density theory for carbon fiber/nylon 6, 6 composites. *Polym Compos* 2005; 26: 671–678.
22. Kirkpatrick S. Percolation and conduction. *Rev Mod Phys* 1973; 45: 574–588.
23. Cheng KB, et al. Electromagnetic shielding effectiveness of stainless steel/polyester woven fabrics. *Text Res J* 2001; 71: 42–49.
24. Vojtech L and Neruda M. Application of shielding textiles for increasing safety airborne systems - limitation of GSM interference. In: *the ninth international conference on networks*. IEEE Computer Society, 2010, pp.157–161.
25. Simon R. EMI shielding through conductive plastics. *Polym Plast Technol Eng* 1981; 17: 1–10.
26. Colaneri N and Shacklette L. EMI shielding measurements of conductive polymer blends. *IEEE Trans Instrum Meas* 1992; 41: 291–297.
27. Chen H, et al. Fabrication of conductive woven fabric and analysis of electromagnetic shielding via measurement and empirical equation. *J Mater Proc Technol* 2007; 184: 124–130.
28. Vojtech L and Neruda M. Design of radiofrequency protective clothing containing silver nanoparticles. *Fibres Text East Eur* 2013; 101: 141–147.
29. Perumalraja R, et al. Electromagnetic shielding effectiveness of copper core-woven fabrics. *J Text Inst* 2009; 100: 512–524.
30. Horn PS. Some easy t statistics. *J Am Stat Assoc* 1983; 78: 930–936.
31. ASTM D257-07:2007. Standard test method for DC resistance or conductance of insulating materials.
32. Safarova V and Militky J. Electromagnetic shielding properties of woven fabrics made from high-performance fibers. *Text Res J* 2014; 84: 1255–1267.
33. ASTM D4935-99:1999. Standard test method for measuring the electromagnetic shielding effectiveness of planar materials.
34. Gonzales RC, Woods RE and Eddins SL. *Digital image processing using MATLAB*. New Jersey: Pearson Prentice-Hall, 2004.
35. Meloun M and Militky J. *Statistical data analysis*. New Delhi: Woodhead Publishing India, 2011.
36. Clingerman ML, King JA, Schulz KH, et al. Evaluation of electrical conductivity models for conductive polymer composites. *J Appl Polym Sci* 2002; 83: 1341–1356.
37. Kim HM, et al. Electrical conductivity and electromagnetic interference shielding of multiwalled carbon nanotube composites containing Fe catalyst. *Appl Phys Lett* 2004; 84: 589–591.
38. Duran D and Kadoglu H. A research on electromagnetic shielding with copper core yarns. *J Text & Apparel* 2012; 22: 354–359.
39. ASTM D1777:2011. Standard test method for thickness of textile materials.

Appendix 10

V. Safarova and J. Militky, "Electromagnetic shielding properties of woven fabrics made from high-performance fibers," Text. Res. J., vol. 84, no. 12, pp. 1255–1267, 2014.

Textile Research Journal

Original article

Textile Research Journal
2014, Vol. 84(12) 1255–1267

DOI: 10.1177/0040517514521118
trj.sagepub.com
SAGE

Electromagnetic shielding properties of woven fabrics made from high-performance fibers

Veronika Šafářová and Jiří Militký

Abstract

The expansion of the electronic industry and the extensive use of electronic equipment in communications, computations, automations, biomedicine, space, and other purposes have led to problems such as electromagnetic interference of electronic devices and health issues. For the reasons given above, the demand for the protection of human beings and sensitive electronic and electrotechnic appliances against the undesirable influence of electromagnetic signals and troublesome charges has been increasing. This paper presents the present state of fabrication and characterization of multifunctional high-performance metal/*m*-aramid hybrid fabrics with increased resistivity to electromagnetic smog while preserving basic properties of textile structures designated for clothing or technical purposes. In this paper, hybrid electromagnetic shielding fabrics made of high-performance fibers are introduced. An effect of metal content is studied and a form of relation between resistivity and total shielding effectiveness is proposed. Furthermore, chosen mechanical properties of developed fabric are evaluated.

Keywords

electromagnetic shielding effectiveness, electrical properties, metal fiber, aramid fiber, hybrid fabrics

According to the World Health Organization,[1] exposure to electromagnetic (EM) fields is not a new phenomenon. However, during the 20th century, environmental exposure to man-made EM fields has been steadily increasing due to growing electricity demand, ever-advancing technologies and changes in social behavior.

Everyone is exposed to a complex mix of weak electric and magnetic fields, both at home and at work. Sources of such emissions could include generation and transmission of electricity, domestic appliances and industrial equipment, telecommunications, and broadcasting. If the EM waves are not isolated effectively, they will cause interference with each other and result in technical errors. If somebody gets exposed under the EM, radiate environment, physical harms may occur to the human body.[2,3]

Metal is considered to be the best EM shielding material due its conductivity and permeability, but it is expensive, heavy, and it may also have thermal expansion and metal oxidation, or corrosion problems associated with its use. In contrast, most synthetic fabrics are electrically insulating and transparent to EM radiation.[4]

In recent years, conductive fabrics have obtained increased attention for EM shielding[5–10] and anti-electrostatic purposes.[11–16] This is mainly due to their desirable flexibility and lightweight properties. One way that conductive fabrics can be created is by using minute electrically conductive fibers. They can be produced in filament or staple lengths and can be incorporated with traditional non-conductive fibers to create yarns that possess varying degrees of conductivity. Another method uses conductive coatings, which can transform substrates into electrically conductive

Faculty of Textile Engineering, Technical University of Liberec, Czech Republic

Corresponding author:
Veronika Šafářová, Faculty of Textile Engineering, Technical University of Liberec, Studentská 2, Liberec 463 17, Czech Republic.
Email: veronika.safarova@tul.cz

materials without significantly altering the existing substrate properties. They can be applied to the surface of fibers, yarns, or fabrics. The most common are metal and conductive polymer coatings.

Meta-aramid is an aromatic polyamide fiber that possesses excellent physical and mechanical properties. Because of its outstanding flame-proof and heat-resisting properties, *m*-aramid fiber can be applied widely in thermal protective apparel. The primary applications in which fabrics are used include firefighting and many industrial areas, such as electrical and molten processing. The EM shielding ability of these protective fabrics is often underestimated. In certain cases, people need to be protected from harmful effects of heat and at the same time they need to be protected from harmful effects of high-level EM radiation (e.g. operators of high-frequency heating or molding apparatus).

There is not enough research on shielding properties of conductive fabrics made of high-performance fibers (designated for protective clothing) produced directly from conductive fibers with increased mechanical properties. Most of the studies focus on composite structures, such as aramid fiber composites.[17–19] For example Zhang et al.[17] prepared cement-based composites by introducing aramid fiber into cement. The effect of the filling ratio and length of fibers on EM and mechanical properties was studied and it was found that both factors had influence on absorption properties, the breaking strength, and the compressive strength of cement. On the other hand, the diameters of the metal fibers utilized in previous studies for EM shielding fabric are too large (0.08–0.15 mm) to be flexible enough to be applied for certain applications.[5,8,12] Therefore, it seems that there is a need for creation of protective fabrics with excellent physical and mechanical properties and at the same time with increased EM shielding ability.

In this study we aimed to design and investigate hybrid high-performance EM shielding fabrics. Woven fabrics are made of hybrid yarns produced by blending extremely thin metal fibers (diameter 0.008 mm) and high-performance *m*-aramid fibers. The design and validation of a low-cost metal composite fabric with EM shielding effectiveness (SE), flexibility, processability, and unique tensile strength is presented. The effect of metal content is studied and a form of relation between resistivity and total SE is proposed. Unique mechanical properties of samples, that have a special ability to shield EM smog, are verified using dynamic mechanic analysis (DMA).

The shielding mechanism

An EM field is built up from electric E and magnetic field H components. An electric field is created by a voltage difference and a magnetic field is created by a moving charge, that is, by a current. Every current is thus accompanied by both an electric and a magnetic field. Electromagnetic interference (EMI) shielding consists of two regions, a near-field shielding region and a far-field shielding region. The amount of attenuation due to shielding depends on the EM wave reflection from the shield surface, absorption of the waves into the shield, and the multiple reflections of the waves at various surfaces or interfaces in the shield. The multiple reflections require the presence of a large surface area (porous or foam) or an interface area (composite material containing fillers with large surface area) in the shields. The loss related with multiple reflections can be neglected when the distance between the reflecting surfaces or interfaces is large compared to the skin depth δ [m] (the penetration depth), defined as:

$$\sigma = \frac{1}{\sqrt{\pi f \mu K}} \tag{1}$$

where f [Hz] is the frequency and μ is the magnetic permeability equal to μ_0. μ_r, μ_0 is the absolute permeability of free space (air $= 4\pi\ 10^{-7}$) and K [S m^{-1}] is the electrical conductivity. An electric field at a high frequency penetrates only the near-surface region of a conductor. The amplitude of the wave decreases exponentially as the wave penetrates the conductor. The depth at which the amplitude is decreased to 1/e of the value at the surface is called the ''skin depth,'' and the phenomenon is known as the ''skin effect.''[20]

Efficiency of EM shields is commonly expressed by the total SE [dB], which represents the ratio between power P_2 [W] obtained when the shield is present and power P_1 obtained when the shield is not present:[18]

$$SE = -10 \log\left(\frac{P_2}{P_1}\right) \tag{2}$$

where $\log(x)$ is decimal logarithm.

The EM shielding efficiency of an element is characterized by its electric conductivity, permittivity, and permeability, parameters of source, and properties of the ambient surrounding.

Whilst we are able to determine SE for metal shields on the basis of their electrical parameters, for samples with a more complex structure, and often heterogeneous composition, such as textile materials, it seems that the SE can be determined only based on measurement.[21] There are several methods available for SE measurements. However, for thin planar structures, there are no standards defining the evaluation of small samples of only several tens of centimeters in size. The following test methods are commonly used

for measuring EM shielding of a given shielding material:[22]

1. the shielded box method;
2. the shielded room method;
3. the coaxial transmission line method.

Each of the above-mentioned methods has some advantages and limitations. For example, the shielded box method is widely used for fast, comparative measurements of test samples of different materials. The test comprises of a metal box that has a sample port in one wall and is fitted with receiving antenna. A transmitting antenna is placed outside the box.[22] Great shielding of surrounding man-made noise is the main advantage of this measurement method. On the other hand, for particularly narrow frequency ranges, a metal box with specific dimensions is required. The coaxial transmission line method (ASTM D4935) is now the most commonly preferred method. The measurements can be done at a specific frequency range (from 30 MHz to 1.5 GHz). The results obtained in different laboratories should be comparable.[21] Tests are carried out on small doughnut-shaped samples, but preparation of the samples is quite time consuming. MIL-STD-285, IEEE-STD-299, and later standards (e.g. EN 61000-5-7) based on the shielded room method are marked as the most sophisticated ones.[22] The test specimen size ranges typically from 0.25 to 2.5 m^2 in area for square samples or round test samples with a diameter of 30 cm.[21] In general, a signal source is placed outside the test enclosure, whilst the measurement device is located inside. The frequency range is from about 100 kHz to 10 GHz.[5] It is expected that the test results obtained for the same material tested at different laboratories can vary, even by as much as several dBs.[21] This is because the opening in the shielded wall of the chamber also affects the measurements. This opening itself forms a type of antenna with the parameters depending on several factors, one of which is its dimensions.

As already mentioned above, the evaluation of EM interference shielding efficiency needs to use special devices. Besides that, there is no measurement method that would singularly define the SE parameters of screening textiles and also no effective method for comparing the results of SE measurement obtained via different test methods based on different physical principles (for example MIL-STD 285 and ASTM D4935).[21] Measurements of volume resistivity or reciprocal values of electric conductivity are simpler. It is known from the theory that at sufficiently high frequencies it is possible to measure characteristics of the electrical part of the EM field only and therefore there should be a direct relation between total SE [dB] and fabric resistivity. Basic proposed numerical models of fabric SE are based either on electrical properties (especially volume conductivity) of the element[23–28] or on analysis of leakage through the opening in the textile.[29]

Experimental details

Hybrid yarns

Hybrid yarns were composed of high-performance meta-aramid fibers and different content of staple BEKINOX stainless steel (SS) metal fibers (1%, 3%, 5%, 10%, 15%, 20%). The aspect ratio (length/diameter ratio, l/d) of the SS used in this study is 6250, since the diameter of the SS is 8 μm and the fiber length of the SS is 50 mm. In this study, CONEX high-performance poly(*m*-phenylene isophthalamide) fiber with a fineness 1.8 dtex and 51 mm length was used. TREVON polypropylene fiber (2.2 dtex/50 mm) was chosen as a comparative non-conductive material. Properties of these fibers are given in Table 1. Hybrid yarns were two-ply yarns; fineness of yarns was 2×25 tex.

Hybrid fabrics

The seven fabrics with the same structure (weft and warp fineness 2×25 tex, warp density 20 1/cm, weft density 19 1/cm and twill weave) were used. Details about the fabrics are given in Table 2. Sample No. 7 was used in order to compare whether the average difference between the chosen mechanical properties of samples with different non-conductive portions is significant.

Table 1. Properties of fibers used for this study

Fiber	Fineness [tex]	Length [mm]	Tensile strength [cN/tex]	Elongation [%]	Young's modulus [cN/dtex]
Meta-aramid fiber (Conex)	1.80	51	34.38	32.2	57.37
Stainless steel fiber (Bekinox)	3.85	50	14.35	1.29	111.56
Polypropylene fiber (Trevon)	2.20	50	34.83	57.57	24.95

Table 2. Characteristics of fabrics

Sample	Composition	Warp/weft count [tex]	Fabric thickness [mm]	Fabric structure	Warp/weft density [1/cm]	Mass per unit area [g/m^2]
1	1% SS/99% *m*-aramid	25 × 2/25 × 2	0.70	2/2 twill	20/19	211
2	3% SS/97% *m*-aramid	25 × 2/25 × 2	0.63	2/2 twill	20/19	215
3	5% SS/95% *m*-aramid	25 × 2/25 × 2	0.57	2/2 twill	20/19	213
4	10% SS/80% *m*-aramid	25 × 2/25 × 2	0.58	2/2 twill	20/19	208
5	15% SS/75% *m*-aramid	25 × 2/25 × 2	0.58	2/2 twill	20/19	212
6	20% SS/80% *m*-aramid	25 × 2/25 × 2	0.57	2/2 twill	20/19	215
7	5% SS/95% PP	25 × 2/25 × 2	0.77	2/2 twill	20/19	230

SS: stainless steel; PP: polypropylene.

Statistical analysis of small samples

Due to the very small sample sizes $4 \le n \le 20$ available for evaluation process, a procedure based on order statistics introduced by Horn[30] was used. This is based on the depths that correspond to the sample quartiles. The pivot depth is expressed by:

$$H_L = \text{int}[(n+l)/2]/2 \text{ or } H_L = \text{int}[(n+l)/2+l]/2$$

according to which H_L is an integer. The lower pivot is $x_L = x_{(H)}$ and the upper one is $x_U = x_{(n+1-H)}$. Note that the $x_{(i)}$ are ordered statistics, that is, $x_{(i)} <= x_{(i+1)}$. The estimate of the parameter of location is then expressed by the *pivot half sum*:

$$P_L = 0.5(x_L + x_U) \tag{3}$$

and the estimate of the parameter of spread is expressed by the *pivot range*:

$$R_L = (x_U - x_L). \tag{4}$$

The random variable

$$T_L = \frac{P_L}{R_L} = \frac{x_L + x_U}{2(x_U - x_L)} \tag{5}$$

has approximately symmetric distribution and its quantiles are given by Horn.[30]

The 95% confidence interval of the mean is expressed by pivot statistics as

$$P_L - R_L t_{L,0.95}(n) \le \mu \le P_L + R_L t_{L,0,95}(n) \tag{6}$$

and analogously hypothesis testing may also be carried out. For small samples ($4 \le n \le 20$), the pivot statistics lead to more reliable results than the application of Student's *F*-test or robust *t*-tests.

Characterization

Electrical properties evaluation. Volume and surface resistivity of the high-performance hybrid fabrics were measured according to the standard ASTM D257-07, at temperature $T = 22.3^{\circ}\text{C}$ and relative humidity $RH = 40.7\%$. Volume resistivity is measured by applying a voltage potential across opposite sides of the sample and measuring the resultant current through the sample. Volume resistivity ρ_V [Ω . cm] was calculated from the following relation:

$$\rho_V = R_V \frac{S}{t} \tag{7}$$

where R_V [Ω] is volume resistance reading, t is thickness of the fabric [cm], and S is the surface area of the electrodes [cm^2].

Surface resistivity is measured by applying a voltage potential between two electrodes of specified configuration that are in contact with the same side of a material under test. Surface resistivity ρ_S [Ω] was calculated from relation:

$$\rho_S = R_S \frac{2\pi}{\ln\left(\frac{R_2}{R_1}\right)} \tag{8}$$

where R_S [Ω] is the surface resistance reading, R_1 is the outer radius of the center electrode [m], and R_2 is the inner radius of the outer ring electrode [m]. The measurement was carried out at 15 different places on the textile samples because of subsequent statistical analysis, $\alpha = 0.05$, $t_{L,0.95}(15) = 0.399$. The mean values estimator (pivot half sums), pivot ranges, and confidence intervals for means of ρ_V and ρ_S are summarized in Table 3.

Electromagnetic shielding effectiveness evaluation. The SE of the high-performance hybrid fabrics was measured according to ASTM D 4935-99,[29] for planar materials

Table 3. Results of electrical properties' evaluation

	Volume resistivity ρ_V [Ω.cm]			Surface resistivity ρ_s [Ω]		
Sample	Pivot half sum P_L	Pivot range R_L	95% CI	Pivot half sum P_L	Pivot range R_L	95% CI
1	4.16E + 08	3.10E + 08	± 1.24E + 08	3.24E + 07	2.68E + 07	± 1.07E + 07
2	6.48E + 06	4.88E + 06	± 1.95E + 06	1.14E + 06	9.83E + 05	± 3.92E + 05
3	1.32E + 06	1.07E + 06	± 4.26E + 05	3.11E + 05	2.43E + 05	± 9.71E + 04
4	6.49E + 04	3.51E + 04	± 1.40E + 04	3.43E + 04	1.81E + 04	± 7.21E + 03
5	1.04E + 04	4.97E + 03	± 1.98E + 03	3.47E + 03	1.44E + 03	± 5.76E + 02
6	6.14E + 03	1.63E + 03	± 6.51E + 02	1.19E + 03	6.28E + 02	± 2.51E + 02

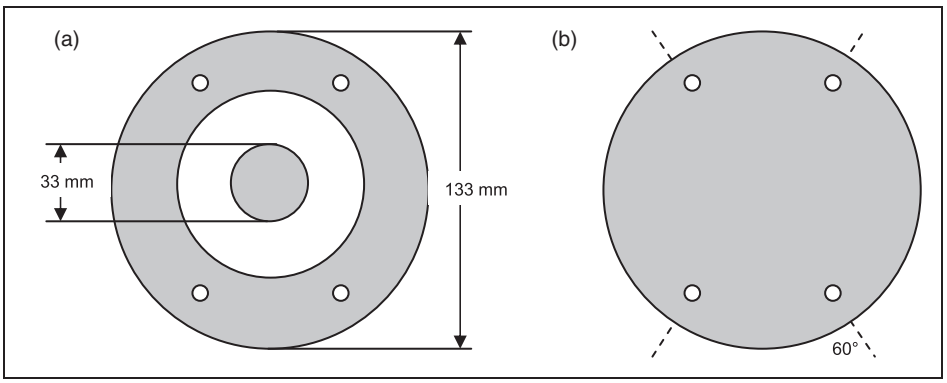

Figure 1. Illustrations of (a) reference and (b) load sample.

using a plane-wave, far-field EM wave. The SE of samples was measured over a frequency range from 30 MHz to 1.5 GHz. The set-up consisted of a sample holder with its input and output connected to the network analyzer. A SE test fixture (Electro-Metrics, Inc., model EM-2107A) was used to hold the sample. The design and dimension of the sample holder follows the ASTM method mentioned above. Network analyzer Agilent E5061B was used to generate and receive the EM signals. The standard mentioned above determines the SE of the fabric using the insertion-loss method. A reference measurement for the empty cell was required for the SE assessment. A "through" calibration with the help of the reference sample was made first. A load measurement was performed on a solid disk-shape sample subsequently. The reference and load specimens must be of the same material and thickness. Sample (both reference and load) geometries according to ASTM D 4935-99 are shown in Figure 1. The measurement was carried out at four different places on the textile samples because of subsequent statistical analysis, $\alpha = 0.05$, $t_{L,0.95}(4) = 0.555$. The mean values estimator (pivot half sums), pivot ranges, and confidence intervals for means of SE for frequency 1.5 GHz are summarized in Table 4.

Chosen mechanical properties' evaluation. Young's modulus E and loss factor $tg\ \delta$ were chosen as representative candidates for mechanical properties' evaluation. These parameters were studied with the help of the DMA method. The DMA method monitors the behavior of materials during mechanical exposure. The viscoelastic property of a sample is studied using DMA where a sinusoidal force (stress σ) is applied to a material and the resulting displacement (strain ε) is measured. This sinusoidal force was chosen as the easiest way to simulate dynamic conditions during wearing, because developed high-performance fabrics are designed for protective clothing. For a perfectly elastic solid, the resulting strain and stress will be perfectly in phase. Viscoelastic polymers have the characteristics in between where the same phase lag will occur during DMA tests. This phase lag represents loss angle δ (see Figure 2). Loss factor $tg\ \delta$ expresses the rate of mechanical loss; it is a portion between loss and storage modulus:

$$\tan\delta = \frac{E''}{E'} = \frac{E\sin\delta}{E\cos\delta} \tag{9}$$

where E is a complex modulus, E'' is a loss modulus, and E' is a storage modulus.

Table 4. Results of electromagnetic shielding effectiveness evaluation

	Electromagnetic shielding effectiveness *SE* [dB] $f = 1.5$ GHz		
Sample	Pivot half sum P_L	Pivot range R_L	95% CI
1	12.97	1.47	±0.59
2	22.36	0.92	±0.37
3	25.9	2.88	±1.15
4	29.58	2.15	±0.86
5	33.51	1.05	±0.42
6	35.98	0.65	±0.26

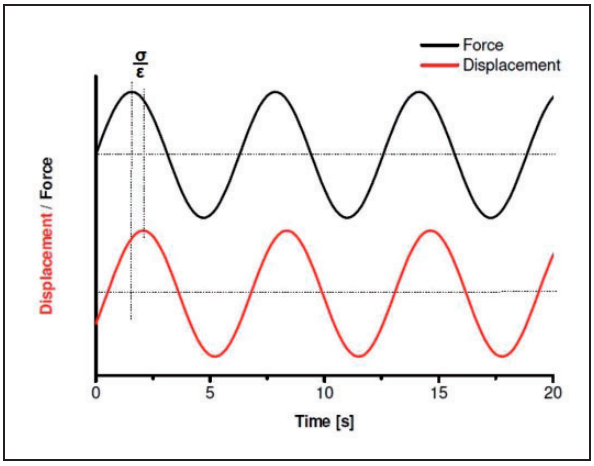

Figure 2. Phase diagram: time behavior of force and diplacement.

Firstly, the conductive component content on the Young's modulus and loss factor was studied. For this purpose, samples containing different portions of SS fiber and identical non-conductive components were used (sample no. 1–6). Although there are many studies comparing the mechanical performances of fibers/fabrics made of *m*-aramid and polypropylene, it was aimed to find out if the non-conductive component itself has a statistically significant effect on the Young's modulus of these hybrid samples designed for protective clothing. Therefore, in the second step, the effect of the non-conductive component on mechanical properties was examined. On this occasion samples with the same content of conductive component (5%) and different material using a similar non-conductive component (*m*-aramid, polypropylene) were evaluated (sample no. 3, sample no. 7). All studied samples have the same structure (weft and warp fineness 2×25 tex, warp sett 20 1/cm, weft sett 19 1/cm, and twill weave). The measurement was carried out at four different places on the textile samples because of subsequent statistical analysis, $\alpha = 0.05$, $t_{L,0.95}(4) = 0.555$. The mean values (pivot half sums), pivot ranges, confidence intervals for means of the Young's modulus, and loss factor are summarized in Tables 5 and 6.

Results and discussion

As described above, textile samples made of yarns containing meta-aramid fibers and different portions of conductive metal fiber (sample no. 1–6) were characterized by their electrical properties (surface and volume resistivity), EM shielding (coaxial transmission line method), and chosen mechanical properties (Young's modulus). Samples with different material using a similar non-conductive component (sample no. 3, sample no. 7) were also evaluated in the terms of the Young's modulus.

In order to get a clear overview of the results, Table 7 summarizes mean values of resistivity, EM SE, and the Young's modulus of samples with different material composition. All statistical parameters of the measured data (mean values, spread, and confidence intervals) are represented in Tables 3–6. Table 7 shows that volume and surface resistivity are decreasing (by about five orders) with increasing content of metal fiber inside the woven fabric. EM SE is increasing (up to 36 dB for samples with 20% of conductive component at frequency 1.5 GHz) with increasing conductivity of samples, which falls in line with the shielding theory. We can observe that the Young's modulus is increasing with increasing metal fiber content in samples for both studied directions.

Electrical properties

Figure 3 depicts the volume resistivity ρ_V and surface resistivity ρ_s metal fiber concentration curve for current samples made of high-performance fibers (sample no. 1–6). A strong correlation was found; the volume and surface resistivity decrease by more than four orders of magnitude between 1% and 20% metal fibers in the hybrid fabrics. This figure also identifies a percolation threshold at a loading of 3% of conductive component. A percolation threshold and drastic decrease in resistivity exists where the volume fraction of the metal fiber portion becomes sufficient to provide continuous electrical paths through the non-conductive component. Generally, the percolation threshold varies considerably with the shape and agglomeration of the conductive phase, as well as the type of non-conductive phase used. It is well known that the resistivity dependence on the amount of conductive component P is different for the range below and above the so-called percolation threshold P_o. The ρ_V and ρ_s show the strongly

Table 5. Details of studied fabric for Young's modulus evaluation

	Young's modulus [GPa]					
	Warp direction			Weft direction		
Sample	Pivot half sum P_L	Pivot range R_L	95% CI	Pivot half sum P_L	Pivot range R_L	95% CI
1	8.95E-02	1.52E-02	±8.44E-03	8.74E-02	1.18E-02	±6.55E-03
2	9.43E-02	1.55E-02	±8.60E-03	1.07E-01	1.63E-02	±9.05E-03
3	9.13E-02	4.70E-03	±2.61E-03	1.07E-01	1.00E-02	±5.55E-03
4	1.03E-01	4.00E-03	±2.22E-03	1.28E-01	1.50E-02	±8.33E-03
5	1.06E-01	8.00E-03	±4.44E-03	1.34E-01	1.33E-02	±7.38E-03
6	1.18E-01	6.00E-03	±3.33E-03	1.44E-01	1.20E-02	±6.66E-03
7	5.96E-02	1.20E-03	±6.66E-04	7.37E-02	7.40E-03	±4.11E-03

Table 6. Details of studied fabric for loss factor evaluation

	Loss factor [-]					
	Warp direction			Weft direction		
Sample	Pivot half sum P_L	Pivot range R_L	95% CI	Pivot half sum P_L	Pivot range R_L	95% CI
1	2.45E-01	3.90E-02	±2.16E-02	2.48E-01	1.60E-02	±8.88E-03
2	2.38E-01	2.30E-02	±1.28E-02	2.54E-01	3.20E-02	±1.78E-02
3	2.59E-01	2.90E-02	±1.61E-02	2.31E-01	1.00E-02	±5.55E-03
4	2.36E-01	1.80E-02	±9.99E-03	2.34E-01	5.10E-02	±2.83E-02
5	2.62E-01	4.20E-02	±2.33E-02	2.24E-01	2.80E-02	±1.55E-02
6	2.64E-01	1.60E-02	±8.88E-03	2.33E-01	5.10E-02	±2.83E-02
7	2.84E-01	6.00E-03	±3.33E-03	2.61E-01	5.00E-03	±2.78E-03

Table 7. Mean values of samples' studied characteristics

Sample	Composition	Volume resistivity ρ_V [Ω.cm]	Surface resistivity ρ_s [Ω]	Electromagnetic shielding effectiveness *SE* [dB], f= 1.5 GHz	Young's modulus [GPa]	
					Warp direction	Weft direction
1	1% SS/99% *m*-aramid	4.16E + 08	3.24E + 07	12.97	8.95E-02	8.74E-02
2	3% SS/97% *m*-aramid	6.48E + 06	1.14E + 06	22.36	9.43E-02	1.07E-01
3	5% SS/95% *m*-aramid	1.32E + 06	3.11E + 05	25.9	9.13E-02	1.07E-01
4	10% SS/80% *m*-aramid	6.49E + 04	3.43E + 04	29.58	1.03E-01	1.28E-01
5	15% SS/75% *m*-aramid	1.04E + 04	3.47E + 03	33.51	1.06E-01	1.34E-01
6	20% SS/80% *m*-aramid	6.14E + 03	1.19E + 03	35.98	1.18E-01	1.44E-01
7	5% SS/95% PP	–	–	–	5.96E-02	7.37E-02

SS: stainless steel; PP: polypropylene.

decreasing function of P below P_o . The ρ_V and ρ_s show the more slowly decreasing function of P in the range above P_o for samples 1–6 . It stands to reason that resistivity will not increase dramatically with additional increasing of the conductive component (above 20%).

The dependence of resistivity (ρ_V, ρ_s) on P can be expressed by a simple power function (see Figure 4; adopted from Clingerman et al.[31]):

$$\rho = \rho_C \cdot P^E \tag{10}$$

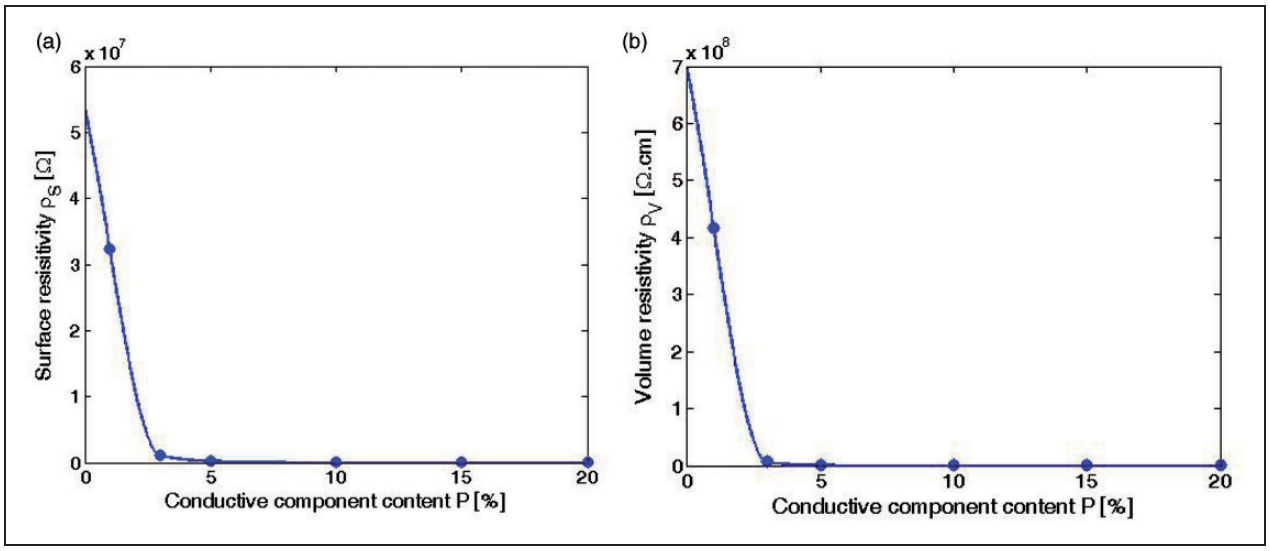

Figure 3. The dependence of (a) surface resistivity and (b) volume resistivity of samples on percentage of conductive component.

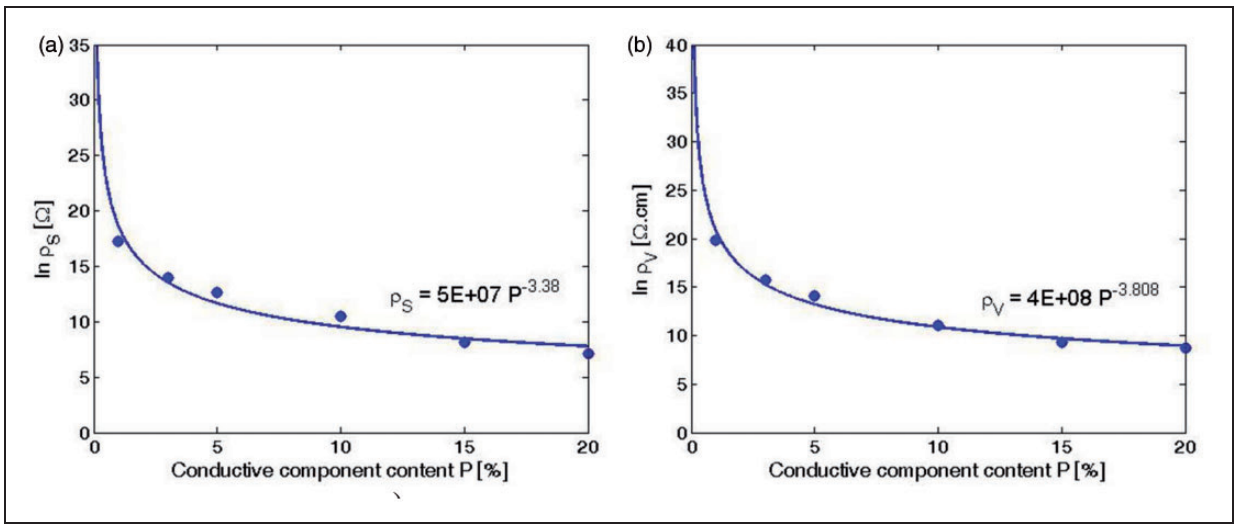

Figure 4. The dependence of the natural logarithm of (a) surface resistivity and (b) volume resistivity of samples on percentage of conductive component approximated by the simple power function.

where ρ is the volume or surface resistivity, ρ_C is the surface or volume resistivity for $P = 1\%$ of the conductive component in hybrid yarn, and parameter E is dependent on the structure of the conductive component.

Electromagnetic shielding efficiency

Figure 5 shows the variation in SE for the six fabrics made of high-performance fibers with incident frequency in the range 30–1500 MHz. The fabric with the highest content of conductive component (metal fiber) has the highest shielding efficiency through the frequency range. The effect of metal content on the SE has been already well established (e.g. Cheng et al.,[4] Duran and Kadoglu,[8] and Kim et al.[32]). It was confirmed in this study that SE increases with increasing metal fiber content. The position of the SE global maximum is possible to observe about frequency 1.1 GHz for all samples. The sample with the highest content of metal fiber reaches 42.9 dB for this frequency. It is possible to observe a shift of the local minimum/maximum to lower frequencies for samples with higher metal content.

The dependence of SE for frequency 1.5 GHz on metal fiber content in yarn is shown in Figure 6(a). We can examine the percolation threshold of the

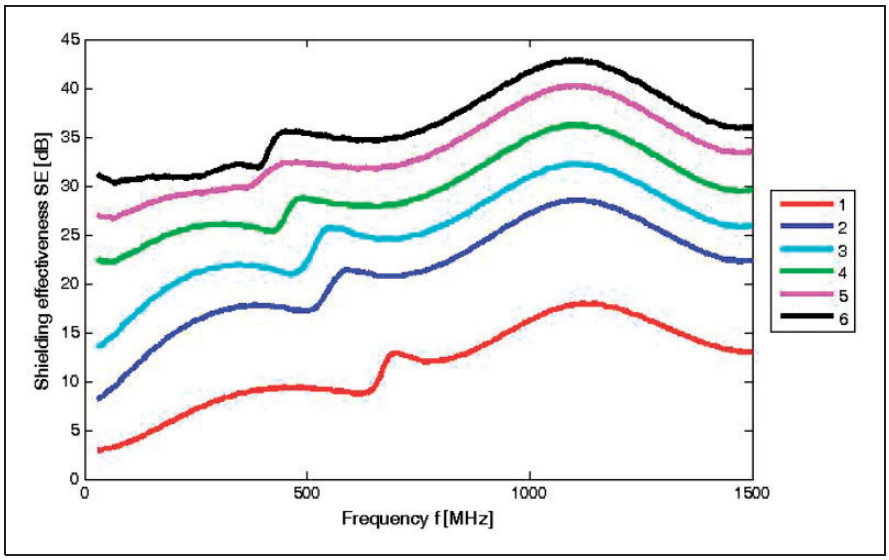

Figure 5. The dependence of shielding effectiveness on frequency for all samples.

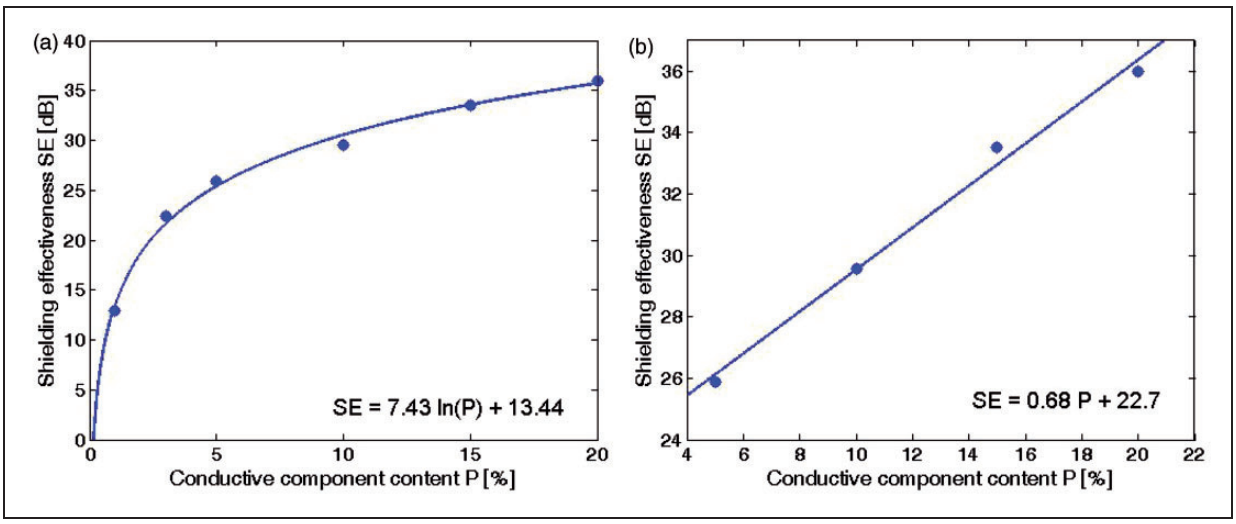

Figure 6. The dependence of shielding effectiveness on conductive component content for (a) the whole range of samples and (b) samples above the percolation threshold.

conductive component, which is about 3%. Even though the SE of samples was obviously frequency dependent, the SE increased logarithmically with metal content. The dependence of SE on P for the range above P_0 can be simply approximated by lines (see Figure 6(b)). The solid line in this graph corresponds to the linear regression model with parameters obtained by the minimizing sum of squared differences. This linear regression model can be used for prediction of the value of P for sufficient shielding. For example, for samples no. 1–6:

$$P = \frac{SE - 22.7}{0,68} \tag{11}$$

For example, $SE = 40\,\text{dB}$ can be obtained at conductive component concentration $P = 25.44\%$. The prediction ability of this line model is restricted to the content of the conductive component above percolation threshold P_o.

Correlation between electric resistance and electromagnetic shielding

It is well known that the SE increases as electric conductivity as well as permittivity of shielding material increases based on the EM shielding theory,[32,33] but there is a lack of experimental verification and

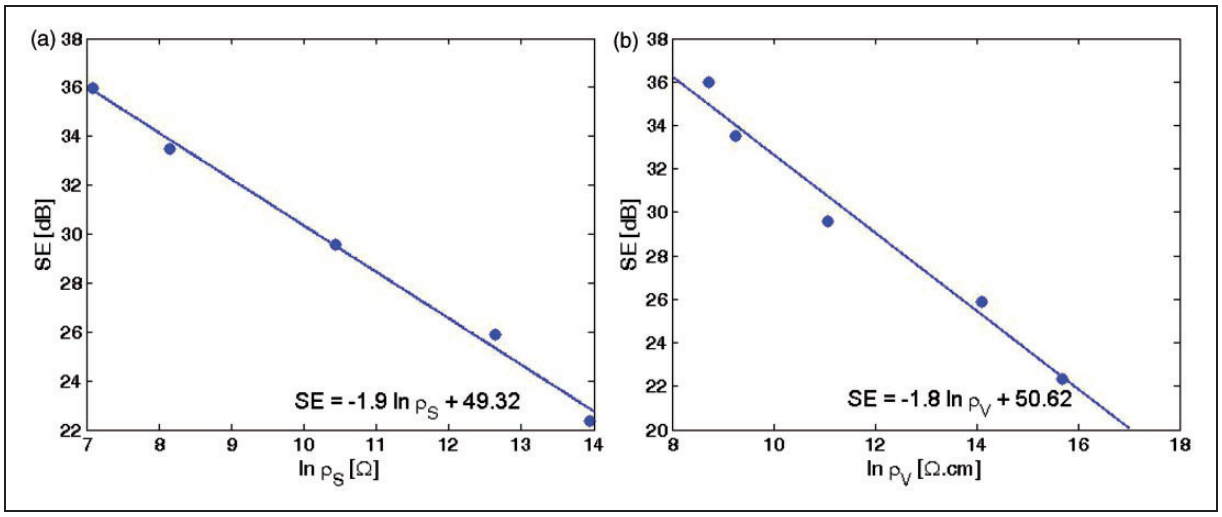

Figure 7. The dependence of shielding effectiveness on the logarithm of (a) the surface and (b) volume resistivity in the area above the percolation threshold.

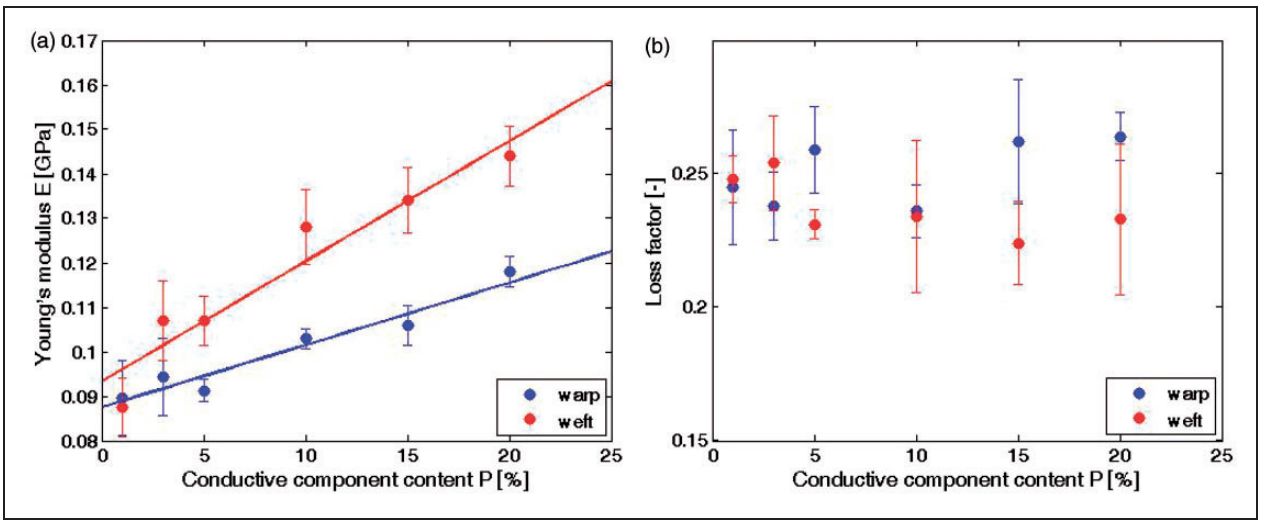

Figure 8. The dependence of (a) the Young's modulus and (b) the loss factor on conductive component content.

exploration of this dependence for fiber structures. In addition, direct measurement of fabrics' EM SE is quite complicated, especially because of the need for special devices and time-consuming preparation of samples. Utilization of the presumption that the electrical part of the EM field dominates for sufficiently high frequencies seems to be simpler. Knowledge of the electrical characteristics, which are easily measurable, could be therefore used for establishment of EM SE of textile samples. That is why correlation between surface and volume resistances and EM shielding efficiency is studied. Samples with content of conductive component higher than $P = 3\%$ were analyzed because they belong to the region above the percolation threshold. The dependence of total SE on logarithms of surface and volume resistivity log ρ_s and log ρ_V is shown in Figure 7. The approximate linearity is visible. The solid lines in this graph correspond to the linear regression model with parameters obtained by the minimizing sum of squared differences. The corresponding correlation coefficient $r = 0.997$, resp. 0.9878 indicates the good quality of fit. This graph clearly indicates that for sufficiently high frequencies it is sufficient to measure only the electric field characteristics. In this graphical evaluation, EM shielding efficiency at only one frequency (1.5 GHz) was studied. This particular frequency is the maximum one for measuring SE by the coaxial transmission line method. During the research it was confirmed that linear regression model is applicable also for other

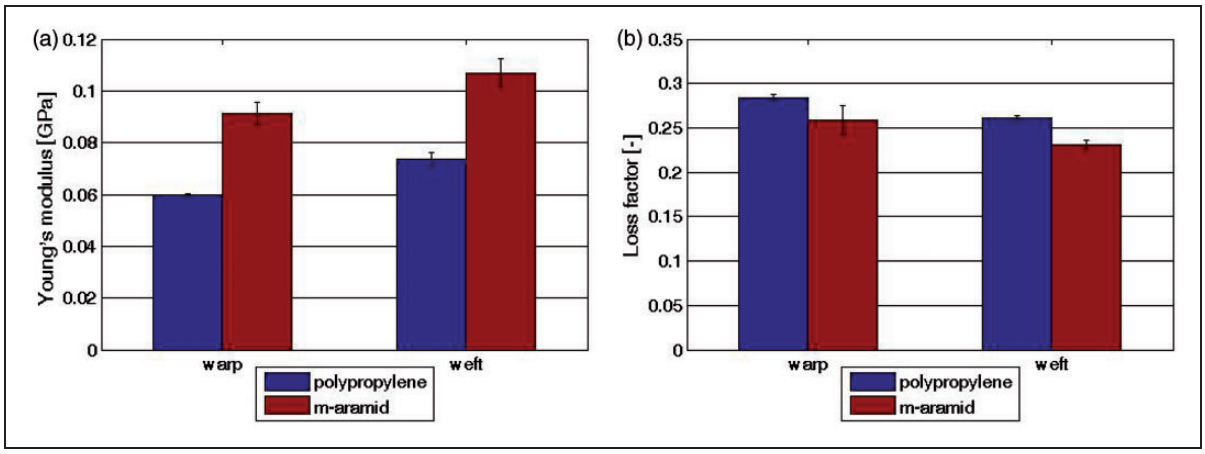

Figure 9. The dependence of (a) the Young's modulus and (b) the loss factor on different types of non-conductive components of samples.

Table 8. Specified requirements of electromagnetic shielding textiles.[34]

Grade	5 Excellent	4 Very good	3 Good	2 Moderate	1 Fair
Percentage of electromagnetic shielding (ES)	SE > 99.9%	99.9% ≥ SE > 99%	99% ≥ SE > 90%	90% ≥ SE > 80%	80% ≥ SE > 70%
Shielding effectiveness (SE)	SE > 30 dB	30 dB ≥ SE > 20 dB	20 dB ≥ SE > 10 dB	10 dB ≥ SE > 7 dB	7 dB ≥ SE > 5 dB

studied frequencies (900 MHz–1.5 GHz) with good quality of fit ($r = 0.99$–0.98).

Chosen mechanical properties

The effect of content of conductive fiber content on Young's modulus is shown in Figure 8(a). The solid line in this graph corresponds to the linear regression model with parameters obtained by the minimizing sum of squared differences. It is clear that the Young's modulus increases with the increasing portion of metal fiber in the sample. The Young's modulus of weft is higher in comparison with the Young's modulus of warp. The same effect on the loss factor is shown in Figure 8(b). There is no clear dependence between the loss factor and conductive component content.

The effect of non-conductive material (*m*-aramid versus polypropylene) on the Young's modulus is shown in Figure 9(a). The same effect on the loss factor is shown in Figure 9(b). As expected, we can observe that the Young's modulus is much higher when *m*-aramid fiber is used. The difference is about 30 MPa for the weft and warp directions. Samples made of *m*-aramid fiber have a lower loss factor in comparison with samples made of polypropylene, which is in agreement with the Young's modulus evaluation. This effect is determined by properties of fibers used in this study (see Table 1). It was confirmed that content of SS fiber (1–20%), as well as the type of non-conductive component (*m*-aramid versus polypropylene fiber), has a statistically significant effect on the Young's modulus.

Conclusion

The EM shielding properties and Young's modulus of conductive woven fabrics made of metal and high-performance fibers were investigated assuming to use these fabrics in protective clothing. As high-performance fibers, meta-aramid fibers were considered. A linear relationship between the conductive component concentration (above the percolation threshold) and SE of the fabrics was also derived.

Weft fabrics with the same structure and different portion of conductive phase in hybrid yarn were studied. Hybrid yarns forming weaves were composed of *m*-aramid and staple SS fiber. Samples were characterized by their volume and surface resistivity (standardized method). Plane-wave shielding properties of the composite high-performance fabric were measured between 30 and 1500 MHz using the coaxial transmission line method.

The so-called percolation threshold, dependence of resistivity, and total SE on the amount of conductive

component in hybrid yarn and dependence of total SE on volume resistivity and surface resistivity was examined. It is clear that the portion of the conductive component has a significant effect on increasing conductivity (decreasing resistivity) and improvement of EM shielding efficiency. Samples with the highest content of conductive component have EM shielding efficiency higher than 35 dB for frequency 1.5 GHz, which means that more than 99.9% (see Table 8) of EM waves were shielded by the high-performance conductive fabrics. It is possible to express dependence between resistivity and percentage of the conductive phase in hybrid yarn by a simple power function adopted from the literature. It is possible to express the dependence between total SE and percentage of conductive phase in hybrid yarn above the percolation threshold P_0 using the linear regression model. A model for prediction of the value P for desired shielding was proposed. It was shown that dependence of total SE on volume and surface resistivity of fabric above percolation threshold V_0 is nearly linear at the frequency of 1.5 GHz. For reasons given above, the existence of the direct relation between electrical properties and the ability of the sample to shield a plane-wave EM field was confirmed.

It was found out that increasing the conductive component content has an effect on increasing the Young's modulus, while *m*-aramid as a non-conductive component of a sample significantly influences the chosen mechanical properties (Young's modulus) of samples. Therefore, so-called high performance was proved.

It was also ascertained that these high-strength fabrics with optimum EM SE can be obtained by controlling the content of the conductive component. Samples prepared in this study have not only a very satisfactory SE level (see Table 8), but they also have very good mechanical properties appropriate for the chosen application (e.g. protective clothing).

Funding

This work was supported by the research project TIP–MPO VaV 2009 "Electromagnetic field protective textiles with improved comfort" of the Czech Ministry of Industry.

References

1. World Health Organization. *Establishing a dialogue on risks from electromagnetic fields*. Geneva: WHO, 2002.
2. Bolte JFB and Pruppers MJM. *Electromagnetic fields in the working environment*. Netherlands: Ministry of Social Affairs and Employment (SZW) report, 2006.
3. Polisky LE. *Radiation hazards issues for telecommunication facility professionals*. Ashburn, VA: Comsearch, 2005.
4. Cheng KB, Cheng TW, Lee TC, et al. Effects of yarn constitutions and fabrics specifications on electrical properties of hybrid woven fabrics. *Composites Part A* 2003; 34: 971–978.
5. Ortlek HG, Alpyildiz T and Kilic G. Determination of electromagnetic shielding performance of hybrid yarn knitted fabrics with anechoic chamber. *Textil Res J* 2013; 83: 90–99.
6. Chen H, Lee KC, Lin JH, et al. Fabrication of conductive woven fabric and analysis of electromagnetic shielding via measurement and empirical equation. *J Mater Process Technol* 2007; 184: 124–130.
7. Shinagawa S, Kumagai Y and Urabe K. Conductive papers containing metallized polyester fibers for electromagnetic interference shielding. *J Porous Mater* 1999; 6: 185–190.
8. Duran D and Kadoglu H. A research on electromagnetic shielding with copper core yarns. *J Textil Apparel* 2012; 22: 354–359.
9. Yidiz Z, Usta I and Gungor A. Electrical properties and electromagnetic shielding effectiveness of polyester yarns with polypyrrole deposition. *Textil Res J* 2012; 82: 2137–2148.
10. Ching IS and Jin TCh. Effect of stainless steel-containing fabrics on electromagnetic shielding effectiveness. *Textil Res J* 2004; 74: 51–56.
11. Knittel D and Schollmeyer E. Electrically high-conductive textiles. *Synth Met* 2009; 159: 1433–1437.
12. Ramachandran T and Vigneswaran C. Design and development of copper core conductive fabrics for smart textiles. *J Ind Textil* 2009; 39: 81–93.
13. Mamunya YeP, Davydenko VV, Pissis P, et al. Electrical and thermal conductivity of polymer filled with metal powders. *Eur Polym J* 2002; 38: 1887–1897.
14. Shateri-Khalilabad M and Yazdanshenas ME. Fabricating electroconductive cotton textiles using graphene. *Carbohydr Polym* 2013; 96: 190–195.
15. Bhat NV, Seshadri DT and Radhakrishnan S. Preparation, characterization and performance of conductive fabrics: cotton + PANi. *Textil Res J* 2004; 74: 155–166.
16. Neruda M and Vojtech L. Verification of surface conductance model of textile materials. *J Appl Res Technol* 2012; 10: 579–585.
17. Zhang Y, Li B, Liu S, et al. Electromagnetic wave absorption properties and mechanical properties of aramid fiber reinforced cement. *Adv Mater Res* 2012; 512–515: 2873–2877.
18. Xue W. Application and molding technique research of aramid fiber composites in radar components. In: *proceedings of 2011 IEEE CIE international conference on radar*, 2011, 2, pp.1402–1405.
19. Hua Y, Yamanaka A and Ni QQ. Electromagnetic shielding properties of super fiber-reinforced composites. *Adv Mater Res* 2010; 123–125: 65–68.
20. Ott HW. *Electromagnetic compatibility engineering*. Hoboken, NJ: John Wiley & Sons, 2009.
21. Wieckowski TW and Jankukiewicz MJ. Methods for evaluating the shielding effectiveness of textiles. *Fibres Textil East Eur* 2006; 14: 18–22.
22. Geetha S, Sathees Kumar KK, Rao Chepuri RK, et al. EMI shielding: methods and materials – a review. *J Appl Polym Sci* 2009; 112: 2073–2086.

23. White D. *A handbook series on electromagnetic interference and compatibility*. Gainesville, VA: Don White Consultants, 1971.
24. Simon R. EMI shielding through conductive plastics. *Polym Plast Technol Eng* 1981; 17: 1–10.
25. Colaneri N and Shacklette L. EMI shielding measurements of conductive polymer blends. *IEEE Trans Instrum Meas* 1992; 41: 291–297.
26. Vojtech L, Neruda M and Hajek J. Planar materials electromagnetic shielding efficiency derivation. *Int J Commun Antenna Propagation* 2011; 1: 1– 10.
27. Keith JM, Janda NB and King JA. Shielding effectiveness density theory for carbon fiber/nylon 6,6 composites. *Polym Compos* 2005; 26: 671–678.
28. Perumalraja R, Dasaradan BS, Anbarasu R, et al. Electromagnetic shielding effectiveness of copper core-woven fabrics. *J Textil Inst* 2009; 100: 512–524.
29. ASTM D 4935-99. Standard test method for measuring the electromagnetic shielding effectiveness of planar materials, June 1999.
30. Horn PS. Some easy *t* statistics. *J Am Statist Assoc* 1983; 78: 930–936.
31. Clingerman ML, King JA, Schulz KH, et al. Evaluation of electrical conductivity models for conductive polymer composites. *J Appl Polym Sci* 2002; 83: 1341–1356.
32. Kim HM, Kim K, Lee CY, et al. Electrical conductivity and electromagnetic interference shielding of multiwalled carbon nanotube composites containing Fe catalyst. *Appl Phys Lett* 2004; 84: 589–591.
33. Yupig D, Shunhua L and Hongtao G. Investigation of electrical conductivity and electromagnetic shielding effectiveness of polyaniline composite. *Sci Technol Adv Mater* 2005; 6: 513–518.
34. Committee for Conformity Assessment on Accreditation and Certification of Functional and Technical Textiles. Specified requirements of electromagnetic shielding textiles, http://www.ftts.org.tw/images/fa003E.pdf (2010, accessed 30 January 2014).